Computational Modeling for Stress Analysis of Overhead Transmission Line Stranded Conductors Under Design and Fretting Fatigue Conditions

by

Gang Qi

April, 2013

Department of Civil Engineering and Applied Mechanics
McGill University
Montreal, Canada

A thesis submitted to McGill University in partial fulfillment of the requirements of the degree of Doctor of Philosophy

In Loving Memory of My Grandparents

Qi-Sheng Qi *(1904 ~ 1986)*

Ti-Wei Li *(1914 ~ 2001)*

Days go by, months go by, and years have gone by, I still miss you much, being there to talk to me, believe in me, and hug me …

You always live in my heart.

Abstract

While great efforts have been made in the electrical utility industry to engineer various stranded conductors with enhanced strength and vibrational characteristics, research devoted to understanding the complex mechanical behavior of complete conductors has been scarce, especially from a computational mechanics perspective. In the meanwhile, the long-lasting problem of conductor fretting fatigue becomes increasingly critical for overhead line design and maintenance, especially with the world-wide aging of electrical transmission grids. Aging of conductors contributes to significant degradation of their local fatigue strength, leading to drastic reduction of their service life. However, the complex mechanical response of stranded conductors cannot be well predicted by either experimental testing or simplified theoretical models, owing to the physical complexity introduced by their multi-layer stranded geometry, nonlinear material properties, substantial frictions among the wires and between the wires and hardware clamping systems, as well as the comprehensive contact interactions amongst their components. Simplified beam models and coarse 3-D models of earlier computational studies also fail to calculate the accurate stress variations inside a conductor strand and capture the stress gradients near the contact interfaces. Moreover, the estimations of fretting fatigue life are very dependent on the high accuracy of the stress predictions in the conductor wires. Therefore, reliable high-fidelity computational models have been long expected for a better understanding of the contact damage of transmission line conductors under both design and fretting fatigue conditions. Nevertheless, the practical difficulties encountered during solving such computationally demanding and highly nonlinear problems for a real conductor have made the task very challenging.

The main objective of this thesis is to study the complex stress states and relevant influencing factors of stranded electrical conductors, using finite element analysis approaches. The research was carried out in three stages.

First of all, a study focused on the finite element (FE) modeling of an optical ground wire (OPGW) cable strand for its detailed stress analysis. A refined 3-D FE model including all essential nonlinear characteristics was successfully constructed. In order to obtain satisfactory accuracy, least computational cost, and reliable solution process, the quality

of the mathematical model and the involved numerical solution techniques were studied thoroughly, including geometric modeling, element selections, mesh design, material models, contact condition establishment, boundary conditions and load treatments, as well as the key numerical solution techniques. As a result, a high-fidelity physics-based macroscopic modeling methodology was developed for detailed and accurate computational stress analysis of stranded conductors.

A 795 kcmil Drake ACSR conductor was then selected as a benchmark conductor to investigate the tensile strength and critical stress states of a complete conductor under extreme design conditions. The computational results under axial loading were discussed in detail and showed agreement with the experimental data provided by manufacturers. Furthermore, a sensitivity study explored the relative importance of friction effects among conductor wires on the mechanical response.

A large scale 3-D FE stress analysis model with comprehensive nonlinearities was developed and implemented to simulate an actual ACSR fretting fatigue test. It was shown to be very beneficial to provide insight into better understanding of the contact states and the associated stress states among the helically stranded conductor wires in the conductor-clamp system under bending fretting fatigue amplitudes. The computational results showed good agreement with some experimental measurements and field observations reported in the open literature. Based on the accurate stress analysis, a practical multi-axial fatigue lifing methodology was developed to estimate local fretting fatigue strength of electrical conductors. Subsequently, a parametric study was performed to examine the influence of fretting amplitudes on the mechanical response of the conductor-clamp system.

In conclusion, this research shows the reliability and significance of using reliable FE modeling in predicting the complex response of stranded conductors, which has contributed to fill some of the current knowledge gaps. Furthermore, the computational modeling and lifing approaches developed in this thesis provide a different perspective from existing practices and may become a starting block of further exploration of the mechanisms of conductor fretting fatigue and future development of improved fatigue lifing methods for the increasingly aging overhead transmission line conductors.

Résumé

Malgré les efforts déployés par l'industrie des lignes de transport d'électricité pour la conception de conducteurs toronnés de haute résistance mécanique, la recherche dédiée à la compréhension physique du comportement mécanique des conducteurs s'est faite plus rare, surtout du point de vue de la mécanique computationnelle. Le problème du vieillissement des conducteurs de lignes aériennes à haute tension, en particulier celui de l'usure en fatigue des brins et torons, n'est toujours pas complètement compris ni donc résolu. Le vieillissement des conducteurs se manifeste par une dégradation importante de leur résistance locale à l'usure en fatigue, réduisant par le fait même leur vie utile et la robustesse mécanique de l'ensemble de la ligne. Il faut reconnaître que les études expérimentales et les modèles théoriques simplifiés ne peuvent pas prédire le comportement mécanique détaillé des conducteurs toronnés à cause de la complexité physique de ces câbles: torons et brins multicouches, matériaux inélastiques non-linéaires, effets des frictions substantielles entre les brins, torons et les surfaces des accessoires d'attache, ainsi que les interactions de contact entre ces éléments. Les modèles simplifiés basés sur la théorie des poutres et les rares modèles d'éléments finis 3-D avec maillages grossiers provenant d'études antérieures ne permettent pas de calculer les variations précises des états de contraintes dans les conducteurs, en particulier les gradients élevés dans les zones de contact. Une estimation raisonnablement précise de la résistance en fatigue des conducteurs dépend directement du degré de précision de l'analyse des contraintes dans les brins et torons.

On a longtemps attendu des modèles computationnels de haute fidélité pour ce type de problème afin de mieux comprendre l'endommagement par contact et usure des câbles (maintes fois observé sur le terrain) et leur réponse mécanique détaillée sous les charges de conception. Néanmoins, ce sont les difficultés pratiques inhérentes à la solution du problème (modèles de grande taille exigeant beaucoup de ressources de calcul, processus numériques complexes dû aux non-linéarités, etc.) qui ont posé les plus grands défis dans les applications réelles.

Le but de cette recherche est de démontrer la faisabilité d'une méthodologie de construction de modèles d'analyse par éléments finis pour l'étude détaillée des contraintes dans les conducteurs toronnés. Les travaux rapportés dans la thèse procèdent en trois étapes principales, décrites ci-après.

La première partie consiste à préparer un modèle de section de câble de garde à fibre optique (CGFO) de construction complexe et d'en faire l'analyse détaillée sous déplacement axial contrôlé. Cette étape a servi à établir les bases de la méthodologie proposée, lesquelles sont discutées de manière exhaustive : la modélisation géométrique des câbles, le choix des éléments finis, la conception du maillage, la définition des modèles des matériaux constitutifs, l'établissement des conditions de contact et des conditions frontières, l'application des charges, ainsi que le choix et la performance des algorithmes numériques. Les résultats prédits par le modèle raffiné du CGFO sont une nette amélioration par rapport à ceux d'études antérieures et la méthodologie est ainsi validée.

La deuxième partie de la recherche porte sur la modélisation raffinée du conducteur de ligne ACSR 795 kcmil qui porte le nom de code « Drake », sélectionné comme cas de référence pour étudier la résistance en traction et les états de contraintes complexes du conducteur sous des conditions de conception extrêmes de conception (contrôlées par l'allongement dans cette deuxième partie). Les résultats obtenus sont discutés en détail et sont en accord avec les données expérimentales fournies par les manufacturiers. Une étude de sensibilité a également exploré l'importance relative des effets frictionnels entre les brins du câble sur les contraintes calculées par le modèle.

Finalement, un modèle détaillé 3-D est créé pour simuler les conditions précises d'un essai typique de fatigue en flexion pour le conducteur « Drake » jumelé à une pince de suspension. Le modèle retient toutes les non-linéarités du problème d'un point de vue mécanique. Les résultats de l'analyse apportent un éclairage nouveau qui permet une meilleure compréhension des interactions de contact et des états de contraintes complexes induits entre les brins et torons des conducteurs ACSR dans la région de contact avec la pince de suspension et pour un cycle complet de flexion du conducteur. Les résultats des analyses computationnelles du « Drake » sont avérés en accord avec certains résultats d'essais et observations d'endommagement par fatigue rapportés dans la littérature. Sur la base des résultats détaillés rendus disponibles par l'approche computationnelle proposée dans cette thèse, l'auteur suggère une méthode pratique pour évaluer la résistance locale en fatigue multiaxiale des conducteurs du type ACSR au droit des points de contact des pinces de suspension. Cette méthode est relativement simple d'application (une fois les analyses de contraintes disponibles) et donne des résultats en accord avec les valeurs recommandées par les manufacturiers pour le câble « Drake ». Par la suite, une étude paramétrique est faite pour vérifier l'influence de l'amplitude des mouvements de glissement sur les états de contraintes déterminés dans le conducteur dans la région de contact avec la pince sous l'effet d'un cycle complet de chargement flexionnel.

En conclusion, cette recherche démontre la faisabilité et la pertinence de l'usage des méthodes computationnelles avancées pour l'analyse des contraintes d'un problème complexe comme celui des conducteurs toronnés multicouches. La méthodologie de construction des modèles est une contribution scientifique importante qui permet d'améliorer notre compréhension du comportement mécanique des conducteurs sous charges extrêmes ou dans des conditions de fatigue flexionnelle. La méthode proposée pour l'estimation de la résistance à l'usure en fatigue est également utile pour l'industrie des lignes de transport et pour les manufacturiers de câbles et il est envisageable que cette recherche servira de tremplins à plusieurs autres études computationnelles pertinentes sur les conducteurs de lignes afin d'améliorer leur fiabilité et leur robustesse mécanique.

Originality and Contributions to Knowledge

To the best of the author's knowledge, this research includes the following original contributions:

1. An essential improvement of existing finite element stress analysis models of overhead optical ground wires (OPGW) is achieved, from which a new-generation refined stress analysis model is created based on state-of-the-art numerical solution technologies.

2. A rational and high fidelity modeling methodology is developed to address effectively the highly nonlinear mechanics behavior of overhead transmission line conductors under extreme design conditions. The same approach can also be applied generally to other complex stranded cable structures and wire ropes used widely in civil and mechanical applications.

3. A sensitivity study is conducted to explore the effects of variations in the frictional coefficients among conductor wires on the mechanical response of helically stranded conductors under axial loading.

4. A computational model for accurate contact stress analysis of stranded conductors under fretting fatigue conditions is developed. This model is capable of describing contact damage of helically stranded conductors with fretting fatigue amplitudes that simulate the effects of conductor aeolian vibration.

5. A practical multi-axial fatigue lifing methodology is proposed to estimate the fretting fatigue resistance of stranded conductors.

6. A numerical parametric study examining the influence of fretting amplitudes on contact damage is conducted, which provides insights into the fretting fatigue mechanisms of transmission line conductors.

7. Much computation and simulation experience is gained throughout the entire research by solving various modeling-related issues, which may benefit other researchers and experts. From a numerical modeling perspective, this study enriches the knowledge of solving a complex nonlinear mechanics problem for cable and wire rope structures using finite element methods.

Acknowledgements

This dissertation represents the culmination of many years of my study, hard work, and commitment in order to achieve my goal. And this doctoral study has been the longest journey among my formal school education, during which too many things happened in my life, going up and down. All are unforgettable !

Compared with a typical progress of a PhD research, it was a tough road, not because of the technical challenges that I had to tackle, but the many distractions that I had to overcome. A North America life was not easy for a new Chinese immigrant family, and making a living was overwhelming rather than pursuing my personal dream. Due to the busy full-time jobs, family commitments and business trips, accomplishing this research (especially the thesis writing) had become a very demanding and lengthy endeavor, far beyond my initial anticipation. But, I never intended to give up and had poured my heart into making it as best as I could. In the past three years, I always carried my laptop, brought along my thick binders, and used every available time slots and possible places to move forward this “my own task”. A considerable portion of this thesis was actually written in hotels and on airplanes, and each completed section became a milestone to me.

Along the way, the person whom I admire and appreciate most is my thesis advisor, Professor Dr. Ghyslaine McClure. She is such a wonderful advisor and mentor! She allowed me complete freedom to conduct this study, while her outstanding expertise in this field had made working with her an inspiring pleasure. Not only her valuable academic guidance, but also her moral supports, constant encouragement, well understanding of my life (my difficulties) and great patience with my progress, have made my doctoral research a great experience. I have felt the honor of being her graduate student. Thank you, my professor !

In addition, I am very thankful to Hydro-Québec and General Cable for their generous assistance by providing us with the OPGW and ACSR mechanical property data and testing results, without which this research would not have been possible to be carried out.

Further, I cheerfully wish to extend my thanks to all the professors who taught me various subjects during my McGill years in “Civil” and “Mechanical” departments. What they had instilled in me was not only the knowledge, but the values and attitude to reshape me to become a confident engineer and researcher.

As always, I have been greatly indebted to my former professors when I studied in China, Changhua Wu, Xi Zhang, Xing Ji, Wanxie Zhong, among others, for showing me the beauty of solid mechanics from different perspectives. In particular, Professor Wu, who was my first mentor, introduced me the fascinating world of nonlinear finite element analysis through his enthusiasm and dedication to scientific excellence, and his friendship. I am truly grateful to each of these individuals, without whose great influence it was impossible for me to decide to devote my career to this science. On this pleasant journey, I have experienced immeasurable joy.

Last but not least, I am deeply grateful to my parents and especially my wife for putting up with my frequent absence from family activities over the years to pursue the (personal and not profitable) goal for which I have a desire to achieve. Also, thank you, Amy, my lovely daughter! While no words can compensate the many weekends and holidays that could have been devoted to you, and precious playtime you expected to have with me, I record herein my immense gratitude as you have been a constant source of joy and love since you were born, and your charming smiles have been making my life so beautiful !!

Finally, it is time to say “Goodbye” to my long student life. I have no doubt that it would be the most precious period in my lifetime, and I do cherish every minute of these times. If people often think that studying for a PhD is such a long and difficult mission, it is because they do not realize how complex to succeed and “feel really good” every single day in a real working world. From this year, my daughter is starting her long student life. I sincerely wish her all the best and enjoy her educational journey as I did.

Contents

List of Symbols

F_n	normal force
F_t	frictional force
D	fretting displacement
N	fretting cycles
h	pitch length
E	Young's modulus
ν	Poisson's ratio
σ	stress
ε	strain
$\{\sigma\}$	smoothed stress vector at a node of an element
$\{\varepsilon\}$	smoothed strain vector at a node of an element
$\{\sigma^*\}$	nodal stress vector calculated directly from FEM
$\{\varepsilon^*\}$	nodal strain vector calculated directly from FEM
$\{\Delta\sigma\}$	stress error vector at a node of an element
$\{\Delta\varepsilon\}$	strain error vector at a node of an element
[D]	stress-strain (constitutive) matrix
Ω	volume of an element
$\| e \|_e$	structural error energy norm of an element
$\| e \|$	structural error energy norm over the entire (or a selected part of the) model
N	number of elements in a model or part of the model
U	strain energy over the entire (or selected part of the) model
η	percentage error in energy norm
μ	static frictional coefficient
P	normal contact pressure
τ_{sy}, τ_{sz}	tangential contact stress in y, z directions
K_n	normal contact stiffness per unit contact width
K_s	tangential contact stiffness per unit contact width
u_n	contact gap
u_s	contact slip distance

e user-defined contact compatibility tolerance

λ_i Lagrange multiplier

${}^{t}\mathbf{R}$ vector of external nodal forces at time t

${}^{t}\mathbf{F}$ nodal stress resultants at time t

${}^{t}\mathbf{K}$ tangent stiffness matrix

F incremental nodal force vector (stress resultant)

U incremental nodal displacement vector

$\Delta\mathbf{R}^{(i-1)}$ residual or out-of-balance load vector

S_{von} Von-Mises stress

ε_{von} Von-Mises elastic strain

ε_{p} equivalent plastic strain

θ lay angle of a given layer

Fi bolt preload

$\mathbf{S_a}$ alternating stress (stress amplitude)

$\mathbf{S_{qa}}$ equivalent von Mises alternating stress

$\mathbf{S_{qm}}$ equivalent mean stress

$\mathbf{S}_{Nf}$ endurance limit

Y_b vertical fretting amplitudes

List of Figures

List of Tables

Chapter 1

Introduction

1.1 Background and Motivation

In the transmission line industry and in collaboration with the research community, numerous structural dynamic studies have been carried out to investigate and predict the transient response of overhead lines (OHL) and their supporting towers (Figure 1.1) to different types of shock loads such as those induced by ice-shedding, seismic loads, sudden tower collapse, conductor breakages, etc. (see for example, McClure et al., 1993, 1998, 2003, 2007, 2008). Conductor breakage has been widely recognized as one of the worst types of shock loads that a line section can experience, as it directly leads to power disruptions and large tension imbalances that may even lead to the failure of transmission line supports, and possibly catastrophic cascading failures of the supports. Then, how do conductor ruptures happen? As a matter of fact, the main cause of direct conductor ruptures under normal in-service conditions is the significant drop in local fatigue strength induced by fretting (Zhou et al., 1994). Therefore it is not surprising that fatigue-weakened conductors would eventually break under conditions that create large overloads.

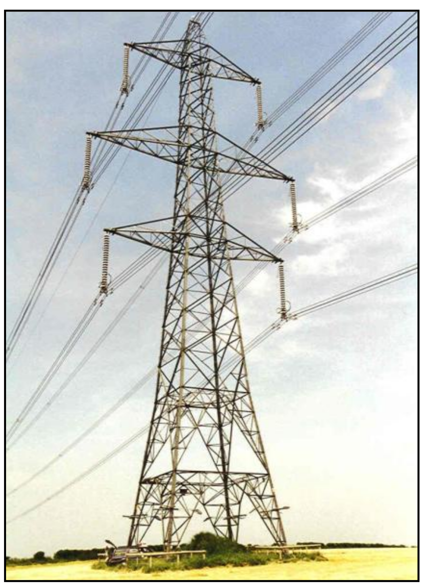

Figure 1.1 Overhead transmission line with tower (http://www.eng.uwo.ca/people/esavory/tower.htm)

Fretting fatigue is widely acknowledged to significantly degrade local fatigue resistance by promoting the initiation of fatigue cracks and their early propagation and this has been identified as one of the most severe problems affecting conductor service life. Under normal operating conditions, transmission line conductors are frequently (not to say almost constantly) subjected to small amplitude aeolian vibrations; in the meanwhile they have to carry their own weight and mechanical tension while undergoing localized heavy compressions from various clamping devices, connectors and spacer hardware. Many laboratory observations and field experiences have shown that the most severe fretting damage usually occurs in suspension clamp edge regions (Figure 1.2), where conductor ruptures happen eventually (EPRI, 2006).

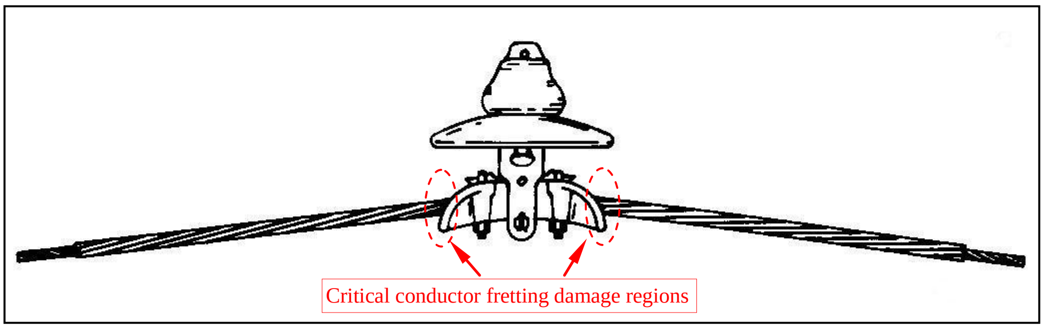

Figure 1.2 Schematic of suspension clamp and conductor

Historically, studies on fretting damage have been mainly concentrated on aerospace applications (aero-engine and airframe structures) due to demanding requirements to the durability and integrity of those components serving in aeronautical systems. However, the contact regions in transmission line multi-layered stranded conductors in their clamping devices are also very susceptible to fretting fatigue damage; they are also difficult to investigate because of the complexity of their combined *material properties*, *contact geometry* and *loading conditions*, as outlined below.

Overhead electrical conductors are typically made of ACSR (Aluminum Conductor Steel Reinforced), which are comprised of outer layers of aluminum alloy strands with a galvanized high-strength steel core also made of stranded wires; they are common in North America (Figure 1.3). The role of the aluminum alloy wires is to carry the electrical current while the central steel core is the main supporting part due to its higher axial rigidity. Another type of construction is the All Aluminum Alloy Conductor (AAAC) where all individual strands are made of the same highly conductive material (Figure 1.4). From the material perspective, aluminum is more deformable and ductile than titanium- and nickel-based aerospace alloy materials and fretting cracks are theoretically easier to initiate and propagate in aluminum strands. In addition, aluminum and aluminum alloys in their clean state usually exhibit very strong adhesion when in self-contact or with other metallic materials. Such a state of strong adhesion could promote surface degradation (wear) and high friction under working conditions. Although the surface wear induced by fretting may be mild, the reduction in local fatigue life can be substantial. Moreover, the geometric configurations of transmission line cable strands make their contact states much more complex than ordinary two-body or three-body contact in mechanical fasteners. Many "hot spots" of fretting damage can develop due to the extensive contact interactions among wires on a given layer, wires of different layers, as well as between the outer layer of the conductor and the suspension clamp, an example of which is shown schematically in Figures 1.5 and 1.6. Furthermore, the multi-axial loading environment of conductor strands not only creates a complex contact stress state in the suspension clamp contact region, but also causes severe stress gradients at the edge-of-contact that potentially foster crack nucleation and growth leading to strand ruptures. Finally, it also should be noted that the local contact stresses under fretting conditions are very sensitive to the configuration (geometry) of the contact bodies, contact loads, materials, and contact surface tribology (friction). Taken together, all these features make transmission line conductors especially prone to fretting fatigue failure, and also make the related fretting study very difficult.

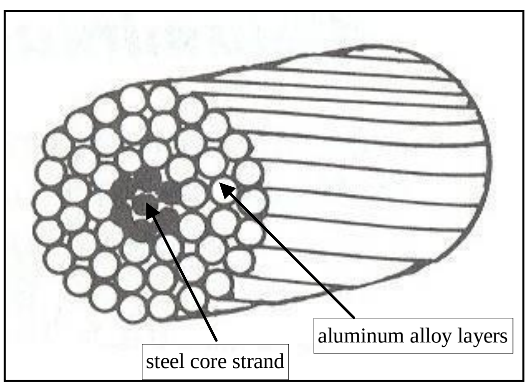

Figure 1.3 ACSR conductor

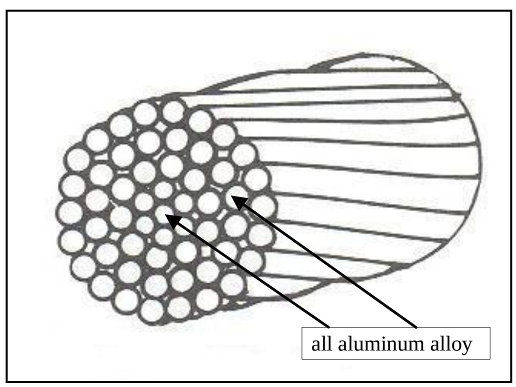

Figure 1.4 AAAC conductor

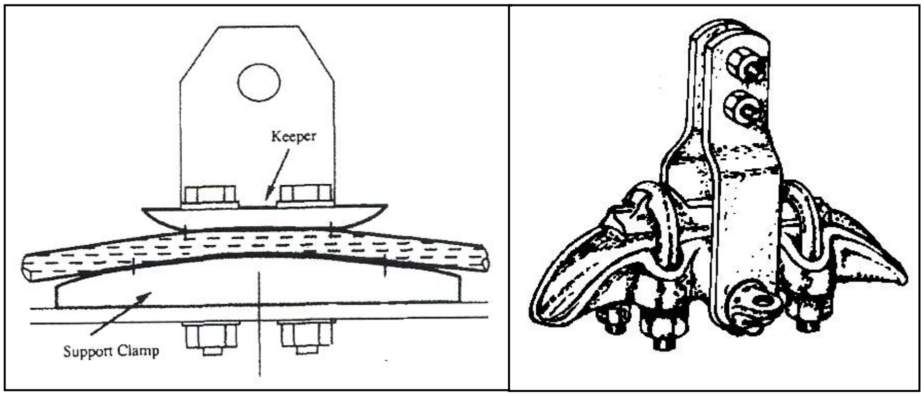

Figure 1.5 Suspension clamp/conductor connections and a typical clamp structure

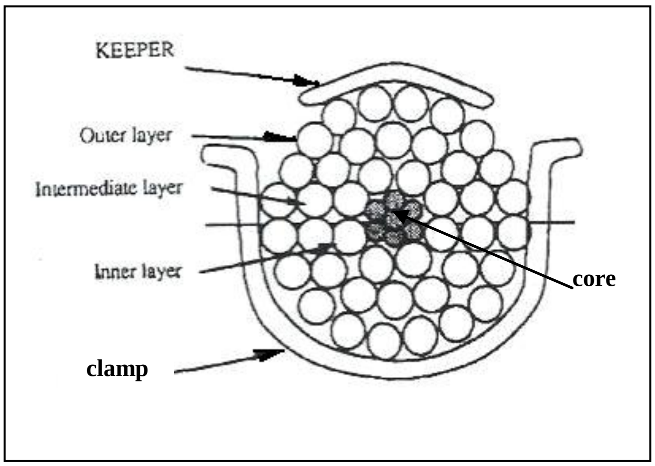

Figure 1.6 Cross-section of a conductor at suspension clamp center (Zhou et al., 1995)

From a methodological perspective, in spite of the existence of abundant experimental studies in the area of fretting damage, which could date back to the 1920s (Tomlinson et al., 1927, 1939), computational approaches have not been very successful to date. Also, it is noteworthy that the current research and development approaches used by cable designers/manufacturers are almost exclusively experimental and limited to specific cable types. However, due to technological limitations, experimental testing alone is insufficient to fully characterize the mechanical response of a stranded conductor. A preliminary study with a simplified and coarse numerical model (Roshan Fekr et al., 1999) has demonstrated that three-dimensional modeling is necessary to describe the mechanical behavior of these cables of complex construction under a variety of loads. Nevertheless, the development of effective computational modeling of the contact damage of transmission line conductors has achieved limited progress afterwards, even for the case under design (tension) load conditions. In the open literature, few published studies have addressed these topics using numerical simulations, although it has been widely acknowledged that computational stress analysis is of great significance in product design and failure investigations. In view of such a situation, it is clear that simulations of contact damage (under both design conditions and fretting fatigue conditions) of transmission line conductors call for in-depth study, which strongly motivated this research.

The study presented in this thesis is original since at present there are no detailed and accurate stress analysis models to describe effectively the mechanical response of overhead transmission line stranded conductors under both design and fretting fatigue conditions. It is anticipated that this research will fill the gap and lead to a better understanding of stranded cable mechanics, and be directly useful for the structural design of overhead line conductors and their suspension clamp systems.

1.2 Problem Description

As mentioned above, the complex mechanical behavior of stranded line conductors under both design and fretting fatigue conditions is difficult to describe and understand with experimental testing or simplified theoretical models. Therefore, reliable computational stress analysis models have been long expected. However, complex cable strand geometries, nonlinear material properties, substantial friction effects, and comprehensive contact interactions make the numerical work very challenging. The problem studied in this thesis is how to overcome the difficulties encountered during the modeling process to develop a rational and high fidelity modeling methodology to describe effectively the detailed mechanical response of each cable component. Based on the accurate stress analysis models, fretting fatigue of transmission line conductors is then studied from a structural mechanics perspective.

1.3 Research Scope and Objectives

The scope of the work presented in this thesis is on the computational prediction of the contact stress states and the study of their relevant influencing factors (such as frictional coefficient, fretting amplitude) in stranded electrical conductors under design and fretting fatigue conditions. The specific objectives are:

- To develop and validate a rational and high fidelity finite element modeling methodology for detailed stress analysis of overhead transmission line conductors.
- To examine the tensile strength and the nonlinear mechanical behavior of a stranded conductor under extreme design conditions.
- To explore the effects of variations in the frictional coefficients among conductor wires on the mechanical response of stranded conductors under axial loading.
- To develop a finite element model for accurate stress analysis of stranded conductors under fretting fatigue conditions, in order to investigate the fretting contact damage of stranded conductors, from an applied mechanics perspective.
- To develop a practical multi-axial fretting fatigue lifing scheme to estimate the fretting fatigue resistance of stranded conductors.
- To demonstrate the influence of fretting amplitude on fretting contact states and fretting fatigue strength in a conductor-clamp system.

The in-depth study of the initiation and propagation of fretting cracks is not included in this thesis, and will be carried out in future work. As for the related issues of fretting fatigue mechanisms, fretting wear process, as well as fretting corrosion, they are beyond the scope of this research. In addition, although experiments were not conducted during the project, the validation of the models and resulting numerical solutions is achieved by comparing them with experimental data provided by some cable manufacturers and in the open literature.

1.4 Thesis Organization

This thesis is organized as follows: Chapter 2 reviews the literature of the last few decades on the study of the mechanical behavior of stranded cables and electrical conductors, with emphasis on fretting damage related studies. In the subsequent three chapters, a logical sequence is followed in the development of the numerical models to achieve the above stated research objectives. In Chapter 3, a refined finite element model for detailed stress analysis of an optical ground wire (OPGW) strand is constructed with reference to a preliminary simplified coarse model prepared by Roshan Fekr (1999). Throughout this initial phase of work, essential analysis procedures and numerical solution techniques using finite element methods (FEM) are explored to overcome the many numerical challenges encountered during modeling such a highly nonlinear and large size problem. This is where the high fidelity modeling methodology is developed and validated. Thereafter, in Chapter 4, a numerical model for stress analysis of an ACSR conductor (Drake type (26/7)) under design conditions is studied using the approach developed in Chapter 3 and further validation is provided. Up to this stage, the modeling approach is proven and the next stage in Chapter 5 is to build a conductor/clamp system stress analysis model that can be used to study the contact damage of a stranded electrical conductor under fretting fatigue conditions. A practical fretting fatigue lifing methodology is also proposed to predict the local contact fatigue resistance of the conductor in critical suspension clamp regions. Chapter 6 summarizes the research and makes some suggestions for future work with great significance from both behavioral and design perspectives.

Chapter 2

Literature Review

This thesis relates to computational solid mechanics applied to stranded cables, and it encompasses several different subjects that have been studied throughout the entire project: finite element modeling procedures, numerical solution technologies for nonlinear problems, contact analysis, cable mechanics, and fretting fatigue. Hence, presenting an extensive literature review of all these areas related to this work in one chapter would be too lengthy. Rather, this chapter includes only a selective overview of the main subjects regarding the research purposes, namely the essential features of the mechanical behavior of electrical conductors, and especially the advances of fretting fatigue studies. The other aspects mentioned above are presented in the relevant numerical modeling chapters.

2.1 Introduction to Fretting Damage

2.1.1 What is Fretting ?

As a matter of fact, the terminology of fretting has not been completely standardized yet, i.e., there is no unified definition of fretting. A number of different terminologies have been used widely in the literature, including fretting, fretting wear, fretting fatigue, fretting corrosion, rubbing fretting, impact fretting, impact-slide fretting, to name the most common. In view of this situation, it has been suggested to use the term "*fretting*" only as a general term to cover all aspects of the related phenomena (Smith, 1998). Despite the multiformity of the definition, the fundamental characteristics of fretting are consistent: Fretting phenomena are induced by the minute relative movement between two contacting interfaces. They occur most frequently among tightly fitting contact surfaces that undergo minute relative movement produced by oscillating forces. The amplitudes of fretting slip are usually as small as the order of μm (even with sliding amplitudes of less than 1 μm). In some cases, fretting could also be the consequence of the contacted members subjected to an external cyclic force or a static tensile stress while being under heavy transverse loads (pressure). As it will be addressed later, fretting phenomena in real situations are very complicated and difficult to analyse. However, according to the types of relative movements, there are four types of fundamental fretting movement modes (Zhou, 2002), as shown schematically in Figure 2.1: **(a)** tangential, **(b)** radial, **(c)** rotational, and **(d)** torsional fretting. It should be noted that, although the last three modes also often occur in reality, most of the studies have been focused on the first mode so that the term "fretting" usually just refers to tangential fretting in the literature. In addition, little attention has been paid to more complex situations, such as two or more fretting movement modes mixed together, or fretting movement combined with other movements (e.g. impact).

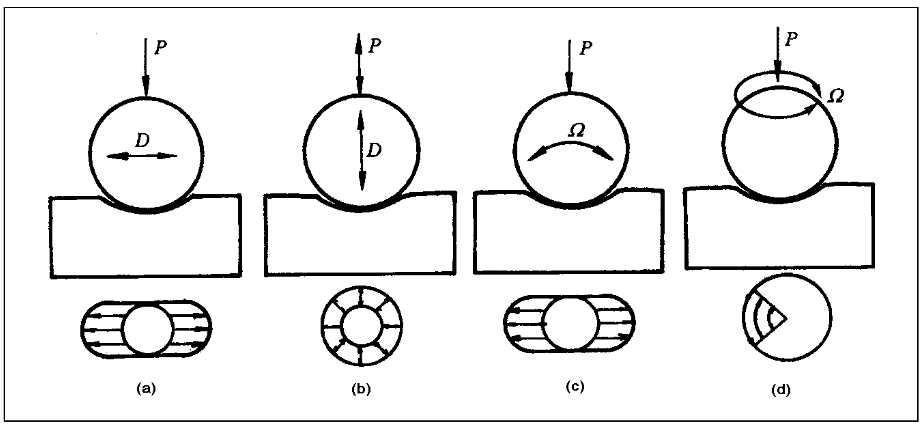

Figure 2.1 Four types of fundamental fretting movement modes (Zhou, 2002)

All failures induced by fretting can be generally called *fretting damage*. As one type of important in-service generated structure failure, fretting damage has been discovered and disclosed in many industries since the beginning of the 20th century. Today, it is well known that fretting can lead to severe material surface wear, which is frequently accompanied by corrosion, thus further speeding up the wear process. On the other hand, it is also widely accepted that fretting can significantly degrade local fatigue strength, resulting in an important reduction in high-cycle fatigue (HCF) life. As a matter of fact, the extensive presence of fretting damage in a variety of mechanical and structural components has become one of the major root causes of these structural failures, especially to those critical components in high-tech applications, such as aerospace, energy, and bio-medical engineering, and thus fretting damage is regarded as a “plague” in these industries (Zhou, 2002). Due to the growing concern about such problems, investigations on fretting damage have been carried out widely in industry and there has been a large amount of research into related areas over the past decades.

The early history of fretting studies can be traced back to 1911 (Eden et al., 1911), followed by the first systematic experimental investigation of the fretting wear process conducted by Tomlinson (1927). However, it was not until 1969[1] that the first review appeared (Campbell, 1969). Thereafter, several review papers (Hurricks, 1970; Waterhouse et al., 1969, 1984, 1992) were published in the open literature, which provide summaries of the state of knowledge at various periods. Up to now, there are mainly two monographs in the English literature, exclusively addressing the fretting subject (Waterhouse, 1972; Hills and Nowell, 1994). In addition, several international symposia were organized over the past 30 years by ESIS (European Structural Integrity Society) and ASTM (American Society for Testing and Materials) to summarize the advances in fretting research (Waterhouse et al., 1981, 1992, 1994; Hoeppner et al., 2000, 2003). Overall, the substantial progress of fretting studies was quite slow before the 1980s, mainly due to the limitations of experimental facilities and computational methods. Indeed, the majority of the research papers on fretting was published in the last 20 years, and fretting has become a very active research area in recent years. In the next section, an overview of the current state of fretting studies will be presented in an attempt to show the “big picture” of this very broad area.

[1] Comyn, R. H. and Furlani, C. W. 1963. Fretting corrosion: A literature Survey. U.S. Army Material Command, Harry Diamond Laboratories, 100 p., a technical report (No. TR-1169), which was initially distributed only in U.S. defense research community and was not available in the open literature at the time.

2.1.2 Categories of Fretting Damage

Although there are many nuances in the definitions of fretting phenomena, and no matter how they are labeled and whatever specific investigations were conducted, most fretting damage studies fall into three categories: *fretting corrosion*, *fretting wear*, and *fretting fatigue*. In addition, it should be mentioned that, due to the close association between fretting wear and fretting corrosion, studies of fretting wear have traditionally been called "fretting corrosion", especially in the early days of fretting studies. Many fretting fatigue studies have also been frequently addressed using this terminology.

(a) Fretting corrosion

The concept of fretting corrosion herein has some different connotation from the conventional one in that a more rigorous explanation is endued. Fretting corrosion is frequently associated with fretting wear. However, among the three major categories of fretting damage studies, there are relatively fewer publications about "genuine" fretting corrosion because most investigations and reported case studies of fretting wear occur under strictly "clean" conditions while fretting corrosion must involve some corrosive agents, such as sea water, acid rain, corrosive gas, and so on. The environmental effects on fretting are the most significant features of fretting corrosion research, with the objectives to reduce the action of corrosive media on the surface of fretting components and to develop corrosion-resistant materials. Therefore, environmental, chemical, and electrochemical knowledge and approaches become crucial to study fretting corrosion; this is obviously beyond the scope of this thesis.

Like other tribology phenomena, the mainstream of fretting research is from either a material or a structural perspective, focusing on the wear mechanisms and mechanics of fretting damage. Different theories and methodologies are thereby employed. Some significant advances in these two aspects are reviewed as below.

(b) Fretting wear

The most significant difference between fretting wear and other types of wear is that fretting wear always occurs on contacting (mating) surfaces that are intended to be fixed in relation to one another but actually undergo minute relative movement. Historically, the largest body of fretting related research was focused on fretting wear. The main objective of this line of fretting study is to explore the mechanisms of fretting wear process by examining the variations of material micro-structures occurring on fretting contact surfaces. Almost all fretting wear investigations were conducted from the material and metallurgy science perspectives, mainly using experimental approaches.

Hurricks (1970) summarized the early studies on this topic, and proposed a theory that explains a fretting wear process in three stages: the adhesion and transfer of contact surfaces in the early stage of fretting; the formation of debris and its oxidation; and the steady state of fretting wear. Waterhouse (1977), the leading investigator on fretting wear (known as "the father of fretting research"), further extended Hurricks' findings, and demonstrated that the delamination theory of wear is also applicable to fretting. This classical "three-stage theory" has had a far-reaching influence on the subsequent studies. Hoeppner (2002) considered metal fretting wear mechanisms from five aspects: influence of surface films; adhesion of contacting surfaces; plastic deformation and smearing; material transfer from one surface to another; and oxide buildup. It is noted that, although there were many other different explanations on the mechanisms of fretting wear process (besides the above mentioned), the role of material oxidation was long regarded as essential during the early development of fretting wear theories. However, this opinion has been gradually discarded due to the fact that fretting wear could also occur in some materials (e.g. diamond) without oxidizing environments. Waterhouse (1955) conducted some fretting experiments under no-oxygen conditions, showing that fretting wear could be induced by strictly mechanical actions. In addition, many early theories exhibited some evident weakness: they were not persuasive and satisfactory in explaining the relations between fretting wear and fretting-induced fatigue cracks. In the past 30 years, some novel fretting wear theories have been developed. An important contribution by Berthier, Vincent and Godet (1988) is a velocity accommodation mechanism of fretting contact interfaces is proposed to address the friction properties and relative movement process. Furthermore, by examining the formation and evolution of wear debris, they proposed the notable "third-body" theory of fretting, with a focus on the load-carrying capacity of wear debris (the so-called "*third-body*") and its positive effects on reducing fretting wear and fretting fatigue (Berthier et al., 1984, 1989, 1990). According to this theory, the formation and escape (removal) of wear debris is a dynamic process, during which both occur continuously and simultaneously. This theory also explains the fretting wear process in three stages: **(a)** Two-body contact stage; **(b)** Transition stage (transition from two-body contact to three-body contact); and **(c)** Three-body contact stage. By this theory, the variation of the frictional coefficient with fretting cycles during fretting wear of metallic materials can be explained (Figure 2.2)**:** At the beginning of fretting wear, the frictional coefficient remains low due to the influence (protection and removal) of contacting surface films; thereafter, it starts to increase rapidly with fretting cycles due to the increase of contact interaction, adhesion, local plastic deformation, as well as smearing. Gradually, wear debris is generated between the two contact surfaces. Wear debris is regarded as the "third-body". Hence, the two-body contact is gradually transformed into three-body contact. Like the effects of solid lubricant, wear debris protects contact surfaces and restrains the contact adhesion, leading to the decrease of the frictional coefficient and frictional force during this second stage. When the third stage begins, the "third-body layer" has been established, which means the continuous formation and escape of wear debris reach a dynamical balance. The friction coefficient and frictional force thus become stable (constant), indicating that fretting wear is reaching a steady state.

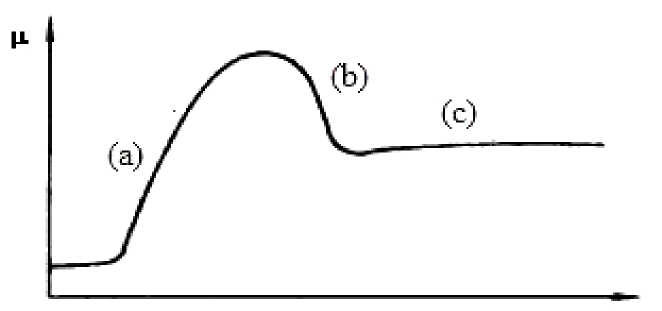

Figure 2.2 Variation of frictional coefficient with fretting cycles during fretting wear of metallic materials (Zhou et al., 2002)

Another very important aspect in fretting wear study is the examination of contact kinematics under fretting conditions, and it is in close association with fretting fatigue studies. A concept of "*fretting map*" was introduced by Vingbo et al. (1988, 1990, 1993). It is a two-dimensional representation of the normal force F_n vs. fretting displacement D, which are both highly significant parameters to identify fretting states. The "fretting map" theory was further extended to two sets of more accurate descriptions: "running condition fretting map" (RCFM) and "material response fretting map" (MRFM) (Zhou et al., 1992). Using fretting maps and the so-called "*friction log*" (a three-dimensional representation of frictional force F_t vs. fretting displacement D with fretting cycles N), three fretting states could be identified corresponding to different characteristics of fretting contact kinematics (contact states), fretting wear, and fretting fatigue. (As seen below, these three aspects are actually related to each other). This methodology has been applied to experimental studies on some metallic materials to demonstrate their fretting wear and fatigue behavior (Zhou et al., 1992, 1993, 1995, 1997). The most important findings using the fretting map theory with the applications in aluminum alloys are reviewed below to illustrate certain points that are related to the work in this thesis.

A complete fretting experiment can be characterized by a "friction log" composed of numerous F_t –D cycles (loops) that generally have different shapes. Also, the variations of frictional force (F_t) may fluctuate with the fretting cycles (N), as shown in Figure 2.3. Although the tribological characteristics of fretting are usually very complex, three main types of F_t –D cycles in a friction log may be identified: **(i)** *Closed cycle*, **(ii)** *Elliptic cycle*, and **(iii)** *Parallelepipedic cycle*. And the transitions among them could happen with the evolution of fretting conditions. These three types of F_t –D cycles expose different contact states in fretting: Closed cycles implicate that no sliding occurs at the interface, and the contact surfaces are mostly in the stick state (static contact). The nonlinear curves of elliptic cycles represent the decrease of the rigidity of the fretting system; in the meanwhile, they also indicate that some small sliding (partial slip contact) occurs at the edge-of-contact, and severe local plastic deformations are usually accompanied. Parallelepipedic cycles appear when complete sliding (gross slip contact) takes place on the contact interface.

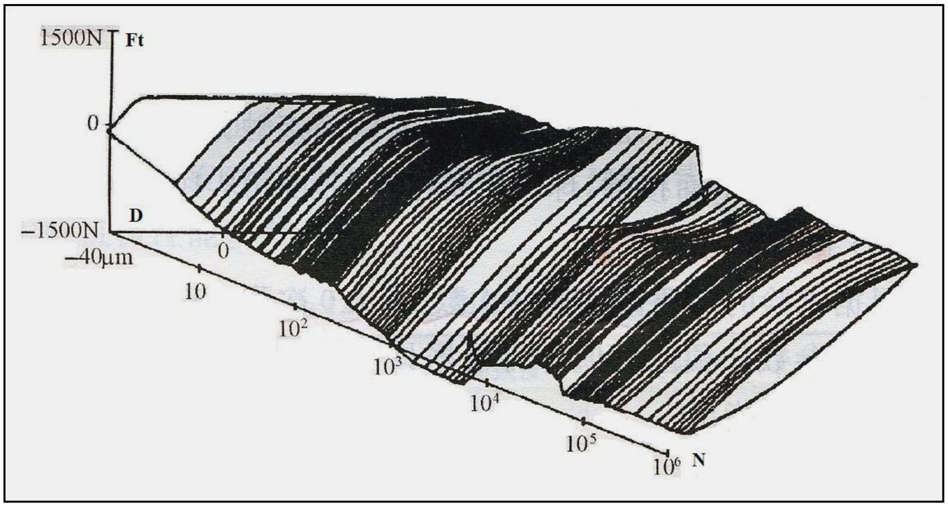

Figure 2.3 Friction log: F_t –*D*–*N* diagram in a fretting test (Zhou et al., 1992)

Different F_t –*D* cycles can remain stable for a certain time during a fretting process. Such a stable period (fretting state) is called a "regime". On a "running condition fretting map" (RCFM), three types of fretting regimes can be identified corresponding to the three types of F_t –*D* cycles: **(i)** *Stick regime* corresponds to the closed cycles. It was found that almost no damage (or just light damage) occurs for the stick regime; few wear debris is generated, and basically elastic deformations and two-body contact are present in the contact area; **(ii)** *Mixed regime* (also called intermediate regime) usually has elliptic cycles. It has been observed that the mixed regime is the most critical regime for fretting fatigue crack nucleation and propagation; **(iii)** *Slip regime* is associated with parallelepipedic cycles. Debris (the third-body) appears during the slip regime; particle detachment and three-body contact are the salient features. While the slip regime undergoes severe fretting wear, fretting fatigue cracks are shown not easy to initiate in this regime. Thus, corresponding to the fretting regimes in RCFM, three "fretting zones" could be identified in a "material response fretting map" (MRFM): **(i)** *No Degradation zone* (ND), **(ii)** *Fretting Cracking zone* (C), and **(iii)** *Particle Detachment zone* (PD). Figures 2.4 to 2.6 present the correspondences of fretting regimes and F_t–*D* cycles. The correspondences of fretting regimes and fretting zones in the two types of fretting maps are illustrated in Figure 2.7. In addition, a summary table (Table 2.1) is proposed by the author to clarify these important corresponding relations. It should be noted herein that, this table is proposed to be helpful to gain a better understanding of this subject, while it is not a rigorous presentation of the correspondences among fretting contact states, fretting wear and fretting fatigue: A real fretting phenomenon is usually very complex so that drawing clear divisions among these definitions is not always attainable. In conclusion, from the above discussions, one can see clearly that fretting wear and fretting fatigue are closely related to each other, constituting the very complex tribological and fatigue phenomenon. Fretting studies thus become very challenging and difficult tasks.

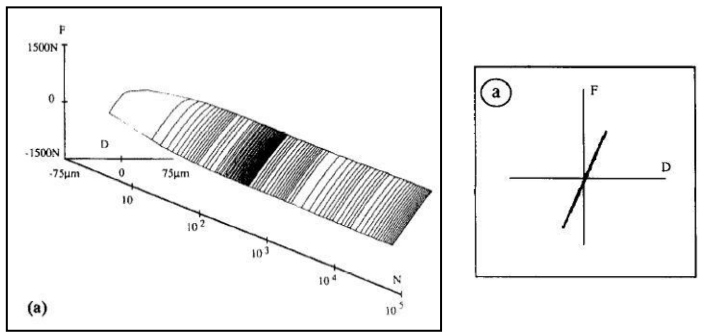

Figure 2.4 Stick regime and Closed cycle (Zhou and Vincent, 2002)

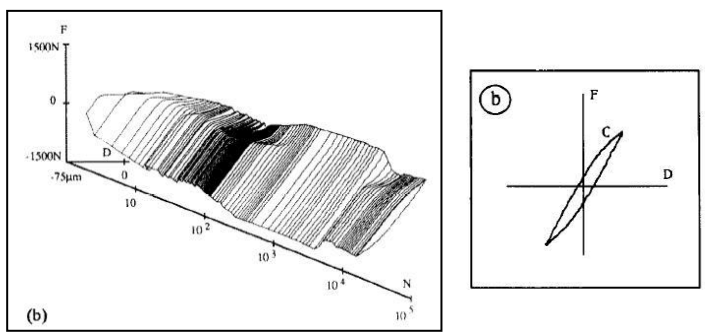

Figure 2.5 Mixed regime and Elliptical cycle (Zhou and Vincent, 2002)

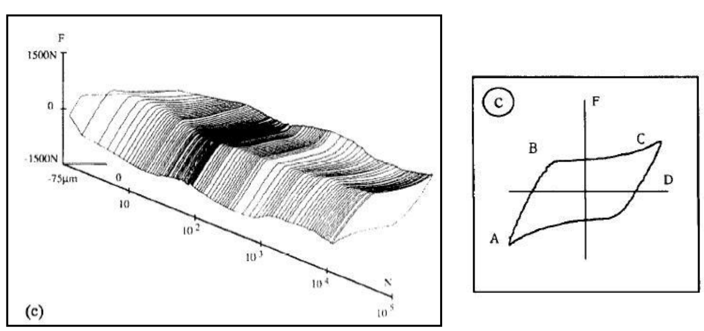

Figure 2.6 Slip regime and Parallelepipedic cycle (Zhou and Vincent, 2002)

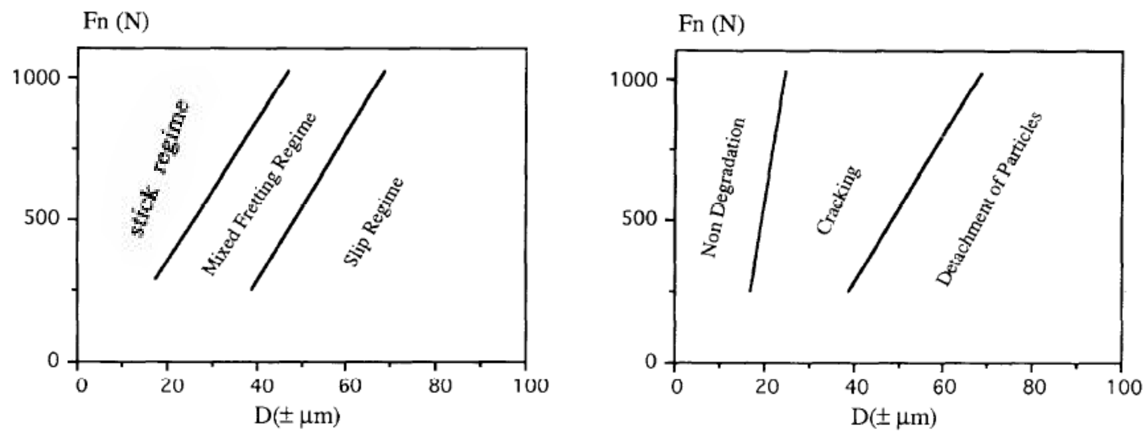

Figure 2.7 Fretting regimes (RCFM) and Fretting zones (MRFM) for aluminum alloy 2091 (Zhou et al., 1997)

Table 2.1 Correspondences among fretting wear, fretting contact and fretting fatigue

Fretting regime	***F_t –D* cycle**	**Contact status**	**Fretting characteristics (Fretting zone)**
Stick regime	Closed cycle	Static contact	No Degradation zone
Mixed regime	Elliptical cycle	Partial slip contact	Fretting Cracking zone
Slip regime	Parallelepipedic cycle	Gross slip contact	Particle Detachment zone

In addition to the investigations of wear mechanisms on fretting contact surfaces (as reviewed above), the effects of many influential parameters on fretting wear have been widely studied. The influential parameters mainly include fretting displacement amplitude, normal load (bearing force), pre-stress, frequency of external tangential force, local plastic deformation, tangential contact stiffness, contact mode, contact surface quality, contact temperature, geometry effects, material properties, to name the most important. Meanwhile, numerous studies investigated the formation of tribological white layer in fretting wear (see for example Griffiths, 1985; Xu, 1995), as well as nucleation related issues occurring in the early stage of fretting (Sauger et al., 1997, 2000a, 2000b).

In summary, fretting wear is a very sophisticated subject. So far, an ideal and widely accepted (generally applicable) fretting wear theory that could be used to satisfactorily demonstrate the mechanisms of fretting wear process has not yet been well established. Moreover, there are still considerable controversies about the effects of various environmental, material and structural factors on fretting wear behavior. Thus, many in-depth studies are to be carried out in this area. In addition, as stated before, fretting wear has been investigated primarily from the perspectives of material and metallurgy science, employing experimental approaches to examine the variations of micro-structures on fretting contact surfaces. Computational methods are not usually used in this research field.

(c) Fretting fatigue

Another and usually more damaging aspect of fretting is fretting fatigue. Numerous field experiences and experimental reports have disclosed that the initiation of fretting cracks and their rapid propagation could significantly degrade local fatigue strength, resulting in a severe reduction in high-cycle fatigue (HCF) life. Extensive fretting fatigue has led to poor performance and unreliable mechanical and structural systems in all engineering industries. For example, for aluminum alloy T7375, a reduction of more than 50% fatigue life due to fretting fatigue was reported (Foulquier, 1988), as shown in Figure 2.8. Therefore, from the perspective of structural durability, the danger and detrimental effects of fretting fatigue are much beyond the other two types of fretting damage.

Compared with other types of fatigue, the most distinctive feature of fretting fatigue is the involvement of complicated tribological phenomena so that fretting fatigue sometimes is also called *contact fatigue*. From the viewpoint of contact mechanics, fretting friction is much more complex than common sliding and rolling frictions due to the occurrences of “partial slip contact” status, accompanied by local plasticity at the edge-of-contact area, and the third-body layer (wear debris) between contacting surfaces. From the viewpoint of fatigue, as opposed to conventional low-cycle fatigue (LCF) failures (less than 10^5 cycles), fretting fatigue is generally associated with high-cycle fatigue (HCF) failure (greater than 10^6 cycles), as well as LCF-HCF interactions (Gallagher et al., 2001). In addition, different from fretting wear investigations, fretting fatigue research typically uses the approaches of applied mechanics to study the initiation and propagation of fretting cracks, estimate fretting fatigue life reduction, and develop means to mitigate fretting fatigue. In the literature in this field, there are more "parametric studies" than "modeling studies". That is to say, the majority of the literature addresses the effects of various factors on fretting fatigue, such as fretting slip amplitude, normal load, shear load, plasticity, pre-stress, external tangential force frequency, tangential contact stiffness, contact mode, contact surface quality, material properties, coefficient of friction, elevated temperature, oxidation, wear debris, stress field effects, geometry effects, and so on[2]. Relatively much less research has focused on the development of methodologies to model fretting fatigue damage.

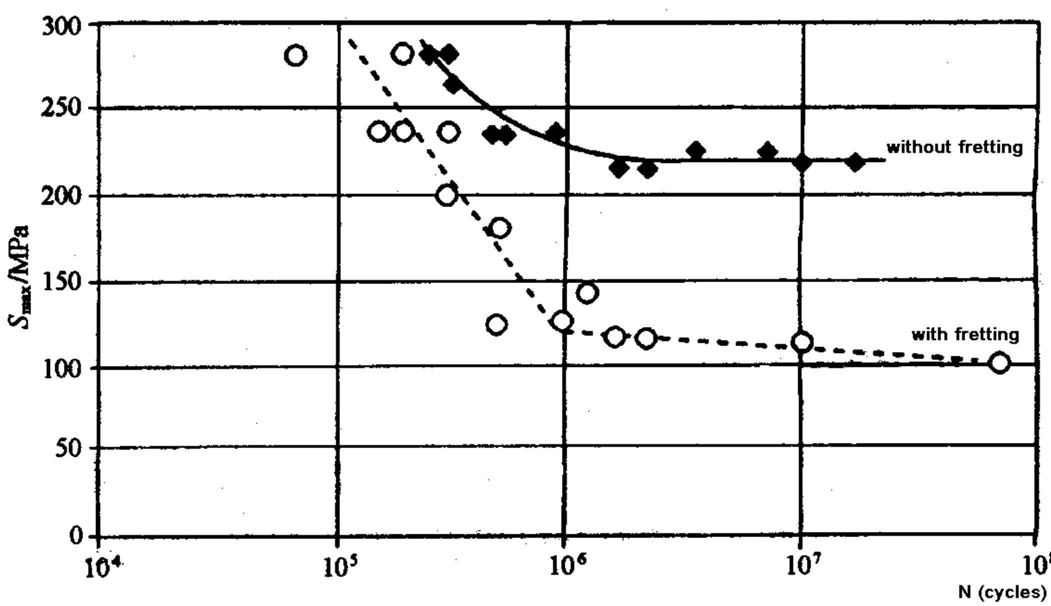

Figure 2.8 HCF life deduction of aluminum alloy T7375 due to fretting (Foulquier, 1988)

While a survey of fretting fatigue studies will be presented in the next section, some general conclusions summarized from the literature review are listed below to outline the most significant and distinctive features of fretting fatigue, which also expose the great challenges in this area of research**:**

[2] Obviously, they are also the influential factors of fretting wear.

(1) The initiation (nucleation) of fretting cracks and their rapid early propagation can significantly reduce local fatigue life of components, and is generally associated with high-cycle fatigue (HCF) life.

(2) Even without external cyclic loading, fretting cracks can also be initiated and propagated by local contact loading in quasi-static loaded assemblies. Furthermore, fretting fatigue may cause failure at surprisingly low stress levels.

(3) Fretting cracks usually occur at the edge-of-contact regions, and mostly initiate from contacting surfaces. This also verifies that tensile stresses on contact surfaces (surface tractions) play a crucial role in fretting fatigue.

(4) Multiple different (not only one) fretting cracks may occur in fretting contact regions. The crack lengths may vary from the order of μm ("microstructurally small" cracks) to the order of mm ("mechanically small" or "microstructurally large" cracks). The longest crack is usually called "dominant crack".

(5) Fretting crack behavior depends on fretting regimes (stick regime, mixed regime, slip regime). In effect, cracks may exhibit different patterns in different fretting regimes, and crack paths may be not consistent even in the same regime. Laboratory observations also revealed that the most severe local contact fatigue usually occurs in mixed regime. In addition, fretting cracks propagate three-dimensionally, and bifurcations might happen during their propagation.

(6) Especially for ductile materials (e.g. aluminum alloy), material slip bands can be observed around fretting cracks, showing the occurrence of severe plastic deformation.

(7) Similar to other types of fatigue, fretting fatigue can also be separated into two evolutionary stages: crack initiation and crack propagation. However, it has distinctive features from other fatigue phenomena**:** In the first stage, fretting fatigue cracks initiate not from free surfaces, but from clamped, bolted or other tightly-fitted mating surfaces suffering vibration or other forms of minor oscillatory loadings. Such a situation may produce significant surface degradation due to

fretting wear so that the small crack initiation is essentially caused by adhesive contact as well as plastic deformation during fretting. At the beginning of the second stage, the propagation of nucleated cracks is still driven by contact stresses imposed by fretting, such as normal contact stress (bearing stress), tangential contact stress, and tensile stress on contact surfaces. The complex multi-axial stress states have been shown to favor or prevent the early cracking, depending on the contact characteristics under study. At the late second stage, cracks may continue to propagate until rupture happens, while contact stresses have no longer a significant contribution.

(8) The nucleation and early propagation of fretting cracks are both strongly affected by many mechanical and material parameters and their synergistic interactions, among which relative slip amplitude and normal load (bearing force) have shown significant effects on fretting crack behaviors.

(9) Careful design can only reduce fretting fatigue, but cannot eliminate it completely in that (minute) vibration is inevitable in reality. The methods that are employed to mitigate fretting fatigue are highly dependent on the specific applications. Some methods that drastically extend fretting fatigue life in one situation could even be detrimental in another application. Only those methods that could increase “baseline” (unfretted) fatigue strength of materials, such as shot peening, are proven to consistently increase fretting fatigue life.

Fretting studies have been outlined in this section according to three failure modes of fretting damage. If categorized by research methodologies applied to this subject, experimental methods are dominant. Theoretical studies are still far from mature. For example, there is clear evidence that the mechanisms of fretting wear and fretting fatigue have not yet been completely understood. Thus new theories and insights are proposed from time to time, with some conclusions proved inconsistent and even controversial. As seen from the above summary of fretting fatigue features, modeling of mechanical behavior induced by fretting has proved extremely difficult (Nicholas, 2006) and thus little research has been done in this area. However, with the increasing power of computing hardware and numerical solution techniques, computational modeling (mainly by the finite element method) is becoming one of the dominant research approaches on this subject, especially for fretting fatigue.

2.2 Overview of Previous Studies on Fretting Fatigue

As one of the main objectives of this thesis is to model the detailed mechanical behavior of stranded transmission line conductors under fretting fatigue conditions, a separate review of the advances of fretting fatigue studies is presented in this section. While there is no attempt herein to provide a complete survey of all aspects of fretting fatigue[3], selected references are chosen with a structural mechanics perspective. It should also be pointed out that the study of fretting fatigue mechanisms is beyond the scope of this thesis since it is usually addressed from a material science perspective due to its intrinsic association with fretting wear. General explanations on mechanisms of fretting fatigue can be referred, for example, to Waterhouse (1972), Hertzberg (1996) and Suresh (1998).

Although fretting fatigue occurs widely at various matting surfaces of mechanical components and structural members, such as in bolted and riveted joints, bearing connections, cable strands, orthopedic implants, to name a few examples, it has long been studied mainly for aerospace applications due to their historical importance. For example, from the overview of typical failure modes of jet engine components, as shown in Table 2.2 (Mattingly et al., 2002), it can be seen that fretting fatigue is a pervasive problem for aerospace and defense industries. Indeed, it has brought about serious concern about mating surfaces of all critical aero-engine components and aircraft joints that are subjected to normal pressure and tangential oscillatory motions. Hence, all major airframe and aero-engine manufacturers, as well as some government organizations have been heavily involved in extensive fretting fatigue investigations since the 1960s: see Harris (1967, 1972); Alic and Kantimathi (1979); Smailys et al. (1987); and also

---

[3] A recent extensive review of fretting fatigue studies can be seen in Section 4.11 in "Comprehensive Structural Integrity", Vol. 4, by Farris et al. (2003).

"Specialists meeting on fretting in aircraft system" (1974). Over the years, the U.S. Air Force and NASA have played key roles to advance the state of the art in fretting fatigue research by launching important programs, such as "ENSIP" (1984, 2002) that have lasted more than 25 years and are still ongoing, as well as by persistently funding relevant scientific projects, for example, those conducted by Heoppner et al. (1994, 1996). Consequently, numerous approaches have been proposed, specific to different components and their operating conditions, to solve fretting and related HCF problems, and a large body of research papers has been published. Today, although fretting fatigue investigations are being largely expanded to many other industries, the majority of literature in this field is still overwhelmingly for aerospace applications. Thus, it is inevitable to refer to those findings when studying on this subject. Moreover, those approaches employed in aerospace actually have brought considerable merit for conducting fretting fatigue research for other applications.

Table 2.2 Typical failure modes of aero-engine components (Mattingly et al., 2002)

Engine section	Component	HCF	LCF	Creep	Erosion	Fretting	TMF	Oxidation	Overload	Buckling	Over temp	Wear	Corrosion
Fan and compressor													
	Blades	X	X	X	X	X	—	—	—	—	—	—	—
	Vanes	X	—	—	X	X	—	—	—	—	—	—	X
	Disks	X	X	X	X	X	X	—	X	—	X	—	—
	Spacers	X	X	X	X	X	X	—	X	—	X	X	—
	Seal teeth	—	X	X	X	X	—	—	—	—	X	X	—
	Shafts	—	X	X	—	X	X	—	X	—	X	X	X
High and low turbine	—	—	—	—	—	—	—	—	—	—	—	—	—
	Blades	—	X	X	X	X	X	X	X	—	X	X	—
	Nozzles	X	—	X	X	—	X	X	—	X	X	X	—
	Disks	X	X	X	—	X	X	—	X	—	X	X	—
	Spacers	X	X	X	X	X	X	X	X	—	X	X	—
	Seal teeth	X	X	—	X	X	X	X	X	—	X	X	—
Cases	—	X	—	—	—	X	X	—	X	X	X	X	—
Mounts	—	X	—	—	—	X	—	—	X	—	—	X	X
Nozzles	—	X	—	X	X	X	X	X	X	X	X	X	—
Combustors	Liners	X	—	X	X	X	X	X	—	X	X	X	—
Frames	—	X	X	X	X	X	X	—	X	X	X	X	X

As stated before, fretting fatigue is usually studied from the applied mechanics perspective, to investigate fretting crack behavior, and to estimate fatigue life under fretting conditions. From the literature, relevant investigations are mainly carried out from one of the following three correlated aspects, with different emphases and approaches:

(a) Estimation of fretting fatigue life;

(b) Prediction of fretting crack initiation;

(c) Examination of fretting crack growth.

As for (a), methodologies conventionally used are mostly empirical (see for example, Nishioka and Hirakawa, 1969; Sato et al., 1986)**:** Experiments are conducted firstly; After acquiring large amounts of data from experiments or directly from field experiences and referring to the values from non-fretting conditions, modified fatigue life calculations (formulas) for fretting can be proposed; afterwards, these formulas are validated by applying them to some other similar situations. The advantage of such empirical approaches is that the resulting calculation methods could be convenient for design (they actually become design tools), while the shortcoming is that they usually lack scientific rigor and generality as they cannot explain the essential physical fretting behavior. That is, these formulas might not be applicable to different situations, and even sometimes they may be misleading when applied outside their range of calibration. Overall, the studies conducted in this line mainly fall into the domain of experimental mechanics. In recent years, some high-cycle fatigue lifing methods (Gallagher et al., 2001) based on numerical stress analyses have been proposed and applied to fretting settings to integrate into experimental work to address this issue.

Regarding (b) and (c), in parallel with experimental work, computational mechanics is playing an increasingly important role, especially for real industrial applications. As in other fields in structural and solid mechanics, it is impossible to consider modeling real fretting fatigue problems by anything other than numerical methods since computational modeling is normally the only practicable and economical way to acquire accurate and detailed stress and strain fields for real engineering structures. With respect to the numerical solution techniques for fretting contact analysis and fatigue lifing, although some methods such as the boundary element methods (Takahashi, 1991), the distributed dislocation technique (Hills et al., 1996), and the emerging meshless methods (Atluri, 2004; Chen and Eskandarian, 2006) have received considerable attention in academia, the most practicable choice usually remains the finite element method (FEM), which is the dominant analysis tool in continuum mechanics applications. However, as stated above, fretting related computational modeling is very challenging. Hence, solving such a problem using FEM requires advanced modeling strategies and robust numerical solution schemes to achieve convergent and reliable solutions. Over the years, some analytical work (theoretical and computational) has been conducted in each of fretting fatigue stages to study different topics.

Obtaining accurate contact stress fields is the first and foremost step to carry out successful fretting fatigue studies. As stated in Section 2.1.2 (b), partial slip appears to be the most critical contact mode for crack initiation. Historically, contact stress fields under the "stick-slip" elastic contact condition were first explored by Mindlin (1949). This pioneering work is now called the classical "Mindlin's elastic contact theory". Mindlin studied the case of a rounded punch on an infinite body with flat surface and identical elastic materials, and considered that the elastic contact region with tangential force can be separated into a stick region and a slip region at the edge-of-contact, the so-called "Partial Slip Contact State" (Figure 2.9-a). The closed-form analytical solutions were derived, which exhibit smoothly distributed normal contact stress but singular tangential contact shear stress at the boundary of stick regions (Figure 2.9-b). The tensile stress on the contact surface is generated due to friction, and it significantly increases with the increase of frictional coefficient, and reaches maximum at the edge-of-contact regions (Figure 2.9-c). Surface traction is currently recognized to play a very important role in fretting fatigue crack initiation.

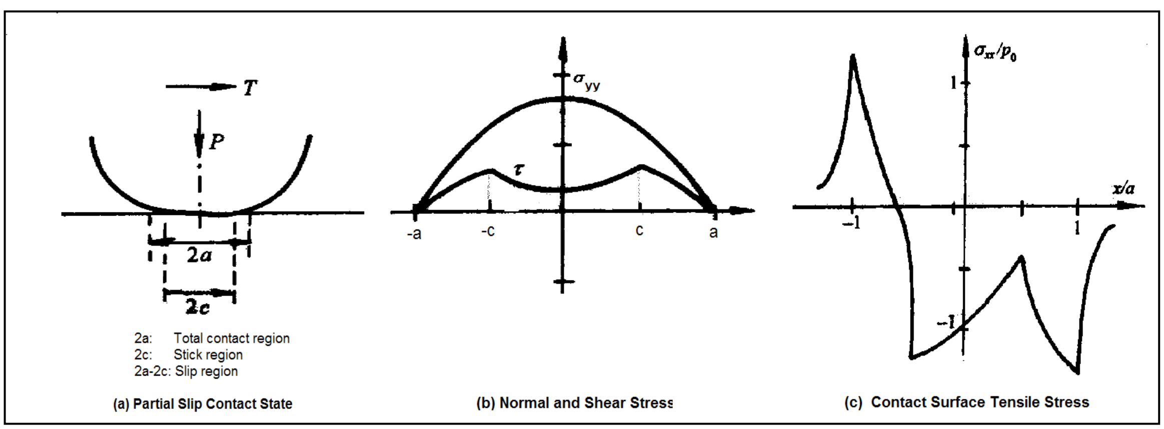

Figure 2.9 Stress fields of partial slip elastic contact in Mindlin's theory (Zhou and Vincent, 2002)

Indeed, high contact adhesion occurs at the fretting interface of ductile materials, such as aluminum alloys, so that frictional coefficients even approaching unity (1.0) are not uncommon (Smith, 1998). An elastic-plastic fretting contact model for a cylinder on flat infinite body contact was studied by Odfalk and Vingsbo (1992) to demonstrate that the singularity of the tangential shear stress disappears owing to ductility, thus the transition of the surface stresses between stick and slip regions is rounded (Figure 2.10). In addition, it was shown that plastic deformation could occur during fretting contact even under rather modest normal loads for most ductile metals (Vingsbo and Odfalk, 1990).

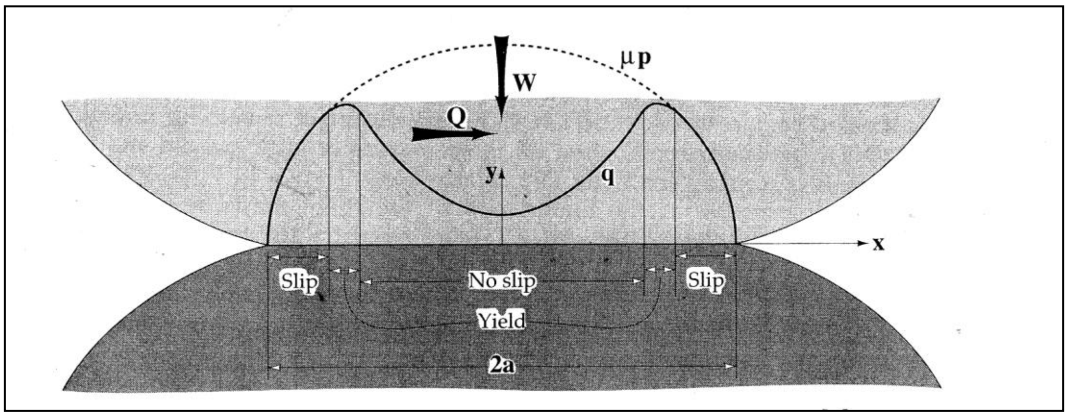

Figure 2.10 Tangential shear stress of partial slip elastic-plastic contact (Odfalk and Vingsbo, 1992)

In effect, Figures 2.9 and 2.10 exhibit important features of stress fields that are also characteristics of fretting contact problems, thus the "cylindrical contact pad" is still widely used in fretting fatigue specimen tests. Certainly, other contact geometries (configurations), especially those in real applications, produce much more complex stress fields in contact regions, which can only be analysed with detailed computational models.

To create proper criteria to predict the initiation of fretting cracks, Hamilton and Goodman (1966) studied this topic by considering the subsurface tensile stress field. The "Fretting Fatigue Damage Parameter" (FFDP) developed by Ruiz et al. (1984) was a widely used model to predict fretting crack initiation, but it is an empirical model, which has the drawback to account for the differences induced by different materials. Nowell and Hills (1990) included more control parameters to predict the initiation of cracks, such as maximum tensile stress on contact surface, tangential contact shear stress, and tangential relative slip amplitude. Maouche et al. (1997) proposed a method from a multi-axial fatigue viewpoint to determine the critical conditions of crack initiation. In addition, experimental investigations (Zhou and Vincent, 1995) have indicated that the mixed regime is generally avoided for brittle materials due to the rapid formation of wear debris and the establishment of the third body layer, thus producing mainly gross slip contact conditions; for ductile materials, however, there are usually longer mixed regimes, so the nucleation of fatigue cracks is facilitated. Furthermore, in mixed regimes of ductile materials, crack nucleation can quickly occur without even any additional external loading and thus cancel the crack initiation period, while small differences in some parameters have been shown to favor or prevent the early cracking. The effects of various mechanical factors on fretting crack initiation, such as the applied normal and tangential forces, coefficient of friction, surface finish, surface plasticity, etc, are being investigated extensively. In summary, so far, many criteria have been proposed to predict the initiation of fretting cracks, which are strongly dependent on contact configurations and their operating conditions. But, a unified criterion has not yet been established, and the investigation of the relationship between fretting crack initiation and various contact interface conditions remains a very active field of research.

The propagation of fretting cracks is another very open research area. Fracture mechanics is still the most popular method for studying this topic (Chan et al., 2001; Nicholas, 2003, 2006). Historically, fracture mechanics was first introduced to fretting by Endo and Goto (1976). Nix and Lindley (1988) demonstrated that the stress intensity factor (Opening mode/Mode I) of fretting cracks is different from that in the conventional crack situations. Later, Nowell and Hills (1990) calculated stress intensity factors of fretting cracks with different lengths and angles, and summarized their study on fretting cracks in their 1994 monograph (Hills and Nowell, 1994). In more recent years, some experimental work was carried out to investigate the crack propagations in aluminum alloy, and demonstrated that the process of crack growth in the plastic domain is fundamentally different from that in the elastic domain. Conventional linear elastic fracture mechanics criteria such as the stress intensity factor are not applicable to the ductile failure observed in the tested aluminum specimens. In addition, it has been shown that the early fretting crack growth (crack path and propagation rate) and the small crack region behavior both have their own features, and are very difficult to analyze. Hence, to gain more insight, fretting crack studies have also been carried out based on fracture mechanics approaches in combination with finite element analysis (McVeigh and Farris, 1999a, 1999b). While some success has been achieved in applying these approaches to simple specimens, practical difficulties are encountered for general applications.

It is also noteworthy that there is much controversy in the literature about the effects of fretting crack behavior on resulting fatigue life, i.e., which stage of cracking is dominant in fretting fatigue, crack initiation or crack propagation? For example, Faanes and Fernando (1994) concluded that the fretting fracture process is dominated by crack growth, and this conclusion was supported by Waterhouse (1992). They observed that fretting crack initiation could contribute only 5% or less of the total fatigue life, while in ordinary metal fatigue, crack initiation may even account for 90% of fatigue life. On the contrary, Hills et al. (1994, 1998) and Szolwinski and Farris (1996) concluded that fretting fatigue is a crack initiation-controlled process, implying that crack initiation is the dominant part of the fatigue life. While no definitive conclusions have been made up to now, it is necessary to indicate that different materials, surface qualities, and loading conditions may perform differently during fretting fatigue, which might lead to completely opposite conclusions.

From the above overview of the current state of fretting fatigue studies, it is seen that: (1) Even for aerospace applications, where fretting fatigue has been investigated and studied extensively, computational modeling approaches are far from successful to be integrated into fretting fatigue failure and lifing analysis; (2) Even if only from an applied mechanics perspective, fretting fatigue is still a multi-disciplinary subject. Contact mechanics and fatigue mechanics are two major theoretical underpinnings for investigating and modeling fretting fatigue failures. While FEA is becoming the dominant analytical tool to conduct fretting fatigue research for real-world applications, modeling and numerical methodologies applied to complex systems are far from mature.

2.3 Advances in Contact Damage of Electrical Stranded Conductors

Structural reliability of overhead transmission line systems has long been emphasized due to its significant economical impacts (El-Fashny et al., 1999; Wong and Miller, 2009), and is regarded as a "key criterion" to design transmission line structural systems (Nickerson, 2006). Because it is well known that the major causes of structural failure of transmission line systems are associated with natural hazard events, such as ice storms, hurricanes, tornadoes, earthquakes, etc., hence, a large amount of studies have been conducted from a structural dynamic perspective, to explain the transient response of transmission lines and towers to shock loads, such as gusty wind loads (Shehata and El-Damatty, 2005; Keyhan et al., 2013), ice-shedding effects (Jamaleddine et al., 1993; Roshan Fekr and McClure, 1998; Anderson and Li, 2006; Kálmán et al., 2007; Keyhan et al., 2011), seismic loads (McClure et al., 1994, 1999, 2000), conductor breakages (McClure et al., 1987, 2003, 2010, 2013), and so on. While concern about various "global" structural failures of transmission line systems remains, "local" failures of line components that may trigger sudden conductor ruptures are preoccupying, especially with the emergence of increasingly severe aging problems of power transmission line systems around the world (Aggarwal et al., 2000; Azevedo et al., 2009). In this regard, fatigue is an important topic since it is the dominant structural failure mode under normal service conditions, and it plays a role as fatigure-weakened components may trigger failures at higher load levels. As stated in Section 1.1, the main cause of conductor ruptures under normal operating conditions is induced by fretting fatigue, which usually occurs in suspension clamp regions. In the past decades, static strength and contact fatigue of electrical conductors have been studied under the framework of general wire ropes and stranded cable structures. The advances of the studies in this field are outlined below.

2.3.1 Theoretical Studies

From a structural point of view, an overhead conductor is essentially the application of a stranded wire rope to the transmission line industry. For example, a typical ACSR conductor can be regarded as a composite stranded cable comprised of multi-layer aluminum wires that are helically wrapped around a central steel core, while the steel core itself is also a twisted cable strand. Therefore, the general classical theories of wire ropes and stranded cable structures are of relevance to gain understanding of the mechanical behavior of overhead electrical conductors.

Accurate stress analysis is fundamental to further assess structural strength and predict fatigue life. Indeed, the majority of related theoretical studies are focused on the static strength of wire ropes under various loadings.

One of the earliest investigations on the mechanical behavior of wire ropes was conducted by Hall (1951). Stress analysis of a wire subjected to axial load was performed based on three assumptions: (i) The axial load was equally distributed amongst all the wires of the strand; (ii) Neither friction nor bending in the wires was considered; (iii) No sliding among the wires was allowed, i.e., “bonded contact” was assumed. Obviously, considering the wire rope as a fully coupled cross section and distributing the load equally amongst its components cannot be realistic and subsequent studies soon revealed that these assumptions were not appropriate. Hruska (1951, 1952, and 1953) claimed that three components of forces (axial tension force, radial force and tangential force) could be produced in a single wire subjected to a pure axial load. He also concluded that the tangential forces and the resulting moments would either cause rotation of the wires in free-ends boundary conditions or would be the moment reactions at fixed supports. Leissa (1959) expended Hruska’s work to a complete wire rope and considered the effects of contact between the single wires. In the same year, Starkey and Cress (1959) proposed a simplified theoretical model to calculate the contact stresses in a wire rope, and the importance of this work is the introduction of fretting in the stress analysis of wire ropes for the first time. Machida and Durelli (1973) used linear expressions to determine the external axial force, bending, torque and corresponding stresses of a strand made of helical wires with a central core and subjected to axial and torsional displacements. However, the effects of friction amongst the wires, Poisson's effect, and the contact pressure between the core and the wires were all neglected. Phillips and Costello (1973) also calculated stresses in twisted wire cables, with fewer assumptions than made in previous studies. They obtained exact solutions from six non-linear equations of equilibrium for each wire to evaluate all stresses (axial, bending, shear, and contact), but without considering the friction among the wires. Nowadays, it has been realized that the theoretical analyses of wire ropes are very inaccurate if frictional forces are neglected. Also, the relative movements of the wires due to tension and twisting of the cable generate resisting forces that are closely related to the contact forces and stresses in the wires. Moreover, for multi-layer ropes, which are the situation in electrical conductors, the frictional contact among adjacent wires, as well as among adjacent layers, makes the stress states very complex.

Uttings and Jones (1987a, 1987b) conducted in-depth theoretical studies on the response of a wire rope to axial tensile loads, and presented the first mathematical model considering the change of helix angle under load, Poisson's effect in the wires, and the effects of friction and wire flattening at the contact surfaces. However, they considered only one layer of helical wires with small displacements. In addition, in the works of both Phillips and Costello (1973) and Uttings and Jones (1987), the cables were considered short and straight, which is not appropriate for transmission lines applications where the catenary configuration of the cable and the large displacements of the wires have significant effects on cable stresses. Raoof and Hobbs (1988) proposed an analytical model for multi-layered structural strands, where each layer of wires was ideally treated as a statically indeterminate orthotropic cylinder with an equivalent modulus of elasticity. LeClaire (1991) also developed a linear theory for wire ropes that considered individual wire geometry and equilibrium and included the effects of contact deformation between the wires. Dry friction and inter-wire slip in a cable under axial load and uniform bending moment were studied by Huang and Vinogradov (1992, 1994, 1996a, 1996b)**:** Two types of contact modes among the helical wires were identified as *"parallel contact"* among the wires of a same layer and *"cross contact"* among the wires of different adjacent layers (Figure 2.11); The thin rod theory from Love (1944) was used for the wires; small deformations and elastic material behavior were assumed and only those friction forces between the wires and the core were considered. Regarding the applications of wire rope theory to transmission lines, after delivering a comprehensive survey (Roshan Fekr, 1998) of the previous work on stress analyses of helical wires, Roshan Fekr (1999) derived the analytical solutions describing the static response of an optical ground wire (OPGW) under axial load, which considered the central tube geometry of the OPGW cable and Poisson's effect. More recently, a theoretical model for the mechanical response of electrical cables under bending was developed by Inagaki et al. (2007), taking into account the friction of the multi-order helical structures but neglecting the contact within the same layer.

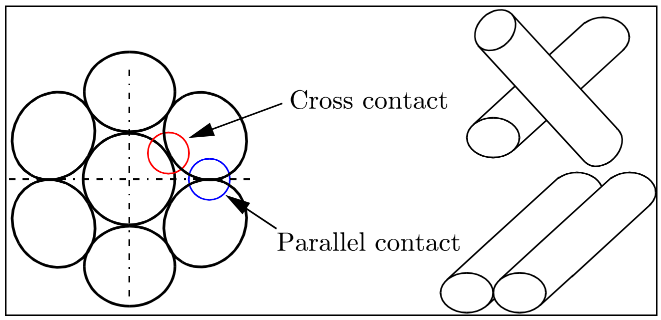

Figure 2.11 Two types of contact modes in a helical wire strand
(Huang and Vinogradov, 1992)

Finally, it should be mentioned that, up to now, several comprehensive literature surveys (Utting and Jones, 1984; Utting, 1994a, 1994b, 1994c) and monographs have been published on the theoretical mechanics of wire ropes. Costello (1997) summarized many findings by his research team and presented their theoretical work on the static response of wire ropes subjected to axial loading, bending and torsion. Contact and friction issues were also discussed, but with very simplified treatments. A large amount of theoretical models of wire ropes under tension and bending were compiled by Feyrer (2010), who summarized more than 80 years of wire rope research in Germany. Kiessling et al. (2010) published a guide book that gives comprehensive descriptions of various electrical conductors, including their mechanical behavior from design and construction perspectives. This recent monograph is also largely based on many years of intensive research in Germany. A small book exclusively on overhead conductors (Rawlins, 2005) includes many useful analytical solutions to calculate the static strength, fabrication stresses and residual stresses of aluminum conductors, which can be directly used for design purposes.

In summary, for all the efforts to derive analytical solutions, many assumptions and simplifications had to be made. Even so, due to the complexity of real wire ropes, developing effective theoretical models for accurate stress analysis purposes (to describe and predict the real mechanical response of wire ropes) has been proven very difficult, and even impracticable. While analytical solutions do bring about some insights into the nature of the subject, like in other real-world mechanics problems, direct use of those closed-form exact solutions can be limited and even not appropriate in the real cases of electrical conductors.

2.3.2 Experimental Studies

Unlike the theoretical studies, experimental studies and testing of wire ropes and overhead conductors have been largely related to fatigue. Early experimental studies on wire ropes were summarized in two comprehensive review papers by Bahke (1985a, 1985b), in which most studies used empirical approaches by means of laboratory tests to generate particular formulas to predict fatigue life of different wire ropes. Based on a modified Goodman diagram, fatigue life of a wire rope was determined by introducing the effective stress to consider the multi-axial stress states of wire ropes (Zhang and Costello, 1996). In combination with analytical formulations to get the stress states, Giglio and Manes (2005) studied the fatigue life of a wire rope subjected to axial and bending loads. It is noteworthy that the majorities of the "fatigue strength" tests of wire ropes in the published literature mainly refer to "*tensile fatigue*" rather than "*fretting fatigue*", and are usually for steel wire cables, for example, the structural ropes used in suspension bridges, instead of electrical conductors (Feyrer, 2010). Fretting-induced contact damage of cable structures, including fretting wear and fretting fatigue, was well summarized by Waterhouse (2003), in which it also refers to steel wire cables mainly used as mooring ropes, haulage ropes, mining ropes, and structural ropes for bridges. Also, from this comprehensive review paper, it is seen that most of the investigations on contact damage of cables have focused on fretting wear and environmental effects, while the very important fretting fatigue problem has not been studied enough.

Furthermore, there are no adequate (standard) failure criteria available for fatigue strength design of cable structures. Besides a damage criterion for transmission line conductors in India, the American Petroleum Institute and Post-Tensioning Institute provides the only specifications in North America that give simplified recommendations for the fatigue design of stranded cables (again, it mainly applies to suspension bridge strands, not to overhead conductors). However, because the above criteria do not take the localized fretting contact fatigue into account, it has been shown that “the criteria give unsafe results” (Papanikolas, 1995) to fatigue strength of cable strands. An experimental study of axial fatigue for bridge steel cables with fretting considerations was thus carried out (Papanikolas, 1995).

Regarding fretting damage of overhead conductors, abundant experimental work has been carried out since the 1960s (see for example, Fricke and Rawlins, 1968; Mocks, 1970). Especially, great efforts were made by the “Research Group on the Mechanics of Electrical Conductors” at Laval University, where a series of fretting fatigue laboratory tests were performed to study the flexural stiffness and fretting behavior of ACSR conductors, particularly at the locations of suspension clamps (Cardou et al., 1985~2001). Their typical fretting fatigue testing rig for a conductor/clamping system is shown schematically in Figure 2.12. Nowadays, it has been well recognized that aeolian vibrations may cause fretting fatigue of individual aluminum wires in overhead conductors and fretting microcracks usually occur in suspension clamp regions (between the keeper edge (KE) and the last point contact (LPC) of the conductor at the mouth of the suspension clamp). The large amount of laboratory test findings and experimental data on this subject (mainly for ACSR conductors) are summarized in the chapters authored by Rawlins et al. in the “EPRI Transmission Line Reference Book” (1979, 2006). The evolution of fretting cracks in an ACSR conductor was explored by metallurgical examinations based on laboratory tests, and fracture mechanics was employed to calculate the stress intensity factors, which were based on simplified assumptions rather than detailed contact stress analysis (Ouaki et al., 2003).

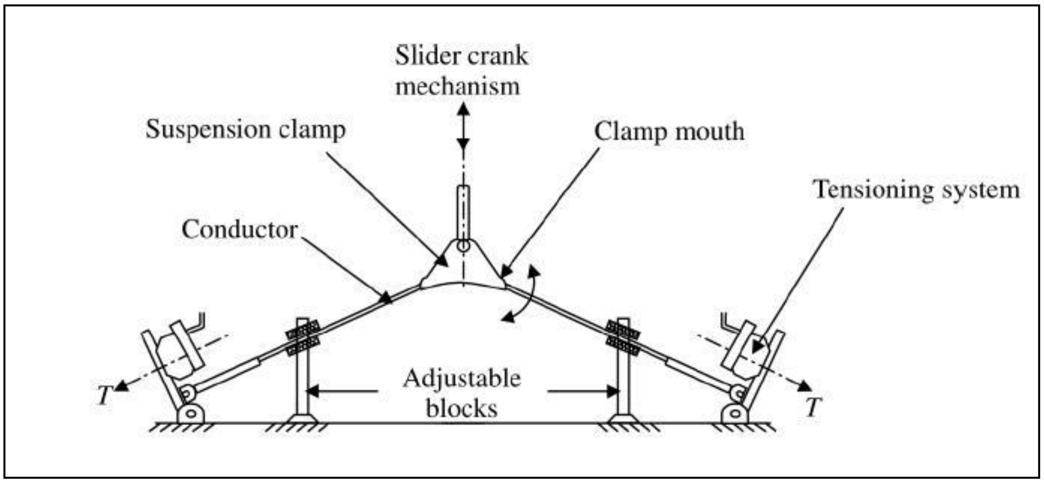

Figure 2.12 A typical fretting fatigue testing rig for conductor/clamping system

Specifically, some typical features of fretting cracks that are characteristics of fretting fatigue of ACSR electrical conductors are summarized below and illustrated in Figures 2.13 to 2.17. Metallographic examinations have shown that fretting cracks may exhibit different cracking modes in three different "fretting regimes" of a conductor/clamping system (Zhou and Vincent, 2002)**:** In the stick regime, while a fretting crack is not easily developed, it is still able to initiate at (or very close to) the boundary of the contact area with increasing fretting cycles, and it usually grows almost perpendicularly inward into conductor wires (Figure 2.13). The mixed regime has been shown to be the most critical regime for crack nucleation and growth (Zhou and Vincent, 1995), where fretting fatigue microcracks often initiate in conductor/clamping edge-of-contact areas under a partial slip contact state, and the initial crack inclines towards the tangential fretting direction. Thereafter, the crack might propagate with one of the three different modes: (a) The crack stops growing deeper, but links up with another crack with opposite crack path, thus generating a large particle debris (Figure 2.14); (b) The crack suddenly changes its initial direction and continues to propagate inward (nearly perpendicular to the contact surface), as shown in Figure 2.15; (c) Bifurcation occurs: one crack would develop according to the first mode, while another crack path would follow the second mode (Figure 2.16). In the mixed regime, the most significant factors are normal contact pressure (bearing force), tangential frictional force and size of contact area. The synergistic effects of these influential factors govern the growing path of the fretting crack. In the slip regime, the location of crack nucleation and the crack path heavily depend on the "competition" between fretting wear and fretting fatigue. The crack might occur from the edge of the fretting wear pit surface (Figure 2.17).

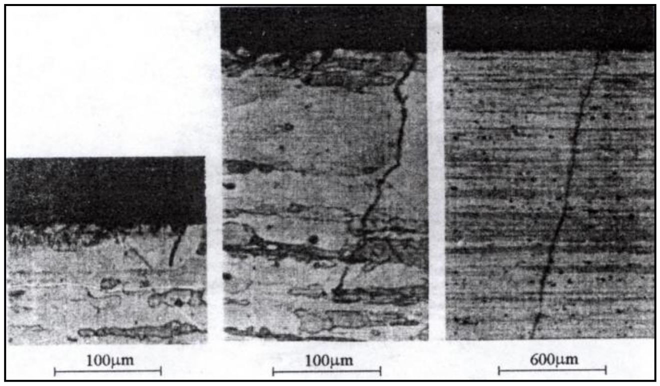

Figure 2.13 Fretting crack path in stick regime (Zhou and Vincent, 2002)

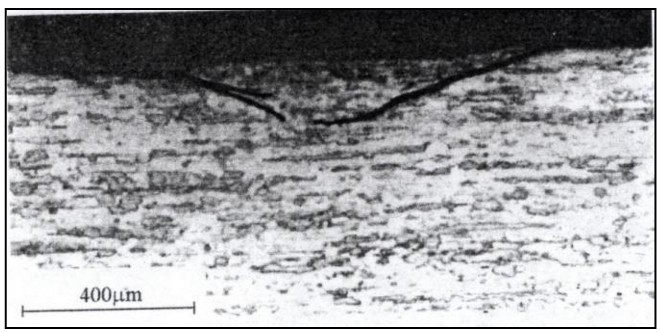

Figure 2.14 Fretting crack path in mixed regime: mode (a) (Zhou and Vincent, 2002)

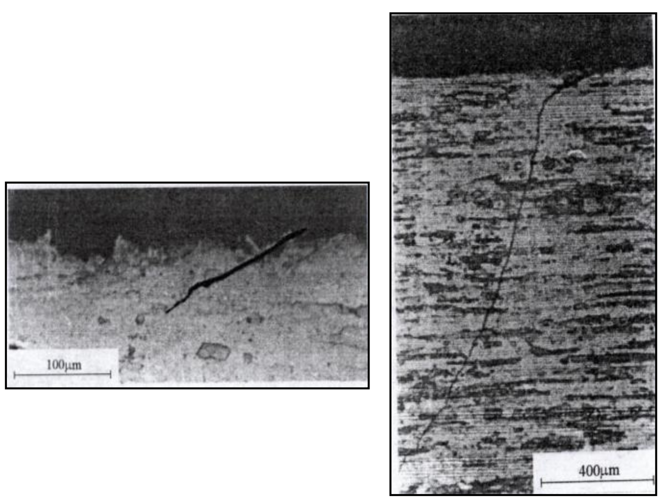

Figure 2.15 Fretting crack path in mixed regime: mode (b) (Zhou and Vincent, 2002)

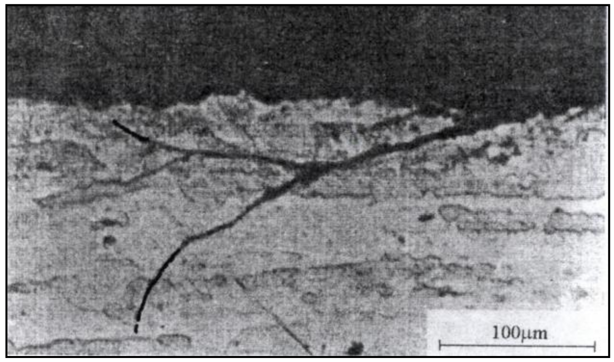

Figure 2.16 Fretting crack path in mixed regime: mode (c) (Zhou and Vincent, 2002)

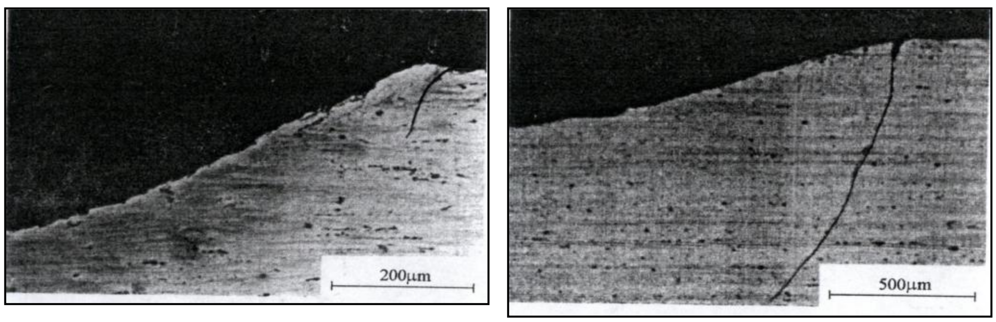

Figure 2.17 One type of fretting crack path in slip regime (Zhou and Vincent, 2002)

Furthermore, it has been shown that fretting conditions also have a crucial influence on fretting cracking behaviors, namely, the nucleation and propagation of fretting cracks strongly depend on material properties, contact geometry configurations and loading conditions, as well as their synergistic effects. Consequently, conductor wire ruptures may in effect occur on either outer layers or inner layers, making it very difficult to predict fretting fatigue of a conductor. The effects of many mechanical parameters, including fretting slip amplitude, clamp pre-stress, number of fretting cycles, frequency of fretting motion, performance of lubricant, and material properties were investigated extensively by Zhou et al. (1992-1999). From the above discussions in this section, it can be concluded that fretting experimental studies are all empirical in the sense that, depending on particular situations (test conditions), quite different research findings have been reported.

In recent years, several field investigations of overhead conductor fretting fatigue failures have been reported. For example, a failure of an all aluminum alloy conductor (AAAC) in a 400 kV overhead transmission line located in Touggourt Biskra (Algeria) was analyzed by Boniardi et al. (2007). Their investigation revealed that all the ruptured wires showed fretting marks associated with intense presence of aluminum oxyde (Al_2O_3) debris; broken and damaged conductors were taken as experimental samples to identify the root cause of the fretting fatigue failure. Another in-depth field investigation by Azevedo and Cescon (2002) related to the catastrophic failure of an ACSR conductor in Brazil[4]. The rupture of the ACSR conductor strands (Figure 2.18) occurred just at the end of the clamping regions. The fracture topography distribution indicated that all the outer and most of the inner aluminum wires had a 45^{o} fracture surface (Figure 2.19), while fretting wear debris was present on the both outer and inner layer surfaces. Recently, the same research group designed a practical testing rig to carry out ACSR conductor fretting fatigue tests and performed metallographic examinations to explore the failure mechanisms (Azevedo et al., 2009). The rig design and the testing parameters of this experimental work have served as important references for the computational work done in this thesis.

Figure 2.18 General view of fretting fatigue rupture of a ACSR conductor (Azevedo and Cescon, 2002)

[4] The blackout in 2002 due to the failure of 460 kV transmission line crossing of the Parana River seriously affected 67 million inhabitants in the southern states of Brazil.

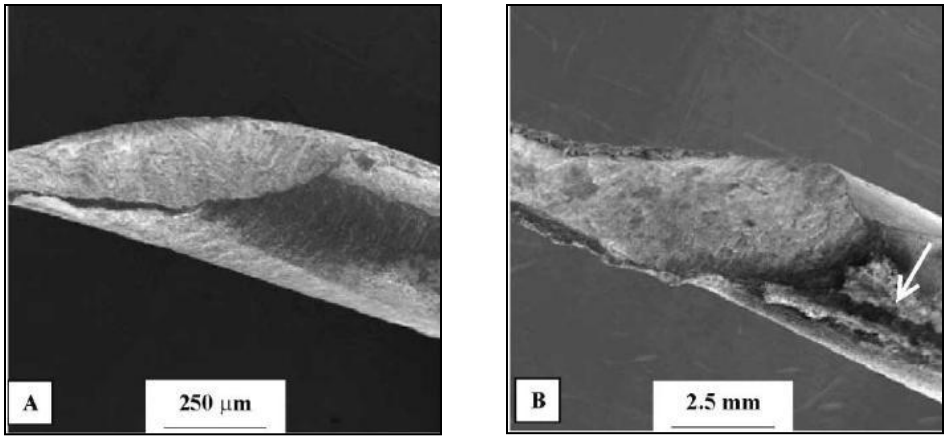

Figure 2.19 ACSR conductor fretting fatigue fracture surface: (A) Outer layer 45^o fracture surface; (B) Inner layer 45^o fracture surface with superficial fretting wear damage (see arrow) (Azevedo and Cescon, 2002)

2.3.3 Computational Modeling Studies

While experimental studies on fretting damage of electrical conductors have been carried out extensively and some fretting fatigue testing methods have been standardized (Cardou et al., 1992), relatively fewer efforts were dedicated to computational modeling of this problem. In effect, due to the great challenges encountered in the modeling process (Ouaki et al., 2003; Azevedo et al., 2009), accurate stress analysis applied to conductor wires and conductor/clamping systems has been a bottleneck to gain a better understanding of the complex strength and fatigue behavior of stranded transmission line conductors. Since the 1990s, only a few related numerical studies have been conducted, all using finite element methods. The salient features of these studies are reviewed next.

One of the first computational studies was reported by Abé et al. (1989), who constructed a 3-D finite element model of overhead ground wires with optical fibers (OPGW). In fact, it modeled only the grooved aluminum spacer (slotted rod) illustrated in Figure 2.20, without considering the other components (the layers of wires and the optical fibers) of the optical fiber cable.

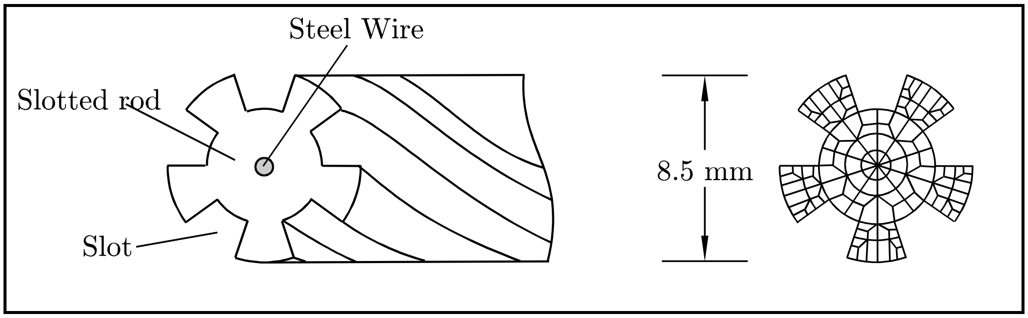

Figure 2.20 Cross section and mesh of an aluminum spacer (Abé et al., 1989)

A finite element analysis of a parallel groove clamp in the bolt-type power connector was conducted by Luo et al. (2000) to address the failure of the connector rather than the conductors. The contact problem was considered in this failure analysis, but without considering fretting. Another wire rope contact stress analysis model was presented to study the interwire motions under axial loading and bending, but with very simplified node-to-node contact treatments (Nawrocki and Labrosse, 2000). Several concise finite element models for a short wire strand sector with very coarse mesh were also built by Chiang (1996) and Jiang et al. (1999a, 1999b, 2000a, 2000b, 2008) to describe the response of a simple strand to axial loads. Contact interactions among wires were considered (Figure 2.21), but it was claimed that accurate boundary conditions would be very difficult to apply, if not impossible. Thus, symmetric boundary conditions were established, which is not accurate for real overhead conductor configurations.

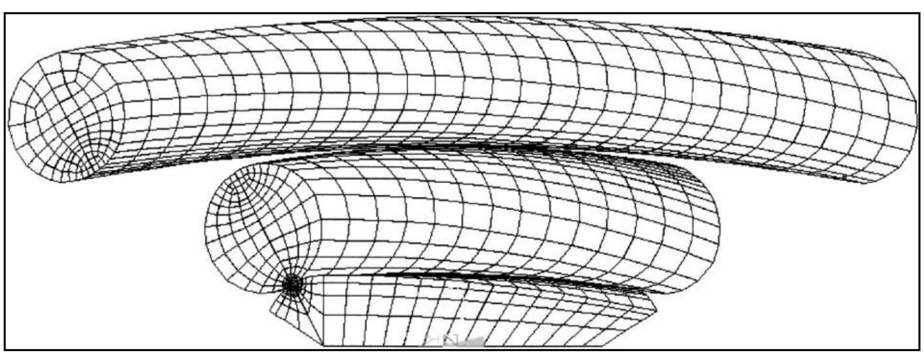

Figure 2.21 Concise FE model for a three-layered wire rope sector (Jiang et al., 2000)

A substantial effort was made by Roshan Fekr et al. (1999) to model a real OPGW strand cable, including the nonlinear material properties, large deformation and frictional contact effects. In that work, the first detailed 3-D finite element model was constructed for stress analysis of an OPGW cable subjected to a prescribed elongation. However, due to the limitations of computing platforms and numerical techniques for solving large nonlinear problems at that time, a very coarse mesh was produced and simplified solid geometric models were built (Figure 2.22) to reduce the model size and analysis running time; also contact surface plasticity was not taken into account. Even so, this work provided an important milestone that served as the starting-point for the computational modeling studies in this thesis.

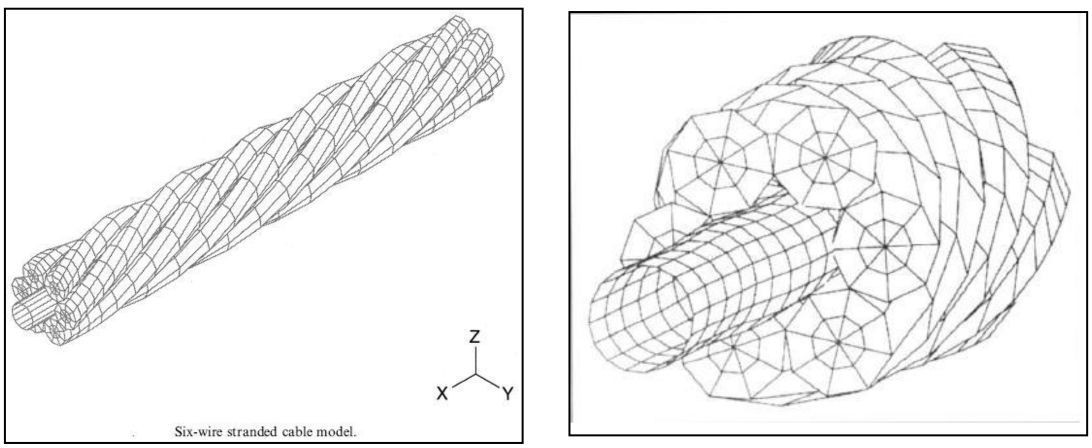

Figure 2.22 A simplified OPGW stress analysis model (Roshan Fekr et al., 1999)

In recent years, Dastous (2005) analyzed stranded conductors using a newly developed beam element with variable bending stiffness based on the so-called tangent stiffness method from Papailiou (1997). Páczelt and Beleznai (2011) developed a p-version FE code to analyze a two-layered wire rope strand based on the curved beam theory. A 3-D finite element analysis for stress concentration at the clamping region of conductors under axial force was studied by Lao et al. (2009). Although contact interactions between the conductor and its suspension clamp were included in that model, the conductor was only regarded as a single elastic solid cylinder rather than a helical cable strand, thus ignoring the essential characteristics of real conductors. Consequently, that model was not able to present the proper stress distributions in the contact region of the conductor/clamping system. A 3-D FE model for multi-layered wire strands under tension was recently built by Stanova et al. (2011). That model considered the inter-layer contact, but with only elastic material behavior, and thus cannot be used to address fretting fatigue behavior. Another recent conductor study involving detailed computational modeling was carried out at the Oak Ridge National Laboratory in the United States (Wang et al., 2008). The objective of the research was to evaluate the integrity of ACSR Drake conductor full tension single-stage splice connector (SCC) systems and their associated effective lifetimes at high operating temperatures. In addition to experiments, 3-D contact stress analysis models were constructed in the investigation. However, coarse models had to be built because it was claimed that the fine meshed model of the real conductor configuration took a very long time to reach a convergent solution. As a result, besides a coarse meshing scheme, the 3-D FEM model had only a single die-set length of 1.5 inches, including the sleeve and the Drake conductor, for simulating the SCC crimping event (Figure 2.23).

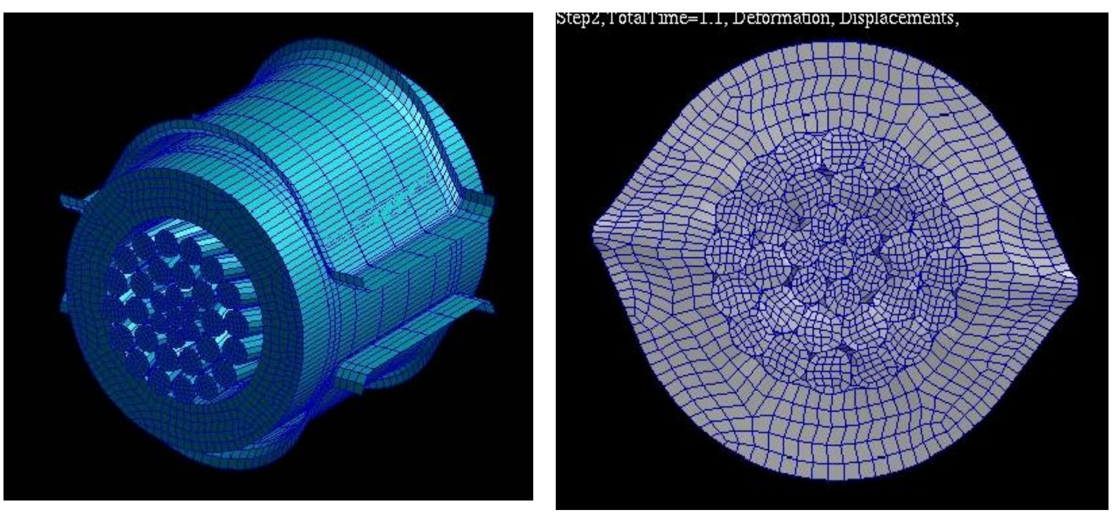

Figure 2.23 ACSR Drake conductor SSC system model (Left) and crimped conductor section at the middle section of the model (Right). (Wang et al., 2008)

From the selective review of this section, one can realize that effective and robust computational models are crucial to accurately analyze and predict the complex mechanical responses in transmission line conductors.

2.4 Summary Remarks

The state of the art of general fretting research, fretting fatigue, as well as contact damage studies of electrical conductors have been reviewed in this chapter. Numerous laboratory tests have been carried out to study the static strength and fretting fatigue of high voltage overhead electrical conductors in the past decades. The effects of a variety of physical parameters on fretting fatigue and fretting wear have been investigated empirically.

Although obtaining accurate stress fields for conductor wires and especially at clamp mouth areas is very important for transmission line design and maintenance against fretting fatigue, the stress states at the contact surfaces among individual wires as well as between the outer wires and the clamp surface are not accessible to direct measurement. Meanwhile, simplified theoretical models are not capable of fully characterizing and explaining real-world situations. Hence, computational mechanics models are the best methodology to accurately and completely determine the complex states of stress and strain for multi-layered composite stranded conductors. However, such numerical work has not been fully successful to date. With the increasing power of computing hardware capabilities and the availability of sophisticated numerical solution techniques, reliable computational models can now be developed to study this problem: this is precisely the scope of the present research.

Chapter 3

Refined FE Modeling for Stress Analysis of an OPGW

3.1 Introduction

As stated in Chapter 1, a refined finite element model for detailed stress analysis of an optical ground wire (OPGW) strand is studied as the first phase of this research. The primary goal in this stage is to develop a high fidelity modeling methodology for reliable and accurate numerical stress analysis of stranded transmission line conductors. A particular type of optical ground wire is selected, for which a simplified coarse model of that OPGW was successfully built by Roshan Fekr (1999). The availability of this model data and its results has enabled a productive starting phase for the purpose of validation and verification of the newly developed finer model. In addition to seeking to achieve the above goal, a significant improvement of that preliminary work had been long expected.

Overhead ground wires with optical fibers (OPGW) have been used widely in high voltage transmission lines to replace traditional steel ground wires, for their telecommunication benefits in power grid control. The primary function of OPGW is to protect the line conductors electrically against lightning, while optical fibers incorporated in the core of the cable serve as telecommunication lines for automatic control of the transmission network. While there has been considerable interest in the power line industry to engineer various stranded transmission line conductors, research devoted to understanding the complex mechanical behavior of complete OPGWs has been scarce in the open literature, especially from the numerical modeling perspective. As mentioned in Chapter 2, the work by Roshan Fekr (1999) produced a simplified model with very coarse 3-D mesh. Considering that friction and contact problems are highly dependent on the geometry of the solids in contact and the problem size, a new-generation refined model with improved solution accuracy is thus to be developed for a better understanding of the detailed mechanical response of the OPGW.

This chapter addresses the construction of a 3-dimensional elastic-plastic, large deformation, multi-body frictional contact finite element (FE) model for a real OPGW conductor. The detailed model attempts to consider all possible mechanical effects, such as contact, friction, elongation, torsion, and bending under maximum design conditions, with a view to describe clearly the detailed mechanical response of each cable component. While nowadays high-end FE software has the capabilities to handle complex problems, this model presents practical difficulties to achieve both convergent and sufficiently accurate solutions due to the helically-stranded cable geometry, the nonlinear cable constitutive properties involving several materials, substantial friction effects, as well as contact interactions amongst its components (i.e., among the wires of different layers, the wires and the tube, and the tube and the spacer). Many challenges have been encountered throughout the modeling process. For example, very fine mesh is imperative in the regions of the comprehensive contact interfaces of all the wires to capture the stress gradient and achieve converged solutions, but how fine does the mesh need to be? What types of elements for contact and non-contact regions work best for this application? What boundary conditions should be specified to properly simulate the effects of the design loads on a short cable section? Which numerical solution techniques (and their combinations) are the most robust and efficient for this type of problem? In this chapter, all these issues are explored and discussed in detail, followed by a comparison of the computational results of this refined model with those obtained with two approximate analytical solutions and from the coarse model developed by Roshan Fekr (1999).

3.2 OPGW Construction and Solid Modeling

The OPGW modeled in this study was manufactured by Phillips-Fitel in Rimouski, Québec (Canada) and used by Hydro-Québec on its first high voltage overhead transmission lines equipped with optical technology. Figure 3.1 shows a schematic cross-section of the OPGW cable strand, and the configuration of the OPGW assembly is illustrated in Figure 3.2: The cable comprises two layers of helically twisted conductor wires, a central aluminum tube, and a spacer that houses the optical fibers in its helical grooves.

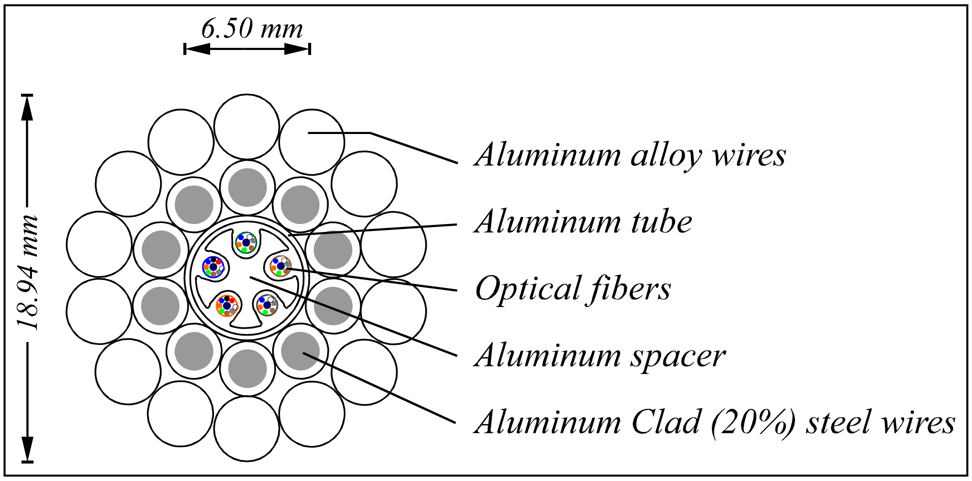

Figure 3.1 Schematic cross section of the 19-mm OPGW (Roshan Fekr, 1999)

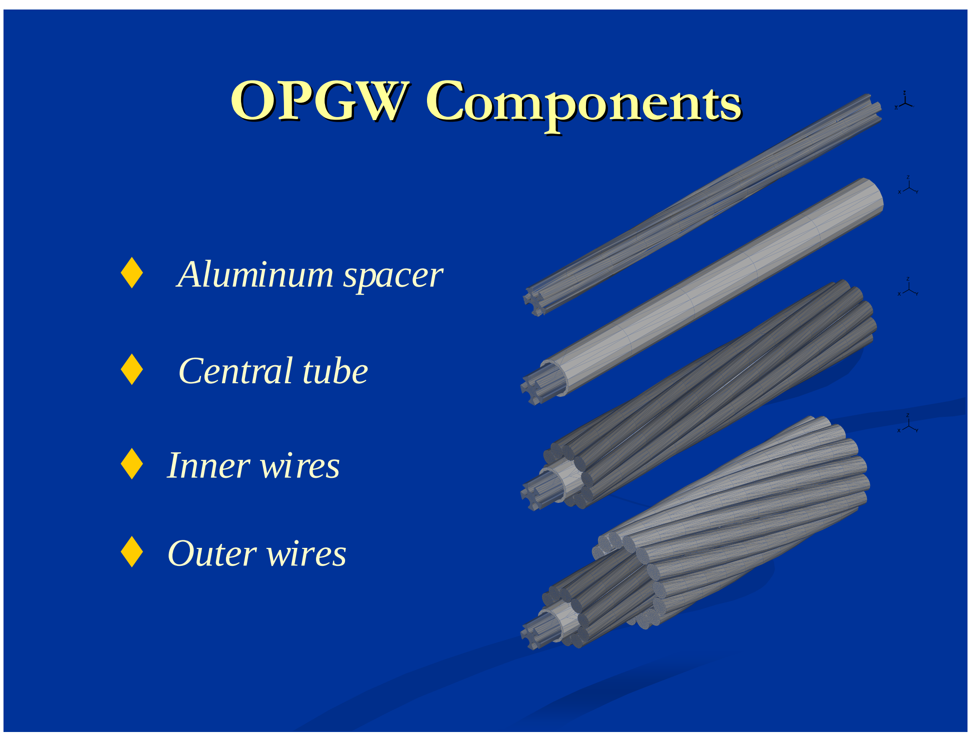

Figure 3.2 The structural components of the OPGW (Roshan Fekr, 1999)

The geometric specifications of the OPGW components are summarized in Table 3.1. The exact external diameter of the cable strand is 18.94 mm. The outer wire layer is made of 14 aluminum alloy wires, whose function is mainly to dissipate the electrical current generated by a lightning strike. These wires are helically twisted around the inner layer wires with a pitch length of 202.16 mm. Acting as the main load-carrying component, the inner layer is made of 10 aluminum-clad steel wires with a pitch length of 265.16 mm and helically twisted in opposite direction to that of the outer wires. The 6.5 mm external diameter and 0.55 mm wall-thickness central aluminum tube encloses the optical fiber strands that are loosely inserted in the five U-shaped grooves of a spacer. The spacer is also made of aluminum alloy and is itself helically twisted along its center with 150 mm pitch length in the same direction as the inner wires. As a result, the helix angles of the outer wires are in the opposite direction of the helix angles of the inner wires and spacer grooves: the outer wires have a Z-shape while the inner wires and spacer are of S-shape. The opposite helical directions of the inner and outer layers are designed to reduce the internal twisting moment of the cable about its longitudinal axis.

Table 3.1 Geometric specifications of the OPGW components

	Diameter (mm)	Area (mm^2)	Pitch Length (mm)	Helix Angle
Outer wire	3.37	8.92	202.16	+ 13.61^o (Z)
Inner wire	2.85	6.38	**265.16**	- 6.32^o (S)
Central tube	6.5 (D_{ext}); 5.4 (D_{int})	10.28	-	-
Spacer	5.15	10.17	150	- 6^o (S)
FE model	External Diameter = 18.94 mm ; Model length = 265.16 mm			

The main software used to build the OPGW solid model is the DesignModeler of ANSYS Workbench 11.0 (ANSYS Inc., 2007). The model comprises all the structural components of the cable strand (Figure 3.3) except the optical fibers. These fibers are designed to remain stress-free under normal operation loads due to their loose insertion in the grooves of the spacer provided by fiber over-length. The relatively larger diameter of the spacer slots with respect to the diameter of the fiber strands provides space for the additional length of the fibers, which is also referred to as *over-length*. Assuming perfect compatibility of strains and displacements amongst cable components, the optical fibers will not experience any elongation and axial stresses until the cable extension exceeds the fiber over-length. The total length of the solid model is based on the longest pitch length among all its structural components, i.e. the inner layer pitch length of 265.16 mm

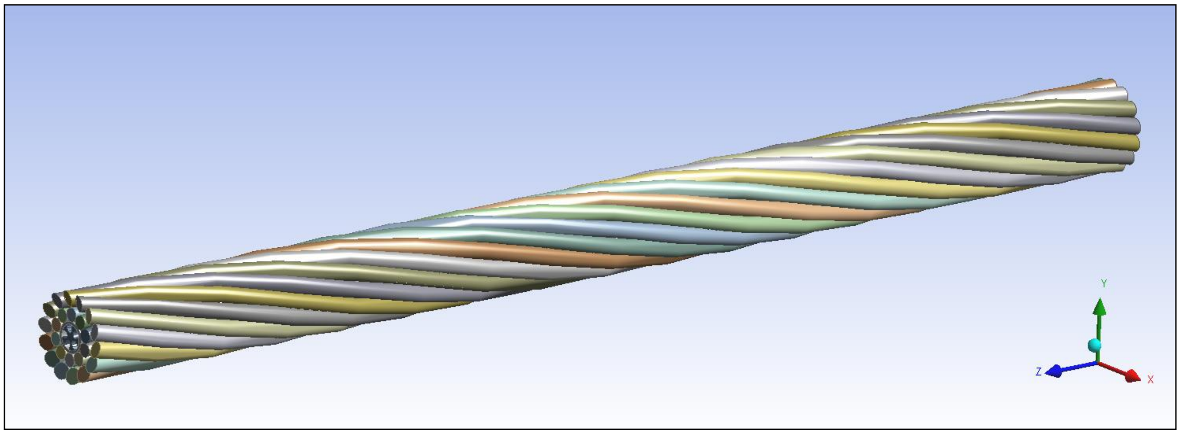

Figure 3.3 Solid model of the OPGW - 265.16 (mm)

In an attempt to build a precise solid model for the purpose of accurate contact analysis, significant improvements had to be made compared to the previous work of Roshan Fekr et al. (1999) to generate the solid bodies and surfaces. The central tube is easily defined by extruding its circular cross-section along the longitudinal axis (z-axis). The spacer (Figure 3.4) is generated using its exact cross-sectional sweep along the z-axis with helical twist based on its pitch length rather than its helical angle as used by Roshan Fekr (A helical angle is an approximate value calculated using the pitch length.), which yields a more accurate geometry.

Building the inner and outer layer wire solid models involves three steps. In step one, two 3-D helical curves are accurately created using I-DEAS software (UGS, 2006) by defining spline function expressions with two sets of helix algebra equations[1], for the inner wire and outer wire separately. The generated helical curves are then transferred (in .igs neutral format) into ANSYS DesignModeler. In step two, an inner solid wire and an

[1] Helix parametric algebra equations: $x= r*\cos\theta$; $y=r*\sin\theta$; $z=h*\theta/2\pi$; $\theta \in [0, 2\pi]$ (h= pitch length)

outer solid wire can be generated separately by sweeping their circular cross sections along the 3-D helical curves defined in step one. In step three, 10 inner layer wires and 14 outer layer wires are built via “circular pattern” to duplicate the helical wires created in the second step. Using this approach, the generated solid wire models may have exact elliptical cross sections on a cutting plane defined by its normal along the z-axis. The geometry of the two cross sections at the fixed-end and free-end is shown on Figures 3.5 and 3.6.

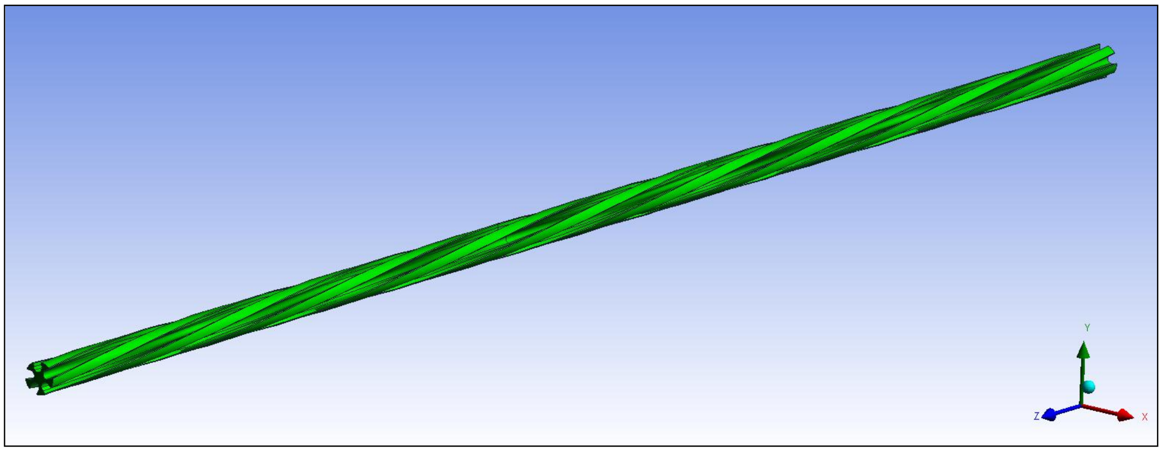

Figure 3.4 Solid model of the core spacer

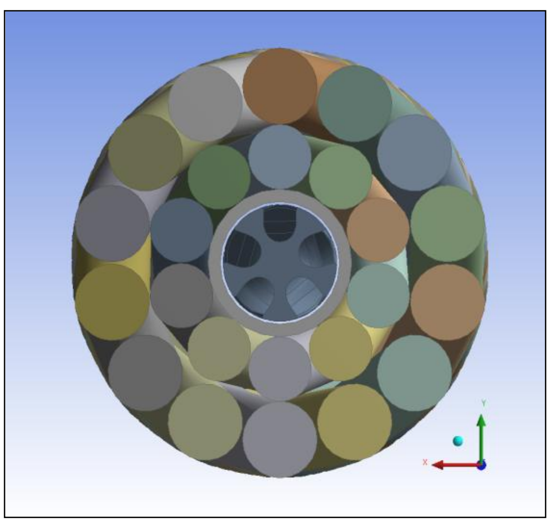

Figure 3.5 Cross section with fixed end

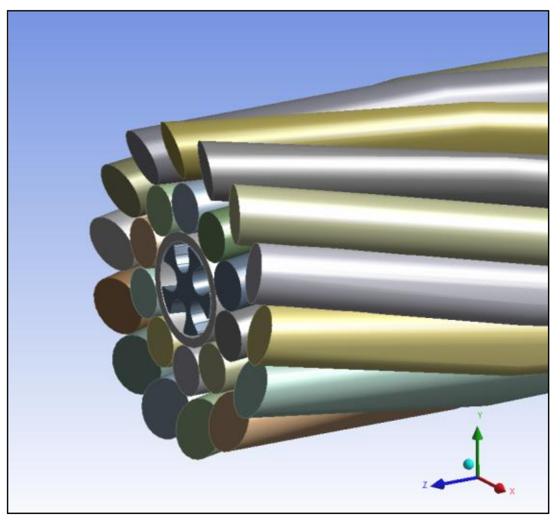

Figure 3.6 Cross section with free end

3.3 Finite Element Modeling

Considering the particular features of the problem and the complex interfacial contact geometry of the cable strand, the finite element method (FEM) is selected for detailed stress analysis. FEM has gained widespread acceptability in industry during the past few decades, and nowadays has been actually the most commonly used tool in various structural analysis areas. However, as mentioned before, a number of modeling challenges were encountered in this application. Especially, the highly nonlinear model exhibits very difficult convergence behavior, which requires extensive numerical experiments as most software-supplied default parameters for numerical solution control and contact settings became inadequate. Keeping in mind the two goals stated in the beginning of this chapter, the focus of the work presented in this section is to gain confidence in the modeling methodology and demonstrate the accuracy of the computational results. Before starting the in-depth discussion of the approaches employed throughout all essential procedures in the FE modeling and its implementation, some comments about the reliability assessment of a FE model are worthy of being addressed, as they provide the author's rationale to carry out all the computational modeling research in this thesis.

The reliability assessment of a numerical simulation (the modeling and its computations) includes two processes, the so-called validation and verification (V&V). Specifically, validation means the examination of the quality of a mathematical model in representing its physical context, and verification addresses the quality of the numerical schemes to solve the mathematical model (Babuška and Strouboulis, 2001). Much research is currently being done on the subject of V&V with the growth of computational modeling (see for example, Babuška et. al., 2011).

Like any other numerical modeling technique, a FE model is essentially a mathematical representation (in this thesis) of a boundary value problem for a set of second-order partial differential equations. Since the actual physical problem to be tackled is almost impossible to model exactly as it is in reality, that is, the actual mathematical model that we seek to solve is generally intractable, and thus it always has to be replaced with a tractable surrogate model. This implies that, even if one gets almost the right answer for the surrogate model, it is still the "wrong" answer for the mathematical model that represents the real problem. Therefore, it is very important to realize that any FE solution can never give more information than that contained in the solved mathematical model (FE model). As any numerical model can only be an approximation to reality, which inevitably contains some uncertainty, a FE model thus must preserve the most important features of the actual physical event so that it could meet the necessary acceptance conditions given the specific goal of the simulation. To answer the question of validation is to address whether the FE model correctly models the physical phenomenon being considered. Hence, an effective FE model is supposed to be the one that can yield the required response with sufficient accuracy and at least cost, and is considered reliable if the predicted response is within the accuracy of the response predicted with a "very comprehensive mathematical model", which is generally a 3-D fine model including all essential nonlinear effects (Bathe, 1996). To this end, an evolutionary development from a coarse model to a fine model is often needed as part of the validation process, which is called *"hierarchical modeling"* (see for example, Oden and Prudhomme, 2002; Bucalem and Bathe, 2011).

As for verification, it essentially involves two aspects: verification of the numerical solution techniques and verification of the code implementing these techniques (Babuška et. al., 2011). To achieve robust numerical schemes, extensive numerical experiments are often required for a highly nonlinear problem. However, *ad hoc* approaches should be avoided to "artificially fix" numerical deficiencies of the computational model. That is, the quality of the numerical schemes should be based on the rational understanding of the numerical solution process and the physical problem that the FE model represents. In addition, error analysis (error estimation) of the FE solution is also crucial for the verification process. Certainly, in engineering practice, it has been always tacitly assumed that round-off error is negligible by using a reliable code. In this thesis, the finite element analysis commercial software ANSYS Workbench 11.0 (ANSYS Inc., 2007) is employed to perform all the FE implementations, due to its proven high-end solver capabilities for large nonlinear problems. The verification aspect of the OPGW modeling will be mainly addressed in Section 3.4, while its validation is discussed next.

3.3.1 Material Properties

All the inner and outer helical wires of the cable strand are assumed linear elastic with large kinematics and small strains, which is in accordance with the experimental results obtained from a 96-hour tension test performed at Hydro-Québec's Research Institute (IREQ, 1994). Uniaxial tension tests were performed at McGill University on the central aluminum tube and spacer separately, to obtain their accurate stress-strain material curves at ambient temperature (22^{o}C). These tests were justified by the significant plastic deformations observed in the IREQ tests. The material nonlinearities of the central tube and spacer are then modeled in ANSYS using multi-linear fits of their experimental curves. The material properties and characteristics of the OPGW components are illustrated on Figure 3.7 and summarized in Table 3.2, where E is Young's modulus, Y is the Yield strength, and UTS stands for Ultimate Tensile Strength.

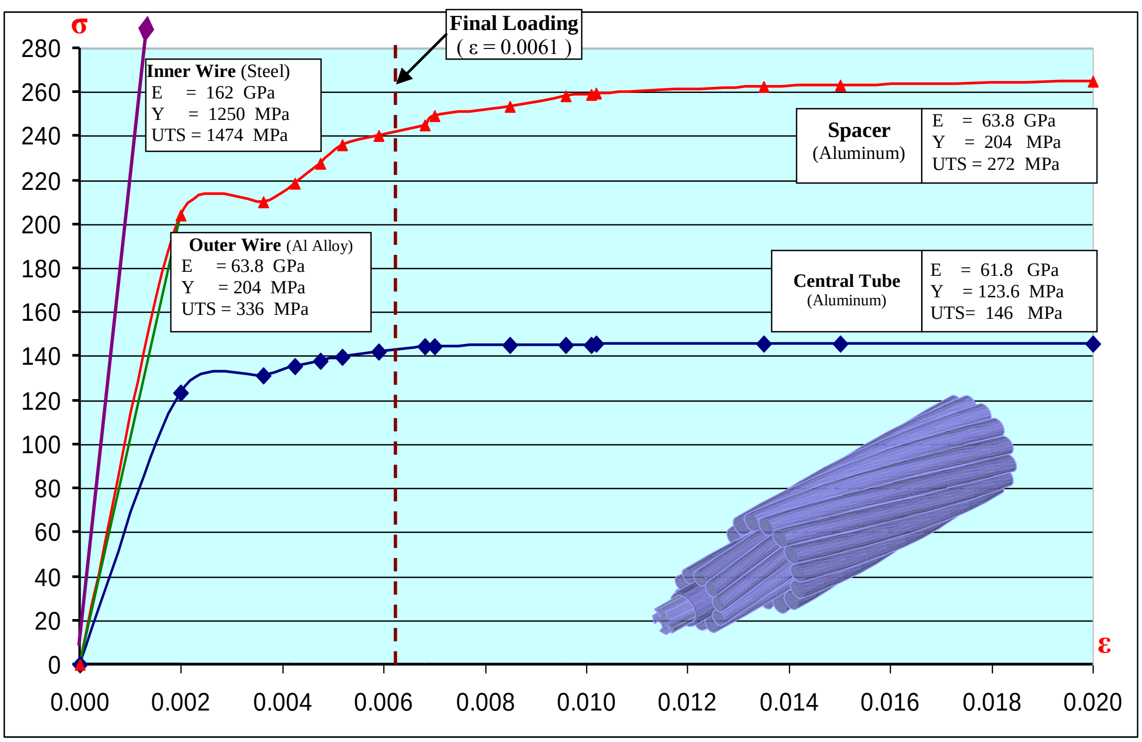

Figure 3.7 OPGW cable strand material curves (**σ** in MPa)

Table 3.2 Material properties and characteristics of the OPGW components

Components	Material	Properties	Characteristics
Outer wires	Aluminum alloy	E = 63.77 GPa; ν = 0.33 Y = 204.05 MPa; UTS = 336 MPa	• linear elastic, • large kinematics, • small strain
Inner wires	Aluminum-clad steel	E = 162 GPa; ν = 0.33 Y = 1250 MPa; UTS = 1474 MPa (main load-carrying component)	
Central tube	Aluminum	E = 61.8 GPa; ν = 0.33 Y = 123.61 MPa; UTS = 146 MPa	• linear elastic to multi-linear plastic, • large kinematics, • large strain
Spacer	Aluminum alloy	E = 63.77 GPa; ν = 0.33 Y = 204.05 MPa; UTS = 272 MPa	

3.3.2 Finite Element Selections and Meshing Studies

The first step of any finite element simulation is to discretize the actual geometry of a structure using a collection of *finite elements*. Each element in the model represents a discrete portion of the physical structure, which is, in turn, represented by many interconnected elements via shared *nodes*. In a displacement-based finite element stress analysis, the displacements of the nodes are the fundamental variables calculated during the analysis. Once the nodal displacements are known, stresses, strains and other physical variables in each element can be determined thereafter, while the displacements at any other point in the elements are obtained by interpolating from the nodal displacements. Therefore, as the fundamental component of a FE modeling, the selection of "correct" element formulations is vital. In effect, the accuracy and efficiency (computational cost) of a stress analysis simulation depend strongly on the types of finite elements in the model, which essentially involve the order of the displacement interpolation functions, the locations of the integration points, and the accuracy of the integrations. Among the large solid element library in ANSYS[2], selecting the best element types for the analyses performed in this thesis is based on the author's understanding and experience about the effects that different element qualities may have on the accuracy for a particular type of analysis. The basic idea is to try to avoid problematic element behavior in solid elements, such as shear locking, volumetric locking and hourglassing. The rationale for the element selections is discussed below.

For a 3-D structural analysis, the most commonly used solid elements are tetrahedral and hexahedral (brick) elements with either linear or quadratic interpolation functions. Higher-order elements are generally not used in practice due to their unnecessary high computational cost for a large size real-world problem. As numerical integrations (commonly Gaussian quadrature for isoparametric elements) are used to calculate various quantities over the volume of each element, the selection of the order of integration (full or reduced integration) can thus have a significant effect on the accuracy of the element for a given problem. For hexahedral elements, either full-integration or reduced-integration scheme can be used, while tetrahedral elements only use a full-integration scheme due to their "complete" polynomial shape functions (Zienkiewicz et al., 2005).

When using full integration, the linear hexahedral element is prone to the problem of *"shear locking"*[3] if flexural effects dominate the response. While the fully integrated quadratic hexahedral element has no shear locking problem, it might still exhibit some *"volumetric locking"*[4] under complex stress states, especially if the element experiences large distortions as is the case for the problem in the thesis. Therefore, a full-integration scheme will not be used in this study. In effect, much experience suggests that a reduced-integration scheme is often preferable in that it has a softening effect and therefore an ameliorating effect on the rather overly stiff behavior of the FE model of a structure

---

[2] In general, the continuum (solid) family of stress/displacement elements has the most comprehensive element library in any general-purpose commercial FE codes.

[3] *Shear locking* causes the elements to be too stiff under bending. i.e., the overall deflection of the elements subjected to bending loads will be under-predicted, and spurious shear stresses would arise as well (see for example, Hughes, 2000).

[4] *Volumetric locking* is another form of element over-constraint that may occurs in fully integrated elements. It causes overly stiff element behavior for deformations that may cause no or little element volumetric changes (see for example, Hughes, 2000).

(Shrivastava, 2005). However, linear reduced-integration elements tend to be too flexible because they suffer from their own numerical problem called *"hourglassing"*, corresponding to the so-called *"zero-energy mode"* (see for example, Cook et al., 2001), and the hourglass mode may propagate in coarse meshes. Fortunately, the hourglass mode has been very effectively controlled (especially in a fine mesh) by some "hourglassing control" techniques (Flanagan and Belytschko, 1981; Belytschko et al., 1984, 2000; Puso, 2000). As a result, these linear reduced-integration elements perform perfectly well under tensile and transverse shear loads, and are very tolerant of element distortions. Hence, it would be ideal to use a fine mesh of these elements for a large mesh distortion (large strain) analysis, as well as for simulations involving complex contact problems. As for the quadratic reduced-integration elements, they rarely experience the problem of hourglassing even in a "normal" (not fine) mesh, and are not susceptible to any locking even when subjected to complicated states of stress. Therefore, these quadratic elements are usually considered the best choice for most general 3-D stress/displacement simulations. Nevertheless, they do not perform better than the linear reduced-integration elements in large-displacement simulations involving large strains and in contact analyses (Dassault Systèmes, 2010). Furthermore, an empirical study (Roshan Fekr, 1999) had indicated that, for contact analysis of a helical wire conductor with a coarse mesh, the increase in accuracy obtained by using higher order brick elements (20- and 27-node elements) compared to linear (8-node) brick elements, is not significant but the additional CPU running time is much longer.

Comparing with hexahedral elements, the main and only advantage of tetrahedral elements (in the author's opinion) is that they can mesh arbitrary geometries using automatic mesh generation supported by reliable free-meshing algorithms (see for example, Georg, 1991; Freitag and Knupp, 2002; Frey and Georg, 2008) that are available nowadays in most FE pre-processors, but the generation of a high-quality pure hexahedral mesh for complex geometries still relies heavily on the expertise of an analyst[5]. Regarding the element quality and computational cost, tetrahedral elements are

---

[5] Despite intensive research in the past decades, to the best of the author's knowledge, no robust and fully satisfactory automatic meshers are yet available to mesh arbitrary geometries completely with hexahedrons, at least for existing commercial FE codes and meshers.

overall not superior to brick elements. The running time of an analysis with tetrahedral elements will typically be longer than an equivalent mesh of hexahedral elements. The 4-node tetrahedral element is too stiff for stress calculations, and thus it has been suggested to be avoided in practice (Dhondt, 2004). The 10-node tetrahedral element is a very flexible element due to its curved shape, and its accuracy is comparable to the 20-node brick element. Also, it is generally well behaved with a fine mesh, especially under tensile and shear deformations.

It should also be noted that in addition to the displacement-based finite elements, there are other two classes of elements: "incompatible mode elements" and "hybrid elements", which are popular for some types of 3-D analyses. The 3-D incompatible mode elements have been developed since the late 1980s (Simo and Rifai, 1990; Wilson and Ibrahimbegovic, 1990) in the attempt to overcome the problem of shear locking in fully integrated, first-order elements, while limiting computational cost. However, these elements are often highly sensitive to mesh distortions, i.e., they can only provide high accuracy when the element distortions are very small. Hence, they are not suitable to be used in models with complex geometries and large deformations. Hybrid elements have been intensively studied historically (Pian and Wu, 2005) and are still popular for some particular types of analysis (Zienkiewicz et al., 2005; Belytschko et al., 2000), especially when the material behavior is, or very close to, incompressible, i.e. the Poisson's ratio is close to 0.5. As for other applications, the improvement of accuracy using hybrid elements is not significant and mainly occurs in the case of a coarse mesh, which is not proper for accurate modeling. Another setback of hybrid elements is that they require much more CPU time than displacement-based elements because their mixed element formulations include additional degrees of freedom to determine stress, strain or pressure in the elements directly.

Based on the above considerations, the best element choice for the problem studied in this thesis is the linear (8-node) reduced-integration hexahedral element, wherever possible, to maximize accuracy and minimize computational cost. For the components with very complex geometries and much less significance (from an analysis purpose perspective), 10-node tetrahedral elements may be employed. Specifically, for the OPGW model, the inner and outer helical wires, as well as the central aluminum tube are all modeled with 3-D 8-node hexahedral elements with “uniform reduced integration and hourglass control”. The spacer is modeled with 3-D 10-node tetrahedral elements. It is also necessary to mention that, due to the thin shell geometric feature of the central tube, it was modeled with shell elements in the work of Roshan Fekr (1999). Thus, the corresponding contact interactions were formulated on the mid-surface of the shell, while in reality, contact occurs on the two-sided shell surfaces. Therefore, in the present study, solid elements are also employed for the tube. For comparison purposes, the element selections for the OPGW stress analysis with the previous coarse model (Roshan Fekr, 1999) and this refined model are summarized in Table 3.3.

Table 3.3 Element selections for the OPGW stress analysis FE models

Components	Element selections and integration schemes	
	Coarse model	Refined model
Outer wires	3-D 8-node hexahedral element (full-integration scheme)	3-D 8-node hexahedral element (reduced-integration scheme)
Inner wires	3-D 8-node hexahedral element (full-integration scheme)	3-D 8-node hexahedral element (reduced-integration scheme)
Central tube	4-node thin shell element (full-integration scheme)	3-D 8-node hexahedral element (reduced-integration scheme)
Spacer	3-D 8-node hexahedral element (full-integration scheme)	3-D 10-node tetrahedral element (full-integration scheme)

Designing a mesh is the second step in FE modeling work after the element types are selected. While coarse meshes may be adequate to predict trends of a mechanical response and to compare structural behavior under different loads, the magnitudes of the results calculated with a coarse mesh are usually not dependable, especially for a real structure and complex nonlinear problems. A fine mesh is certainly required for accurate modeling, and mesh convergence study is often necessary to ensure the solution accuracy from a mesh discretization perspective. In fact, it was shown that the coarse mesh produced in previous work was not fully capable of presenting the subtle stress variations inside the OPGW cable strand and capturing the stress gradients in the regions near the contact interfaces, and a fine mesh is therefore imperative to obtain sufficient accuracy.

It is well understood that the greater the mesh density, the more accurate the FE analysis results, which trend to converge to a unique solution. However, the structural characteristics and the high nonlinearities of the OPGW model complicate its mesh refinement. A very fine mesh for the spacer turns out to be impracticable as the resulting deformed mesh under large kinematics becomes severely distorted (elements with negative *"Jacobian"* [6]), not only deteriorating the results but also becoming a bottle-neck to obtain a converged solution, which implies a limit for its mesh size. Our numerical experiments have also shown that very fine meshes on the inner and outer wire contact interfaces may reduce significantly the rate of convergence, and could even jeopardize convergence. Hence, the effects of mesh refinement on convergence and accuracy have to be investigated.

In addition, the mesh shape has been given careful consideration. A radial mesh for the cable wires was designed in previous work (Figure 3.8). However, recent studies indicated that radial grids would not perform well in the implementation of numerical methods for partial differential equations (PDEs) in circular or spherical domains, in that the solution accuracy close to the center is poor; some numerical difficulties may also arise at the circular/spherical center where all the radial grid lines intersect (see for example, Calhoun et al., 2008). An alternative approach that is well suited to discretizing such regions is to use quadrilateral grids (Topping et al., 2002; Liseikin, 2009). Consequently, the mesh schemes for the inner and outer conductor wires are completely re-designed (Figure 3.9) rather than following the same pattern as in the previous coarse model.

---

[6] Badly distorted element may result in the negative determinant of the element geometric transformation matrix, known as "*Jacobian matrix*", during its volume integral, and consequently the computation will be terminated prematurely (Hughes, 2000).

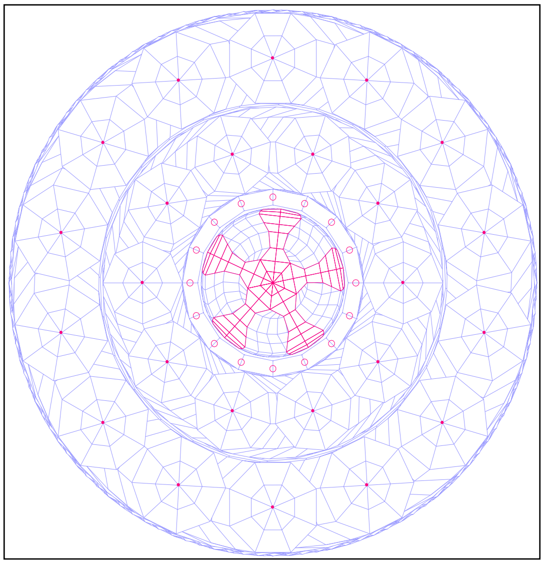

Figure 3.8 Cross-section meshing in the coarse model

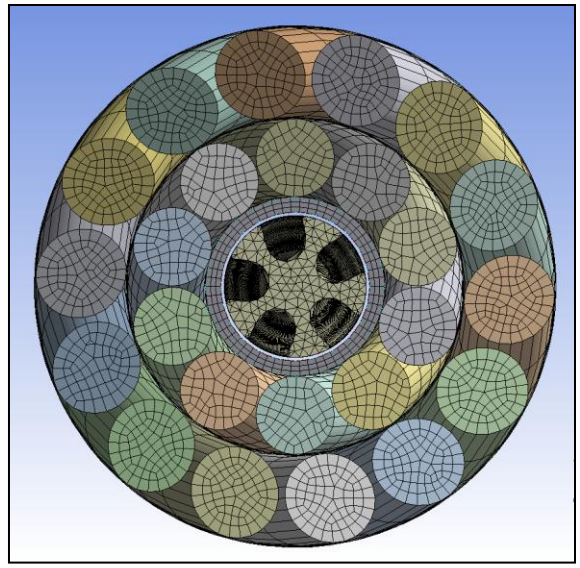

Figure 3.9 Cross-section meshing in the refined model

Another related issue that has been studied empirically in this thesis is the error analysis for the mesh convergence. Error estimation from mesh discretization for a finite element computation is a vast and rich subject that has been extensively investigated since the 1970s, from both the engineering mechanics and the applied mathematics perspectives (Szabo and Babuška, 1991, 2011). In close connection to this subject, those well-known *"adaptive"* FE technologies may immediately come to mind. In effect, performing an automated adaptive meshing has become nowadays a standard consideration when tackling the mesh convergence issue. Despite the present popularity of adaptive mesh refinement (when dealing with linear problems) and the fast development of the so-called *h-version*, *p-version*, and *hp-version* (Babuška, 1988; Babuška and Suri, 1990), error-controlled adaptive finite element mesh design for nonlinear solid and structural mechanics problems (especially for 3-D elasto-plasticity deformations and contact problems) is still very challenging (Stein, 2003; Wriggers, 2006, 2008). The construction of adaptive schemes for nonlinear problems and the robustness of the corresponding algorithms are nowadays research topics that are beyond the scope of this thesis. Of course, the reliable software implementations of adaptive FE methods for nonlinear problems in the general purpose FE codes are far from mature and need to be further developed (Stein et al., 2005). Furthermore, one great difficulty in practical applications is that, the execution of an adaptive method for a large size nonlinear problem with a complex structure (like the cases in this thesis) is not yet affordable (for practical design) due to the resulting extremely high numerical cost during the adaptive refinement, which is an iterative solution process starting from a initial "base" mesh. And last but not least, for a 3-D analysis, the current adaptive techniques can perform well only with tetrahedral mesh shape (In ANSYS for example, an adaptive refinement starting from a hexahedral or hex-dominant mesh will result in re-meshing of the structure with pure tetrahedrons.), while adaptive mesh resizing algorithms for pure hexahedral mesh may be not only very slow to converge due to the larger number of re-meshing iterations that are required, causing an excessively expensive adaptive process, but also very prone to arise singularities to fail the process in achieving the target error. In view of all the above considerations, adaptive meshing strategies are not employed during the FE analysis conducted in this thesis. Instead, the mesh convergence studies have been performed empirically by numerical experiments to control the mesh discretization errors.

The "structural error" examined in this thesis is the error estimate based upon the difference between smoothed stresses within the domain and the stresses actually calculated by the FEM for each element in the mesh. The values are expressed in (strain) energy norm calculated for each element. In other words, using numerical experiments with gradually denser meshes, errors are computed in energy norm, and the "exact" energy norm[7] and the finite element energy norm are compared. The relationship between these two energies is then considered in the light of an error theory used, and the so-called *"posteriori"* error is estimated using a specific estimator, as explained later.

In general, we do not know the exact stresses and strains of a real problem, and the displacement-based FE formulations yield discontinuous stress and strain fields, which are not true in the real physical phenomenon. Although piecewise continuous stresses and strains inside the elements can be obtained from direct FE computations, they are generally discontinuous across the element boundaries. For a homogeneous domain, they

[7] "exact" energy norm means the energy norm of the continuous estimate of the exact energy of a real problem using some specific error estimation theory.

are expected to be continuous since a continuous estimate of the exact stresses and stains is obviously more accurate than the piecewise estimates. To this end, various methods have been proposed to obtain "smoothed" nodal stresses and strains that will yield a continuous solution over the domain. The most common approach in early FEM development was simply an averaging based on the number and/or size of elements contributing to a node. That is, the continuous nodal stresses and strains are obtained by averaging the values from surrounding elements. However, this simple averaging process does not have any mathematical foundation relative to the original problem and thus is not proper to construct an effective error estimator (Akin, 2005). Many error estimation methods were therefore proposed in recent years. Even though up to now there is no error estimator that is the "best" under all circumstances (Babuška et. al., 2011), some estimators have been successful in solid mechanics applications: (1) residual-based error estimators (Babuška and Rheinboldt, 1978; Ainsworth and Oden, 1993), which are very frequently used for elastic solid mechanics problems; (2) error estimators based on "Super-convergent Patch Recovery" (SPR) techniques developed by Zienkiewicz and Zhu (1987, 1990, 1992). The ZZ method shows a practical way to achieve accurate continuous (smooth) nodal stresses and strains, and thus it has been used in many FE codes; and (3) error estimators based on "dual principles" (Becker and Rannacher, 1996), which have been applied to contact problems (Wriggers, 2006, 2008). All these error estimators were firstly developed for elasticity problems and then were extended to some nonlinear applications. The essential features of the error estimation method for 3-D stress analysis in ANSYS (2007) that is used to perform the mesh convergence study in this thesis are outlined below:

The element nodal stresses are firstly averaged based on the ZZ method. The smoothed nodal stresses and strains from the SPR process are denoted by $\{\sigma\}$ and $\{\varepsilon\}$, which are constructed to be continuous across element boundaries. Let $\{\sigma^*\}$ and $\{\varepsilon^*\}$ be the nodal stresses and strains calculated directly from FEM, which are discontinuous across those boundaries. So, the stresses and strains errors at a node can be written as:

$$\{\Delta\sigma\} \approx \{\sigma\} - \{\sigma^*\}; \quad \{\Delta\varepsilon\} \approx \{\varepsilon\} - \{\varepsilon^*\} \tag{3.1}$$

Then, returning to element level, the structural error energy norm $\| e \|_e$ for each element, which also corresponds to the so-called $\boldsymbol{L_2}$ norm in a finite element space, is defined as:

$$\| e \|_e = \left[\frac{1}{2}\int_{\Omega}(\{\varepsilon\}-\{\varepsilon^*\})^T \cdot [D]\cdot(\{\varepsilon\}-\{\varepsilon^*\})d\Omega\right]^{\frac{1}{2}} \tag{3.2}$$

$$= \left[\frac{1}{2}\int_{\Omega}(\{\varepsilon\}-\{\varepsilon^*\})^T \cdot(\{\sigma\}-\{\sigma^*\})d\Omega\right]^{\frac{1}{2}} \tag{3.3}$$

$$= \left[\frac{1}{2}\int_{\Omega}\{\Delta\varepsilon\}^T \cdot\{\Delta\sigma\}d\Omega\right]^{\frac{1}{2}} \tag{3.4}$$

$$= \left[\frac{1}{2}\int_{\Omega}\{\Delta\sigma\}^T \cdot[D]^{-1}\cdot\{\Delta\sigma\}d\Omega\right]^{\frac{1}{2}} \tag{3.5}$$

where:

$\{\sigma\}$ and $\{\varepsilon\}$= smoothed stress and strain vectors at a node of an element;

$\{\sigma^*\}$ and $\{\varepsilon^*\}$= nodal stress and strain vectors calculated directly from FEM;

$\{\Delta\sigma\}$ and $\{\Delta\varepsilon\}$ = stress and strain error vectors at a node of an element;

[D] = stress-strain matrix;

Ω = volume of an element.

So, the structural error energy norm over the entire (or a selected part of the) model is:

$$\| e \| = \sum_{i=1}^{N}\|e\|_e \tag{3.6}$$

where:

N = number of elements in the entire model or a selected part of the model

A relative percentage structural error in energy norm against the strain energy can be defined as:

$$\eta = 100 * \frac{\|e\|}{U+\|e\|} \tag{3.7}$$

where:

η = percentage error in energy norm;

U = strain energy over the entire (or a selected part of the) model. ■

By trial and error through many numerical experiments, an optimal fine meshing scheme for the OPGW model with good solution accuracy is achieved, as shown in Table 3.4 and Figures 3.10 and 3.11. The global structural error over the entire OPGW model due to mesh discretization is well controlled to remain below 5% (based on linear elastic analysis). At the middle cross-section of the OPGW model, the main location of interest in this study, the structural error is only 1.4 % (Figure 3.12). For comparison purposes to illustrate the gains in accuracy of the meshing scheme, the mesh results in the previous coarse model are also summarized in Table 3.5.

Table 3.4 An optimal meshing scheme for the 19-mm OPGW fine model

<table>
<tr><th>Meshing scheme</th><th>Mesh summary</th></tr>
<tr><td>Global element size = 0.5 mm</td><td rowspan="7">Total nodes = 221,816
Total solid elements = 234,119
Total contact elements = 182,340
Total elements = 417,059 *****
(* Including 600 spring elements to stabilize the nonlinear solution)</td></tr>
<tr><td>Inner & Outer wires edge divisions = 24 each edge</td></tr>
<tr><td>Outer wires face element size = 0.40 mm</td></tr>
<tr><td>Inner wires face element size = 0.48 mm</td></tr>
<tr><td>Tube edge divisions = 60; Tube radial divisions = 3</td></tr>
<tr><td>Longitudinal direction sweep divisions = 90 (Bias = 3)</td></tr>
<tr><td>Spacer body element size = 1 mm</td></tr>
</table>

Table 3.5 Mesh summary of the 19-mm OPGW previous coarse model

<table>
<tr><th>Meshing scheme</th><th>Mesh summary</th></tr>
<tr><td>Inner & Outer wires: Total 16 elements on each wire cross-section</td><td rowspan="3">Total nodes = 15,087
Total solid elements = 12,672
Total shell elements = 448
Total elements = 13,120</td></tr>
<tr><td>Central Tube: Total 16 shell elements on cross-section (1 element through thickness)</td></tr>
<tr><td>Longitudinal direction sweep division = 28</td></tr>
</table>

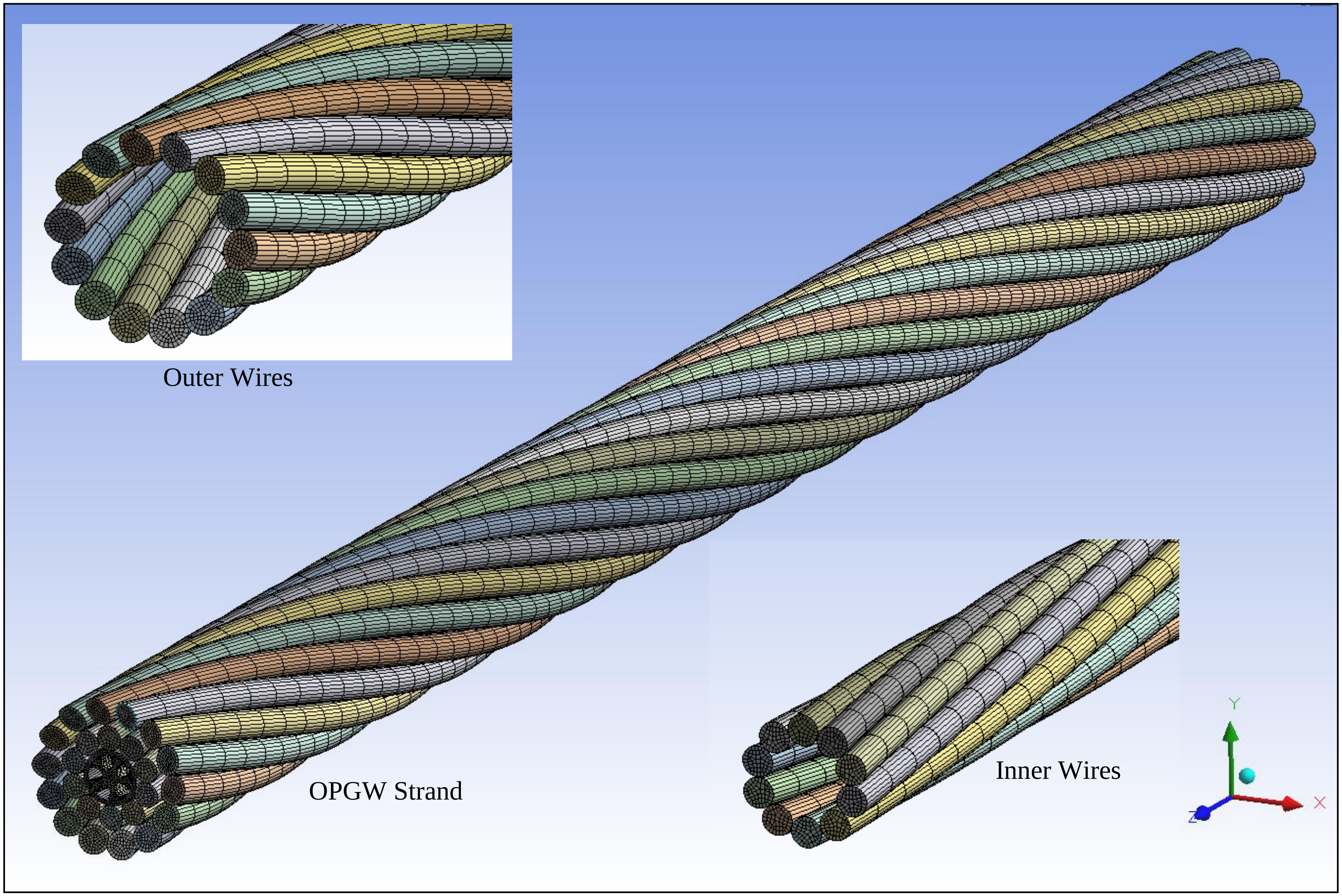

Figure 3.10 Finite element fine mesh of the 19-mm OPGW cable strand - 265.16 (mm)

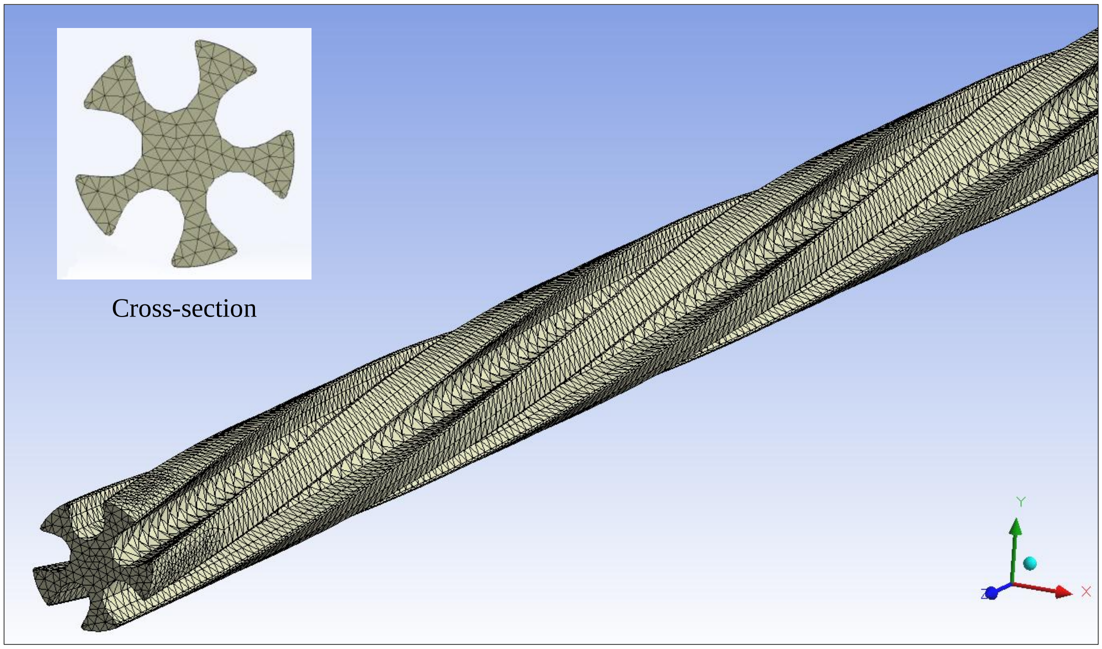

Figure 3.11 Finite element fine mesh of the aluminum spacer

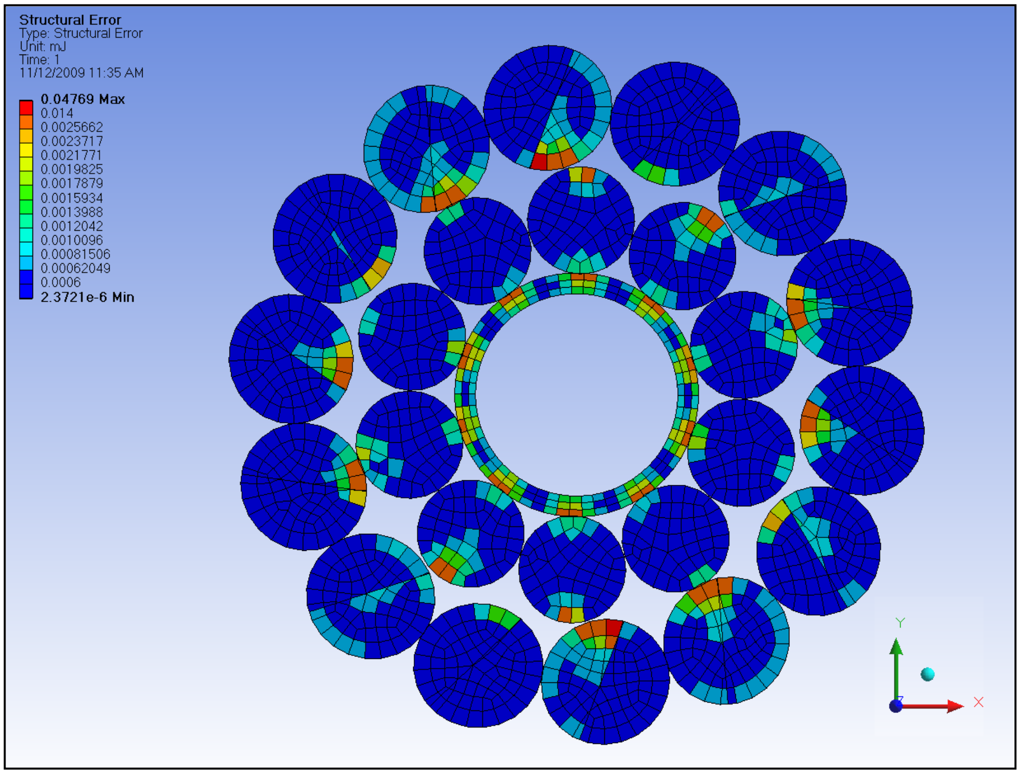

Figure 3.12 Structural error of the OPGW refined model due to mesh discretization

3.3.3 Contact Conditions

The comprehensive contact interactions amongst the OPGW cable components are all considered as *"flexible-to-flexible"* deformable body contact, and *"surface-to-surface frictional"* contact type is defined on all contact regions. For each contact region, a *"contact pair"* is created and composed of "contact" and "target" surfaces, which are discretized with many contact elements. These 3-D 8-node surface-to-surface contact elements (CONTA174 in ANSYS) overlie the underlying solid elements like a "skin" on the surfaces of the contacting regions, providing the relationship among the components. Gauss integration points of the contact elements are designated as contact detection points as they may provide more accurate results than those using the nodes themselves (Cescotto and Charlier, 1992; Cescotto and Zhu, 1994). The classical Coulomb isotropic friction model is used with static frictional coefficient μ=0.33 (Davis, 1994) assigned for all contact surfaces. As a result, in total, 27 contact pairs (Table 3.6) and **182,340** contact elements are generated for the entire OPGW model.

Table 3.6 Surface-to-surface contact pairs of the OPGW model

Contact region	Contact pairs
Inner wires & Inner wires	10
Outer wires & Outer wires	14
Inner wires & Outer wires	1
Inner wires & Central tube	1
Central tube & Spacer	1

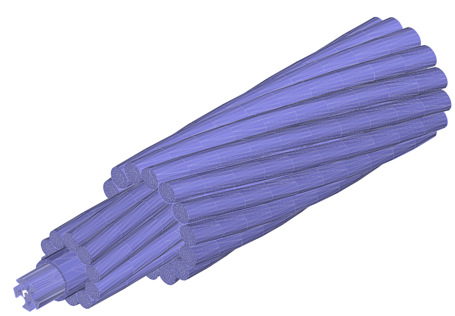

Achieving a robust converged solution to this large-size contact model with material and geometry nonlinearities was very challenging. In the context of contact settings[8], after exploring all important contact properties, it was found that the *"normal contact stiffness factor"* is the most critical and sensitive contact parameter affecting both convergence behavior and accuracy of the calculated response, and could only be examined by

[8] Numerical solution strategies for this highly nonlinear large-size problem will be addressed in Section 3.4.

numerical experiments to obtain a set of appropriate values. A high normal stiffness reduces contact penetrations physically [9] to yield better accuracy, but can result in ill-conditioning of the global stiffness matrix so that many equilibrium iterations have to be implemented for reaching convergence of residual force and displacement increment [10] in each load incremental step, and then the numerical instability ("oscillating" convergence) may eventually lead to outright divergence. Conversely, lower normal stiffness decreases solution accuracy, and very low convergence rate (even global divergence) may be caused due to excessive penetrations. (Many more iterations in each load incremental step are used only for "contact convergence" to within the penetration tolerances rather than for force and displacement convergence.) Many computational experiments had been therefore conducted to obtain appropriate contact stiffness factors. Moreover, it turned out that no uniform normal stiffness factor could work for the entire model, and different factors must be determined for each different contact region to overcome the convergence difficulty. By trial-and-error, a set of good "normal contact stiffness factors" for the OPGW model have been obtained, as shown in Table 3.7, which yielded satisfying convergence rate and solution accuracy. In addition, all normal and tangential contact stiffnesses are specified to be updated (raised, lowered or leave unchanged) after each equilibrium iteration based on the physics of the model (mean stress of the underlying elements, allowable penetrations, contact pressure, as well as slips). The benefit of updating contact stiffnesses throughout the solution is to further enhance robust convergence, while achieving minimal penetrations.

---

[9] Although contacting bodies do not interpenetrate physically, i.e. ensure the so-called "*contact compatibility"*, finite amounts of penetrations are required mathematically to generate contact forces at the interfaces to maintain equilibrium to implement the contact algorithm employed in the analyses.

[10] Residual force and displacement increment are two convergence criteria employed in the solution for nonlinear equations, which will be addressed in Section 3.4.2.

Table 3.7 Normal contact stiffness factors used in the OPGW model

Contact region	Normal contact stiffness factor	Resulting contact stiffness (N/mm^3)
Inner wires & Inner wires	0.002	3288
Outer wires & Outer wires	0.005	3163
Inner wires & Outer wires	0.005	3162
Inner wires & Central tube	0.5	3166
Central tube & Spacer	0.1	6350

3.3.4 Displacement Boundary Conditions and Loadings

In a static FE analysis, displacement boundary conditions (B.C.s) must be applied to constrain the model against rigid body motions in any direction; otherwise, unrestrained rigid body motions will cause the global stiffness matrix to be singular and stop the simulation prematurely. Displacement B.C.s and loadings applied on the OPGW model are in accordance with the ones used by Roshan Fekr (1999), but different means are taken for more accurate treatments.

In reality, the exact details of the attachment of a conductor to a transmission line tower vary with tower types. Inasmuch as possible, the continuity of the OPGW cable is assured and the cable is gripped in a suspension clamp. The stress and strain states in the cable are very complex in the vicinity of a clamp region and require a more delicate modeling, which is not the purpose of the analysis presented in this chapter [11]. On the other hand, from a structural design point of view, a very important consideration for conductor manufacturers is the OPGW tensile strength. Hence, the OPGW cable can be assumed under uniform tension far from its clamped ends. To model such a condition, one end of the cable segment is assumed completely fixed, i.e., at the fixed-end surfaces, the whole cable is fixed in all translational and rotational degrees-of-freedom (DOFs), while tensile loading is applied at the other end (free-end).

[11] Such a study has been carried out for an ACSR conductor, which will be discussed in-depth in Chapter 5.

From the laboratory tension test performed at Hydro-Québec's Research Institute (IREQ, 1994), corresponding to the maximum tension in normal operation set to **83.5 kN**, the equivalent cable elongation of the FE model is **0.61%** of the cable model length, i.e. **1.618 mm** ($\Delta l = \varepsilon l = 0.61\% \times 265.16 = 1.618\ mm$). In the test, it was not possible to ensure that the internal components of the OPGW (the inner wires, the central tube, and the aluminum spacer) deform the same as the external envelope (the outer wires) and the global cable elongation was only measured on the outer wires. However, for a short segment of a straight cable, the displacement compatibility can be assumed, that is, all components (the outer, inner wires, the tube, and the aluminum spacer) are assumed to stretch equally along the cable axis (z-axis). In this case, the direct "*load-control*" approach turned out to be improper. Neither a uniform distributed load on the cross section nor a concentrated load at the center of each component can achieve equal elongations due to the effects of contact, material differences, and the helical geometry. In other words, it would be necessary to find the exact axial forces applied to each component of the OPGW to generate equal stretch, which is obviously impracticable before the analysis. Therefore, the so-called *"displacement-control"* approach is used to apply the tensile load that ensures the displacement compatibility of the components. Specifically, on the model free-end surfaces, all components are assigned the same prescribed axial displacement, **1.618 mm**, while two in-plane translational DOFs (along x and y axes) of the wires are fixed to prevent unwinding of the cable wires. A distinction from the previous work is that the displacement is applied on the free-end surfaces of all cable components rather than to the interior nodes of the surfaces. Also, to circumvent the over-constraint due to the prescribed displacement and concurrent contact conditions on the perimeter nodes at the free-end cross-sections, the so-called *"Remote Displacement"* approach is used to apply the axial displacement on the entire free-end surfaces. This is a specific treatment in ANSYS Workbench to handle difficult B.C.s and help prevent convergence difficulties. It makes use of the *"Multi-Point Constraint"* (MPC) contact formulation that can override other contact settings or boundary conditions for the same degrees-of-freedom of selected nodes.

3.4 Numerical Solution Techniques

In the preceding section, the validation aspect of the OPGW FE modeling was discussed in detail, including element quality, mesh design and mesh convergence study, contact establishment, B.C.s and loads. In this section, the verification aspect of the numerical work will be addressed, i.e. the quality of the numerical strategies developed to solve this FE model.

ANSYS Workbench 11.0 x64-bit version (2007) was selected as the computing platform for all the FE models analysed in this thesis. All computations were implemented on a customized high-end Dell Precision T5500 Workstation with state-of-the-art computer hardware techniques. It features 24GB tri-channel DDR3 1333MHz memory, and a Shared-Memory Parallel processing (SMP) enabled Quad-Core Intel Xeon X5570 server processor, operating up to 2.93GHz with a full 8MB of L3 shared cache and a 6.4GT/s QPI link. Even with this powerful computing facility, solving the refined conductor FE models still proved very difficult and computationally demanding. One of the essential requirements for the solution method of a nonlinear analysis is its capability to overcome the potential numerical convergence and accuracy problems associated with the nonlinear behavior. Since there exists up to now no robust and efficient numerical solution method (solver) that can guarantee convergence and accuracy for all nonlinear solid mechanics problems (Wriggers, 2008), an optimal strategy may only be tailored to the physics and problem size of a specific application.

The key numerical solution techniques to solve the conductor FE models in this thesis involve computational contact algorithms, solution of nonlinear algebraic equations and solution for large linear algebraic systems. No attempt is made herein to deliver comprehensive reviews for any of these three areas, and each of them has been well documented by applied mathematicians and engineering researchers in the field of “computational science and engineering” (refer to Strang, 1986, 2007, in particular for enlightening and limpid presentations). Instead, since the scope of this research is computational modeling of real engineering problems, our attention is mainly focused on the discussion of the various optional techniques available in the ANSYS code. Indeed, they are all well-established algorithms from an applied mathematics perspective, and are also widely coded in other leading nonlinear FE software systems, such as ADINA (ADINA R&D, Inc. 2008), Abaqus (Dassault Systèmes, 2010), Marc (MSC Software Corporation, 2010), etc., to name the most widely used in North America. As such, the numerical strategies developed in this section serve essentially to form the building blocks of a reliable solution methodology to suit the class of problems studied in the thesis, no matter which FE code is chosen. Comparative studies and numerical experiments are conducted for the selections and configurations of a set of proper solution methods and their combinations for the OPGW FE model. The solution methodology developed successfully for the OPGW model has been applied later to other FE models in Chapters 4 and 5.

3.4.1 Contact Algorithms

Only a brief account of the mathematics and physics of "contact" will be presented below with the modest attempt to show the necessary background of "contact problems" to an extent that is germane to the computational implementation issues discussed in this section.

A contact problem is commonly called a changing-boundary-conditions nonlinearity from the structural analysis point of view. It may involve specific boundary conditions that govern the motion of the moving interfaces and possible boundary singularities. For typically encountered contact phenomena in solid continuum mechanics, such conditions usually refer to the impenetrability constraint, the action-reaction law (Newton's third law), and the surface friction law (such as the classical Coulomb's law). The normal contact constraint prevents mutual penetration of immiscible solid media, while the tangent contact constraints represent friction between the contacting bodies. It is well known that boundary-value problems can be formulated in differential, integral or variational forms. For the mathematical analysis of contact problems, the variational formulations, especially the formulations in terms of variational inequalities, play a central role (Stampacchia and Lions, 1967; Panagiotopoulos, 1985; Hlavacek et al., 1988;

Eterovic and Bathe, 1991). The contact boundary conditions can thus be treated as various constraints in the variational equations by means of Lagrange multipliers or penalty functions. Studies devoted to the theoretical foundations (such as existence and uniqueness) and mathematics of contact problems have been dealt with in depth in such monographs as Kikuchi and Oden (1988), Eck et al. (2005), Leine and Wouw (2008), Studer (2009), and Sofonea and Matei (2012).

For the solution of contact problems, historically, there have been an overwhelming number of publications on analytical formulations for (elastic) contact calculations that could be dated back to the famous work of Hertz (1882), and several classical monographs have been published to summarize these important analytical studies (Gladwell, 1980; Johnson, 1985; Goryacheva, 1998; Galin, 2008). As of the past half a century, extensive research on numerical contact analysis has been carried out around the world, a research domain that is currently called "computational contact mechanics" (Wriggers, 1999, 2006, 2008; Laursen, 1995, 2002); and this is still a very active research area with a great number of new numerical procedures being designed. The numerical solution of a contact problem generally involves two aspects: (a) perform a contact search (contact detection) procedure to identify the regions that possibly can come into contact and (b) impose appropriate conditions to prevent the penetration and correctly calculate the contact interactions between the contact bodies. Up to now, these numerical approaches mainly include boundary element methods (Takahashi, 1991; Aliabadi and Brebbia, 1993; Eck et al., 1998, 1999), mathematical programming methods (Conry and Seireg, 1971; Klarbring, 1986, 1988; Bjorkman et al., 1995; Zhang et al., 2006), finite element methods (Kardestuncer and Norrie, 1987; Crisfield, 1997; Belytschko et al., 2000; De Borst et al., 2012; Yastrebov, 2013), meshless methods (Belytschko et al., 1994, 1996; Gunther and Liu, 1998), and more recent mortar methods (McDevitt and Laursen, 2000; Puso and Laursen, 2004; Yang, 2009). Finite element contact algorithms play the dominant role in computational analysis of practical engineering contact applications.

Since all contact algorithms virtually provide only approximate solutions, it is easy to understand that they may have different strengths and limitations to tackle different contact situations; that is, no algorithm can solve all problems. The simultaneous existence of numerous contact algorithms has clearly indicated this point. Meanwhile, the choice of an appropriate algorithm for a specific application is important due to its effects on solution accuracy and computational cost. Hence, a comparative evaluation of various contact algorithms is necessary when conducting a contact analysis. In effect, this turned out to be a critical issue in this thesis due to the physics and problem size of the conductor FE models. Here again, the following discussions on the contact algorithms are from the "practical problem solving" perspective rather than in the form of computational mathematics. The performance and the salient characteristics of the algorithms will be discussed to present useful engineering insights based the author's numerical experiences, while detailed mathematical formulations are omitted.

For *surface-to-surface* static and quasi-static contact[12] (as described in Section 3.3.3), several different contact types can be defined according to the configurations of contact regions, as summarized in Table 3.8. Consequently, the contact solutions can be either linear or nonlinear. The simplest contact type is usually called "*bilateral contact*", including "Bonded" and "No Separation" contact. For "Bonded" contact, the contact region is considered as bonded ("glued") from the very beginning and throughout the entire analysis, so no separation and sliding between contact surfaces are allowed. "No Separation" contact can be considered in such cases: No separation of contact surfaces occurs again during the analysis once the initial gap is closed under the loads, but very small amounts of tangential frictionless sliding are allowed. The "bilateral contact" allows for a linear solution since the contact status will not change during the load history. Three other contact types ("Rough", "Frictionless", and "Frictional") are often referred to as the so-called "*unilateral contact*", in which separations (gaps) could occur between contact bodies depending on loading and the normal contact pressure vanishes if separations happen. The case of "Rough" unilateral contact corresponds to the theoretical case of an infinite frictional coefficient ($\mu=\infty$) between the contacting bodies, so no sliding is allowed while separation can happen under loading. "Frictionless" means the

[12] Dynamic contact problems (such as impact) are beyond the scope of this thesis. Correspondingly, the explicit algorithms that are usually best suited to dynamic contact will not be addressed and can be referred, for example, in Zhong et al. (1993, 1994). Only implicit algorithms are discussed herein.

theoretical case of a zero coefficient of friction (μ=0), thus allowing free sliding. "Frictional" contact is the most difficult (and realistic) case: The contacting surfaces can carry tangential shear stresses across their interfaces, and may slide relative to each other with any friction coefficient. All solutions for "unilateral contact" are nonlinear because the contact areas may change with the varying loads, i.e. the so-called "boundary nonlinearity". In particular, three-dimensional multi-body frictional contact generally exhibits a very strong nonlinearity to arrive at a converged solution because both the normal and tangential contact stiffnesses may change significantly with the changing contact status, and the non-predictable sliding paths further greatly complicate the solution process. Actually, by monitoring the computational implementations of the conductor models, it was observed that most of the computer runtime had been spent on the contact search and the calculations of slide directions and contact tractions (contact pressure and frictional stress).

Table 3.8 Summary of *surface-to-surface* contact types

Contact types		Contact status under loading			
		Separation (Gap)	Slide: Frictionless (free, μ = 0)	Slide: Frictional (μ)	Contact solution
Bilateral Contact	Bonded	x	x	x	linear
	No Separation	x	√	x	linear
Unilateral Contact	Rough	√	x	x	nonlinear
	Frictionless	√	√	x	nonlinear
	Frictional	√	√	√	nonlinear
Note: x: not allowed; √: allowed.					

In finite element contact analysis, contact algorithms have to be implemented within every incremental load step to enforce contact compatibility at the contact interfaces. This implementation is incorporated into the solution scheme for the nonlinear equilibrium equations and is of essential importance for the global convergence and efficiency. Five different implicit contact algorithms are available in ANSYS code for static and quasi-static contact:

- Pure penalty method (Kikuchi and Oden, 1988)
- Pure Lagrange multiplier method (Francavilla an Zienkiewicz, 1975)
- Augmented Lagrangian method (Simo and Laursens, 1992)
- Normal Lagrange multiplier method (Wriggers, 2006)
- Multi-Point Constraint method (Abel and Shephar, 1979)

(1) Pure penalty method (PM)

The pure penalty method is the most widely used contact algorithm (Wriggers, 2006) as it is coded in most commercial nonlinear finite element analysis systems. Essentially, it introduces penalty functions (penalty parameters) in contact variational formulations, and a penalty parameter behaves as a uni-directional contact "spring" to establish the relationship between two contact surfaces. The spring stiffness is called the contact stiffness. So, this method requires both normal and tangential contact stiffnesses. Assuming the frictional plane with normal x, the contact traction vector can be written as:

$$\{P, \tau_{sy}, \tau_{sz}\}^T \tag{3.8}$$

where:

P = normal contact pressure, which represents the normal contact conditions

τ_{sy}, τ_{sz} = tangential contact stress in y, z directions, which represent the frictional contact conditions

The normal contact pressure is defined as:

$$P = 0 \qquad \text{if } u_n > 0 \tag{3.9}$$

$$P = K_n * u_n \qquad \text{if } u_n \leq 0 \tag{3.10}$$

where K_n is the normal contact stiffness per unit contact width, and u_n is the contact gap.

The frictional contact stress in the yz plane can be defined by Coulomb's law:

$$\tau_s = K_s * u_s \qquad \text{if } \tau_s = \sqrt{\tau_{sy}^2 + \tau_{sz}^2} - \mu * P < 0 \quad \text{(stick)} \tag{3.11}$$

$$\tau_s = \mu * K_n * u_n \qquad \text{if } \tau_s = \sqrt{\tau_{sy}^2 + \tau_{sz}^2} - \mu * P = 0 \quad \text{(slide)} \tag{3.12}$$

where K_s is the tangential contact stiffness, u_s is the contact slip distance, and μ is the coefficient of friction.

The main drawback of this method is that the amounts of penetration between two contact surfaces strongly depend on the contact stiffness. It is clear from equation (3.10) that higher normal contact stiffness values decrease the amount of penetration for a given contact pressure. Physically, the penetration should be zero, but then equation (3.10) would result in the contact stiffness being infinite. While a very small penetration is required mathematically to obtain the contact pressure and achieve sufficient solution accuracy, a too high K_n can lead to ill-conditioning of the global stiffness matrix and to convergence difficulty because any small variation of penetration Δu_n yields a very large change in contact pressure ΔP. On the other hand, a too low K_n can cause an excessive penetration, which would not only deteriorate the contact results, but also jeopardize convergence as it will be difficult to meet the criterion of "contact compatibility". In addition, due to the practical difficulties of iterative solvers to solve ill-conditioned matrices, direct solvers are recommended to be used with this method.

(2) Pure Lagrange multiplier method (PLM)

Lagrange multipliers are used on both normal and tangent contact conditions. Instead of solving the contact pressure and frictional contact stress in a displacement-based manner as in penalty-based methods, they are treated as separate (additional) DOFs (Lagrange multipliers), which means that they are solved directly. The benefit of such a treatment is that the impenetrability condition can be satisfied without dealing with any "contact stiffness": It enforces "zero penetration" when contact is closed and "zero slip" when sticking contact occurs. As a result, PLM does not require normal and tangential contact stiffnesses as control parameters, and thus the problems induced from penalty-based methods are bypassed. However, "*chattering*", which is defined as the effect of abrupt changes in the contact status, may have to be controlled. In the mathematical treatment with PLM, it requires two "chattering" control parameters: a maximum allowable penetration tolerance, *e*, and a maximum allowable normal contact pressure, P_{max}, to provide stability to the contact models. Even so, this method might still experience "chattering" problems due to contact status changes between open and closed or between sliding and sticking. In addition, as it adds contact traction components (i.e., Lagrange multipliers) to the model as additional variables for each contact element and thus additional iterations are required, consequently it increases the computational cost. Moreover, PLM introduces zero diagonal terms in the stiffness matrix, so iterative equation solvers cannot perform well with this method and thus only direct solvers are suggested to be used with this method.

(3) Augmented Lagrangian method (AL)

The Augmented Lagrangian contact algorithm is essentially a penalty-based method with penetration control using Lagrange multipliers (Simo and Laursens, 1992, 1993; Laursen and Oancea, 1994). It uses an iterative series of penalty methods with the penalty updates to find the Lagrange multipliers (i.e., unknown contact tractions) to enforce contact compatibiltiy. Different from the pure penalty method, the normal contact pressure can be defined by:

$$P = 0 \qquad \text{if } u_n > 0 \tag{3.13}$$

$$P = \lambda_{i+1} \qquad \text{if } u_n \leq 0 \tag{3.14}$$

where:

$$\lambda_{i+1} = \lambda_i + K_n{}^* u_n \qquad \text{if } |u_n| > e \tag{3.15}$$

$$\lambda_{i+1} = \lambda_i \qquad \text{if } |u_n| < e \tag{3.16}$$

e is the user-defined contact compatibility tolerance, and λ_i is the Lagrange multiplier component of contact pressure at equilibrium iteration i., which is computed locally (for each contact element) and iteratively (during each equilibrium iteration).

From equations (3.14) ~ (3.16), if the penetration at a given equilibrium iteration exceeds this maximum allowable penetration tolerance (*e*), the contact stiffness for each contact element is augmented with its Lagrange multipliers for contact tractions. This process is repeated until the contact penetration is smaller than the allowable tolerance *e*.

As a result, the augmented Lagrangian method overcomes some of the shortcomings of both the pure penalty method and the pure Lagrange multiplier method. Compared with the pure penalty method, AL has less degree of ill-conditioning (better conditioning) and less sensitivity to the magnitudes of both normal and tangential contact stiffness due to the improved "selection" of the contact stiffnesses for each element. Compared with the pure Lagrange multiplier method, AL has less "chattering" caused by abrupt changes in contact status and its stiffness matrix is always positive definte, and thus both iterative and direct solvers can work well with this algorithm. In some cases, AL may require additional equilibrium iterations due to the penetration control, especially if the deformed mesh becomes excessively distorted.

(4) Normal Lagrange multiplier method (NLM)

This is the method that Lagrange multiplier method is applied on the normal contact pressure and a pure penalty method on the tangential contact stress conditions. This method enforces "zero penetration" when contact is closed (Normal contact stiffness is thus not applicable) and allows only a minute amount of slip for a sticking contact condition. While NLM still requires "chattering" control parameters, as well as a maximum allowable elastic slip parameter, u_{smax}, it overcomes some of the "chattering" problems of the pure Lagrange multiplier method (i.e., has an enhanced convergence in tangential direction). Therefore NLM can handle frictional contact problems with small sliding better than the pure Lagrange method. Compared to the Augmented Lagrange method, NLM often has an increased computational cost as it adds contact tractions to the model as additional DOFs and thus requires additional iterations to stabilize their associated contact conditions. Similar to PLM and PM methods, iterative equation solvers cannot perform well with this method and only direct solvers are suggested.

(5) Multi-Point Constraint method (MPC)

In this method, an internal multipoint constraint algorithm based on contact kinematics is used to create the multipoint constraint equations to tie the contact surfaces, and the degrees of freedom of the contact surface nodes are eliminated. No normal and tangential contact stiffnesses are required. For small deformation problems, this represents true linear contact behavior and no iterations are needed to solve the system of equations. For large deformation problems, the MPC equations are updated during each equilibrium iteration to overcome the small strain restriction. This method only works for “Bonded” and “No Separation” contact surface behavior, and thus is not applicable to frictional contact problems.

Based on the foregoing comparative study of the pros and cons of several contact algorithms and on our numerical experiments using all the above available options, the **Augmented Lagrangian method** was finally selected. The AL method proved the best choice to yield a stably convergent solution process with accurate results for frictional sliding contact analysis of the OPGW FE model, while the other options led to either convergence difficulties or inaccurate results.

3.4.2 Solution for Nonlinear Algebraic Equations

For a nonlinear FE computaion, the fundamental problem is to find the state of equilibrium of a system corresponding to the applied loads and boundary conditions. Assuming that the external loads are described as a function of time, the equilibrium conditions of the finite element model can be expressed as

$$ {}^{t}\mathbf{R} - {}^{t}\mathbf{F} = \mathbf{0} \qquad (3.17) $$

where ${}^{t}\mathbf{R}$ is the vector of external nodal forces at time t, and ${}^{t}\mathbf{F}$ is the nodal stress resultants, i.e. the nodal forces that correspond to the element stresses.

The equilibrium relation in equation (3.17) represents a system of nonlinear algebraic equations stemming from the finite element discretization. It includes all nonlinearities of the model and must be satisfied throughout the complete load history. It should be noted that, for a static time-independent problem, time is only a convenient variable to denote the load and solution history (load steps) rather than an actual variable in a dynamic analysis or a static time-dependent problem (such as creep) to describe the actual physical situations with a real time concept. The use of the time variable in a nonlinear solution process therefore represents a very general approach for all types of nonlinear problems.

A nonlinear analysis is carried out using a step-by-step incremental solution process with a number of time steps (or load steps) to finally reach the total applied loads. The basic idea is to obtain the solution for discrete time t+Δt, while the solution for the discrete time t is known. Δt is a properly chosen time/load incremental step. Hence, equation (3.17) at time t+Δt becomes

$$^{t+\Delta t}\mathbf{R} - {}^{t+\Delta t}\mathbf{F} = \mathbf{0} \tag{3.18}$$

Since the solution is known at time t, $^{t+\Delta t}\mathbf{F}$ can be written as:

$$^{t+\Delta t}\mathbf{F} = {}^{t}\mathbf{F} + \mathbf{F} \tag{3.19}$$

where **F** is the incremental nodal force vector (stress resultant) that corresponds to the increment in element displacements and stresses from time t to t+Δt. In nonlinear FE methods, the approximation of **F** can be made using a tangent stiffness matrix $^{t}\mathbf{K}$, which encompasses the geometric, material and contact conditions of the model at time t:

$$\mathbf{F} \approx {}^{t}\mathbf{K}\mathbf{U} \tag{3.20}$$

where **U** is the incremental nodal displacement vector.

Substituting equations (3.19) and (3.20) into (3.18):

$$^{t}\mathbf{K}\mathbf{U} = {}^{t+\Delta t}\mathbf{R} - {}^{t}\mathbf{F} \tag{3.21}$$

and then solving for **U** yields an approximation of the nodal displacements at time t+Δt:

$$^{t+\Delta t}\mathbf{U} \approx {}^{t}\mathbf{U} + \mathbf{U} \tag{3.22}$$

As equation (3.20) is used, $^{t+\Delta t}\mathbf{U}$ is an approximation to the exact nodal displacements at time t+Δt that correspond to the external loads $^{t+\Delta t}\mathbf{R}$. The approximated element stresses and resulting nodal forces at time t+Δt can then be evaluated before proceeding to the next time step. Obviously, the approximation errors may be significant depending on the time step size. Therefore, an iterative solution process is required to solve equation (3.18) to obtain satisfactory accuracy.

The most commonly used iteration methods for the solution of nonlinear algebraic equations in a nonlinear FE analysis is the *"Newton-Raphson"* technique and its variants. Corresponding to the above formulations, the equations used in Newton-Raphson iterations (Bathe, 1996) can be written as follows, for iterations i = 1, 2, 3, ...

$$\Delta\mathbf{R}^{(i-1)} = {}^{t+\Delta t}\mathbf{R} - {}^{t+\Delta t}\mathbf{F}^{(i-1)} \tag{3.23}$$

$$ {}^{t+\Delta t}\mathbf{K}^{(i-1)}\,\Delta\mathbf{U}^{(i)} = \Delta\mathbf{R}^{(i-1)} \tag{3.24}$$

$$ {}^{t+\Delta t}\mathbf{U}^{(i)} = {}^{t+\Delta t}\mathbf{U}^{(i-1)} + \Delta\mathbf{U}^{(i)} \tag{3.25}$$

with the initial conditions

$$ {}^{t+\Delta t}\mathbf{U}^{(0)} = {}^{t}\mathbf{U}; \quad {}^{t+\Delta t}\mathbf{K}^{(0)} = {}^{t}\mathbf{K}; \quad {}^{t+\Delta t}\mathbf{F}^{(0)} = {}^{t}\mathbf{F} \tag{3.26}$$

These equations are obtained by linearizing the response of the FE model about the conditions at time t+Δt, while the conditions at (i-1) are obtained by solving the system of linearized equations in (3.24). In each iteration, the residual or out-of-balance load vector $\Delta\mathbf{R}^{(i-1)}$, which expresses the system "force error" in predicting the nodal stress resultants (hence the nodal force imbalance), is calculated that yields a displacement increment $\Delta\mathbf{U}^{(i)}$ when solving (3.24). If $\Delta\mathbf{R}^{(i-1)}$ corresponds to an external load vector ${}^{t+\Delta t}\mathbf{R}$ that is not yet balanced by element stress resultants, then an increment in the nodal displacements is required. This updating of the nodal displacements ${}^{t+\Delta t}\mathbf{U}^{(i)}$ in the iteration is continued until the out-of-balance loads and corresponding incremental displacements are smaller than a predetermined error tolerance threshold. This method is called a *"Full Newton-Raphson"* scheme in the sense that the tangent stiffness matrix, ${}^{t+\Delta t}\mathbf{K}^{(i-1)}$, is recalculated at every time step and every iteration within a time step.

Different variants of Newton's method have been developed (Kelley, 2003; Quarteroni et. al., 2007) to save computational effort in the evaluation of the tangent stiffness matrix, such as the "Modified Newton-Raphson method", "Quasi-Newton method", "Damped

Newton method”, etc., and the effectiveness of these methods depends on the degree of nonlinearity of specific applications and the problem size. In our work, the “Full Newton-Raphson” method is chosen due to its proven robustness in terms of convergence (Bathe, 1996) despite its higher computational cost.

Frictional contact yields a non-symmetric tangent stiffness matrix in the Newton-Raphson method due to the non-associative character of the frictional constitutive equations (Wriggers, 2008). In view of the fact that an unsymmetric solver is generally more computationally expensive than a symmetric solver, some symmetrization algorithms were developed, such as the famous one by Laursen and Simo (1993), so that a frictional contact problem can be solved still using those solvers for symmetric systems. However, when frictional effects are substantial, i.e. when frictional stresses have a significant influence on the displacement fields and the magnitude of the frictional stresses are highly solution-dependent, any symmetric approximation to the stiffness matrix may lead to a low rate of convergence. From our numerical experiences, it turned out that, in the case of the OPGW FE model, the use of an unsymmetric solver proved more computationally efficient.

As a result, the scheme of “**Full Newton-Raphson**” with support for **unsymmetric** matrix is employed for our OPGW stress analyses, in which the tangent stiffness matrix is updated at every equilibrium iteration. In addition, it generates and uses unsymmetric matrices for the frictional contact analyses.

Another important issue related to the solution of nonlinear equations is the selection of realistic convergence (error tolerance) criteria in relation to the out-of-balance nodal forces and incremental displacements, which will have to be imposed to terminate the iterations. A suitable pre-defined convergence tolerance needs to be used as a check at the end of each iteration to determine whether equilibrium is reached or more iterations are still necessary within that time step. Too loose a tolerance may result in inaccurate results, while a too stringent one may be very costly. Ideally, an energy-based convergence criterion would be the most attractive for this work, such as the one proposed by Bathe and Cimento (1980). In that criterion, the amount of work done by the out-of-balance loads on the displacement increment is compared with the initial internal strain energy increment during each iteration. Unfortunately, such an option is not available in ANSYS, so a compromise had to be made. As a result, **both force and displacement convergence criteria** are used: The iterations within a time step will terminate only when both the residual force and displacement increment are smaller than their set tolerances. Therefore the solution must satisfy two individual criteria rather than a “combined” one in the form of residual strain energy.

3.4.3 Solution for Large Linear Algebraic Equations

A linear equation solver may have substantial influence on the accuracy and efficiency of the solution of a nonlinear finite element analysis. This is due to the fact that linearization is a key component in iterative solution schemes. A nonlinear iterative procedure (a series of iterations for the system equilibrium) is accomplished via the solutions of successive linear sub-problems. Specifically, for the implementation of the “Full Newton-Raphson” scheme, a linear equation system of full size has to be solved in each iteration step *i*, thus becoming a very time consuming part in a large nonlinear FE computation.

Two classes of methods to solve the system of simultaneous linear algebraic equations are *iterative methods* and *direct methods* (not requiring iterations), and the effectiveness of a method depends on the character and size of the problem under consideration. The fundamental theories and algorithms about these linear solvers have been well established and thoroughly documented in many excellent numerical linear algebra textbooks, such as the ones by Golub and Van Loan (1996), Quarteroni and Valli (1997), Demmel (1997), Trefethen and Bau (1997), Strang (2005), and Watkins (2010). Therefore, only a brief discussion is made to explain our selection of a linear solver used for this work, and a numerical experiment is performed to verify our choice.

Regarding the iterative methods, there are usually several options available in most commercial FE codes. The typically used ones in structural analysis are the Jacobi Conjugate Gradient method (JCG), Incomplete Cholesky Conjugate Gradient method

(ICCG), Algebraic Multi-grid method (AMG), and Pre-conditioned Conjugate Gradient method (PCG). The JCG solver is mainly based on the algorithm developed by Mahinthakumar and Hoole (1990), which is more suitable for well-conditioned problems. The ICCG solver is generally more robust than the JCG method for handling ill-conditioned matrices that are often obtained in models containing highly distorted elements or contact elements. The AMG solver (Saad, 2003) typically performs better than the ICCG and PCG solvers in a shared-memory parallel environment (such as a multi-processor computer) to handle indefinite matrix and ill-conditioned problems for nonlinear analyses. While the AMG delivers about the same level of performance for ordinary problems, it usually uses much more memory than other iterative solvers. The Pre-conditioned Conjugate Gradient (PCG) method is nowadays the most popular iterative method applied in solid mechanics FE computations (Wriggers, 2008) due to its efficiency and reliability for most types of large linear and nonlinear problems: for example, contact analyses that use either penalty-based or augmented Lagrangian-based algorithms can work well with this method. The PCG solver in ANSYS is valid for large equation systems with sparse, symmetric, definite or indefinite stiffness matrices, and it is usually about 4~10 times faster than the JCG solver for models with 3-D solid elements, and time savings tend to increase with problem size, while its memory usage is very affordable (roughly speaking, only 1 GB per million nodal DOFs).

Overall, iterative solvers (such as AMG, PCG) are advantageous for solving very large FE equation systems because they require much less memory, less processing time (the total number of operations is less) and more scalable parallel performance when compared with direct solvers (Hackbusch, 1994; Kelley, 1995; Saad, 2003, Braess, 2007). However, iterative solvers are in general not as robust as direct solvers. Especially for problems with numerical challenges such as ill-conditioned or even nearly-singular matrices (matrices with small pivots) or matrices that include Lagrangian multipliers, iterative solvers are less effective or may even fail, whereas direct solvers are much more reliable.

Direct solvers refer to the numerical methods that solve linear equation systems without an iterative process. These algorithms are fundamentally based on “Gauss elimination”

(Bathe, 1996). Comparing with iterative methods, the most attractive advantage of direct solvers lies in their robustness in solving very ill-conditioned and negative definite systems of equations (Wriggers, 2008), which are a concern in nonlinear applications. For a highly nonlinear problem, not only the convergence of using iterative methods is not guaranteed, but also the number of iterations required to obtain sufficient solution accuracy may be so large that direct methods become faster. In such cases, a direct solver may be the best choice. On the other side, the main shortcoming of direct solvers is their very high requirements for large in-core memory and the number of operations. This is the main reason why those commonly used direct FE solvers in the last century, such as the “Frontal” (Wavefront) methods and the “Block elimination” methods, have been abandoned for large FE computations, and replaced with the modern “Sparse Direct” solvers developed in the 1990s (Timothy, 2006).

Currently, sparse matrix solving technologies have advanced to a mature stage so that almost all commercial FE codes have added them as solution options (Nguyen, 2006). Specifically, the ANSYS “Sparse Direct” solver works well for large sparse symmetrical and unsymmetrical equation systems. It can run completely in computer in-core memory if sufficient memory is available (roughly, 10 GB per million nodal DOFs) and thus drastically increase computational efficiency. If the available memory is less than that required for in-core processing, this solver can still run efficiently in an optimal out-of-core mode, while it requires large disk space to store the factorized matrix. In addition, it can also be implemented in parallel computing on a shared memory architecture machine (like the one used in this research), which will further reduce running time.

Based on the above considerations and the high computing capability used for this work, the “**Sparse Direct**” solver was employed for the solutions of linear systems of equations in each iteration step of the “Full Newton-Raphson” scheme. To justify our selection, a numerical experiment was performed on a simplified OPGW 3-D elastic beam contact model (Figure 3.13). Keeping the same parameters for all the other solution settings, PCG and Sparse Direct solvers are specified to run this model separately to compare their total numbers of iterations and elapsed CPU-time (Table 3.9). It turned out that PCG, the most popular iterative solver for large FE problems, is much less effective than the

Sparse Direct solver for this application. The Sparse Direct solver saved more than 30% CPU-time compared to the PCG solver, while triple memory space was used by the Sparse Direct solver. It is anticipated that the advantages of using the Sparse Direct solver will be even more significant for the refined OPGW model with a large number of 3-D solid elements and stronger nonlinearities.

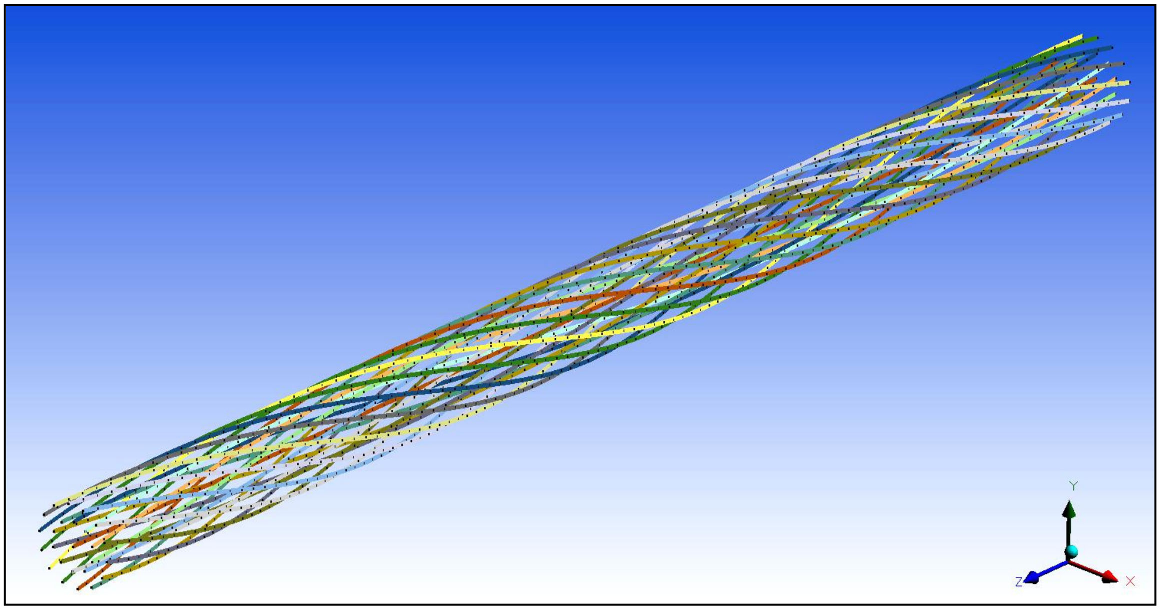

Figure 3.13 A simplified OPGW 3-D elastic beam contact model

Table 3.9 Comparison of Sparse Direct and PCG solvers for a OPGW beam model

	Sparse Direct	PCG
Number of iterations	601	565
Memory usage	914.4 (MB)	308.2 (MB)
Total CPU time	43139 (sec.) --- 12.0 hours	63444 (sec.) --- 17.6 hours

3.4.4 Stabilization Considerations

During the FE implementations of the refined OPGW model, several convergence enhancement tools were employed within the Full Newton-Raphson iterations, including “automatic time stepping”, “weak spring element”, “line search” and “time step bisection”. These techniques were shown to be very advantageous in stabilizing the model by either accelerating the solution process or reducing the numerical instability.

Due to the practical difficulties for the OPGW model to reach a converged solution, the time step size (load incremental step) must be very small to gradually apply the loads. Even so, the solution process still deteriorated in some stages. Therefore, using a constant time step size throughout the whole load history is not practicable. In view of this, only the initial (first) time step was user-specified, and then the *"automatic time stepping"* algorithm was activated to internally estimate and adjust the subsequent time step size in response to the out-of-balance state of the analysis (to make proper adjustments of the incremental loads that are to be applied). In ANSYS, both the "minimum time step size" and "maximum time step size" need to be user-defined to serve as the range of values for which the automatic time stepping algorithm can work. Indeed, it was found that the "minimum time step size" was a key solution control parameter to show significant effect on the convergence behavior of the OPGW model. A very small limit of t_{min}=0.001 was selected to ensure a "smooth" computation; otherwise the solution process becomes unstable or even divergent.

Although very small load steps had been specified, "chattering" was still encountered during the computations; sudden system stiffness changes deteriorated the solution process and led to convergence difficulty. Hence, to enhance numerical stability, some weak spring elements were added to the assembly with negligible assigned spring stiffness compared with the system stiffness to ensure that they had no effects on the solution accuracy.

The "Line search" algorithm incorporated into the Newton-Raphson iterations has been shown to significantly improve the robustness of Newton's method (Bonet and Wood, 2008; Ibrahibegovic, 2009), and thus was activated in this study. The use of *"time step bisection"* combined with the "automatic time stepping" was also beneficial: the calculated response was reviewed at the end of each load step to examine whether excessive contact penetrations, abrupt contact status changes, and overly large residual forces had occurred. If so, the next load incremental step would be bisected (reduced by half) and the iterations continued. In effect, the "bisection" occurred several times when around 40% loading was applied on the OPGW model, thus showing the effectiveness of this technique to stabilize the solution process.

3.5 Computational Results and Discussion

Using the modeling strategies developed in the preceding sections, the OPGW model was solved with both stable convergence and sufficient accuracy. The computational process is very costly due to the refined mesh (large problem size) and high nonlinearity of this 3-D model. In total, 102 load incremental steps were applied and lead to 428 cumulative interations. The elapsed CPU running time for one analysis implementation (under a share memory parallel processing environment) was 503247 seconds (5 days, 19 hours and 47 minutes).

Computational results of this refined OPGW model are presented in this section, and are compared with the ones obtained with the previous coarse FE model by Roshan Fekr (1999), as well as two approximate analytical solutions based on the work of Machida and Durelli (1973) and Phillips and Costello (1997). In addition, it should be indicated that, most of the results discussed below refer to the cable cross section at mid-length of the model (z = 132.58 mm).

3.5.1 Conductor Wires

The total deformation of the OPGW model under the prescribed elongation (a simulation of extreme design conditions) is shown in Figure 3.14, and the overall longitudinal displacement field Uz (z-axis) of the conductor wires at the mid-length cross section is shown in Figure 3.15 (Spacer is not included herein.). First of all, it is seen in Figure 3.15 that all similar components have a similar response pattern and the displacement distributions in each wire are not uniform. Meanwhile, the displacement trends of the outer and inner wires are opposite due to their opposite helical angles. In addition, the results confirmed that the outer wires have larger axial displacements and steeper displacement gradients than those in the inner wires. The largest and smallest axial displacements both occur on the outer wires with the values 0.8299 mm and 0.8006 mm (Figure 3.16), while the maximum and minimum displacements calculated on the inner wires are 0.818 mm and 0.810 mm, respectively (Figure 3.17). The axial displacement of the central tube is uniform at 0.8204 mm.

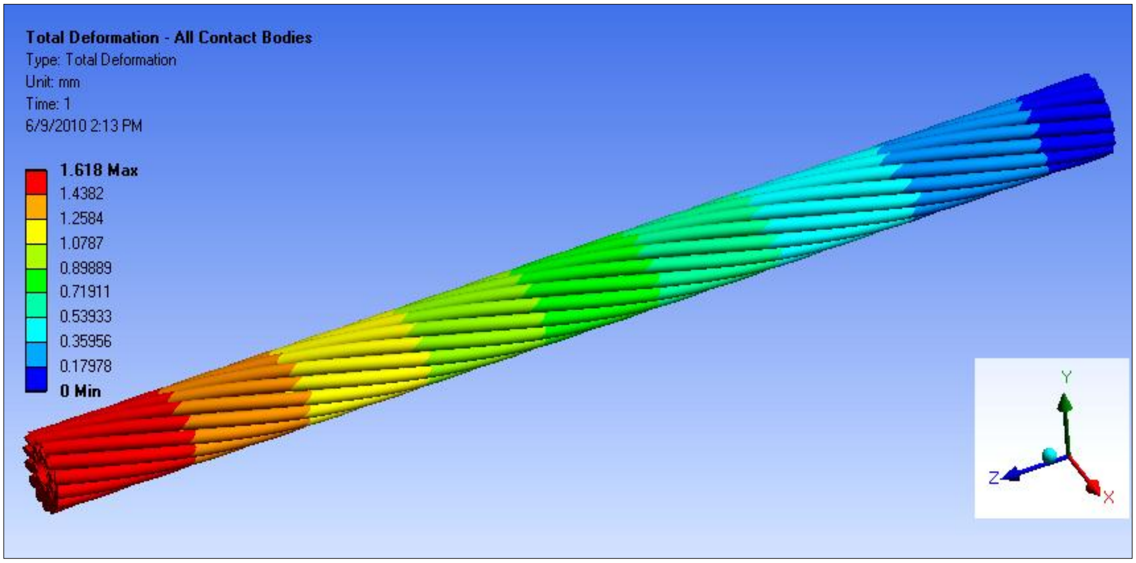

Figure 3.14 Total deformation of the OPGW model under prescribed elongation

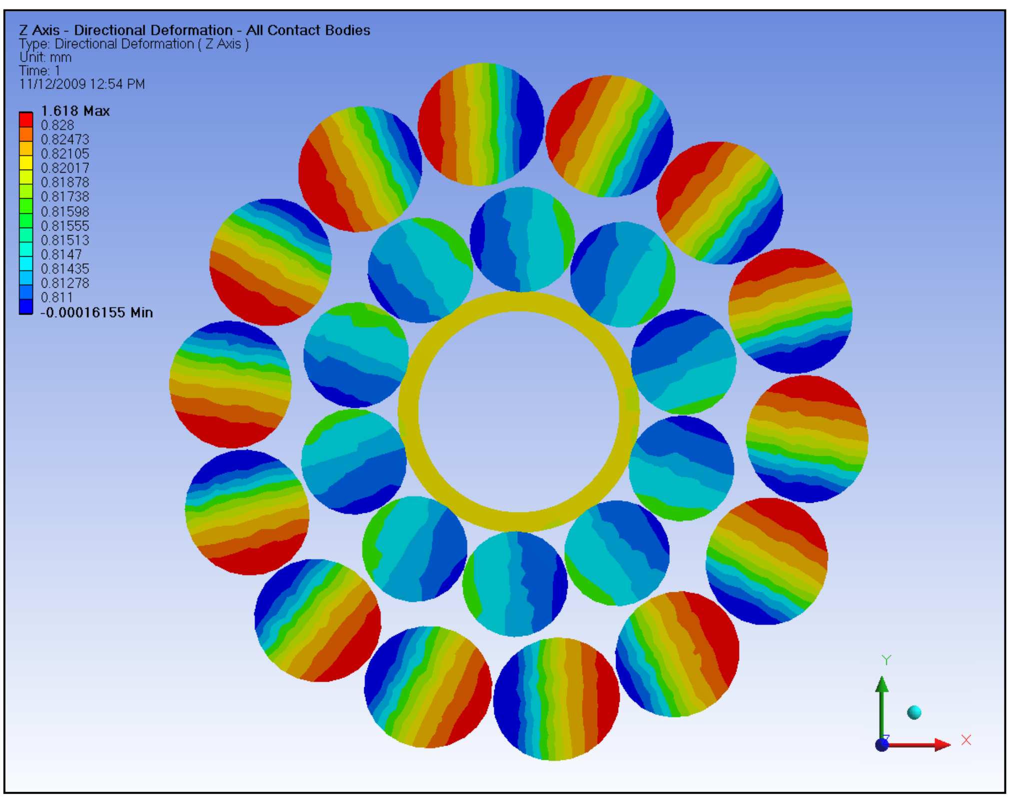

Figure 3.15 Axial displacement (Uz) of OPGW wires at mid-length cross section

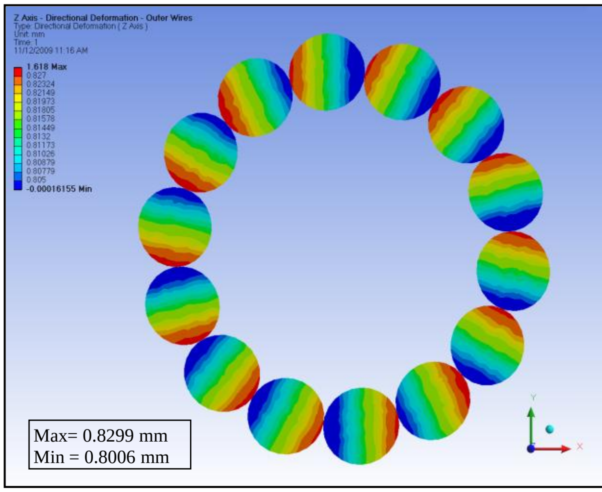

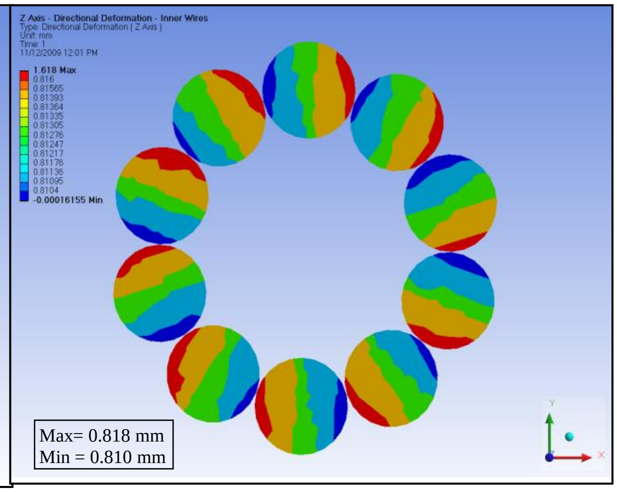

Figure 3.16 Uz of OPGW outer wires

Figure 3.17 Uz of OPGW inner wires

The non-uniform Von-Mises stress distribution in the conductor wires (Figure 3.18) clearly indicates the structural role of the inner steel wires (acting as the main load-carrying components of the cable), while the external aluminum alloy wires experience considerably less stress.

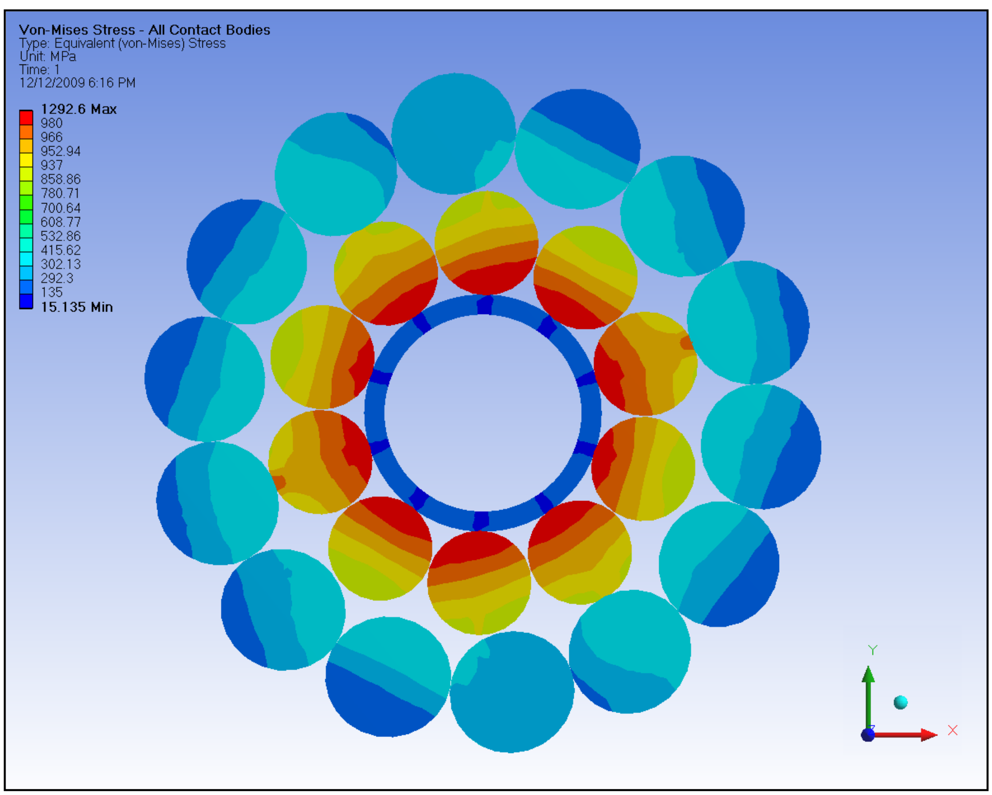

Figure 3.18 OPGW Von-Mises stress (S_{von}) at mid-length cross section

The maximum Von-Mises stress (1029.1 MPa) occurs on the steel inner wires (Figure 3.19); their yield strength is defined at 1250 MPa, so they are still in the elastic range. The minimum Von-Mises stress (268.54 MPa) occurs in the aluminum alloy outer wires (Figure 3.20); their yield strength is 204 MPa, so they have entered their inelastic response range.

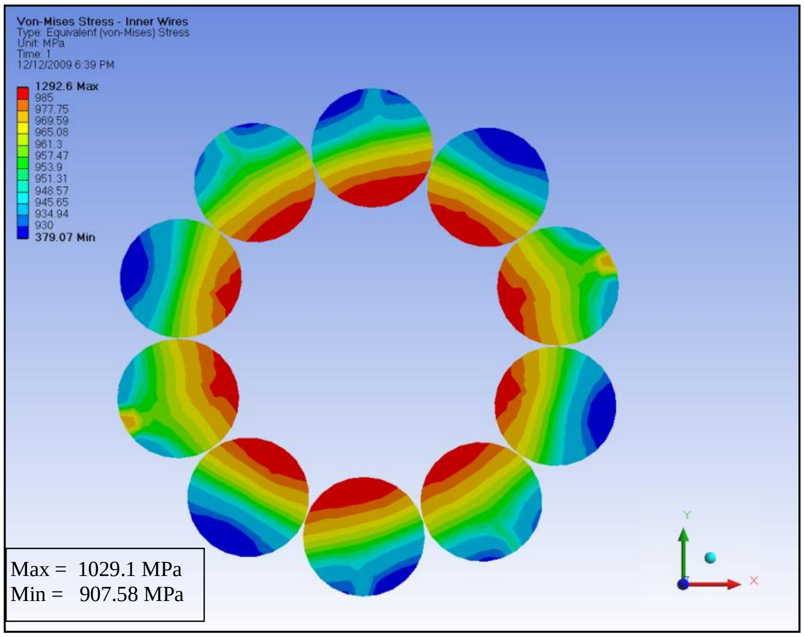

Figure 3.19 Inner wire Von-Mises stress (S_{von})

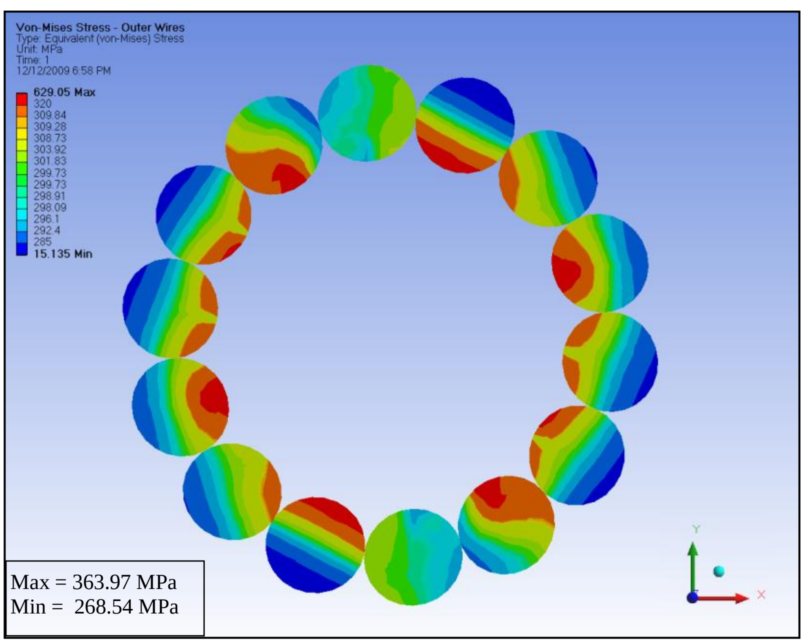

Figure 3.20 Outer wire Von-Mises stress (S_{von})

The corresponding Von-Mises stain (ε_{von}) distribution is similar to the stress fields for the elastic response of the inner wires (Figure 3.21), and the peak Von-Mises strain decreases by as much as 50% from the inner to the outer wires (Figures 3.22 and 3.23).

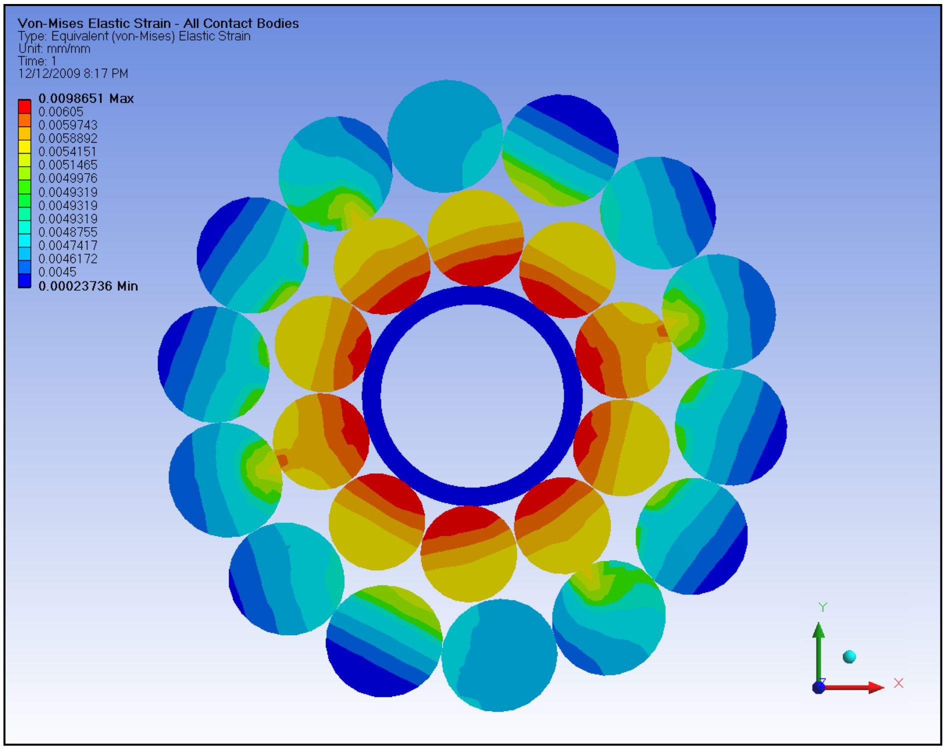

Figure 3.21 OPGW Von-Mises strain (ε_{von}) at mid-length cross section

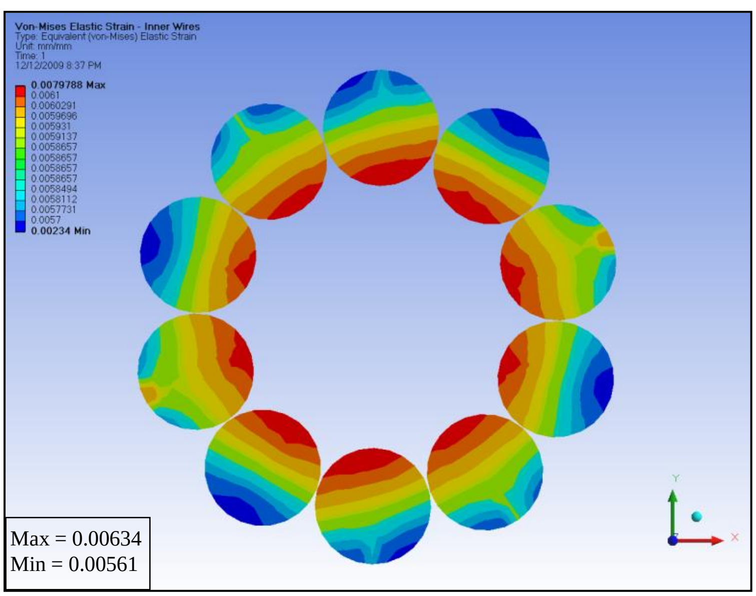

Figure 3.22 Inner wire Von-Mises strain (ε_{von})

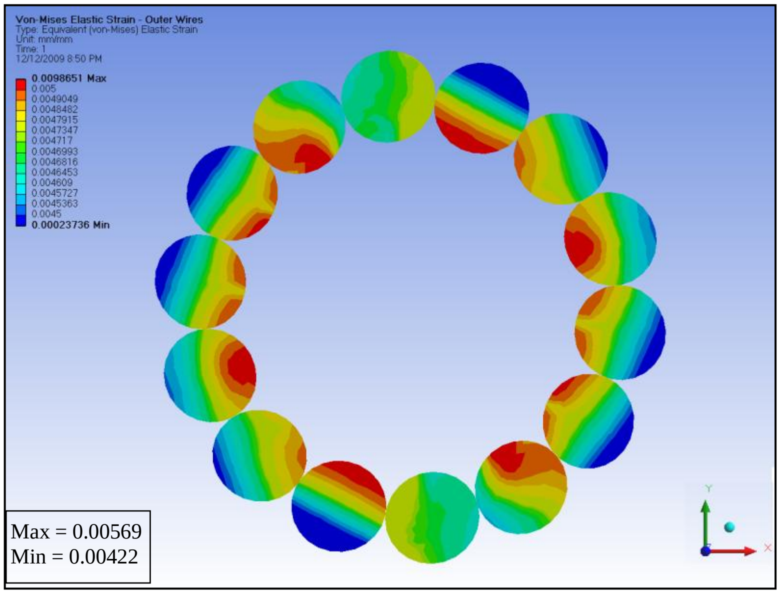

Figure 3.23 Outer wire Von-Mises strain (ε_{von})

The OPGW axial stress field (S_{zz}) at the mid-length cross section is shown in Figure 3.24. The maximum S_{zz} occurs on the inward side of the steel inner wires, and the variation of S_{zz} on the inner and outer wires is presented in Figures 3.25 and 3.26. The effects of the friction shear stresses at the contact interfaces on the distribution of the tensile axial stress are clearly shown on the figures.

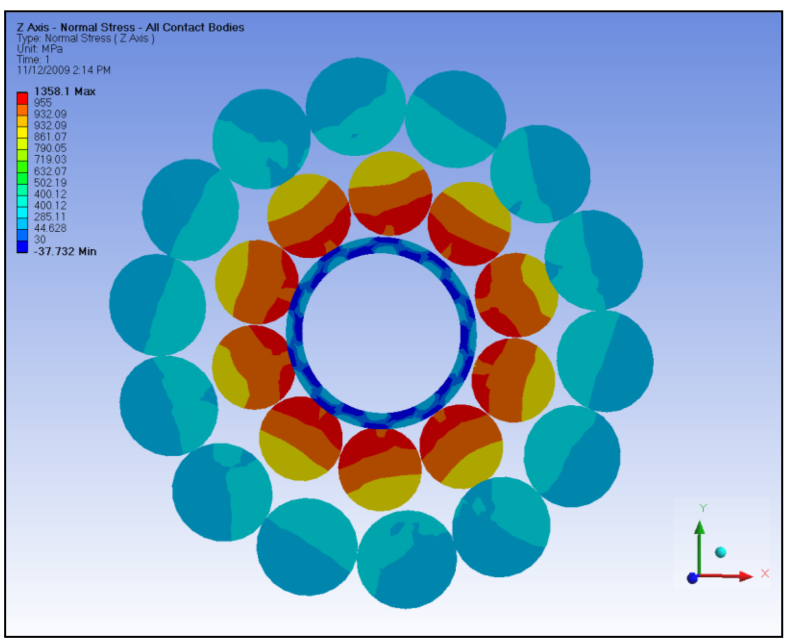

Figure 3.24 OPGW axial stress (S_{zz}) at mid-length cross section

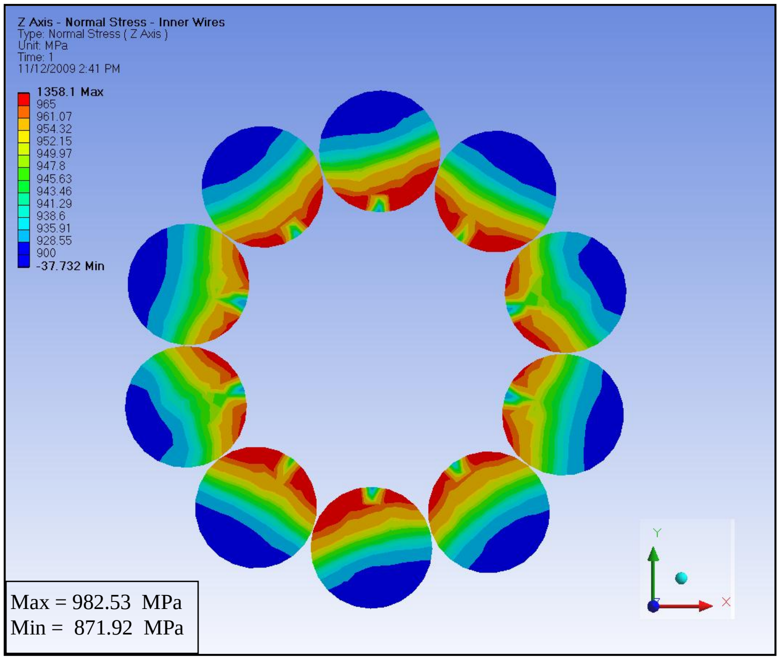

Figure 3.25 Inner wire axial stress (S_{zz})

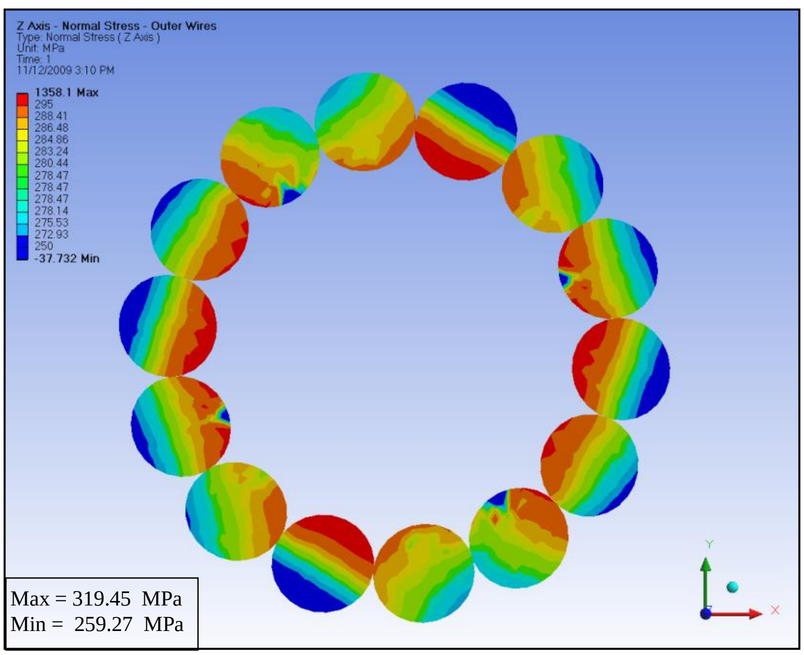

Figure 3.26 Outer wire axial stress (S_{zz})

The OPGW axial strain (ε_{zz}) at the mid-length cross section is shown in Figure 3.27. It needs to be mentioned that the strain displayed on the tube is only the elastic strain and not the total strain. The plastic strain of the central tube will be presented later. The maximum axial strain occurs in the inner wires, 0.00607; the minimum strain occurs in the outer wires, 0.00395, decreasing by 35%. (See also Figures 3.28 and 3.29).

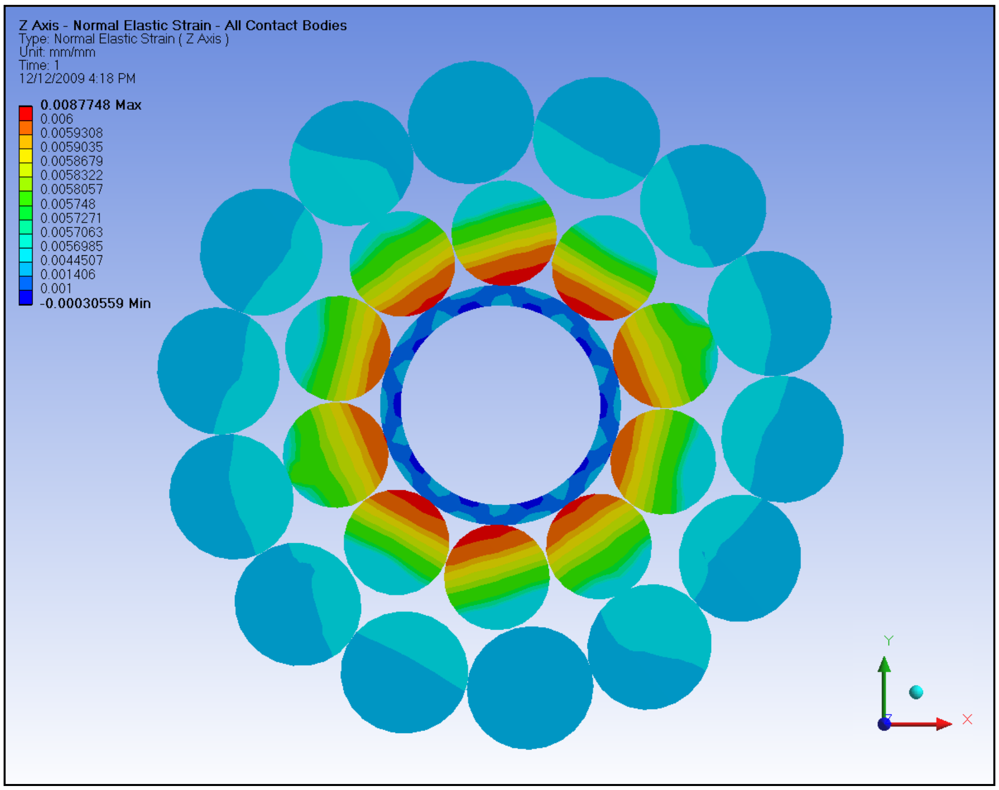

Figure 3.27 OPGW axial stain (ε_{zz}) at mid-length cross section

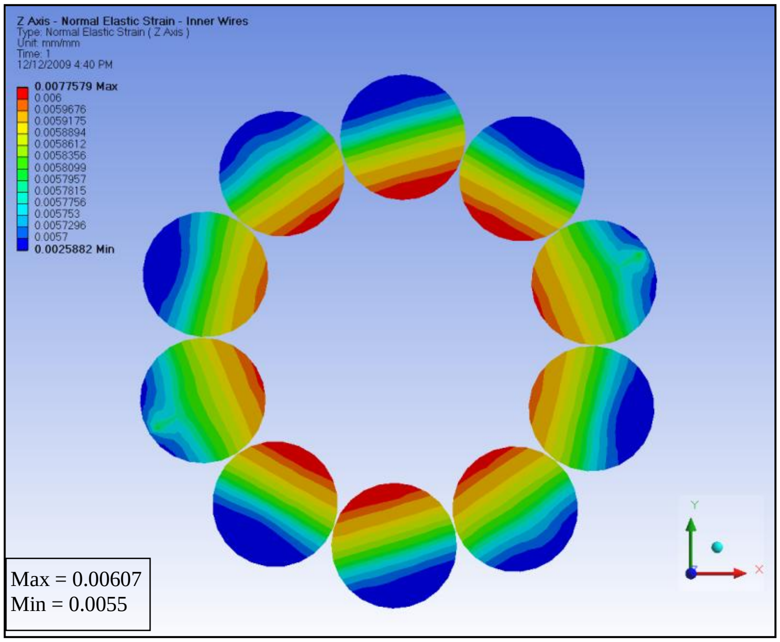

Figure 3.28 Inner wire axial stain (ε_{zz})

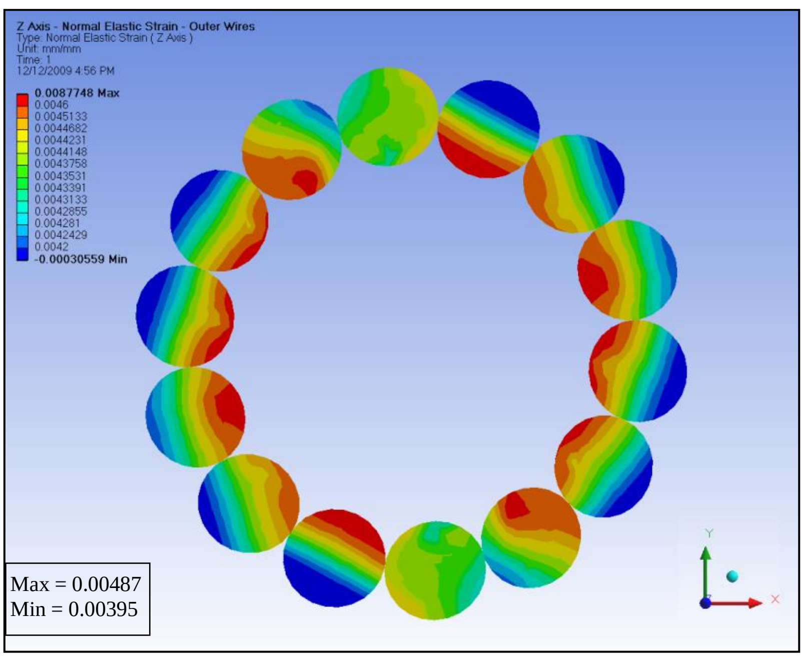

Figure 3.29 Outer wire axial stain (ε_{zz})

Tables 3.10 and 3.11 summarize the comparisons of the maximum principal stress (S_1) and maximum shear stress (S_τ) of the outer and inner wires at the mid length cross-section obtained from this refined model and the ones from the previous coarse FE model and two analytical models, from which the refined model clearly exhibits significant improvements on the stress predictions. Because the two analytical models were not able to consider friction, they thus overestimated the maximum principal stress, and their predictions of the maximum shear stress are generally larger and more uniform than those calculated with the two FE models that show the strong effects due to friction. In the refined FE model, the maximum shear stresses of all the outer wires occur on their contact surfaces with the inner wires, and the maximum shear stresses of all the inner wires occur on their contact surfaces with the central tube. Compared with the coarse model, the upper-limit values (representing the stresses without frictional effects) from the refined model are much closer to the resuts from the analytical models. On the other hand, the much smaller lower-limit values from the coarse model indicate that it could not provide sufficient accuracy to present the frictional contact response.

Table 3.10 Comparisons of analysis results for outer aluminum wires

Analysis method	**Max. Principal Stress** (MPa)	**Max. Shear Stress** (MPa)
Machida & Durelli (1973)	349 - 367	175 - 183
Phillips & Costello (1997)	353 - 373	177 - 186
Coarse FE model (1999)	54 - 292	39 - 157
Refined FE model (2011)	240 - 339	135 - 197

Table 3.11 Comparisons of analysis results for inner steel wires

Analysis method	**Max. Principal Stress** (MPa)	**Max. Shear Stress** (MPa)
Machida & Durelli (1973)	969 - 984	485 - 492
Phillips & Costello (1997)	967 - 982	483 - 491
Coarse FE model (1999)	790 - 932	406 - 473
Refined FE model (2011)	883 - 996	461 - 527

3.5.2 Central Tube

Due to the contact interactions, the stresses and strains in the central aluminum tube exhibit complex patterns, as shown in Figure 3.30 for the Von-Mises stress (S_{von}) and in Figure 3.31 for the axial stress (S_{zz}). The central tube experiences significant plastic deformations especially in the zones close to the contact surfaces with the inner wires. Plasticity occurs after the maximum Von-Mises elastic strain, ε_{von}=0.00234, is exceeded (Figure 3.32). At the end of the loading phase, the tube has permanent deformations with a maximum equivalent plastic strain ε_p=0.0085, corresponding to a Von-Mises stress of 144.77 MPa, which is clearly beyond its yield strength (123.6 MPa). Results for the axial elastic strain (ε_{zz}) and equivalent plastic strain (ε_p) in the central tube are shown in Figures 3.33 and 3.34.

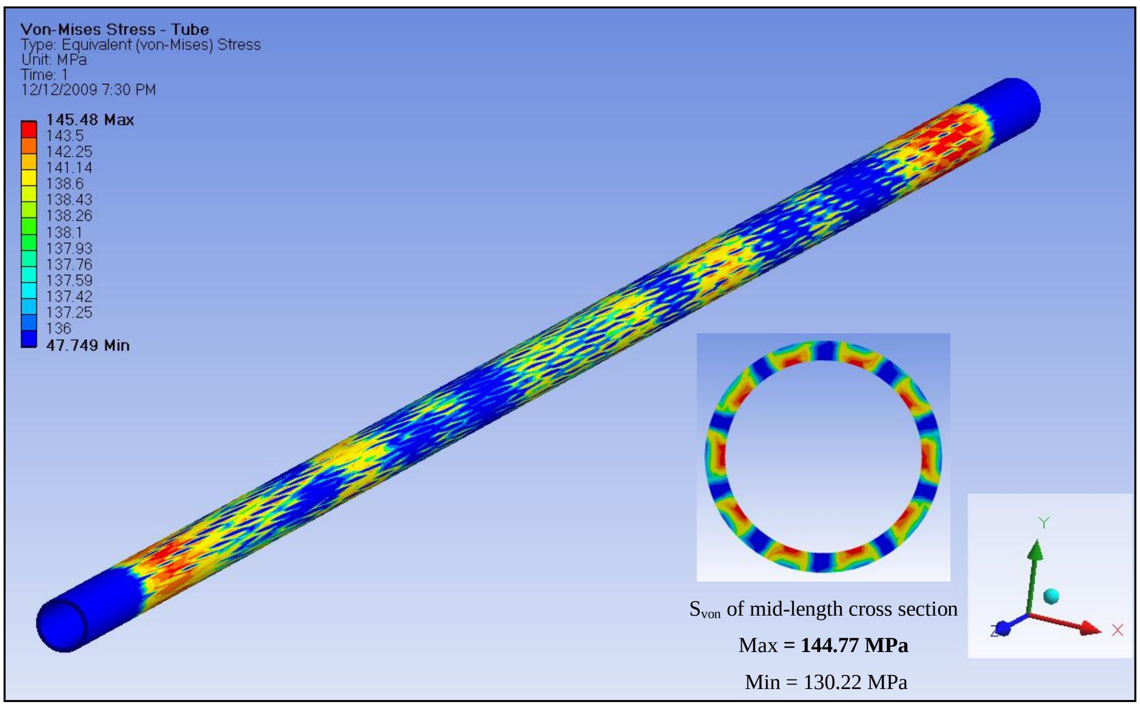

Figure 3.30 Von-Mises stress (S_{von}) in central tube

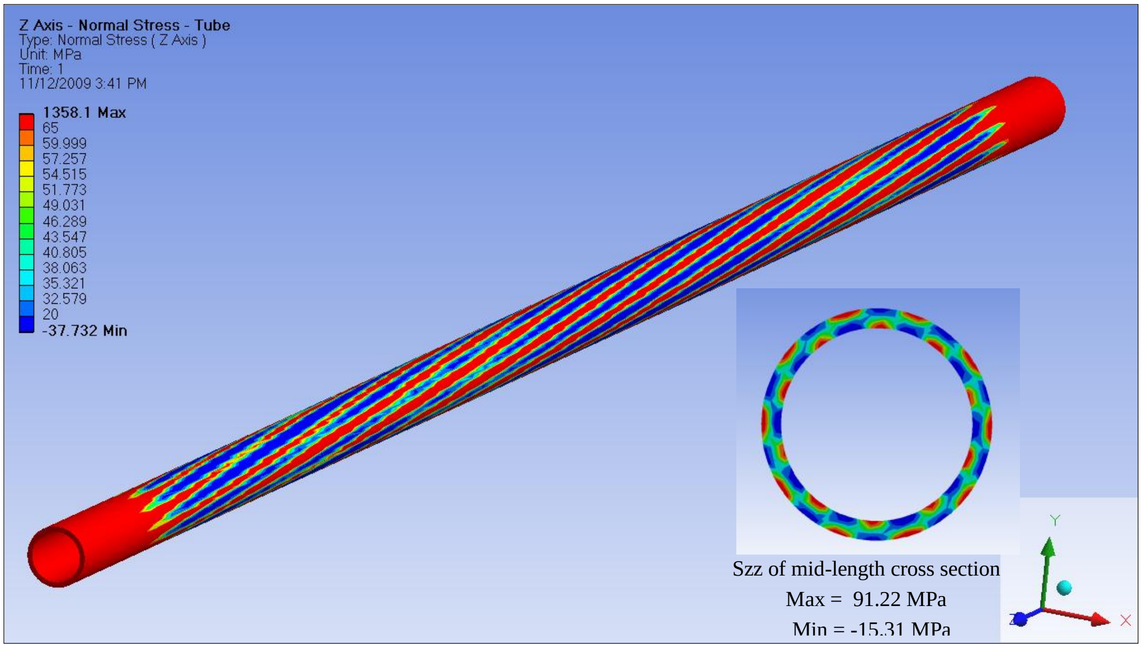

Figure 3.31 Axial stress (S_{zz}) in central tube

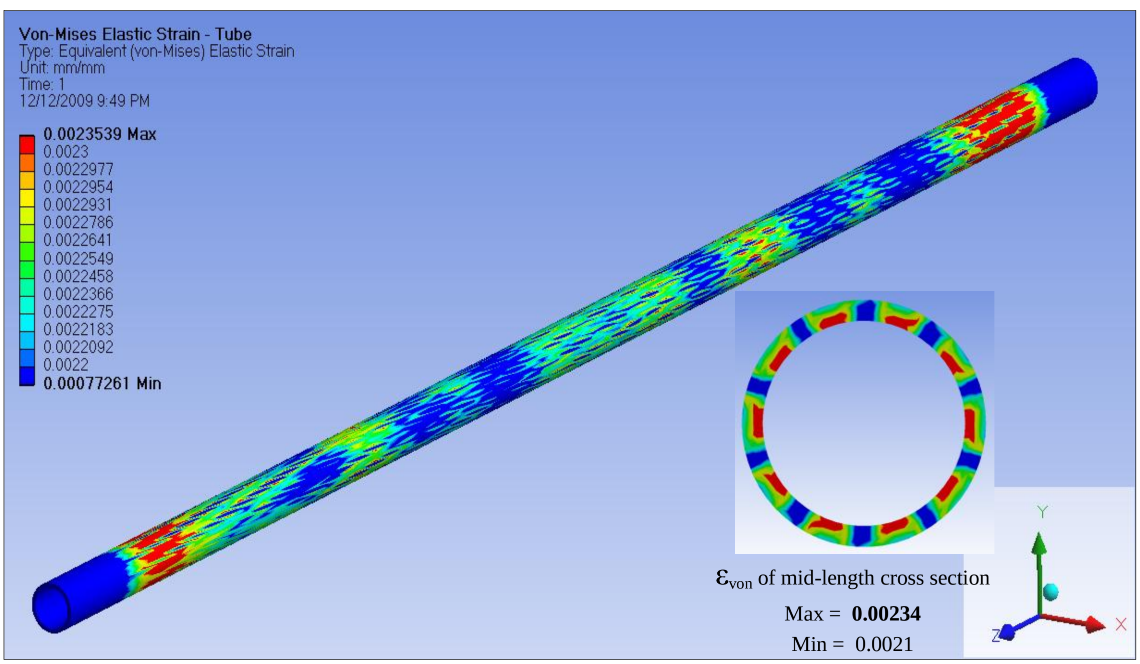

Figure 3.32 Von-Mises elastic strain (ε_{von}) in central tube

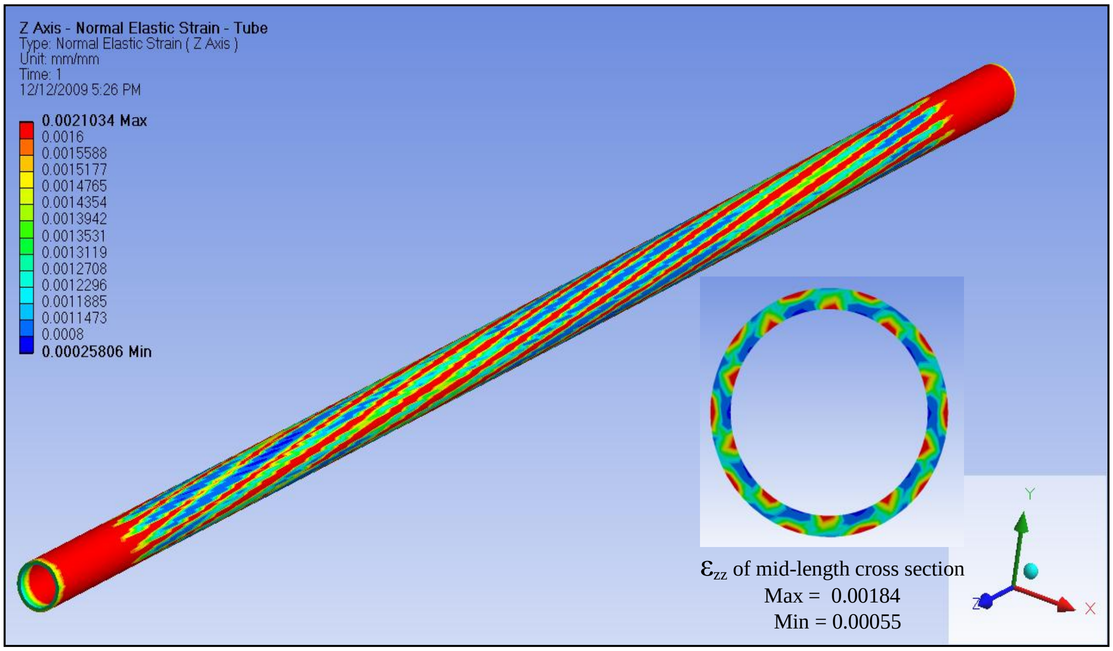

Figure 3.33 Axial elastic strain (ε_{zz}) in central tube

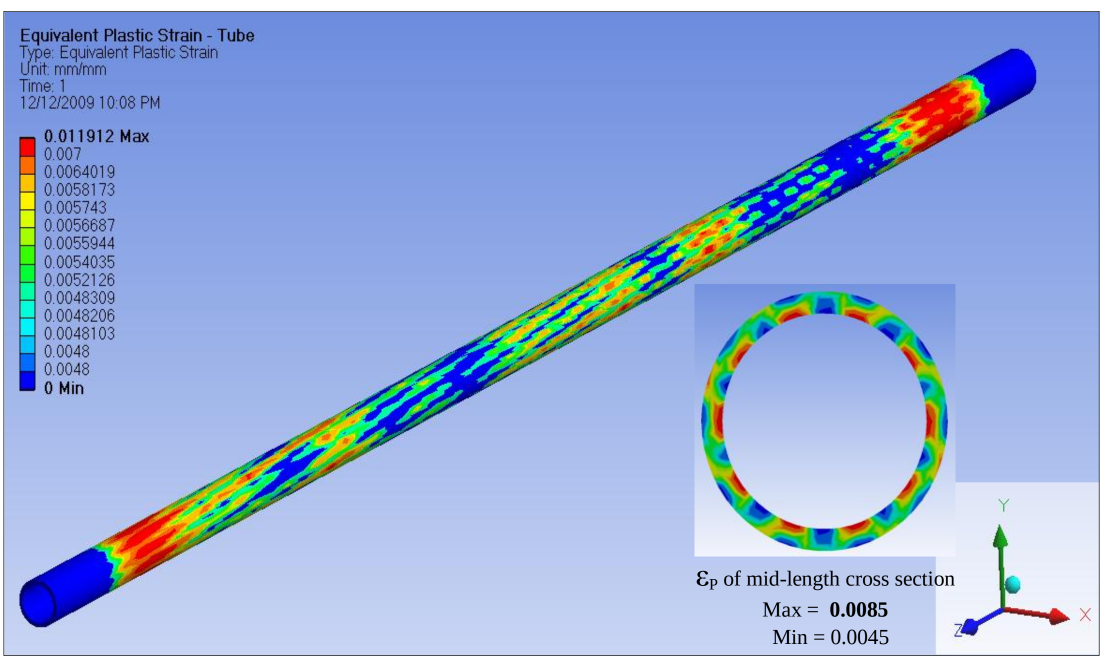

Figure 3.34 Equivalent plastic strain (ε_p) in central tube

3.5.3 Aluminum Spacer

The spacer's Von-Mises strain (ε_{von}), axial elastic strain (ε_{zz}), and plastic strain (ε_p) are shown in Figures 3.35~3.37. The results indicate that the aluminum spacer experiences no interaction with the central tube during the analysis as the initial clearance (0.125 mm) between them is relatively too large to produce contact under the prescribed axial elongation.

At the end of the loading, however, the spacer has already experienced strong plasticity. Although the colour scale used in the legend of the following figures suggests some variations on the cross section for visulizaion purposes, the strains are quite uniform throughout with an axial elastic strain (ε_{zz}=0.0032) and equivalent plastic strain (ε_p=0.0031). The subtle stress and strain variations are due to the spacer's cross-sectional and helical configurations, and their peak values both occur at the bottom of one of the grooves instead of the center of the spacer.

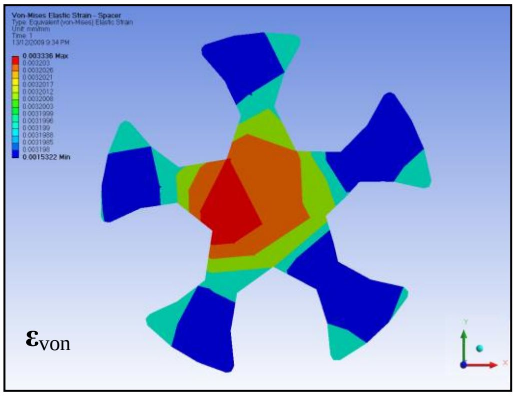

Figure 3.35 Von-Mises strain (ε_{von}) at mid-length cross section of the spacer

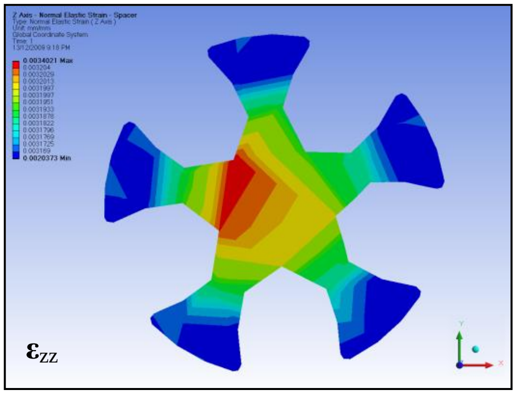

Figure 3.36 Spacer axial elastic strain (ε_{zz})

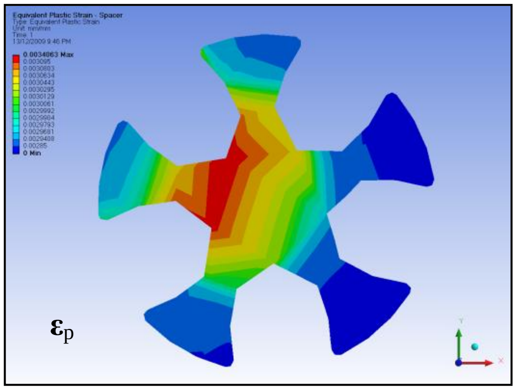

Figure 3.37 Spacer equivalent plastic strain (ε_p)

3.6 Summary Remarks

This chapter focused on the refined FE modeling of an OPGW for its detailed stress analysis under design elongation conditions. The cable strand has two-layer wires with 19-mm outer diameter, an inner tube core and spacer - a tight core OPGW construction typically used in overhead transmission lines. A 3-D elastic-plastic, large deformation, frictional contact FE model was constructed. The model comprises all the structural components of the cable strand - two layers of helically-twisted wires, a central aluminum tube (enclosing the optical core), and a spacer that houses the optical fibers in its helical grooves - adding up to **221,816** nodes, **234,119** solid elements, and **182,340** surface-to-surface contact elements. Great modeling challenges were encountered to arrive at converged solutions for this highly nonlinear large size model. Extensive numerical experiments had to be conducted to achieve an optimal solution strategy.

All key procedures in the FE modeling and related numerical techniques were studied thoroughly to overcome the very difficult convergent behavior of the fine model without compromising its solution accuracy. Specifically, the effects of element qualities and mesh refinement on convergence and accuracy were investigated empirically with rational error estimation (control); proper treatment of boundary conditions and loads were carefully considered; various numerical solution techniques in the implementations of the nonlinear FE model were examined to develop a robust solution scheme.

The computational results show agreement with the analytical solutions and significantly improve on a previous coarse FE model. By means of this study, a faithful physics-based macroscopic modeling methodology for detailed numerical stress analysis of stranded transmission line conductors was developed successfully, and it is essentially code-independent. The quality of the FE model is considered to be highly satisfactory.

Chapter 4

Computational Modeling for ACSR Conductor Strength Study

4.1 Introduction

Electrical conductors and ground wires are both essential components of overhead transmission lines. As already seen in Chapter 3, the complex mechanical behavior of an OPGW cannot be well understood by either experimental testings or theoretical models. In the field of general cable strand (wire ropes) modeling, many analytical models have been proposed, of which most are single-layered strands and are based on various simplifying assumptions. Several coarse numerical models have been published, but have limited success to describe the behavior of multi-layered strands. To the best knowledge of the author, detailed high-fidelity conductor computational models have not yet been available in the open literature. Therefore, an effort is made herein to fill this void.

In view of the fact that the tensile strength is currently the standard structural design specification for electrical conductors (see for example, American Society for Testing and Materials (ASTM), 2004), the study carried out in this chapter aims at modeling the mechanical behavior of individual stranded wires under axial design load, to investigate the tensile response of a complete conductor.

Aluminum alloy stranded conductors with a galvanized steel core (ACSR) have been extensively used worldwide on high-voltage overhead transmission lines for their many economical and technical advantages (EPRI, 1979, 2006). Actually, the combination of the light weight and efficient conductivity of aluminum with the high tensile strength and stiffness of steel has made ACSR conductors the most economical solution for overhead power transmission lines, even under extreme weather conditions. Hence, a particular type of ACSR conductor is chosen to conduct this study by using the FE modeling methodology developed in Chapter 3.

In addition, with a view to enrich the research effort in solving the critical conductor fatigue problems that continue to challenge overhead line design, this study will not only contribute to the understanding of the complex contact and friction mechanics of conductors under extreme design conditions, but also serve as a rational basis for the development of a practical computational approach (presented in the next chapter) to study the fretting fatigue of overhead line conductors.

4.2 Drake Conductor Construction and Solid Modeling

In reality, there exists a wide spectrum in each manufacturer's ACSR product catalogue, offering many design configurations on the market. In this thesis, a two-layer 795 kcmil [1] (26/7) "Drake" type ACSR overhead conductor is selected as the benchmark conductor for the modeling study due to its widespread use throughout the electrical utility industry.

A "Drake" is a composite concentric-lay-stranded conductor, comprising a steel central core strand surrounded by two layers of helically wound aluminum alloy strands. The steel core (a 7-wire concentric helical strand) is essentially the load-carrying component of the conductor, and the steel wires are protected from corrosion by galvanizing (zinc coating). The outer two layers strands are wounded alternately in right-handed and left-handed helices with a total of 26 individual wires made of 1350-H19 aluminum alloy (10 inner wires and 16 outer wires). The opposite helical directions of the different layers are designed to reduce the internally unbalanced torque of the conductor. The exact external diameter of the bare conductor is **28.133** mm. Its configuration is illustrated in Figure 4.1, and its schematic cross section is shown in Figure 4.2.

[1] 1 kcmil = 1000 cmil = 785.4 * 10^{-6} in^2 = 0.5067 mm^2. This is a measure of the aluminum alloy cross-sectional area and is directly related to the electrical conductivity of the cable.

Figure 4.1 Drake configuration

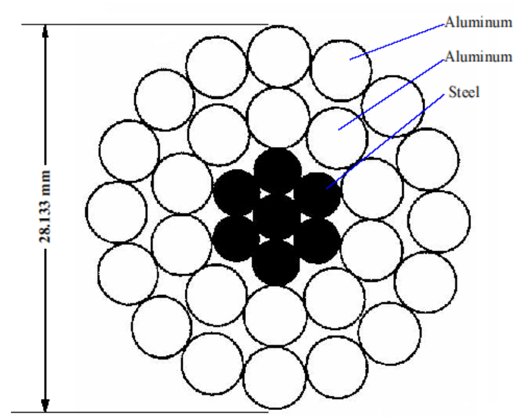

Figure 4.2 Drake schematic cross-section

While some of the geometric specifications (overall conductor and individual wire diameters, strand configuration) of a Drake conductor are standard, which need to be in compliance with the industry standards, such as those in ASTM B232, the pitch lengths and thus the lay angles of the different layers may actually differ among manufacturers. Although lay angles are generally ignored in most theoretical models when calculating the bending stiffness of a conductor, they do have significant effects on the mechanical response of a helically stranded cable. The effects of lay angles and their design strategy have been discussed in-depth by Rawlins (2005). The geometry parameters (Figure 4.3) of a helical wire can be defined with the following relations:

$$\theta = \arctan(\pi * D_{mean} / P)$$

$$P = \pi * D_{mean} / \tan(\theta)$$

$$L.R. = P / D_{ext}$$

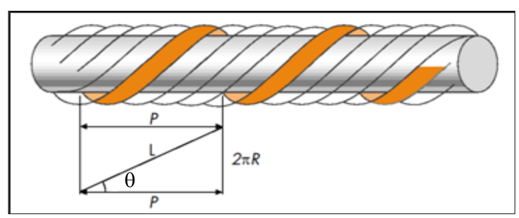

Figure 4.3 Helical wire geometry parameters

where:

θ = lay angle of a given layer, being positive for right-handed helices and negative for left-handed helices;

D_{mean} = mean diameter of a given layer (R in Figure 4.3 is the mean radius);

P = pitch length (also called lay length) of a given layer, which means the axial length of one complete revolution of a helical wire;

L.R. = “Lay Ratio”;

D_{ext} = external diameter of a given layer.

The so-called “*lay ratios*” rather than the lay lengths (or lay angles) are actually used by most manufacturers as basic measurements when designing a conductor, and they are specified in various “Standards” by a range of values (instead of specific values) for any particular conductor. It is noted that too small a lay ratio may cause interferences among wires in one layer so that “a lay ratio less than 10 is prohibited” (Rawlins, 2005); on the other hand, too large a lay ratio would leave substantial gaps between adajacent wires (although small gaps are permitted in ASTM 9 and IEC 10 standards, and they may be inevitably generated). In addition, the internal unbalanced torque of a conductor that is induced when the conductor is tensioned will be different with the different angles among the layers. A small increase of the angle between adjacent helical layers may result in large unbalanced torque, which would significantly twist the conductor even in normal stringing conditions. Furthermore, from the numerical modeling perspective, a subtle lay angle difference may result in quite different lay lengths, which can change significantly the problem size of the resulting nonlinear FE model. Hence, defining a set of pitch length values of all the helical layers becomes crucial for the Drake FE modeling study.

By means of several design parameters provided by General Cable (2007, 2010) and a combination with the data suggested by ASTM B232, a set of pitch lengths are determined and the geometric specifications of the Drake conductor are summarized in Table 4.1.

Table 4.1 Geometric specifications of the Drake conductor model

<table>
<tr><td>Helical Wire</td><td>Wire Diameter (mm)</td><td>Pitch Length (mm)</td><td>Lay Angle</td><td>Lay Ratio</td></tr>
<tr><td>Outer wire</td><td>4.44246</td><td>358.14</td><td>+ 11.74° (Z)</td><td>12.73</td></tr>
<tr><td>Inner wire</td><td>4.44246</td><td>274.32</td><td>- 9.62° (S)</td><td>14.25</td></tr>
<tr><td>Steel wire</td><td>3.4544</td><td>259.08</td><td>+ 4.79° (Z)</td><td>25</td></tr>
<tr><td>Drake Conductor</td><td colspan="4">Overall external diameter = 28.133 (mm)
Angle between outer wires and inner wires = 11.74° + 9.62° = 21.36°
Angle between inner wires and steel wires = 9.62° + 4.79° = 14.41°
FE Model total length = 358.14 (mm)</td></tr>
</table>

Employing the same solid modeling approach as described in Chapter 3, an accurate Drake conductor solid model is created in DesignModeler of ANSYS Workbench 11.0 (ANSYS Inc., 2007). The model is composed of all 33 conductor wire solid bodies (Figure 4.4), and its total length is based on the longest pitch length among the three helical layers, i.e. the outer layer pitch length of **358.14 mm**.

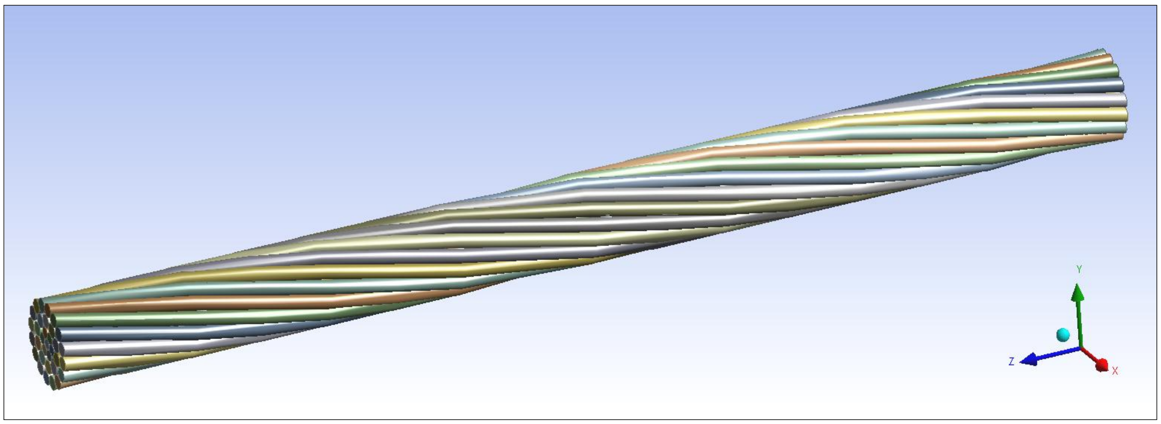

Figure 4.4 Drake conductor solid model for strength study - 358.14 (mm)

4.3 Finite Element Modeling

In this thesis, the numerical study of the Drake ACSR strength can be regarded as an application of the methodologies developed in Chapter 3. That is, the same finite element modeling procedures are applied, and thus they will be discussed briefly, while the different features of this study will be addressed in detail.

4.3.1 Material Properties

Firstly, it should be indicated that high-quality material data are often difficult to obtain in practice, especially for complex nonlinear material properties, and in consequence the validity of the analysis results is certainly limited by the accuracy and extent of the constitutive material data. Unlike in the OPGW study, in this Drake ACSR FE modeling for its strength study and subsequent fretting fatigue study (next chapter), the availability of very precise material properties of the Drake individual wires are actually not achievable due to a lack of testing data, although the conductor overall mechanical properties are provided by General Cable (2010). As a result, the open literature becomes the main resource, from which the published material data are reviewed and selected to best fit the model used in this study.

All Drake individual wires are assumed with large kinematics and small strain under design conditions. The stress-strain curves used for the aluminum wires (1350-H19) and the galvanized steel core wires (IEC60888) at ambient temperature (20^{o}C) are presented in Figures 4.5 and 4.6, respectively, and they were originally taken from uni-axial tensile experiments conducted by Alcoa Inc. (Rawlins, 2005). Table 4.2 summarizes the wire material properties and characteristics used in the Drake FE models. It is clear that both wire materials exhibit significant plasticity in the tests. The aluminum wire yields beyond a 0.1% axial strain, and the steel wire would not yield until 0.3%. The material nonlinearities of the Drake wires are then modeled using multi-linear fits of their experimental material curves in ANSYS to describe their inelastic constitutive behavior.

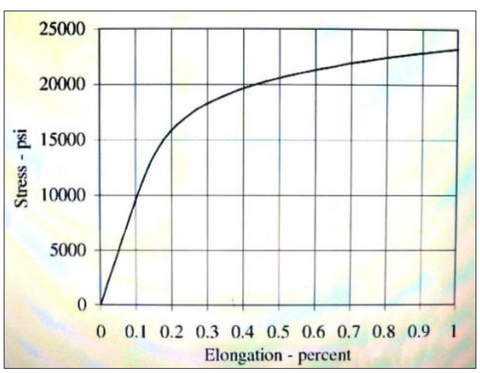

Figure 4.5 1350-H19 Al. wire material curve

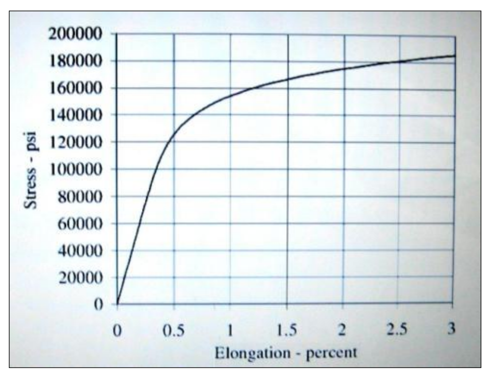

Figure 4.6 IEC60888 steel wire material curve

Table 4.2 Drake wire material properties and characteristics

Wires	Material	Properties	Characteristics
Outer & Inner layer wires	Aluminum 1350-H19	E = 68.95 GPa; ν = 0.33 Y = 68.95 MPa; UTS = 186.1 MPa	• linear elastic to multi-linear plastic, • large kinematics, • small strain
Steel core wires	Steel IEC60888	E = 206.84 GPa; ν = 0.29 Y = 620.52 MPa; UTS = 1846 MPa	

Finally, it is noteworthy that the conductor wire properties specified by manufacturers generally refer to the "apparent modulus" that is based on the force equilibrium and elongation compatibility of a cable segment subject to a prescribed axial elongation. Consequently, the wire properties obtained either from the cable experimental stress-strain curves directly or from calculations by designated polynomial equations have incorporated their mechanical response as the components of a cable, rather than the constitutive material properties of the individual wires that may be used in the FE model. In this context, the stress-strain curves of the Drake wire materials, wire components, and overall composite cable (General Cable, 2010) are summarized in Figure 4.7.

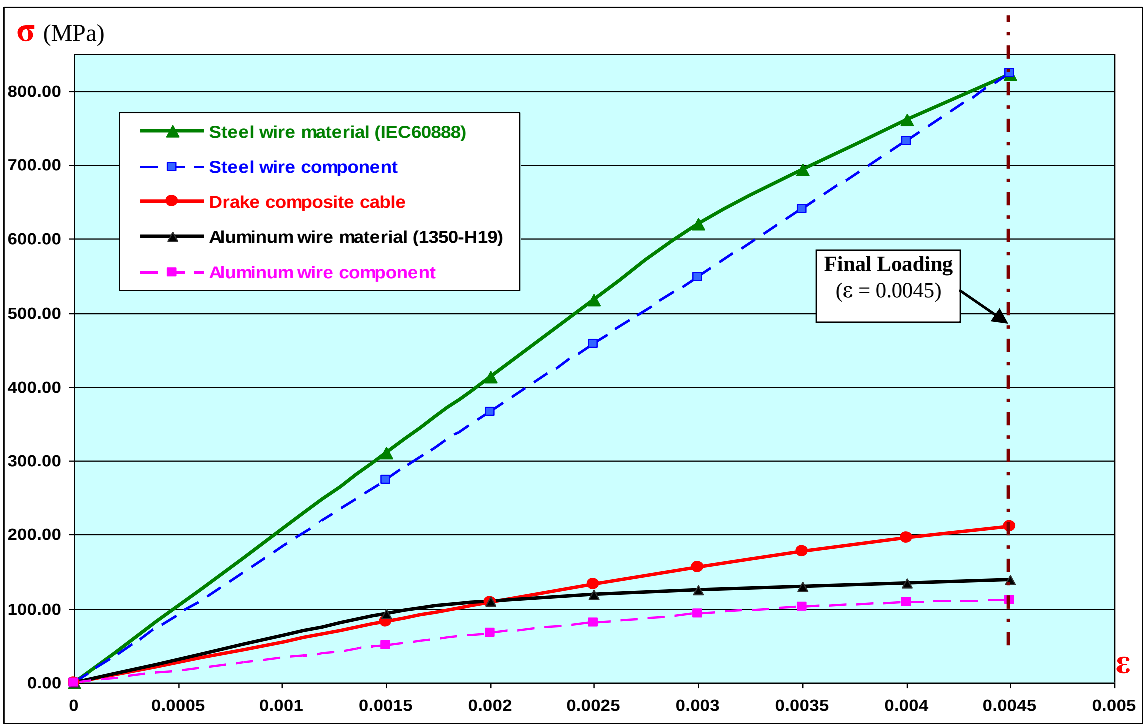

Figure 4.7 Stress-strain curves of Drake wire materials, wire components, and composite cable

4.3.2 Finite Element Meshing

For optimal solution accuracy with minimum computational cost, all Drake outer, inner, and steel core wires are modeled using 3-D 8-node reduced-integration hexahedral elements with hourglass control. By means of numerical experiments, an optimal fine meshing scheme (Table 4.3) is designed for the Drake strength model to ensure stable convergence and sufficient accuracy. The error analysis for mesh convergence indicates that the global structural error due to mesh discretization of the entire Drake strength model is well controlled below 3% (based on linear elastic analysis). At the middle cross section of the model (Z = 179.07mm), which is the location of interest in this study, the structural error is reduced to about only 0.4 % (Figure 4.8). Figure 4.9 shows the finite element mesh of the entire model as well as the mesh configuration on its cross section.

Table 4.3 An optimal meshing scheme for the Drake strength model

Meshing scheme	Mesh summary
Global element size = 0.6 mm	Total nodes = **276,998**
Outer & Inner wires face element size = 0.55 mm	Total solid elements = 232,740
Outer & Inner wires edge divisions = 22 each edge	Total contact elements = **263,088**
Steel wires face element size = 0.45 mm	Total elements = 496,620 *****
Steel wires edge divisions = 20 each edge	(* Including 792 spring elements to stabilize the nonlinear solution)
Longitudinal direction sweep division = 108 (Bias = 3)	

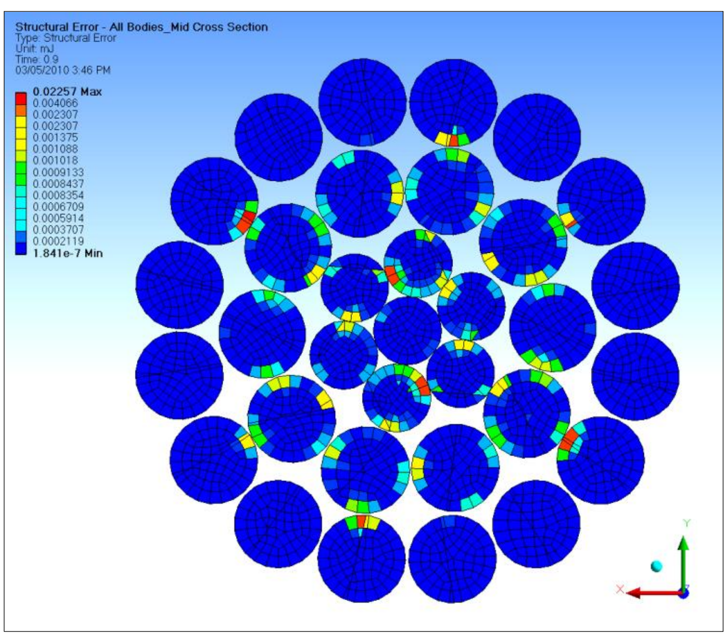

Figure 4.8 Structural error of the Drake strength model due to mesh discretization

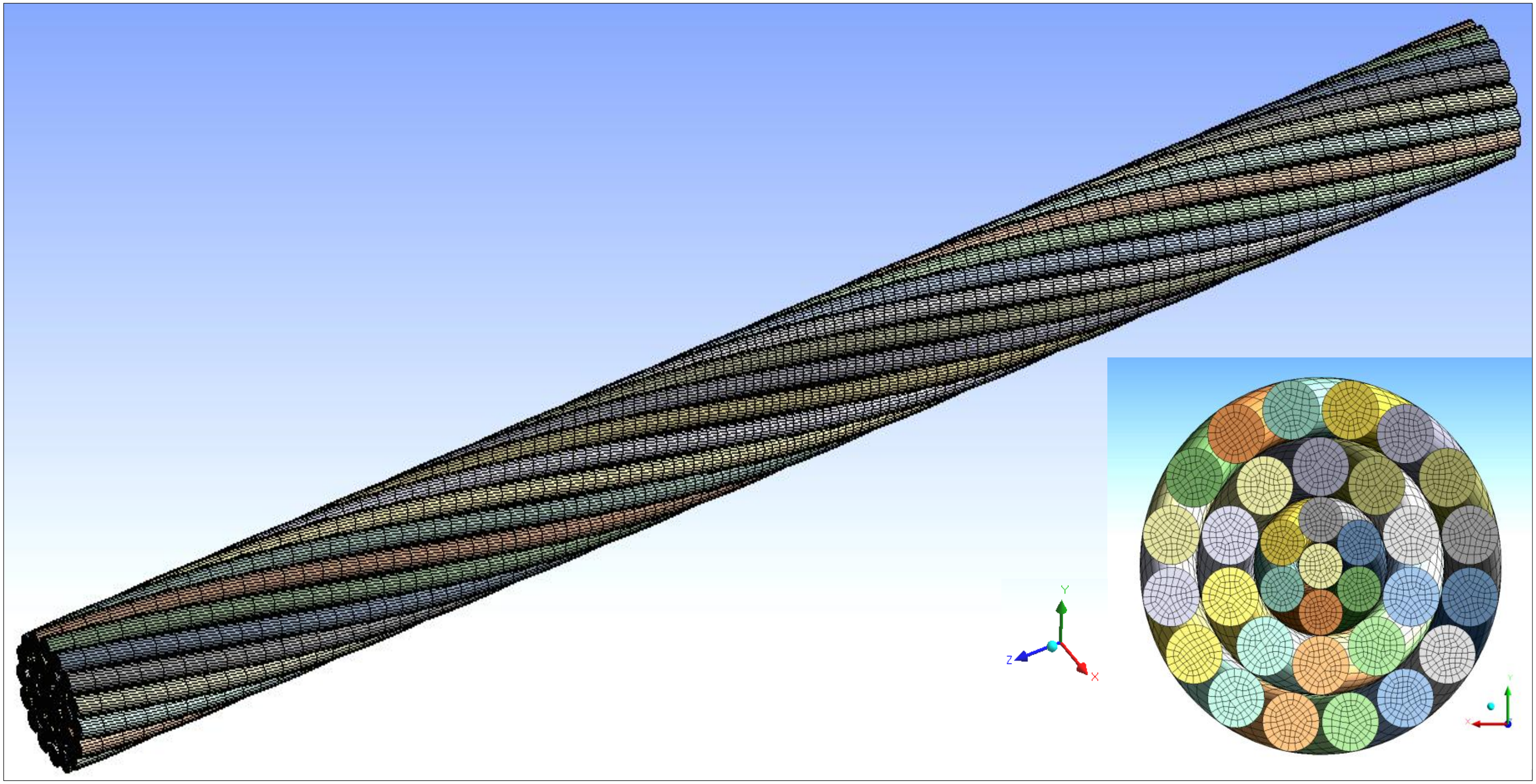

Figure 4.9 Finite element mesh of the Drake strength model - 358.14 (mm)

4.3.3 Contact Conditions, Boundary Conditions and Loadings

The comprehensive contact interactions amongst the Drake wires are all considered as *"flexible-to-flexible"* deformable body contact, and *"surface-to-surface frictional"* contact types are defined on all contact regions. For each contact region, many *"contact pairs"* are created and composed of "contact" and "target" surfaces, which are discretized with 3-D 8-node surface-to-surface contact elements (CONTA174 in ANSYS). As a result, in total 35 contact pairs and **263,088** contact elements are generated for the entire Drake strength model. The classical Coulomb isotropic friction model is used with different frictional coefficients among the contact pairs (Serway, 1995; Kurtus, 2005), and all the assigned μ_s are static frictional coefficients for clean, dry surfaces sliding against each other. Regarding the contact parameter control, normal contact stiffnesses are still the primary factors to control the solution convergence. Many computational experiments had to be conducted to obtain a set of optimal "normal contact stiffness" factors to overcome the convergence difficulties and to achieve high solution accuracy for this large-scale contact model combined with material and geometric nonlinearities. Table 4.4 summarizes the major contact setting parameters of the model.

Table 4.4 Contact settings used in the Drake strength model

Contact region	Contact pairs	Normal contact stiffness factor	Resulting contact stiffness (N/mm^3)	Frictional coefficient (μ_s)
Steel wires & Steel wires	6	0.15	2353.3	0.60
Inner wires & Inner wires	10	0.50	2575.9	0.33
Outer wires & Outer wires	16	0.50	2523.7	0.33
Steel wires 1-6 & Steel wire 0	1	0.15	2356.6	0.60
Steel wires 1-6 & Inner wires	1	0.50	2573.4	0.45
Inner wires & Outer wires	1	0.50	2573.4	0.33

Displacement B.C.s and loading applied to the Drake strength model are in accordance with the laboratory tension test performed by General Cable (2010). And subject to the axial design load, the Drake conductor is assumed to have uniform horizontal tension far from its ends. To model such a condition, the fixed-end surfaces of the conductor (at Z =

0) are fixed in all translational and rotational degrees-of-freedom (DOFs), while tensile loading is applied at the other end (free-end, Z = 358.14mm). Based on the assumption of displacement compatibility for a short segment of a straight cable, the same "*displacement-control*" approach as in the previous OPGW study is used to assign a prescribed axial displacement to all the free-end surfaces. Under ambient temperature, the equivalent elongation of the FE model is **0.45%** of the model length, i.e. **1.61163 mm** ($\Delta l = \varepsilon l = 0.45\% \times 358.14 = 1.61163\ mm$).

4.4 Computational Results and Discussion

Employing the same numerical solution strategies developed in Chapter 3 for the OPGW model, the Drake model was solved with both stable convergence and good accuracy. Certainly, the solution process is still costly due to the large contact problem size and strong triple (material, geometry and contact) nonlinearities of this 3-D model. Computational results of the Drake strength model are presented in this section, and the numerical results are validated through comparisons with experimental data provided by General Cable (2010). As in the case of the OPGW model, all stresses and strains discussed below refer to the cross section at mid-length of the model (Z = 179.07mm).

The total deformation of the Drake strength model under the prescribed elongation (corresponding to extreme design condition) is shown in Figure 4.10. Figures 4.11~4.13 illustrate the longitudinal displacement field Uz (z-axis) of the wires at the mid-length cross section. The Uz distributions of both the outer and inner aluminum wires are symmetric with respect to the conductor center (z-axis). As it will be seen later, this observation will also apply to all stress (and strain) distributions since only tension loading is applied on the strength model. In addition, all the wires in a given layer have the same longitudinal displacement pattern, and they are opposite between adjacent layers. The non-uniform displacement distributions in each wire are induced by their helical geometric configuration, opposite lay angles, and the resulting unbalanced torque. The largest axial displacement occurs on the steel helical wires and the smallest one is on the outer layer aluminum wires. The variations in axial displacements in each layer are summarized in Table 4.5. The largest variation is obtained among the outer wires due to their larger helical angle (11.74^{o}), while the axial displacements in the steel core wires are quite uniform due to their very small helical angle (4.79^{o}).

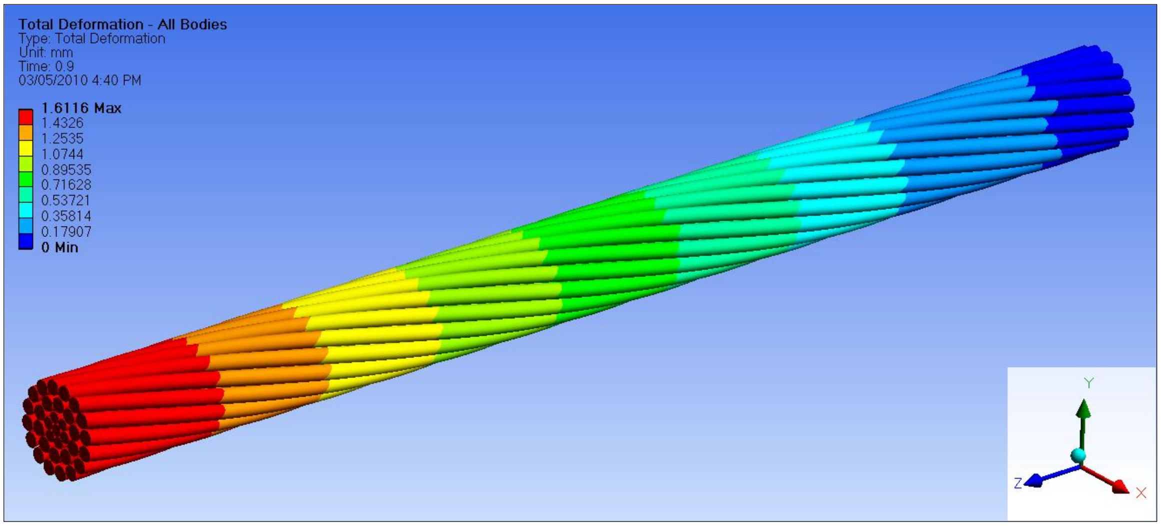

Figure 4.10 Total deformation of the Drake strength model under elongation

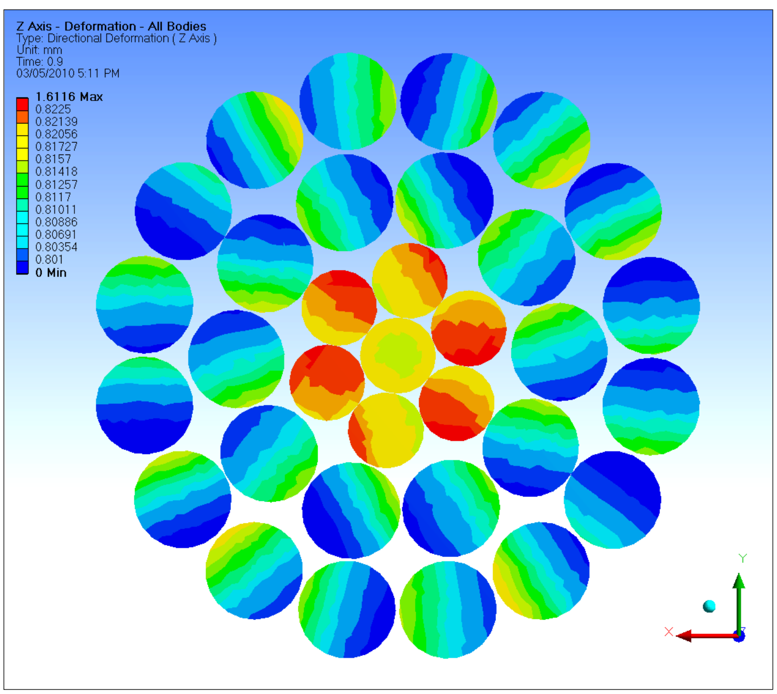

Figure 4.11 Axial displacement (**U**z) of Drake wires at mid-length cross section

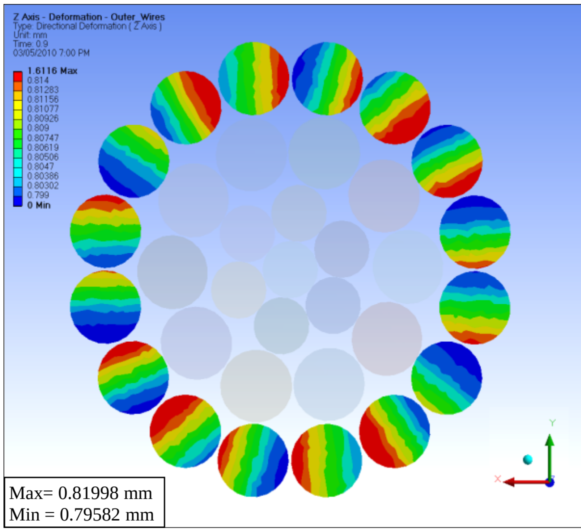

Figure 4.12 Uz of Drake outer wires

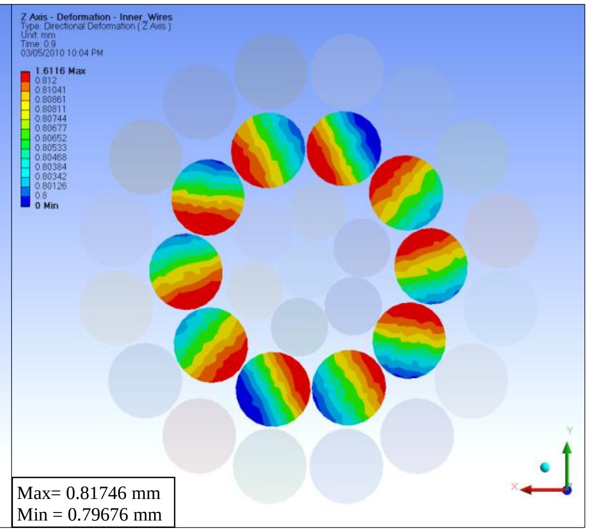

Figure 4.13 Uz of Drake inner wires

Table 4.5 Variations of axial displacement in Drake wires at mid-length cross section

Wires	Max. Uz (mm)	Min. Uz (mm)	ΔUz (mm)
Outer aluminum wires	0.81998	**0.79582**	0.02416
Inner aluminum wires	0.81746	0.79676	0.02070
Steel wires	**0.82495**	0.81609	0.00886

The Von-Mises stress field of the Drake conductor at its mid-length cross section is shown in Figure 4.14. It clearly indicates the structural role of the steel wires due to their higher axial rigidity, the steel wires carry the largest portion of the tensile loads with much higher stresses than in the aluminum wires. While the stresses in the steel wires are rather uniform (671.2 MPa ~ 682.1 MPa), the outer aluminum wires have larger stress gradients than the inner wires (see Figures 4.15 and 4.16). Also, the results indicate that the Von-Mises stresses of both the steel and aluminum wires are far beyond their respective yield strengths (Y_{Steel} = 620.52 MPa; Y_{Al}=68.95 MPa), so the whole cable is undergoing significant inelastic deformations at the end of the loading.

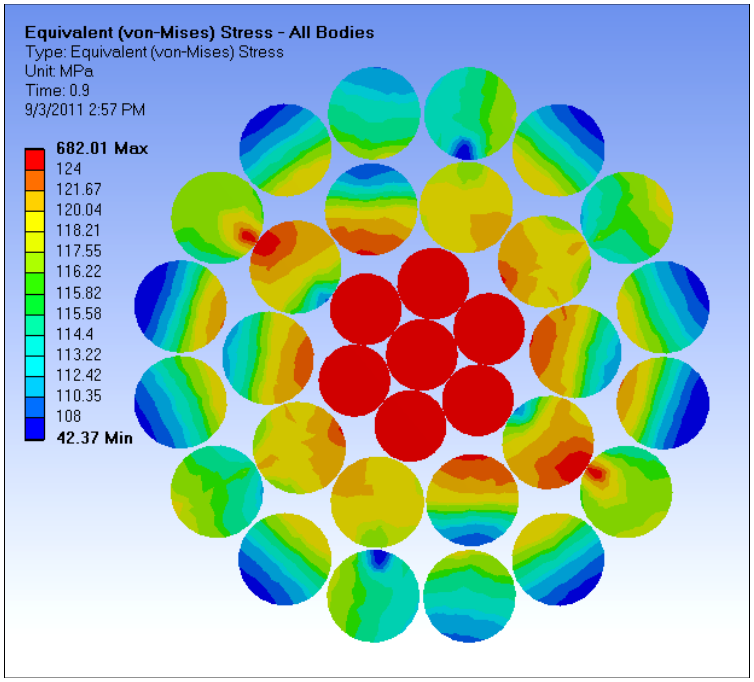

Figure 4.14 Drake Von-Mises stress (**S**$_{von}$) at mid-length cross section

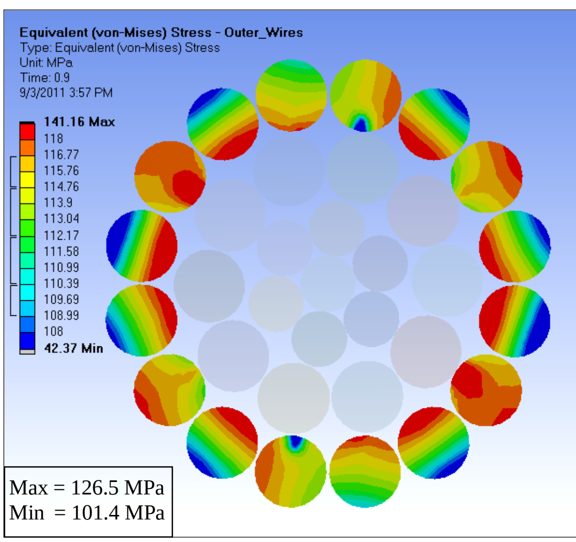

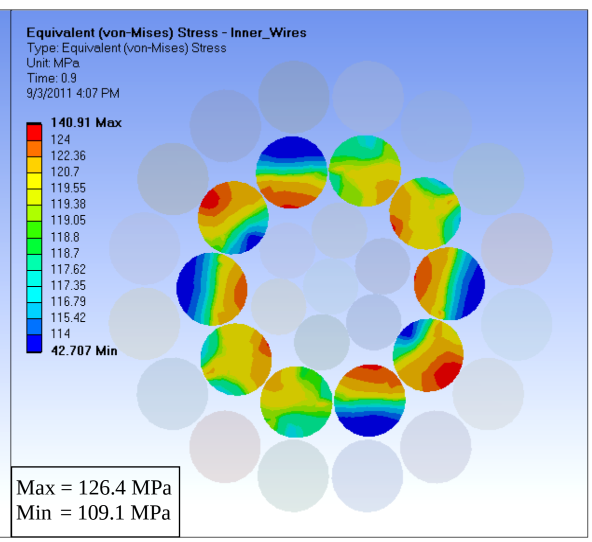

Figure 4.15 **S**$_{von}$ of Drake outer wires

Figure 4.16 **S**$_{von}$ of Drake inner wires

The Drake axial stress field (S_{zz}) at the mid-length cross section (Figure 4.17) exhibits a very similar pattern to the Von-Mises stress field as only tensile loading is applied. The maximum S_{zz} occurs on the steel wires, and the detailed distributions of S_{zz} on the outer and inner aluminum wires are presented in Figures 4.18 and 4.19, from which one can see the effects of friction on the tensile stresses in the vicinity of the contact surfaces.

On a particular cross section, for those wires that do not contact with adjacent layer wires, under the interactions of tension and unbalanced torque, their wire cross sections have the same axial stress distribution: inboard is larger, outboard is smaller (i.e., stresses are decreasing outward). However, once frictional contact exists, this pattern reverses. Actually, without any exception (during the entire loading history), the minimum axial stresses in the outer and inner aluminum layers, as well as the steel layer are all attributed to frictional contact: Tangential contact stresses (in the opposite direction) significantly reduce the tensile stresses in the contact regions. For the outer layer, the minimum axial stress occurs at the location of a contact surface between the outer and inner wires (Figure 4.18); for the inner layer, the minimum axial stress occurs at the location of a contact surface between adjacent inner wires (Figure 4.19). In addition, it is also observed that stress concentrations may occur in the steel wires at some load incremental steps, which increase significantly their peak axial stresses. These stress concentrations occur when the tangential contact stress is in the same direction as the tensile stress, causing a superposion of the stresses in the axial direction.

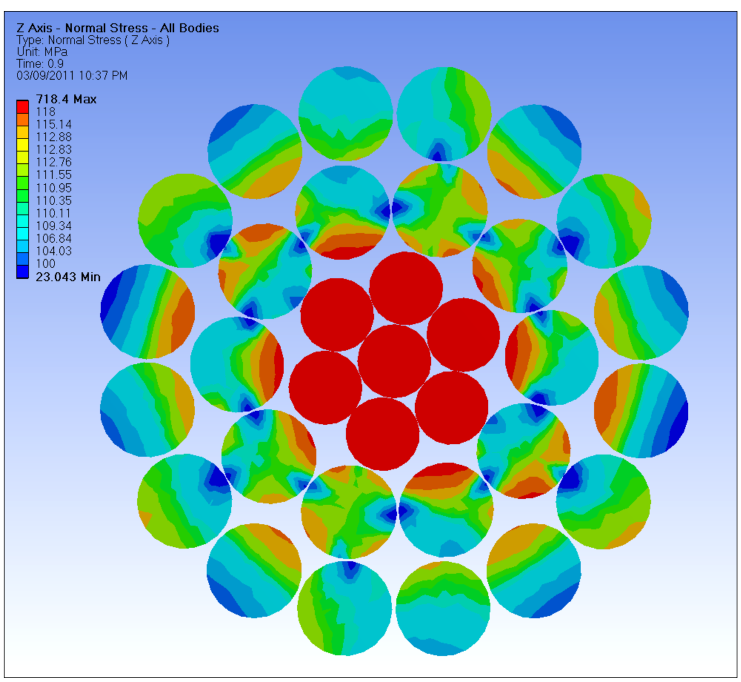

Figure 4.17 Drake axial stress ($\mathbf{S}_{zz}$) at mid-length cross section

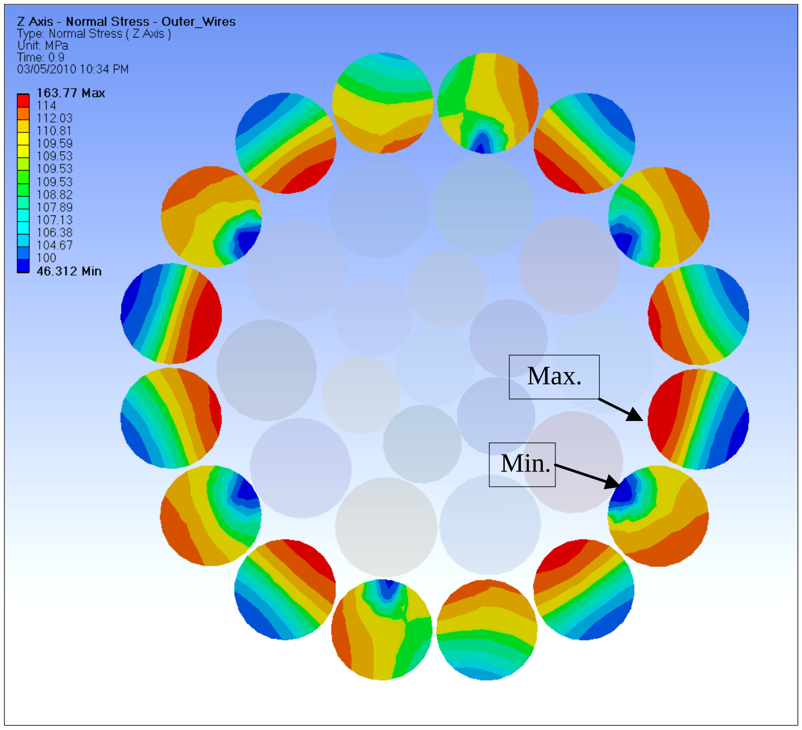

Figure 4.18 Drake outer wire axial stress ($\mathbf{S}_{zz}$)

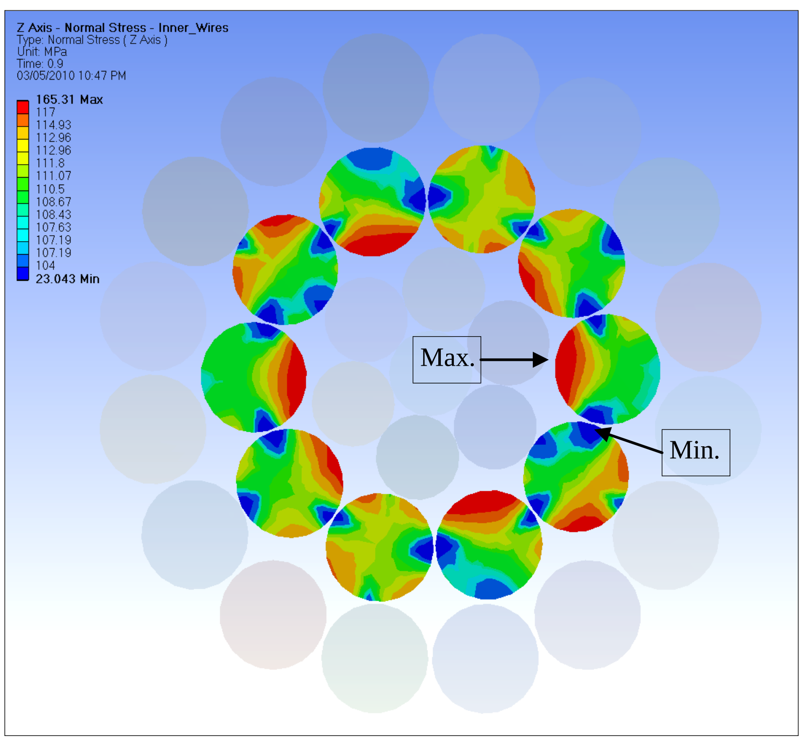

Figure 4.19 Drake inner wire axial stress ($\mathbf{S}_{zz}$)

A comparison of the axial stresses of the Drake wires obtained by FEA and experimental data (General Cable, 2010) is illustrated in Figure 4.20, which clearly shows their overall agreement along the entire loading history, especially for the aluminum wires. This validation shows again that the conductor FE modeling methodology and related numerical solution strategies developed in the thesis are successful and reliable. In the meanwhile, it can be noticed that, at the end of the loading, the computed stress of the aluminum wires is 7.2% higher than the experimental value, while the computed steel wire result is 12.7% lower. Besides the assumed material properties of the computational model (as explained before) and the inevitable modeling errors, another important factor that may contribute to the stress differences between the FE model and the test data is the magnitudes of the static frictional coefficients among the different contact surfaces; these coefficients have uncertainty and thus have to be estimated in the numerical model. As observed earlier, the axial stress, Szz, is the combination[2] of the tensile stress and tangential contact stress, while the effects of tangential contact stress induced by friction are significant. Following these observations, a sensitivity study on the effects of frictional coefficients is motivated and the results are presented in the next section.

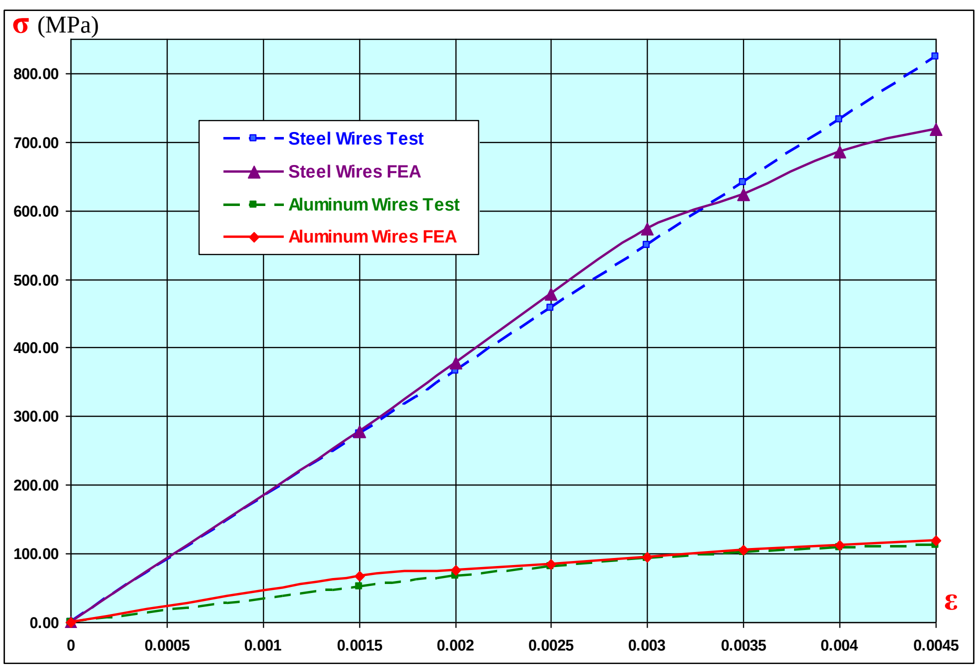

Figure 4.20 Comparison of Drake $\mathbf{S}_{zz}$ obtained by FEA results and testing data

[2] Szz is not a simple algebraic superposition of tensile stress and frictional stress in that the directions of tangential contact stress vary at different locations due to the helical configuration of the conductor wires.

4.5 Sensitivity Study of Frictional Coefficients

First of all, it is worth mentioning that the real frictional coefficient for a particular material combination as well as its nominal value measured by engineering laboratories is actually affected by the problem environment and various experimental conditions, such as temperature, relative humidity and the quality of the contact surfaces (surface roughness, surface oxidation, presence of surface films - dirt, water, grease, etc.), which all can dramatically change the coefficient of friction. When a metal surface is perfectly dry and clean, the friction is much higher than the nominal accepted value and seizure can easily occur. For instance, the static frictional coefficient between dry and clean steel surfaces may be as much as 3 times higher than that on their oxidized surfaces (Kurtus, 2005). In view of this, a major problem when using the values established by others, such as those published in the literature, is that the exact testing protocol and surface conditions of the tested materials are not known. Furthermore, even for the basic dry Coulomb friction model, the frictional coefficients may still depend on the contact time, magnitude of the normal force and the sliding speed (Popov, 2010). Therefore, although great care may be taken, an accurate determination of the coefficients of friction to be implemented in a FE model is generally very difficult if not impossible, and a range of realistic values might have to be considered. (This is actually a pratical challenge in the validation of a FE model.)

As stated in section 4.3.3, the classical isotropic Coulomb's law of static friction is used in this thesis. Because the main purpose of this sensitivity study is to examine the effects of different frictional coefficients on the predicted stress states on the contact surfaces of the aluminum wires, only the frictional coefficient values among the contact pairs of aluminum wires are varied, while the frictional coefficients involving contact with steel wires are kept constant (see Table 4.6). Based on several sources (Serway, 1995; Kurtus, 2005; Ramsdale, 2006), the selected values of frictional coefficient for aluminum surfaces vary from 0 to 1.35, thus covering the entire spectrum of μ_s from ideally frictionless contact to lubricated conditions, up to complete dry and clean surfaces sliding against each other.

Table 4.6 Frictional coefficient schemes in Drake strength model

Contact regions (Contact Pairs)	Frictional coefficient (μ_s)				
	Case 1	**Case 2**	**Case 3**	**Case 4**	**Case 5**
Steel wires & Steel wires (6)	0.60	0.60	0.60	0.60	0.60
Inner wires & Inner wires (10)	***0***	***0.33***	***0.57***	***1.05***	***1.35***
Outer wires & Outer wires (16)	***0***	***0.33***	***0.57***	***1.05***	***1.35***
Steel wires 1-6 & Steel wire 0 (1)	0.60	0.60	0.60	0.60	0.60
Steel wires 1-6 & Inner wires (1)	0.45	0.45	0.45	0.45	0.45
Inner wires & Outer wires (1)	***0***	***0.33***	***0.57***	***1.05***	***1.35***

The conclusions from the parametric study can be summarized as follows:

(1) The results confirm that the frictional coefficients have no significant effects on the normal contact stresses since the model is under tensile loading.

(2) The axial stresses in the inner and outer layer wires with different μ_s are presented in Figures 4.21 and 4.22, respectively, confirming the significant effects of frictional coefficients on the conductor axial stresses. During the entire loading process, the ideal frictionless contact condition generates the maximum axial stress field. Once friction is introduced, the axial stress field is affected (reduced) differently on the outer and inner wires with increased loading.

(3) Due to their larger helical angles, the frictional effects on the outer layer wires are relatively higher than on the inner wires in that the increase in normal contact force is more important. For the inner layer wires, the maximum axial stress difference among the different μ_s values considered can reach 6.8%; for the outer layer wires, the frictional contact can even contribute up to 16.2% stress reduction under the extreme design load.

(4) After the μ_s value was increased above 0.57, the stress differences calculated with different frictional coefficients were negligible. This observation implies that the calculated axial stresss will remain insensitive to variations in the frictional coefficient as long as the conductor aluminum wire surfaces remain in dry and clean working conditions.

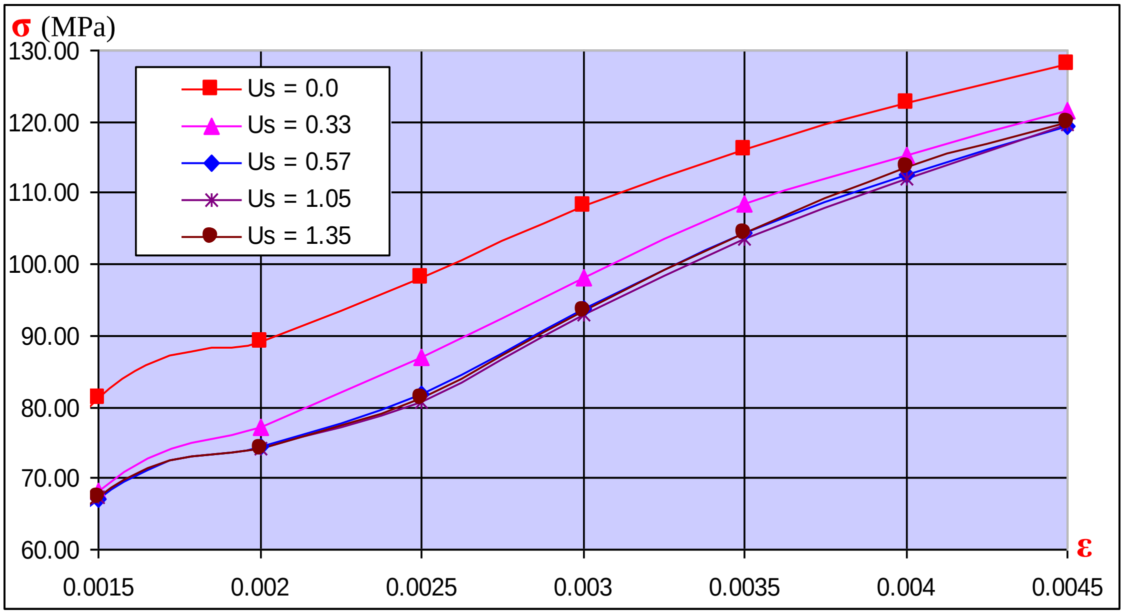

Figure 4.21 Peak axial stress in Drake **inner** layer aluminum wires with different μ_s

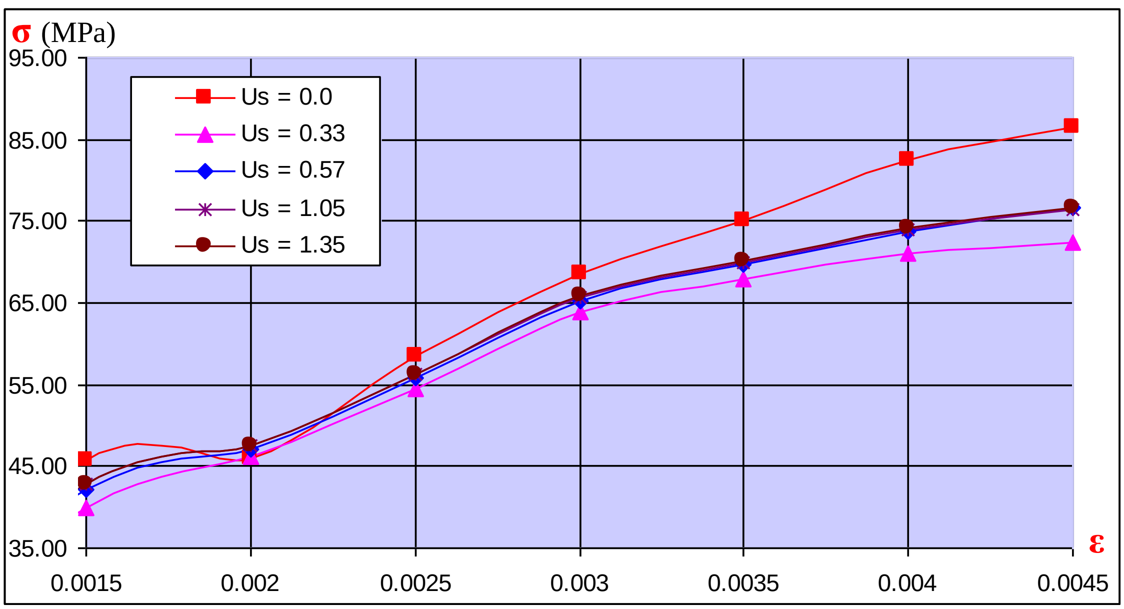

Figure 4.22 Peak axial stress in Drake **outer** layer aluminum wires with different μ_s

4.6 Summary Remarks

The study conducted in this chapter is to model the mechanical behavior of transmission line conductor wires under axial design load with a view to investigate the tensile strength of a complete conductor. The 795 kcmil Drake ACSR conductor is selected as the benchmark conductor for the modeling study. It is made of two conductive layers comprising a total of 26 aluminum wires and a structural steel core of 7 wires, for an overall diameter of 28.13 mm. A 3-D elastic-plastic, large kinematics, multi-body frictional contact finite element model of a 358.14-mm section of this conductor was constructed successfully based on its nominal material properties and selected geometric specifications. The detailed model comprises all components of an ACSR conductor strand, and attempts to consider all possible mechanical effects under extreme design conditions. In total the FE model is defined by **276,998** nodes, **232,740** solid elements, and **263,088** contact elements.

Employing the modeling methodology and numerical strategies developed in the preceding chapter, good solution accuracy is obtained with stable convergence process. The results of the static stress analysis show agreement with the experimental data provided by Drake manufacturers. Furthermore, a sensitivity study explored the effects of variability in the friction coefficients among the conductor aluminum wires on their stress response. Again, as for the OPGW model of Chapter 3, this study demonstrates the capability and significance of using refined FE modeling in predicting the detailed mechanical response of a complex conductor cable, as well as the validity of the modeling approaches developed in this thesis.

Chapter 5

Computational Modeling for ACSR Conductor Fretting Fatigue

5.1 Introduction

Up to this stage, based on the success shown in the preceding chapters in developing a sound modeling methodology for detailed stress analysis of electrical conductors under extreme design conditions, some confidence has been gained to launch a computational study of conductor fretting fatigue, which becomes increasingly critical for overhead line (OHL) design and maintenance.

OHL conductors are exposed mainly to static or quasi-static loading in their normal service. The effects of these external loads are essentially to cause fluctuations in the cable tension. Other localized loads on the conductors are those local compressive forces exerted by the clamping devices of suspension clamps or other hardware components such as vibration dampers, spacer-dampers, etc. During most of their lifetime, however, conductors are subjected to external loads that are only a fraction of their peak design requirements. Meanwhile localized bending effects often associated with conductor fatigue have been widely recognized as the most dangerous threat to the conductor's mechanical reliability. Conductor fatigue can drastically reduce the conductor service life, especially in the presence of Aeolian vibrations that occur at high frequency. These oscillations generate alternating bending stresses in conductors at their junction with clamping systems or any hardware device that constrains the vibrations. Aeolian vibrations promote fretting fatigue failure of individual conductor wires in suspension clamp regions and may lead to entire conductor rupture (see for example, Ramey and Townsend, 1981; Zhou et al., 1994, 1995, 1996; Aggarwal et al., 2000). Moreover, many overhead transmission lines around the world are reaching middle age (25~40 years old and more) and aging conductors are showing evident signs of deterioration (Azevedo and Cescon, 2002). Accordingly, the structural optimization and maintenance of overhead conductors also depend heavily on the systematic investigation of the fretting fatigue mechanisms in conductor/clamping regions (Azevedo et al., 2009).

As reviewed in Chapter 2, a large number of laboratory tests on conductor fretting fatigue were performed over the past decades. Although it is true that some general trends can be found from experimental studies, such as the ones summarized in Chapter 2, it is well acknowledged that, fretting fatigue behavior of conductor wires is very difficult to predict and characterize owing to their synthetic geometry, material and loading complexities. For instance, wire fractures were actually observed on either external or internal layers depending on different test conditions; fretting crack propagations may have quite different modes and different contributions to total fatigue life, and so on.

From the structural mechanics perspective, accurate description and prediction of the conductor stress states at the clamp mouth regions are fundamental to provide a clear explanation of the mechanical behavior of stranded conductors under fretting fatigue conditions and to identify the fatigue damage initiation (fretting crack nucleation). Furthermore, even small stress variations (only by a small percentage) can make a significant difference in the fatigue life of overhead lines. As we have seen from the work presented in Chapters 3 and 4, the complex (contact) stress states among individual conductor wires as well as the ones between the external wires and the clamp surfaces are not accessible to direct measurements, while the theoretical fatigue-life assessment models based on semi-empirical formulae and linear elastic hypotheses can only predict idealized nominal stresses (see for example, Cardou et al., 1993; Papailiou, 1995, 1997; Jolicoeur and Cardeau, 1996). Numerical modeling thus appears the only effective approach to achieve this goal although such an effort has been claimed to be a daunting task (Azevedo et al., 2009).

To the author's knowledge, no such a numerical work is available yet in the open literature that presents a rational mechanics-based model to describe the fretting fatigue phenomena in electrical conductors. Hence, the main goal of the present study is to develop a faithful FE model to explore the mechanical response of a typical stranded conductor-clamp system under bending fretting fatigue conditions. Local stress and strain fields in the suspension clamp mouth regions of fretting are predicted by detailed 3-D elastic-plastic multi-body contact analyses with friction. Computational results are validated by comparing them with published experimental data. Based on the accurate stress analyses, a practical fatigue lifing method is proposed to asses the conductor service life. Thereafter, a parametric study is conducted to examine the effects of fretting amplitude on the fretting fatigue in this application.

5.2 Assumptions for Numerical Modeling of Fretting Fatigue

The simulations of fretting phenomena in real conductor situations are currently intractable. Accurate description of the mechanics states of a conductor under fretting and prediction of its fretting fatigue life during normal operation conditions are still beyond our engineering capability. As reviewed in Chapter 2, the damage mechanisms of fretting fatigue are complex and their description may require numerous parameters. Thus, some simplifying assumptions are necessary to make the numerical models manageable in size and complexity, while still ensuring reliable results. It should be mentioned that this work should be seen as a preliminary computational study on this topic. In order to preserve the key features of the actual physical event rather than to expose all factors involved in conductor fretting failure mechanism, the following six assumptions and simplifications are made:

(1) As indicated in Chapter 2, fretting debris might be generated in the “mixed regime”, which means that the so-called “third-body” contact might exist in some local contact regions, and the effects of the debris on fatigue cracks are not negligible. However, the extremely complicated mechanisms of the formation and evolution of fretting debris (involving fretting wear, tribological white layer, oxidation, etc.) and the uncertainty of its characterization make the simulation of the debris very difficult. Hence, in this study, fretting debris is not considered in the FE models.

(2) The forcing frequency of the external cyclic loading induced by wind and the ensuing fretting motion may have some effects on the initiation and propagation of fretting cracks, mainly owing to their influence on fretting debris (Zhou and Vincent, 2002). Since no debris is included in the models, the fretting frequency is not a studied parameter in the analyses, i.e. the models are only subjected to static loads.

(3) In practice, some forms of lubricant (mainly lubrication grease) might be included in the cables to lessen fretting wear. A comprehensive experimental study of the influence of lubricants on conductor fretting fatigue was carried out by Zhou et al. (1992-1999). It was shown that the effectiveness of lubrication grease on lessening fretting fatigue is not significant under heavy clamping forces and minute amplitude of fretting slips. Hence, only unlubricated, clean and dry contact surfaces of the conductor are assumed in the fretting models.

(4) The frictional coefficient does vary with the number of fretting cycles (refer to Figure 2.2), which is mainly due to the dynamical process of the formation and escape of fretting debris. In addition, fretting displacement amplitude, normal load (clamping force), and other factors may also significantly affect the magnitude of the frictional coefficient. Nevertheless, due to the limited availability of relevant data, the frictional coefficients among the conductor components are considered to remain constant during the entire loading history.

(5) The tangential contact stiffness (K_s) is an important factor in fretting, and it is determined by both the material properties and the size of the contact areas. It may also vary with the number of fretting cycles. From some experimental observations (Zhou and Vincent, 2002), the variation of K_s with fretting amplitude is practically negligible under low fretting cycles (N usually $<10^5$, i.e., within the stage of fretting crack nucleation). Thus, the initial K_s is assumed to remain constant during the parametric study of the effects of fretting amplitude.

(6) The conductor sag angle (usually about 10 degrees) in conductor/clamp systems is ignored in the numerical models. Comparing with the real testing conditions, this is the only geometric approximation in the 3-D solid modeling.

5.3 Drake Fretting Fatigue Solid Model Construction

Even if considered in a controlled laboratory testing environment, different fretting conditions may have crucial influence on the conductor fretting cracking behavior; the nucleation and propagation of local fretting cracks strongly depend on the material properties, contact geometry configurations and loading conditions, as well as their synergistic effects. Accordingly, for the purpose of developing a modeling methodology, the FE model needs to correspond to a particular conductor-clamp system.

In practice, to hang electrical conductors to insulator strings or hang the ground wires to tower arms/peaks through link fittings, "*suspension clamps*" have been used. A suspension clamp assembly (see Figure 5.1) includes typically a lower clamp body with a lengthwise groove for receiving the lower side of a conductor, an elongated upper keeper to apply to the upper side of the conductor, as well as two U-bolts and nuts that connect the clamped conductor assembly. The suspension clamp is a critical line hardware component because of its paramount function of connecting the conductor to the tower supports, and it must be designed carefully to avoid damaging the conductor by premature wear, fretting, etc.

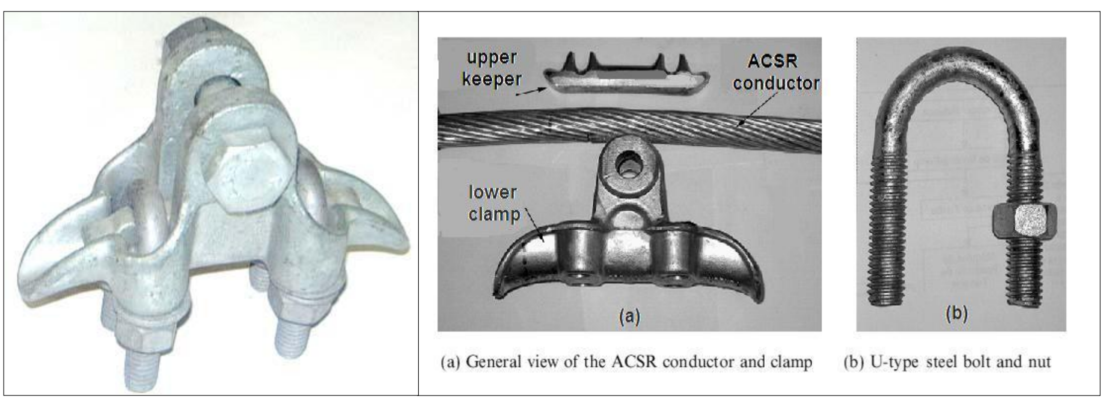

(a) General view of the ACSR conductor and clamp (b) U-type steel bolt and nut

Figure 5.1 Suspension clamp and conductor installation (Azevedo et al., 2009)

Similar to the situation for conductor design, although the general shapes of suspension clamps are quite standard, different manufacturers have their own types, configurations and materials to design a suspension clamp assembly for different types of conductors, and the dimensions of a suspension clamp may vary with the conductor diameter, leading to numerous commercial suspension clamp products on the market (see for example, Liling Orient Power Co., Ltd., 2009). Therefore, a set of definite specifications has to be determined for a specific suspension clamp assembly to be used in this study.

First of all, the common "*envelope type*" suspension clamp is chosen, which is actually also the one used in most transmission line fretting fatigue lab tests. To build the suspension clamp 3-D model, the shape of the lower clamp body is defined according to the design data available from EMI Transmission Ltd. (2007), Preformed Line Products Ltd. (2009) and Liling Orient Power Co., Ltd. (2009). The profile of the upper keeper is also referred to an early invention by Eddens and Reed (United States Patent No. 3602956) with improved grooved shape to prevent cable fretting fatigue breakage. In addition, from a fretting fatigue point of view, the critical zone of a suspension clamp is located between the *keeper edge* (**KE**) and the *last point of contact* (**LPC**) of the clamp body, and thus the lengths of the clamp body and the keeper are the most important geometric parameters to affect contact stresses, fretting regions and crack initiation. In accordance with the experimental work reported in the literature that will be used for model validation, these two key dimensions are those used in the DRAKE conductor fretting fatigue tests performed by Zhou et al. (1994, 1995), as schematized in Figure 5.2.

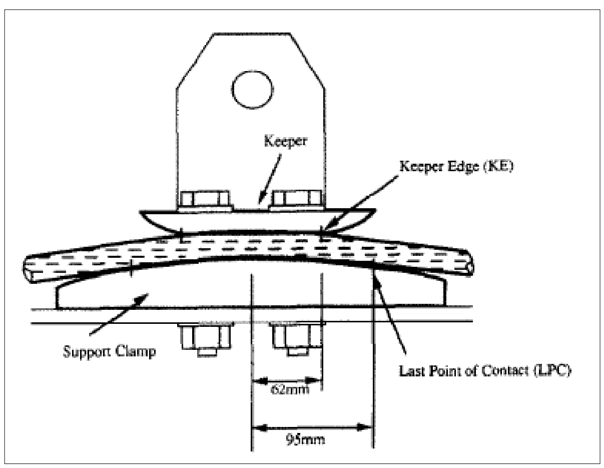

Figure 5.2 Key dimensions of the clamp body and keeper (Zhou et al., 1994)

As a result, a generic "*envelope type*" suspension clamp assembly is designed, shown in Figures 5.3 and 5.4. It is a 216 mm clamp with a 124 mm keeper that are both made of permanent mould-cast aluminum. The upper keeper is pressed on a conductor with two stainless steel U-bolts and nuts.

The "Drake" conductor is selected because it is widely used worldwide and extensive fretting fatigue testing data is available in the open literature for this conductor. Accordingly, the same 795 kcmil "Drake" type ACSR described in Chapter 4 is used for the fretting fatigue study. The conductor cross section with numbered wires in each layer referring to the suspension clamp center (**SCC**) is shown in Figure 5.5.

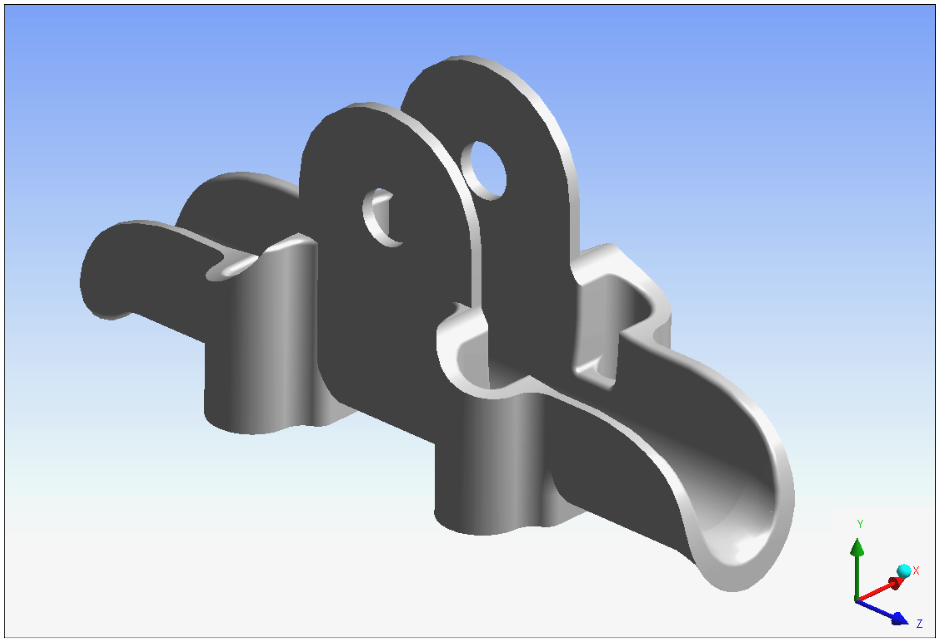

Figure 5.3 The suspension clamp lower body solid model

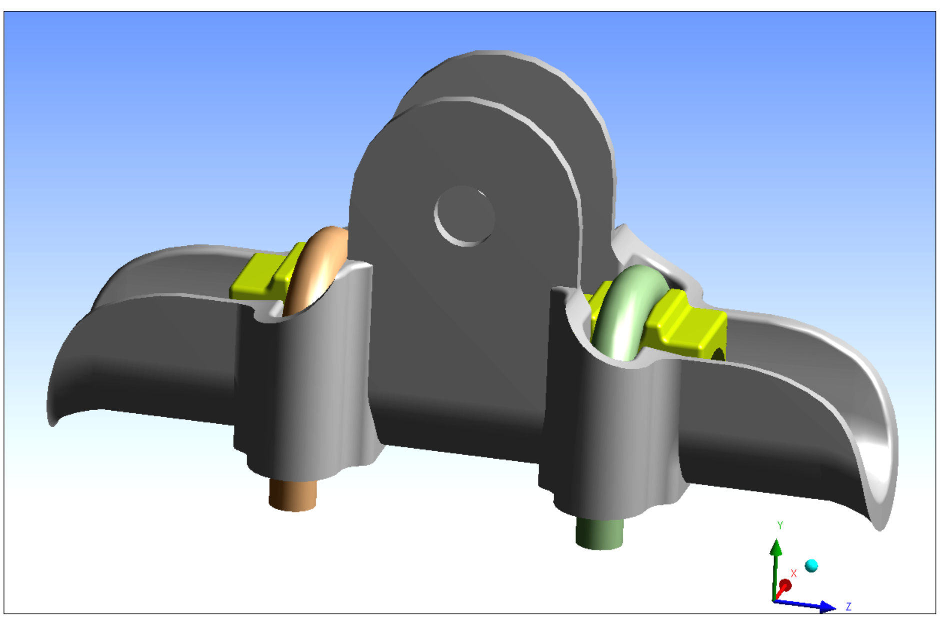

Figure 5.4 The suspension clamp assembly solid model

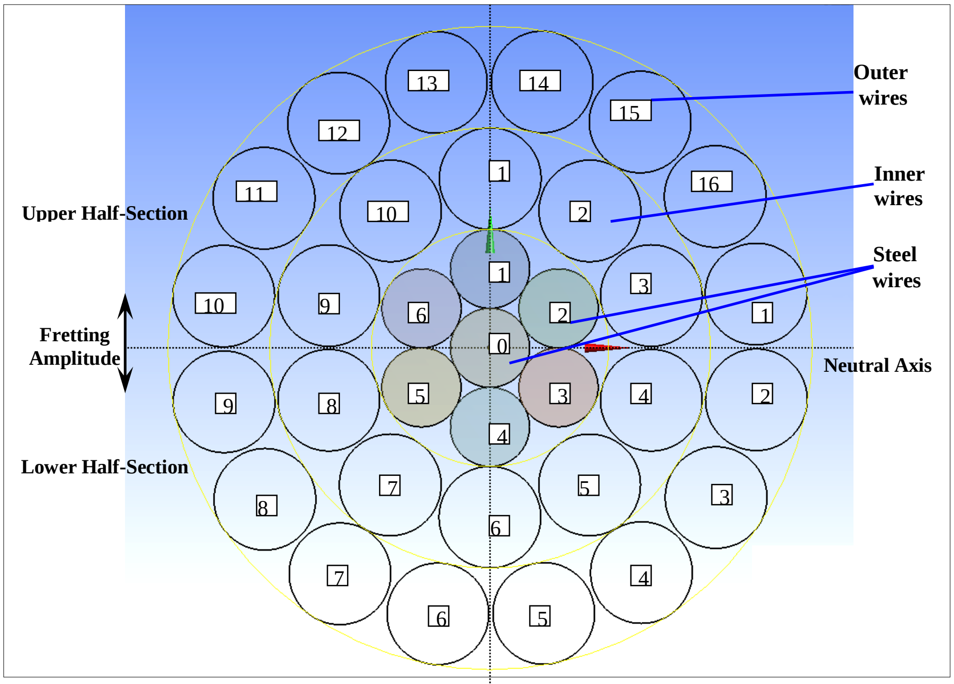

Figure 5.5 Drake cross-section with wire numbering for bending fretting fatigue study

The experimental setup for a bending fretting fatigue test of a conductor-clamp system has been standardized in the IEEE standard (1966) and the EPRI Transmission Line Reference Book (1979, 2006). Two very similar testing benches are typically used (see for example, Zhou et al., 1996; Ouaki et al., 2003), one of which is shown schematically in Figure 5.6, while another may be found in Figure 2.12 of Chapter 2. These test set-ups share the same principle of operation that can be described herein:

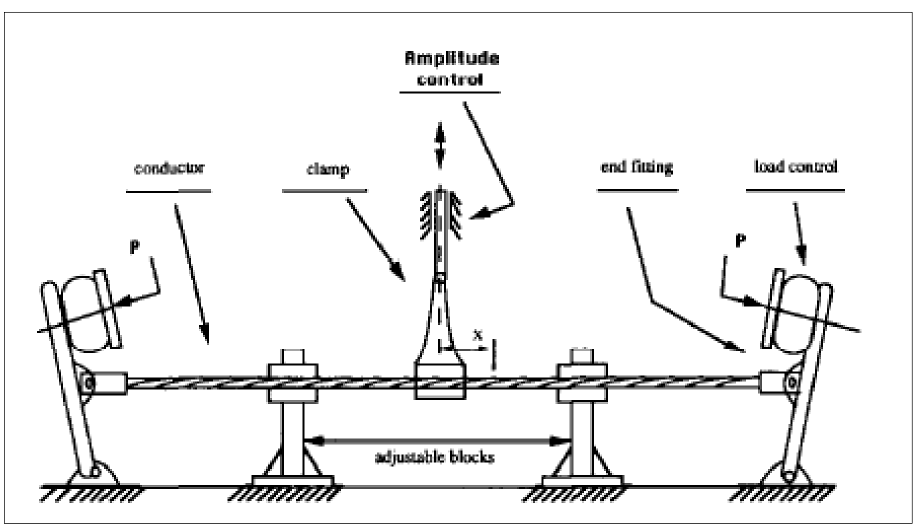

Figure 5.6 Schematic of conductor bending fretting fatigue test bench (Zhou et al., 1996)

In compliance with the above standards, the imposed transverse peak-to-peak relative fretting amplitude (**Y_b**) needs to be measured at a distance of **89mm** (3.5 inches) from the last point of contact (LPC) between the conductor and the suspension clamp. This bending amplitude is imposed on the conductor specimen via an adjustable slider-crank mechanism where the suspension clamp is attached to the slider. The up-and-down motion of the clamp induces a slight variation of the conductor angle at the clamp mouth. For a given location on the conductor axis, this motion corresponds to the bending amplitude with respect to the clamp, where the clamp can be considered as fixed. To be accurate, two adjustable blocks located on both sides of the clamp can be moved horizontally, vertically and angularly to obtain the desired relative amplitude. Both ends of the conductor specimen are fixed to a tensioning system in order to maintain a constant tensile pre-load during the entire test period, which is usually taken as 18% ~ 25% of the conductor *"Rated Tensile Strength"* (**RTS**). The cycling frequency is typically limited to 10 Hz in order to avoid undesirable dynamic effects. This forcing frequency is also representative of field conditions in the lower frequency range. The tests can be run from 0 (static test) up to about 2 x 10^7 cycles (over 23 days at 10 Hz).

Recently, a practical and proven effective bending fretting fatigue testing rig for overhead conductors was designed by Azevedo et al. (2009) with the same operational principle as described above. The test is controlled by a prescribed vertical fretting displacement measured by a laser sensor positioned at **89 mm** from the LPC between the conductor and the clamp, as illustrated in Figure 5.7. This rig design and some of the testing parameters in this experimental work are adopted in the present numerical modeling. As stated before, the axial position of KE is located at **62 mm** from the clamp transverse symmetry plane (i.e. suspension clamp center, SCC) that is defined as the origin of the model. The LPC is positioned at **95 mm** from the origin.

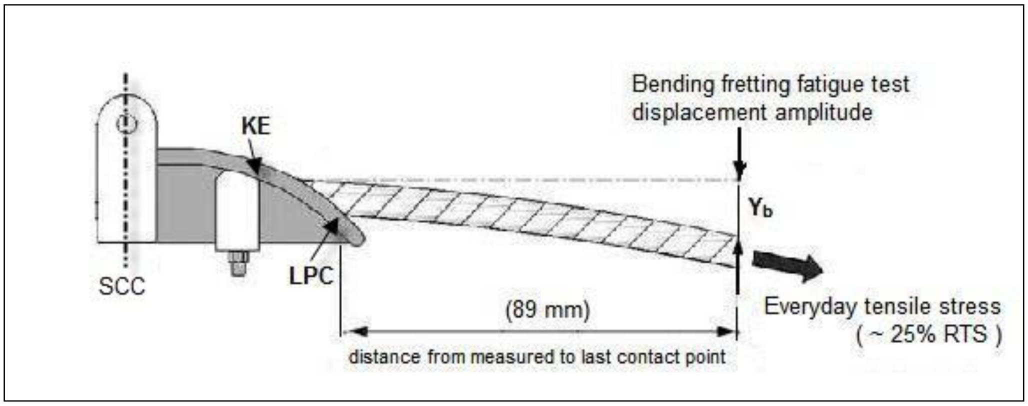

Figure 5.7 Schematic of conductor bending fretting fatigue model (Azevedo et al., 2009)

The 3-D Drake conductor fretting fatigue solid model assembly is also built using DesignModeler of ANSYS Workbench 11.0. Due to the symmetric configuration in the test, only half of the assembly is used for the FE model, as shown in Figure 5.8. The model is comprised of a total 36 solid bodies: 33 conductor wires, the suspending clamp body, the upper keeper and the U-bolt. The total conductor length in the model is the half length of the suspension clamp up to the LPC, 95 mm, plus the measurement distance at fretting amplitude, 89 mm. That is, the total model length is: **L = 95 + 89 = 184 (mm).**

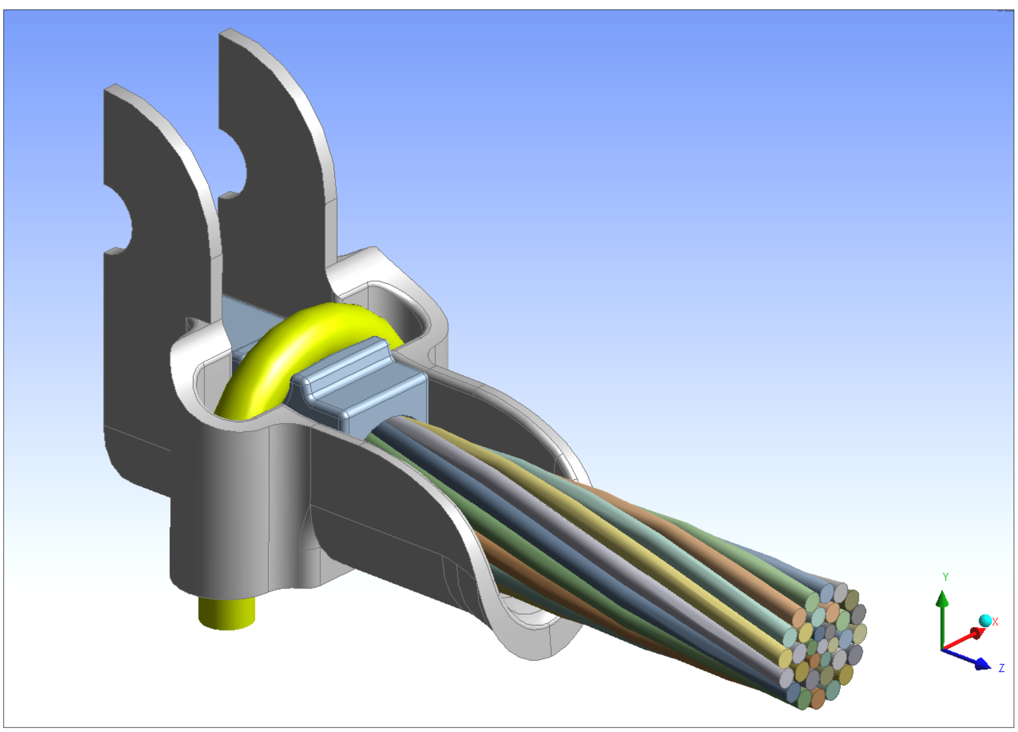

Figure 5.8 Drake conductor-clamp solid model for fretting fatigue study (184 mm)

5.4 Finite Element Modeling

While some of the methodologies developed in the preceding chapters are proven still effective for this study, new challenges are encountered due to the unique features of the problem. The detailed FE modeling procedures are summarized in this section.

5.4.1 Material Properties

Certainly, the Drake conductor wire material properties are the same as the ones used in Chapter 4: all individual wires are assumed elastic-plastic, with large kinematics and small strain under fretting fatigue loading.

As for the clamping device, the suspension clamp lower body and upper keeper are both made of common aluminum alloy and U-bolt is made of galvanized stainless steel. Their elastic properties can be easily available from the open literature. Although some experimental tests exposed that plastic deformations were observed on the clamps, we will focus only on the conductor wires instead of the clamping devices in this study, and thus the plastic material properties of the clamping device are not considered. Indeed, comparing with all previous work on this topic, modeling the clamping devices as elastic contact deformable bodies is already a big step forward since previous theoretical studies (without exceptions) always regarded the suspension clamp body, upper keeper and bolts as perfect rigid bodies. For completeness, the material properties and characteristics for the Drake fatigue model are summarized in Table 5.1.

Table 5.1 Drake conductor-clamp system material properties and characteristics

Component	Material	Properties	Characteristics
Outer & Inner layer wires	Aluminum 1350-H19	E = 68.95 GPa; ν = 0.33 Y = 68.95 MPa; UTS = 186.1 MPa	• linear elastic to multi-linear plastic, • large kinematics, • small strain
Core steel wires	Steel IEC60888	E = 206.84 GPa; ν = 0.29 Y = 620.52 MPa; UTS = 1846 MPa	
Clamp body & Keeper	Aluminum 135-T6	E = 72.40 GPa; ν = 0.33 Y = 179 MPa	• linear elastic, • small deformation, • small strain
U-Bolt	Galvanized Steel	E = 206.84 GPa; ν = 0.29 Y = 620.52 MPa	

5.4.2 Mesh Refinement

Regarding the element selection, for the best solution accuracy with minimum computational cost, all components in the entire assembly are discretized using only 8-node reduced-integration hexahedral solid elements with hourglass control.

The fine meshing scheme designed for the Drake conductor strength model in Chapter 4 was initially adopted. While a converged solution could be obtained for the fatigue model, its solution accuracy in the critical fretting contact regions was much below expectations. Due to quite small fretting amplitudes, a very fine mesh is shown to be required near the contact interfaces in the clamp mouth regions to capture the stress gradients in the conductor radial directions. In addition, referring to the author's past research experience (Qi et al., 2000, 2001), four layers of elements near the contact surfaces are suggested to obtain accurate results for the purpose of a FE-based fatigue analysis. However, after the mesh was further refined, this FE model experienced high difficulty to converge due to excessive element distortions and inadequate contact control settings.

A number of numerical experiments were then conducted and the trial-and-error process was very time-consuming since each trial had to perform a large-size nonlinear solution for the entire model. As a result, an optimal refined meshing scheme was finally achieved, leading to a much larger computational size than the initial model – adding up to 323,731 nodes, 309,805 solid elements and 274,478 contact elements. This very fine model will ensure sufficient solution accuracy while maintaining stable convergent behavior provided that robust solution control and contact control settings are determined carefully. The comparison of the two meshing schemes for the Drake wires is summarized in Table 5.2., seen also in Figures 5.9 and 5.10 about the cross-sectional meshes. The finite element mesh of the entire conductor-clamp fretting fatigue model is presented in Figure 5.11.

Table 5.2 Two meshing schemes for the Drake fretting fatigue model

<table>
<tr><th colspan="2">Drake conductor fatigue model meshing scheme</th><th>Initial</th><th>Final</th></tr>
<tr><td colspan="2">Outer & Inner wires edge divisions for each edge</td><td>22</td><td>36</td></tr>
<tr><td colspan="2">Outer & Inner wires face element size (mm)</td><td>0.55</td><td>0.26</td></tr>
<tr><td colspan="2">Steel wires edge divisions for each edge</td><td>20</td><td>20</td></tr>
<tr><td colspan="2">Steel wires face element size (mm)</td><td>0.45</td><td>0.45</td></tr>
<tr><td colspan="2">Conductor longitudinal sweep length divisions</td><td>60</td><td>66</td></tr>
<tr><td colspan="2">Number of element layers near Al. wire contact surfaces</td><td>1</td><td>4</td></tr>
<tr><td rowspan="4">Computational size for entire assembly model</td><td>Total nodes</td><td>169,161</td><td>323,731</td></tr>
<tr><td>Total solid elements</td><td>167,185</td><td>309,805</td></tr>
<tr><td>Total contact elements</td><td>183,166</td><td>274,478</td></tr>
<tr><td>Total elements*</td><td>351,215</td><td>585,147</td></tr>
<tr><td colspan="4">(* Including 864 spring elements to stabilize the nonlinear solution process)</td></tr>
</table>

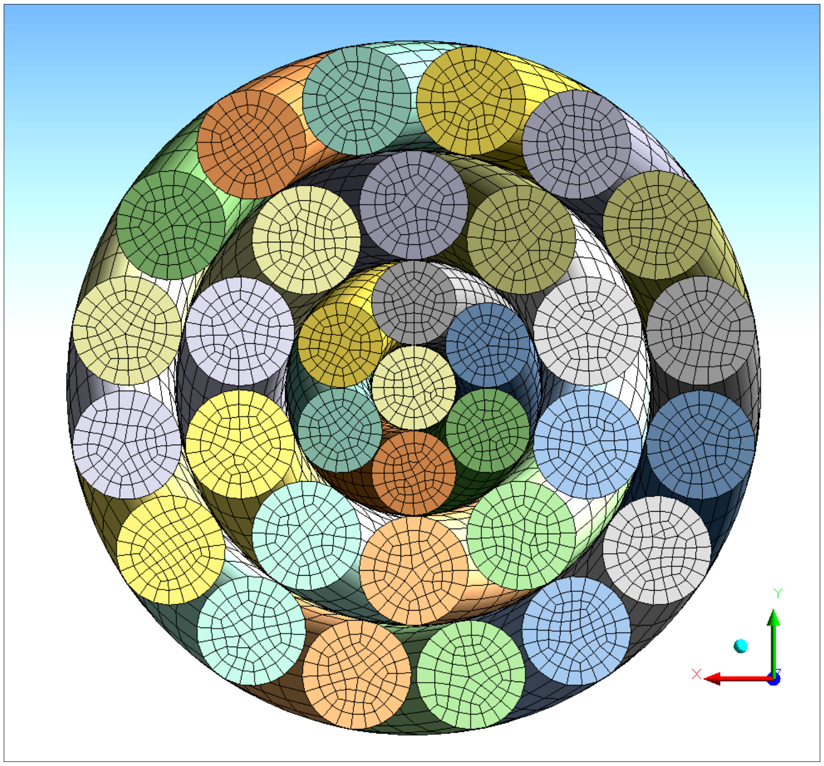

Figure 5.9 Initial mesh scheme of Drake conductor fretting fatigue model

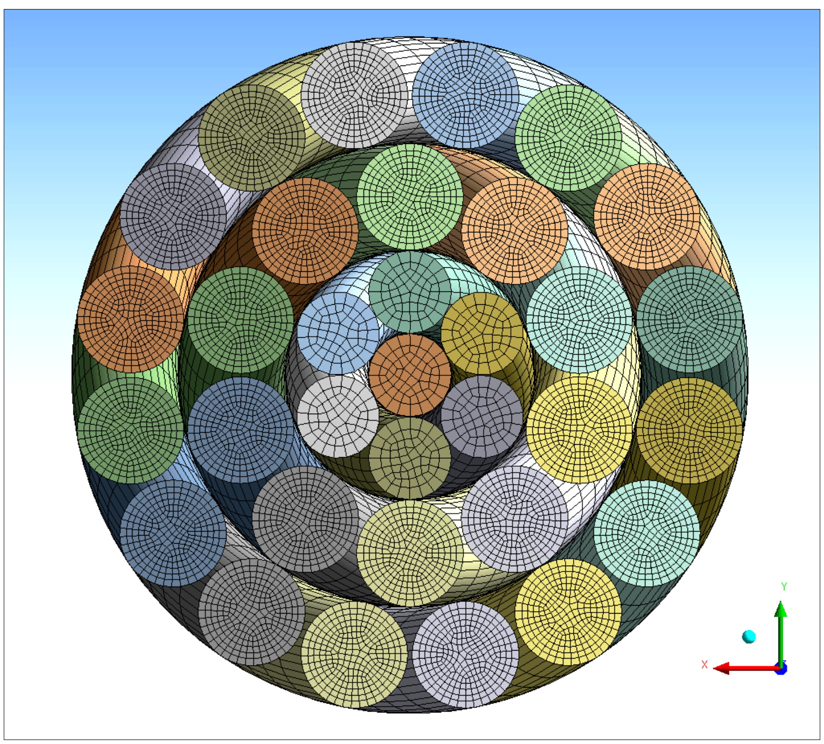

Figure 5.10 Final refined mesh scheme of Drake conductor fretting fatigue model

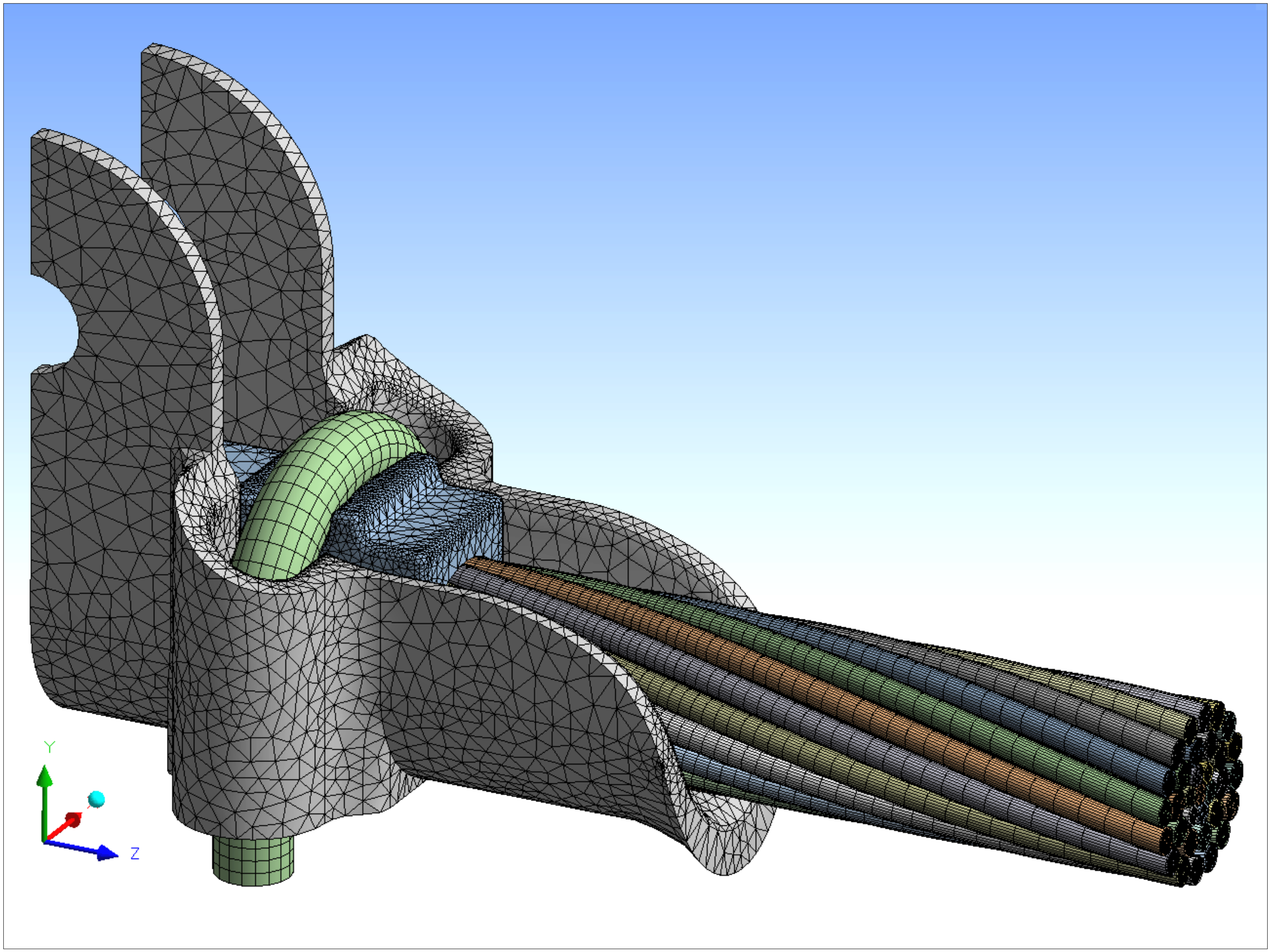

Figure 5.11 Finite element mesh of the Drake conductor-clamp assembly fretting fatigue model (184 mm)

5.4.3 Contact Conditions

The comprehensive contact interactions amongst the entire assembly model are all considered as *"flexible-to-flexible"* deformable body contact, and *"surface-to-surface frictional"* contact types are defined on most contact regions except between the Upper Keeper and U-Bolt. The so-called "*bonded contact*" type is defined for this contact region to facilitate the computations. That is, no separation and no sliding are allowed for the interaction between the Upper Keeper and U-Bolt, which is realistic. For each contact region, many *"contact pairs"* are created and composed of "contact" and "target" surfaces that are discretized using 3-D 8-node surface-to-surface contact elements (CONTA174 in ANSYS). As a result, in total 38 contact pairs and **274,478** contact elements are generated for the entire model. The classical Coulomb isotropic friction model is used with different frictional coefficients among the contact pairs, and all the μ_s are static frictional coefficients for clean, dry surfaces sliding against each other. It is noted that $\boldsymbol{\mu_s = 1.05}$ is assigned for all conductor aluminum wires contact in this study.

The same numerical solution strategies developed in Section 3.4 of Chapter 3 are inherited in this study. Due to the critical effects of a contact algorithm on the accuracy and convergence for a complex contact analysis, an effort was made to empirically compare and evaluate the available contact algorithms applied to this model. It was confirmed that the "*Augmented Lagrangian*" method is still the most robust contact formulation for this application, while other options either significantly increase the convergence difficulties or cause inaccurate results.

As mentioned before, this model exhibits difficult convergent behavior with the increase of its mesh density. Actually, the final fine mesh model experienced divergence if applying the same contact control parameters used in the initial model. Moreover, different convergent issues were experienced in different loading stages, while only "one-time" contact control parameters can be set up for the whole load history. Especially, it was observed that the numerical performance (stability and accuracy) of the model was very sensitive to variations of the prescribed normal contact stiffness factors. Therefore, designing a fine mesh (as discussed before) and configuring a proper set of contact parameters as well as the solution control settings are three interdependent aspects that have to be considered together to ensure a successful solution. Such an endeavor reflects essentially the nature of the so-called “*hierarchical modeling process*” (Bathe et al., 1990, 2011) for solving a complex nonlinear problem, during which the mathematical model that represents the physical event is from simple to complex in order to gain more benefits (engineering insights), and meanwhile developing a reliable analysis approach as well as robust modeling procedures becomes increasingly difficult. As such, “***To perform an effective analysis is an art***”. (Bucalem and Bathe, 2011)

Many numerical experiments were conducted by monitoring the computational processes and adjusting the schemes accordingly based on the same approach used in the "Drake strength model". Eventually, a good solution scheme with a set of optimal normal contact stiffness factors was obtained, which overcame the convergence difficulty and achieved high solution accuracy. Table 5.3 summarizes the key contact setting parameters for the Drake fatigue model.

Table 5.3 Contact settings used in the Drake fretting fatigue model

Contact regions	Contact pairs	Frictional coefficient (μ_s)	Normal contact stiffness factor	Resulting initial contact stiffness (N/mm^3)
Steel wires & Steel wires	6	0.60	0.15	2558.4
Inner wires & Inner wires	10	1.05	0.50	2861.3
Outer wires & Outer wires	16	1.05	0.50	2845.6
Steel wires 1-6 & Steel wire 0	1	0.60	0.20	3422.7
Steel wires 1-6 & Inner wires	1	0.45	0.40	2288.8
Inner wires & Outer wires	1	1.05	0.40	2288.8
Outer wires & Upper Keeper	1	1.05	0.25	1422.7
Outer wires & Clamp body	1	1.05	0.2	1138.1
Upper Keeper & U-Bolt	1	“Bonded”	0.042	11378.0
* Contact algorithm: “Augmented Lagrangian” method				

5.4.4 Multi-Step Loading Process

The loads applied to the model are in compliance with the bending fretting fatigue laboratory tests performed by Zhou et al. (1994, 1996), leading to a multiple load stepped analysis implemented sequentially to complete the entire load history for one bending fretting cycle. In ANSYS, a load case is defined as a “Step”, which refers to a set of loads and boundary conditions corresponding to a particular loading condition. In this study, the complete load history consists of four load cases, i.e. four load “Steps”: **(1)** clamping pressure from U-bolt, **(2)** pre-tension of the conductor, ((1) and (2) constitute the pre-stressed state of the fretting test.) **(3)** fretting amplitude is imposed, and **(4)** return to pre-stressed loading condition.

In the first step, a symmetric displacement B.C. is applied on the clamp transverse symmetry plane (SCC) and a fixed displacement B.C. is applied on the clamp fastener hole bottom surface to remove the rigid body motions of the system. (These B.C.s will propagate to the following three load steps.) In the meanwhile, a constant clamping pressure is maintained on the Drake conductor during the test by applying a torque 47 N·m (35 lbf · ft) each to the two nuts that are attached to the pair of U-bolts (Zhou et al., 1994). This tightening torque will generate a bolt preload $\boldsymbol{Fi \approx 19.6}$ **(kN)**[1] to lock the conductor/clamp system. In the model, Fi is applied on each of the two bottom surfaces of the U-bolt.

In the second step, the pre-tension of the conductor is defined. During the whole period of the test, the axial tensile load on the conductor is maintained at **25%** Rated Tensile Strength[2] (RTS) of the conductor. According to General Cable (2008), the RTS for the 795 kcmil Drake ACSR is 295.77 MPa, corresponding to a rated tensile load 138.6 (kN). So, the resulting static tensile force applied on the conductor: T=138.6*0.25=34.65 (kN). Using the same “*displacement-control*” approach as in the preceding chapters, an equivalent elongation can be calculated as $\boldsymbol{\Delta l = 0.2484}$ **(mm)**, which is applied as the

[1] This bolt pre-tension force is calculated using the torque formulae referred to several Handbooks (Avallone et al., 1997; Kutz, 1986; Oberg et al., 1996; Shigley, 1972).

[2] Rated Tensile Strength is usually regarded as a mechanical property of a cable, which is some value obtained from test, and usually between cable Yield strength and Ultimate Tensile Strength.

prescribed axial displacement on all the free-end surfaces of the conductor. This elongation corresponds to an overall axial strain of 0.135%. So, this implies that, under the 25% RTS pre-load tension, the conductor aluminum wires have already entered into their inelastic range.

The third step simulates the imposed bending fretting amplitude induced by Aeolian vibrations. A vertical displacement (**Y_b = 1.3 mm**[3]) is gradually imposed to the free-end surfaces of the conductor. The fourth (last) step is a process of reducing the fretting amplitude to zero. That is, the conductor returns to the pre-stressed state (at the end of the Step 2) to complete the entire fretting cycle. The entire loading history is summarized in Table 5.4.

Table 5.4 Multiple-Step loading process for the Drake fretting fatigue model

Loading history	**Bolt preload** (Fi, kN)	**Conductor static pre-tension** 25% RTS (Δl, mm)	**Bending fretting amplitude** (Y_b, mm)
Step 1	19.6	-	-
Step 2	19.6	0.2484	-
Step 3	19.6	0.2484	$0 \rightarrow 1.3$
Step 4	19.6	0.2484	$1.3 \rightarrow 0$

Each "load step" analysis is implemented within a period of "time," for which the response of the model to the specified loads and boundary conditions is calculated. As stated in Section 3.4.2, unlike in a dynamic analysis where "time" represents actual, chronological time concept, "time" is simply used as a tracking parameter in this analysis to identify a loading history, as well as the load incremental steps within each loading period. In detail, each (time) step corresponds to a different load scenario, and each time sub-step corresponds to an increment of load, during which a series of equilibrium iterations (and contact states related computations) are carried out to arrive at a converged solution for that intermediate load values.

[3] A parametric study about some effects of different fretting amplitudes will be discussed in Section 5.7.

It is worth to note that the time increments in this model must be set very small to avoid abrupt changes in the load increments; otherwise, either the normal contact forces undergo large oscillations or large contact penetrations are experienced, which could jeopardize the solution quality. In effect, it was shown that time sub-step was a very sensitive solution control parameter to help maintain a stable convergence process and it also significantly influenced the computational cost, and it needs to be adjusted at each different load step. By numerical experiments, a set of optimal time sub-step control settings are obtained (Table 5.5) that make the computations very stable and efficient for every load incremental step. Even so, the total running time for one fretting cycle is still about 85 hours (3.5 days), clearly indicating the high computational scale and complexity of this fretting fatigue model.

Table 5.5 Time step settings in the Drake fretting fatigue model

Load Step	Initial time step	Min. time step	Max. time step
Step 1 (0s ~ 1s)	0.01	0.001	0.02
Step 2 (1s ~ 2s)	0.01	0.005	0.03
Step 3 (2s ~ 3s)	0.01	0.01	0.05
Step 4 (3s ~ 4s)	0.01	0.01	0.1

5.5 Stress Analysis Results and Discussion

Selective results of the Drake conductor/clamp fretting fatigue model under fretting amplitude **1.3mm** will be reported. First of all, it should be noted that the purpose of the presentation in this section is to expose the local stress-strain states to gain a clear understanding of the mechanics behavior of the conductor under fretting fatigue conditions, as well as to show the validation of the FE model through comparisons with published experimental data. As for the stress results that are used for the conductor fatigue lifing analysis, they will be discussed in Section 5.6.2. In addition, since the critical zone for conductor fretting crack initiation is located between the keeper edge

(KE) and the last point of contact (LPC) with the clamp, the discussion will mainly focus on this region. Furthermore, the most severe mechanical response of the conductor is clearly shown (as expected) occurring at the end of Step 3, when the fretting amplitude being fully applied. Therefore, most of the results presented will refer to at this "time point" unless otherwise indicated.

The total deformation of the Drake conductor under fretting condition is shown in Figure 5.12. The maximum deformation is 1.324 mm, which occurs at the end surface of the transverse bending amplitude being applied. At the cross section of LPC, the conductor total deformation and bending deflection exhibit similar displacement distributions and very close peak values (Figures 5.13 and 5.14). This indicates that bending dominates the mechanical response under the fretting condition. In addition, the maximum bending deflection (0.413mm) that occurs on the outer layer aluminum wire does deviate from the top center line of the cross section due to the wire helical configuration and multi-body contact interactions.

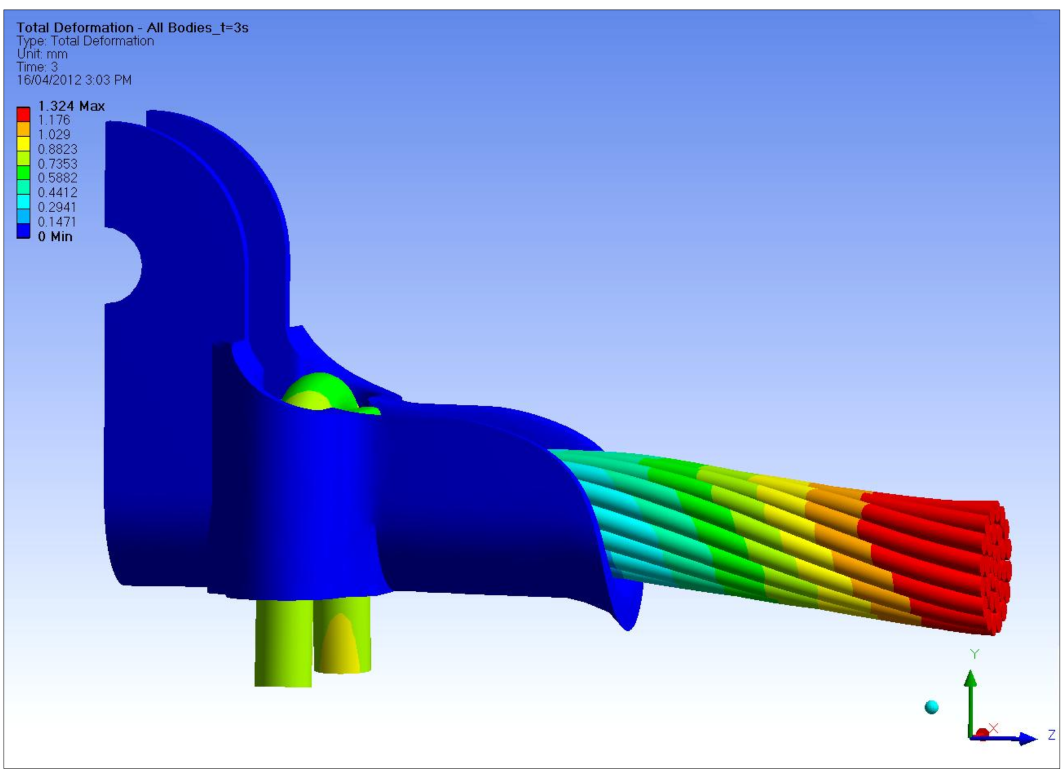

Figure 5.12 Total deformation of Drake conductor under bending fretting condition

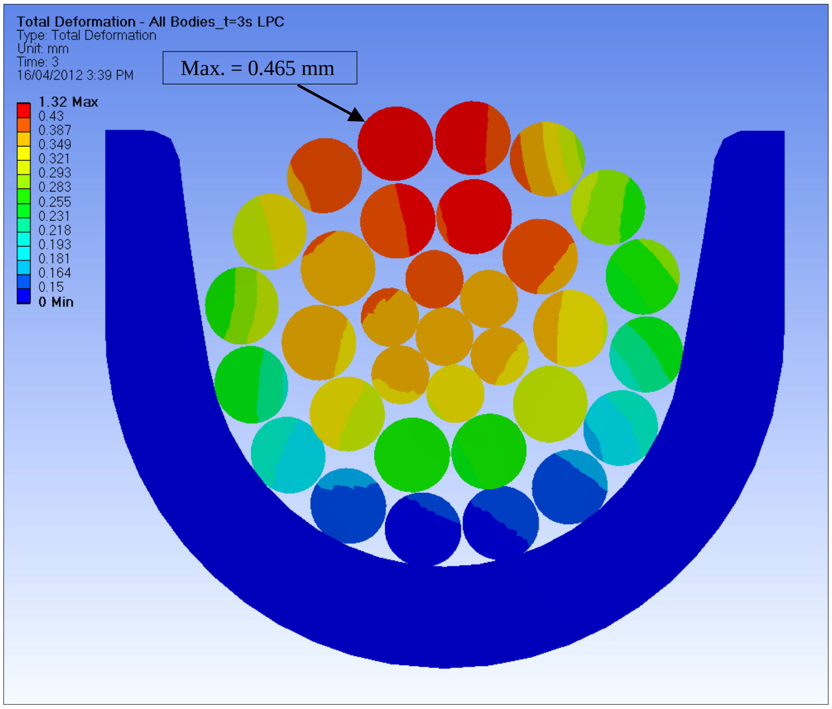

Figure 5.13 Total deformation of Drake conductor at LPC cross section

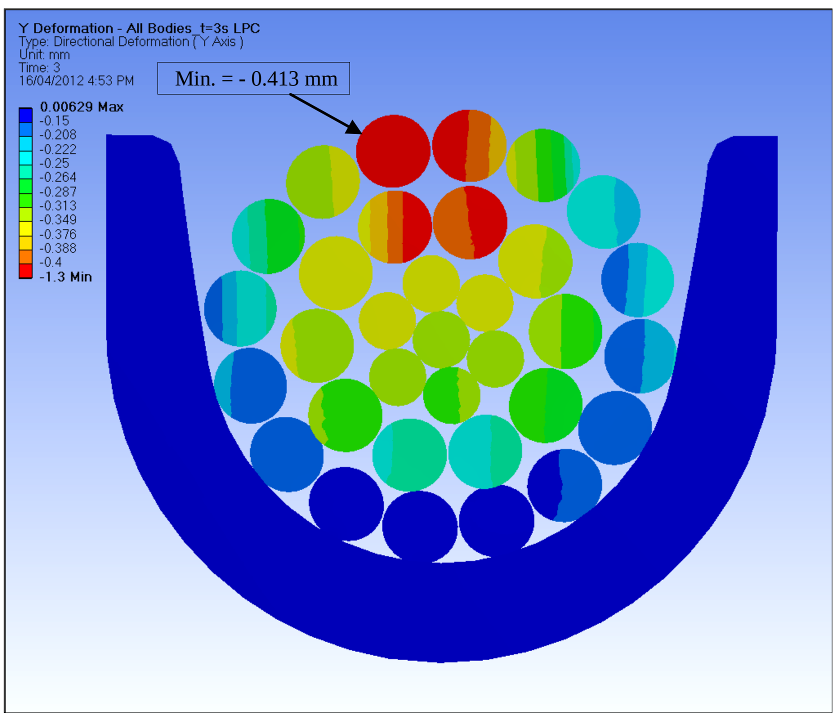

Figure 5.14 Bending deflection of Drake conductor at LPC cross section

The contact kinematics states in the conductor fretting region show overall good agreement with the experimental and field observations, as explained below**:**

Three characteristic fretting contact states (referring to “fretting map” theory described in Chapter 2) can be identified by the relative sliding on the wire contacting surfaces**:** In the section from SCC to the bolt, there are basically no relative slips on both outer and inner layers due to the large clamping force and high friction. The conductor wire mating surfaces exhibit very good adhesion when they are in contact, which indicates that they are mostly in the ***stick*** state. In the meanwhile, the ***slip*** state has been predicted outside the clamping region (beyond the LPC) because global relative slips take place among the corresponding contact interfaces. ***Mixed*** regimes are clearly exposed in the clamp mouth area on both the outer and inner layers as some very small and localized relative sliding occurs, which exhibits the occurrences of the “partial slip contact” state (See Figures 5.15 and 5.16).

Furthermore, the numerical results show that the partial slip contact state may be accompanied by local plasticity on the fretting contact surfaces, as evidenced by the fretting marks in Figures 5.17 and 5.18. As stated in Chapter 2, there are two types of contact modes among the conductor helical wires: *cross contact* and *parallel contact*. In the mixed regime, the cross contact between the inner and outer layers generates elliptical fretting marks due to the opposite lay angles of the contacting layers; these elliptical marks are much more critical than the very narrow-banded fretting marks resulting from the parallel contact among the wires of the same layers. These fretting mark distributions are also consistent with those in the “fretting chart” based on experimental observations (Zhou et al., 1994, 1996). The majority of the fretting marks (indicating inelastic deformations) spread between SCC and KE, and the peak plastic strain of the outer layer occurs on the mating surface with the upper keeper and is very close to the KE. In particular, the elliptical plastic marks on the inner layer exhibit a very similar pattern to the one reported in an ACSR field failure analysis (see Figure 5.19 that is extracted from Azevedo et al., 2009).

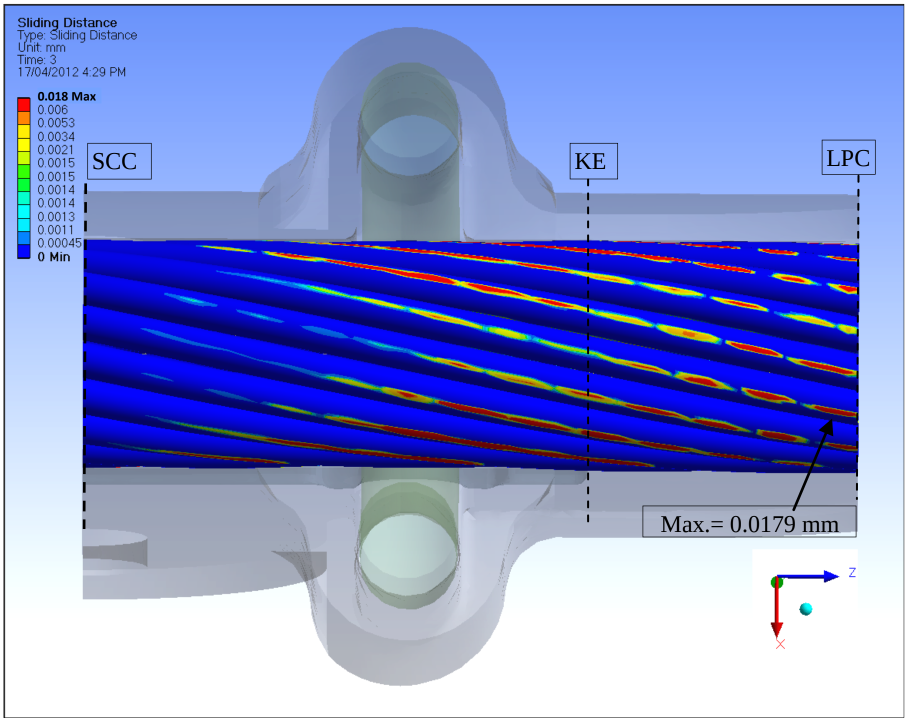

Figure 5.15 Partial slip contact state on the outer layer (between SCC and LPC)

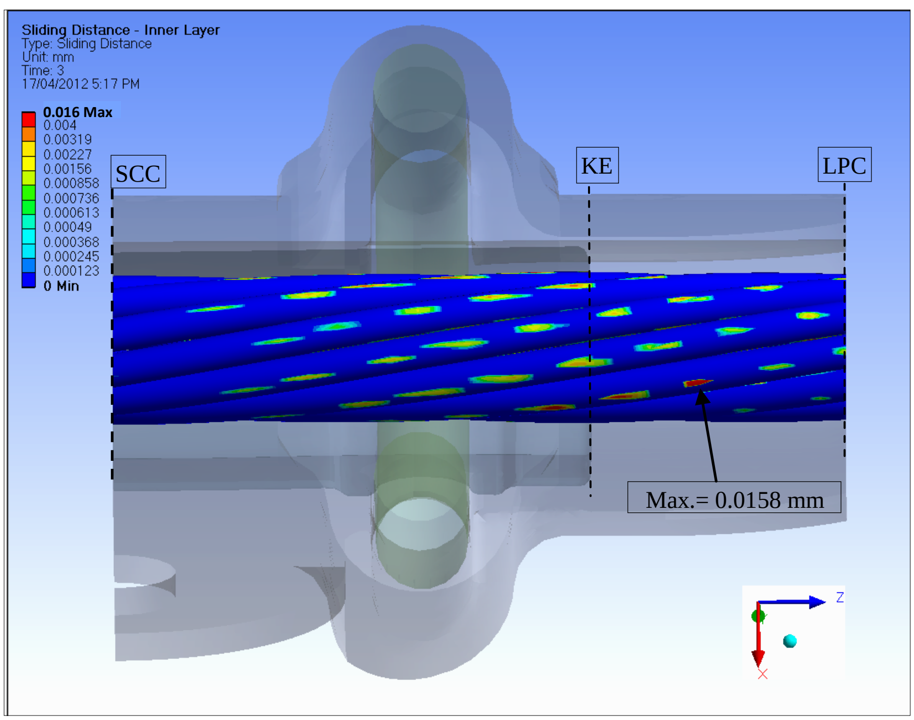

Figure 5.16 Partial slip contact state on the inner layer (between SCC and LPC)

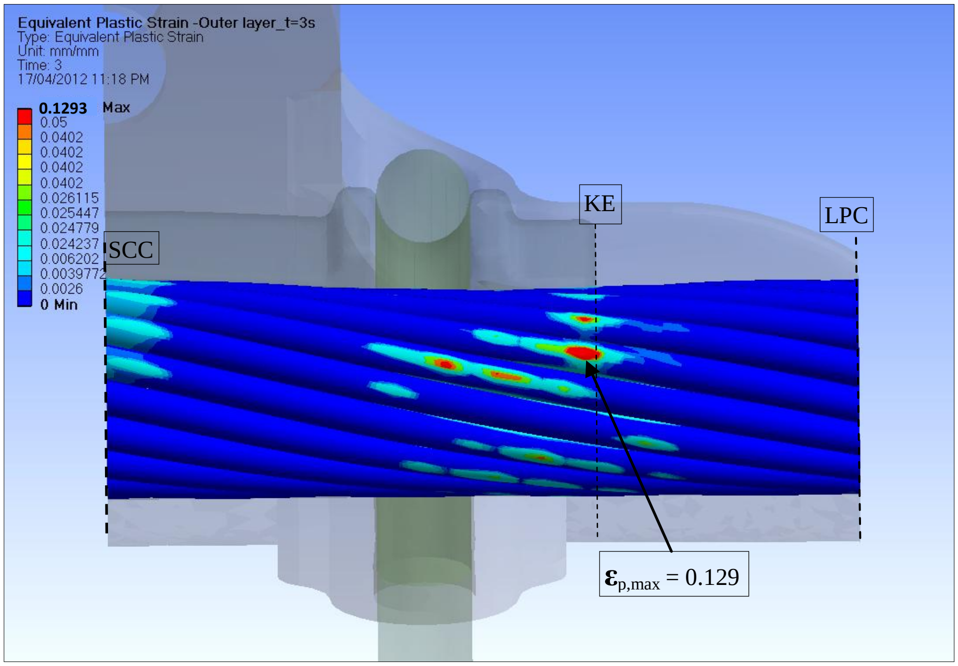

Figure 5.17 Equivalent plastic strain ($\boldsymbol{\varepsilon}_{\mathbf{p}}$) on the outer layer (between SCC and LPC)

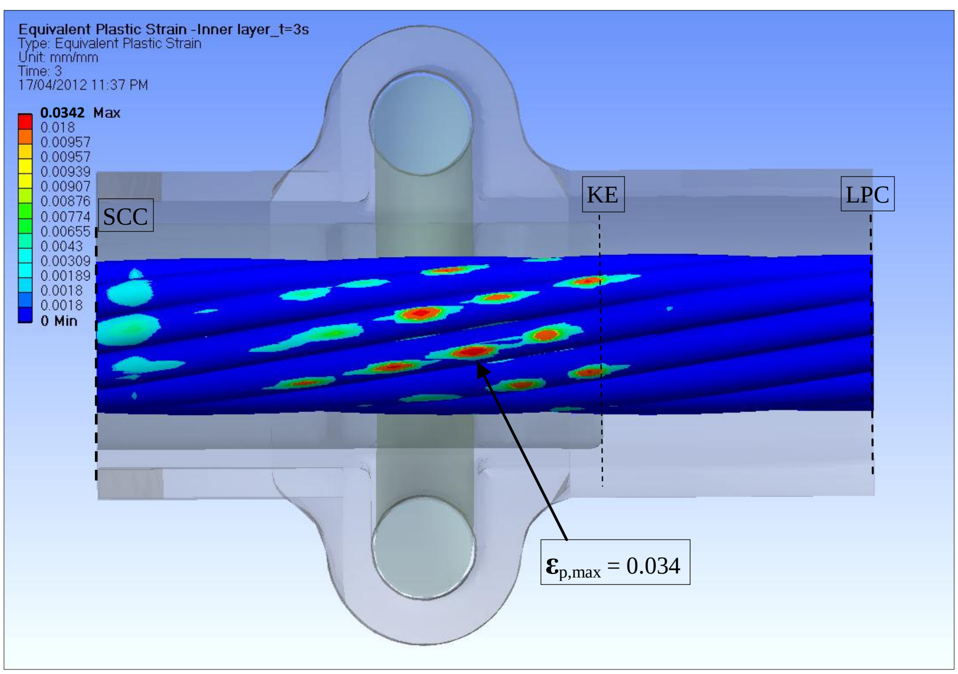

Figure 5.18 Equivalent plastic strain ($\boldsymbol{\varepsilon}_{\mathbf{p}}$) on the inner layer (between SCC and LPC)

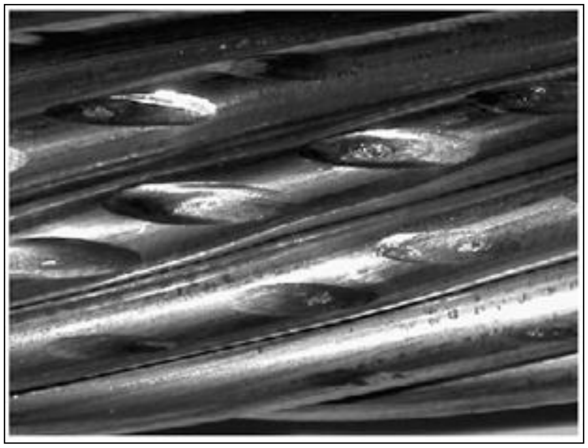

Figure 5.19 ACSR plastic fretting marks on inner layer (Azevedo et al., 2009)

The Von-Mises stress distribution of the Drake conductor at the cross sections of LPC and KE are shown in Figures 5.20 and 5.21, respectively. As expected, the core steel wires have much higher stresses (230 MPa ~ 380 MPa) than the aluminum wires as they are the main load-carrying structure of the conductor. The aluminum wires at KE exhibits much more complex stress states with higher peak values than at LPC owing to the more severe multiaxial loading provided by the suspension clamp.

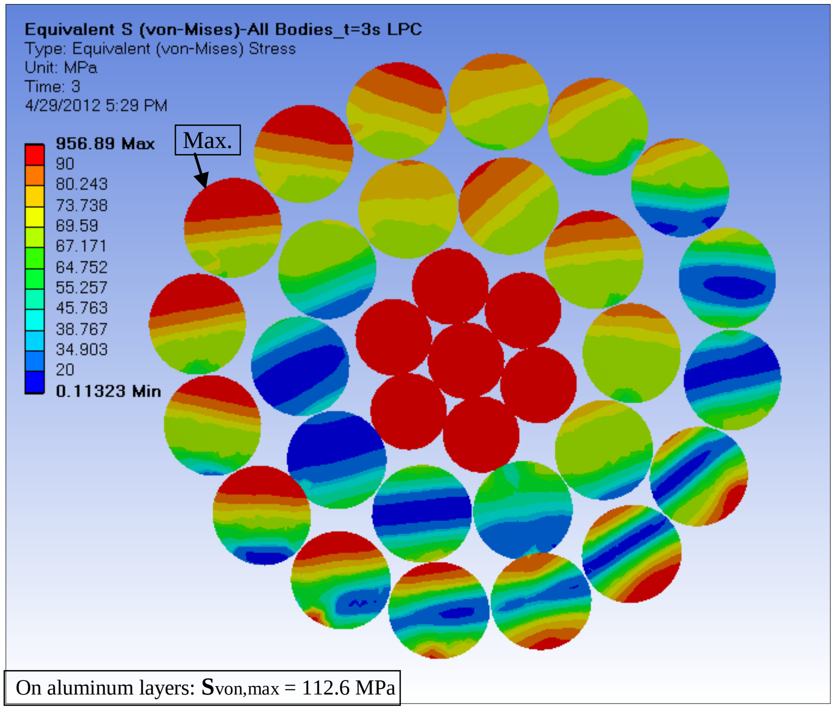

Figure 5.20 Drake conductor Von-Mises stress ($\mathbf{S}_{von}$) at LPC

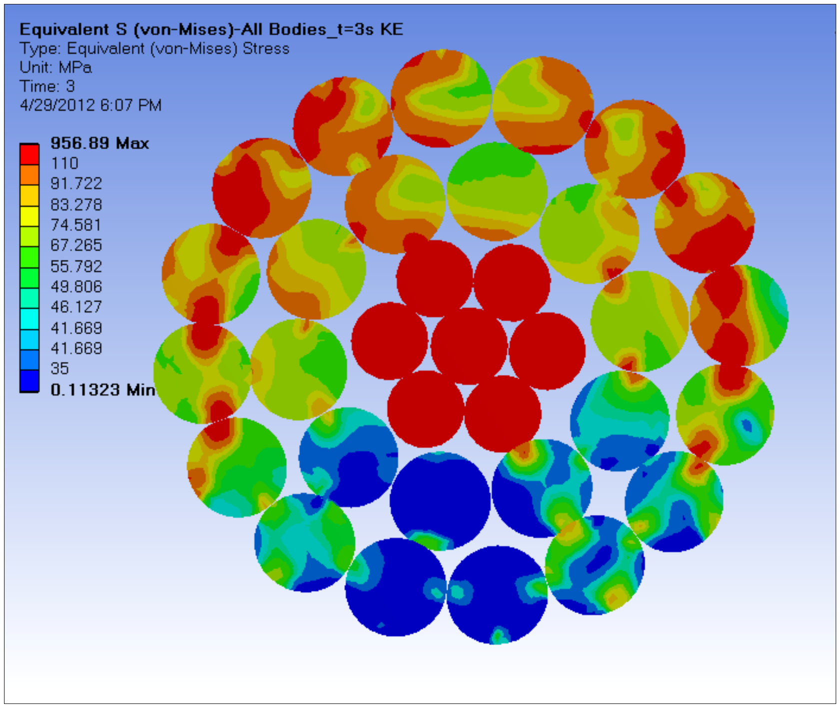

Figure 5.21 Drake conductor Von-Mises stress (S_{von}) at KE

Mainly occurring in the "Upper Half-Section", plasticity is present on the contact surfaces of some wires on both the outer and inner layers, while the outer layer carries a higher peak stress and stress gradient than the inner layer (Figures 5.22 and 5.23).

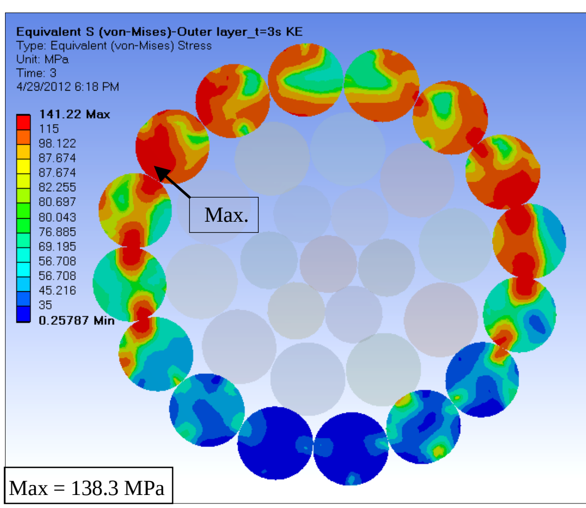

Figure 5.22 S_{von} of outer layer at KE

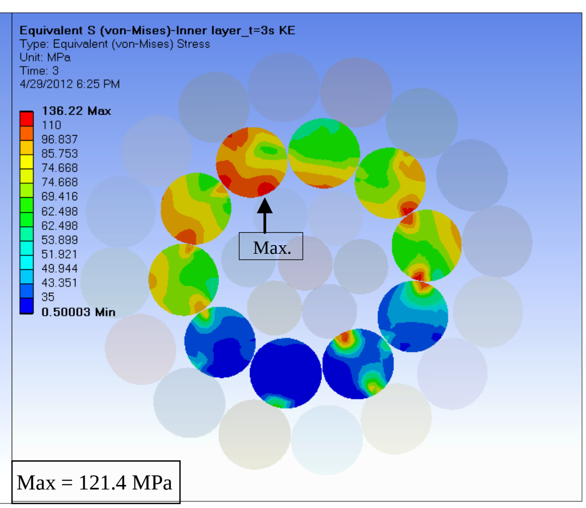

Figure 5.23 S_{von} of inner layer at KE

The maximum (**S**$_1$) and minimum (**S**$_3$) principal stress fields of the conductor aluminum layers at the KE and LPC cross sections are presented in Figures 5.24 ~ 5.27. The same observations as for the Von-Mises stress fields apply**:** All peak values of **S**$_1$ and **S**$_3$ on both the outer and inner layers occur on contact surfaces. Again, the outer layer exhibits higher peak stress and steeper stress gradient than the inner layer. The vicinity of KE appears more critical than LPC as summarized in Table 5.6, where Δ represents the difference between S1 and S3.

Table 5.6 Peak maximum and minimum principal stresses at KE and LPC in MPa

Aluminum layer		**KE** cross section		**LPC** cross section	
Outer Layer	**S**$_1$	113.67	Δ = 365.74	112.86	Δ = 257.76
	S$_3$	-252.07		-144.9	
Inner Layer	**S**$_1$	108.06	Δ = 283.89	94.91	Δ = 166.35
	S$_3$	-175.83		-71.44	

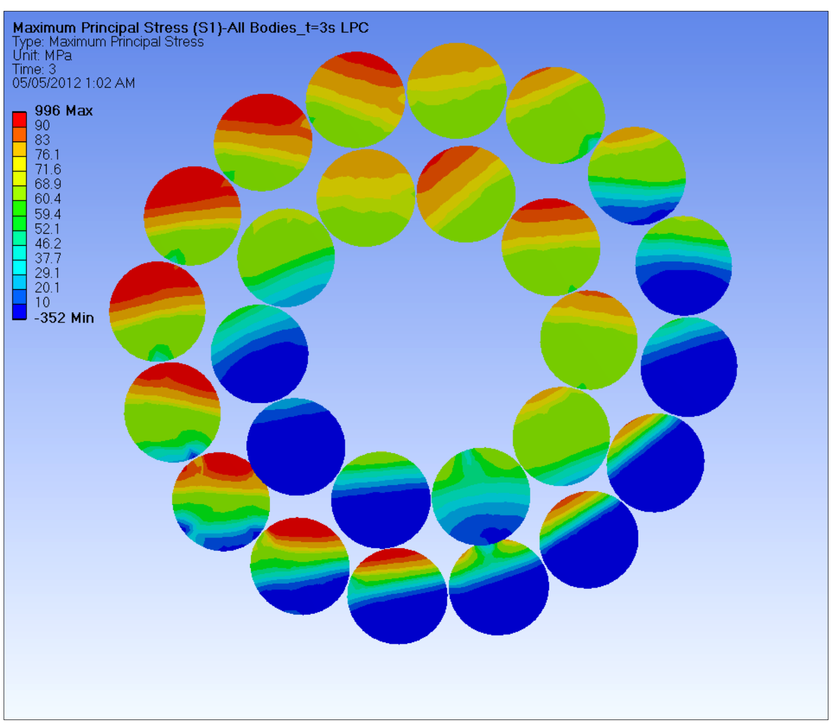

Figure 5.24 Drake conductor Al. wires maximum principal stress (**S**$_1$) at LPC

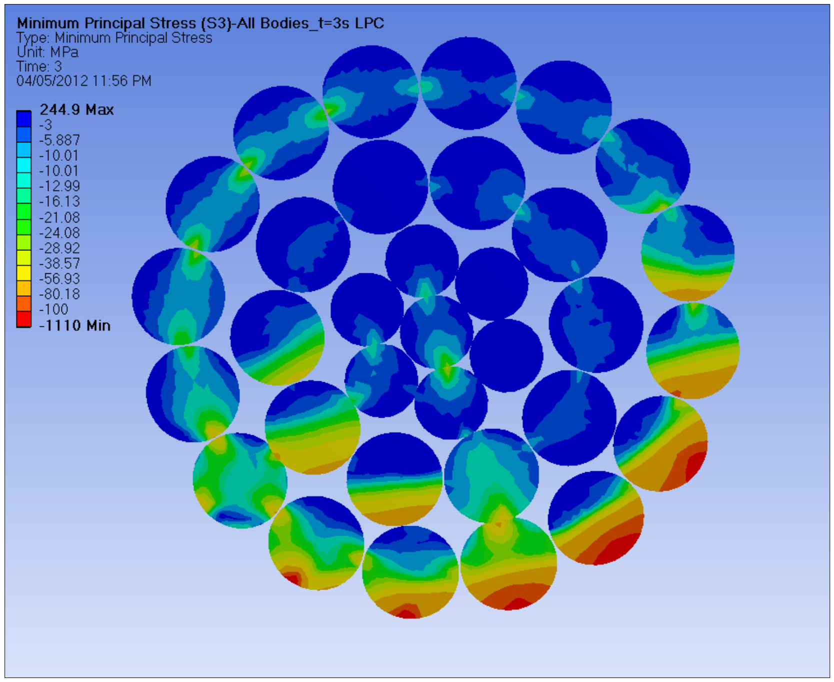

Figure 5.25 Drake conductor minimum principal stress (**S_3**) at LPC

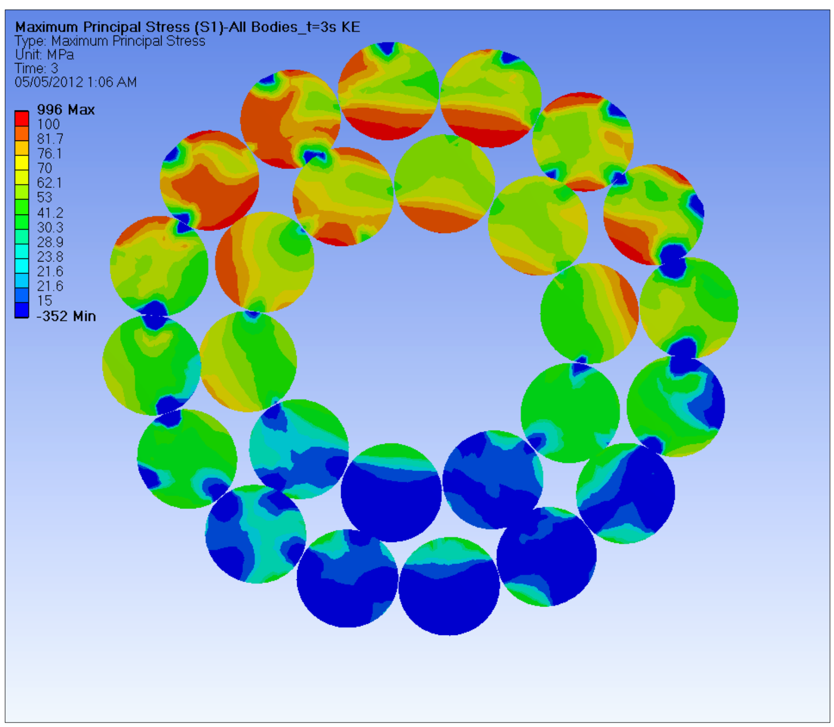

Figure 5.26 Drake conductor Al. wires maximum principal stress (**S_1**) at KE

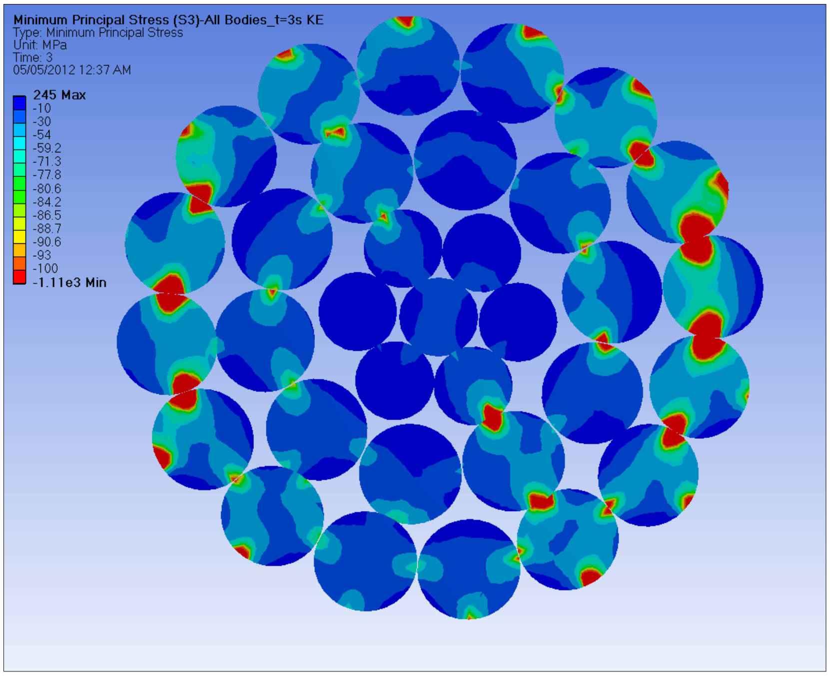

Figure 5.27 Drake conductor Minimum Principal Stress ($\mathbf{S_3}$) at KE

The conductor longitudinal (axial) stress $\mathbf{S}_{zz}$ is resulting from the combination of normal stresses due to bending, tension, friction as well as the unbalanced internal torque. From Figure 5.28, it is clearly demonstrated that the calculated $\mathbf{S}_{zz}$ stress field can be well validated by experimental tests and field observations**:** The critical zone for conductor fretting fatigue is located in the suspension clamp mouth region between KE and LPC, and the fretting micro cracks mostly initiate from contacting surfaces under partial slip contact state (i.e. mixed regime), during which the axial stress plays an essential role.

At both the KE and LPC cross sections, the peak axial stresses (max. and min.) occur on the outer layer, as shown in Figure 5.29. The minimum axial stress does happen on the contact surfaces, demonstrating the significant effect of high interfacial friction (high tangential contact stress) and the resulting steep stress gradients. Under the 25% RTS prescribed (constant) tension, the nominal average axial stress of the aluminum wires is about 59 MPa (Zhou et al., 1994, 1996), but with the occurrence of fretting, very high local stress concentrations are predicted (Table 5.7).

Table 5.7 Peak values of axial stress $\mathbf{S_{zz}}$ at KE and LPC in MPa

Aluminum layer		**KE** cross section	**LPC** cross section
Outer Layer	Max.	109.46	108.82
	Min.	-173.53	-128.59
Inner Layer	Max.	101.08	92.08
	Min.	-96.07	-70.2

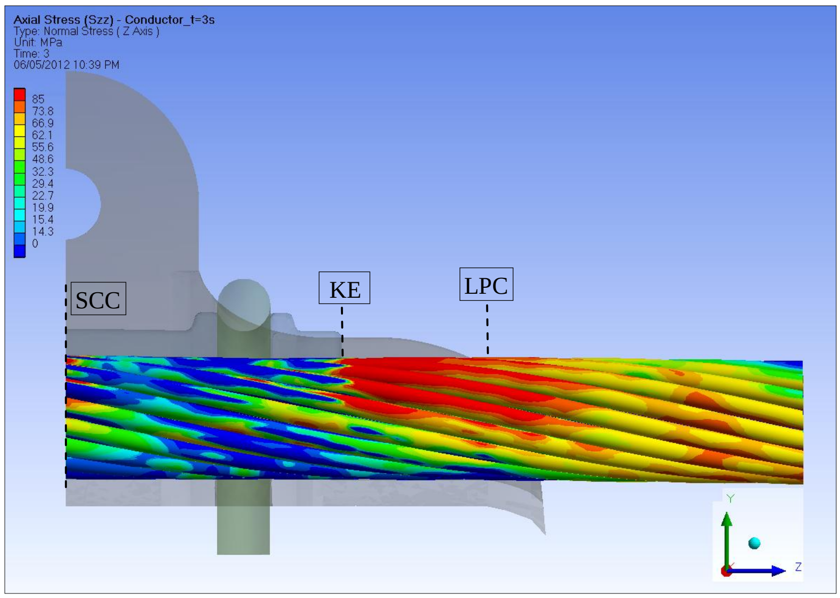

Figure 5.28 $\mathbf{S_{zz}}$ of Drake conductor under bending fretting condition

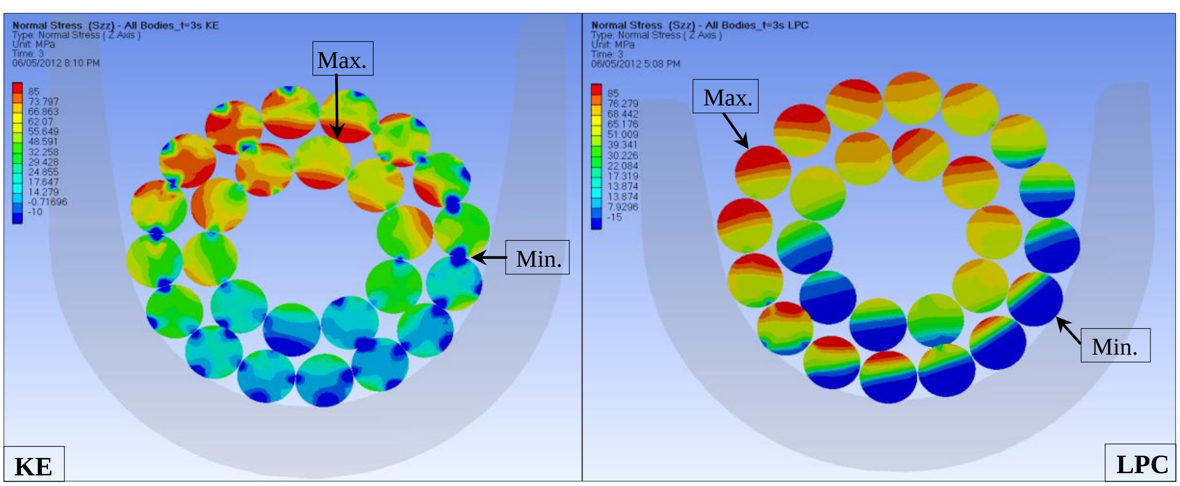

Figure 5.29 $\mathbf{S_{zz}}$ of Drake conductor aluminum wires at KE and LPC

5.6 Conductor Fretting Fatigue Lifing

Metal fatigue analysis (also called "lifing" in practice) has been studied extensively for over 150 years, during which a very large amount of literature has been accumulated. For example, the state of the art of metal fatigue up to early the 1970s was summarized by Frost et al. (2011); Broad historical reviews of this subject can be found in Schütz (1996) and Paris (1998), and can be also referred to the authoritative general survey by Suresh (1998). A recent 10-volume comprehensive compilation on structural integrity (Milne et al., 2003) provides a definitive reference for metal fatigue researchers. Therefore, only a brief overview of metallic lifing methods is presented in this section without great rigor and by no means meant to be complete. Instead, the author's intention is to provide general background and help to justify the rationale of the method employed in the present study. After that, a practical multiaxial lifing scheme is proposed to estimate fretting fatigue life of overhead line conductors.

5.6.1 Selective Overview of Metal Fatigue Lifing Methods

Research on metal fatigue has been from both the metallurgical and mechanical perspectives. While metallurgical descriptions focus on fatigue mechanisms, mechanical descriptions draw much larger industrial interest in that they emphasize the mechanical response of the materials and structures under fatigue loading conditions and the prediction of their service lives to avoid catastrophic fatigue failures, which are more practical from an engineering point of view.

Historically, the majority of the studies on metal fatigue analysis are experimental as it is largely a descriptive subject. Based on laboratory results, numerous empirical models have been developed to predict material and structure fatigue lives, although some of them are seriously misleading due to the lack of an appropriate applied mechanics and mathematics framework (Schütz, 1996; Pook, 2007). In the past four decades, more and more fatigue analyses have been conducted effectively using numerical techniques (largely by FEM) with the increasing power of computers so that some metal fatigue lifing approaches have become established engineering tools in many applications, especially for aerospace and automotive industries. Over many years, various lifing methods have fallen into three primary groups: ***stress-based*** methods, ***strain-based*** methods, and ***fracture mechanics-based*** methods (they are essentially energy-based methods). Correspondingly, a large number of uniaxial and multiaxial metal fatigue criteria (models) have been developed in both the low- and high-cycle fatigue regimes.

The stress-life methods are the most classical methods, which can be traced back to the pioneering work of August Wöhler on railway axle failures (in 1867). They are typically presented as *S-N* curves (also known as Wöhler curves). These are plots of alternating stress ($\mathbf{S_a}$) versus number of load cycles ($\mathbf{N_f}$) to failure, with appropriate curves fitted through the individual experimental data points. $\mathbf{N_f}$ is called fatigue life. Among the effects of many factors on metal fatigue, the effect of mean stress ($\mathbf{S_m}$) has drawn especially great interest and was thus studied thoroughly. It is well understood nowadays that, in general, the fatigue strength expressed in terms of alternating stress would decrease as the tensile mean stress is increased. Many efforts have been made to establish the relationship between mean stress and alternating stress, such as the diagrams by Gerber (1874), Goodman (1899), Soderberg (1930), Morrow (1960), Heywood (1962), and so on. In practice, the Goodman diagram is the most widely used relationship for fatigue strengths at given endurance limits in that it is a simplified, conservative and meanwhile reasonable approach and most experimental fatigue data of metallic materials lie just above the Goodman line. Other influences, such as surface finish and treatments, temperature, environment, have also been investigated empirically and quantified as various modification factors applied to the baseline *S-N* curves (see for example, Bannantine et al., 1990; Stephens et al., 2001.)

In general, stress-life methods are best suited for long life applications, i.e. high cycle fatigue (**HCF**) situations, and the stresses and strains need to be predominantly within elastic range. As these methods do not distinguish between fatigue crack initiation and crack propagation, but directly deal with "*total life*" (the life up to final failure), and are simple to use compared with the other two types of methods, they have become the most preferred approaches in engineering design. The fundamental weakness of stress-life methods is that they are basically empirical (The models are derived from the curve fits of particular tests.) and lack the physical insights into the mechanisms of fatigue and damage (Bannantine et al., 1990).

Strain-life methods were first formulated by Coffin (1954) and Manson (1953) when they worked independently on thermal fatigue problems, and the Coffin-Manson (power law) relationship formed the basis for characterizing fatigue life based on plastic strain amplitude. Strain-life methods take into account the actual stress-strain response of the materials, and thus can model more accurately the plastic strains that lead to crack initiation. Nowadays, strain-life methods have gained definitive acceptance by ASTM (1996, 2002) and SAE (Rice, 1997) in low cycle fatigue (**LCF**) analysis and to deal with local fatigue for notched components, where local stress levels are high, causing appreciable plastic strains. However, they generally have no advantages over the stress-life methods for HCF problems, and have no capability to predict crack propagation life. In addition, they often involve more complicated analyses, mainly due to the use of power law relationships in the strain-life calculations and the determination of the associated material fatigue property constants in the strain-life models being still very empirical. While strain-life methods may be mainly appropriate to determine crack initiation life (or crack initiation-dominated total fatigue life) because crack growth is not explicitly accounted for in their models, linear elastic fracture mechanics (LEFM) methods can be employed to predict crack growth until eventual fracture.

Starting from the groundwork of Irwin (1957) by introducing the stress intensity factor, which is now commonly accepted as the basis of LEFM lifing methods (see for example, Broek, 1982, 1988; Anderson, 2005; Gdoutos, 2005), LEFM has been well developed to estimate fatigue crack propagation life from a known or assumed initial crack size up to some specified length or final failure, typically using the famous Paris' law (1961, 1963). It is worth noting that LEFM methods are currently the only means with the capability to deal directly with the propagation of fatigue cracks. However, due to the assumptions of LEFM, they often have difficulties to estimate the initial crack size in situations where there are no pre-existing crack flaws. It is now understood that in many cases the initial crack size might have a significant influence on total fatigue life. As such, LEFM methods used alone are best in crack propagation-dominated fatigue life situations, such as on the large structures in aerospace and nuclear industries. Therefore, LEFM methods sometimes need to be used in conjunction with strain-life methods to predict a total initiation-propagation life, by either simple sum of these two estimates or some combined approaches, for example the ones proposed by Dowling and Socie (2006), among others (Ellyin, 1996; Dowling, 2006).

The majority of fatigue research, especially in the early years of metal fatigue study, has been carried out under uniaxial loading conditions. In contrast, almost all in-service engineering components are subjected to complex stress-strain states due to multiaxial loadings, particular geometries, as well as contact with adjacent components. Many multiaxial fatigue criteria have been reported in the past decades. The reviews and comparisons of existing multiaxial fatigue models can be found elsewhere (see for example, Garud, 1981; McDowell and Ellis, 1993; You and Lee, 1996; Wang and Yao, 2004; Sonsino and Zenner, 2004). In general, the stress-based multiaxial fatigue criteria can be divided into three categories: **(i)** *Equivalent stress* or *stress invariants* approaches; **(ii)** *Critical plane* approaches; **(iii)** *Dang Van's multiscale* approach.

The fundamental philosophy of the equivalent stress approaches, such as the "equivalent von Mises criterion" suggested by ASME (1979) and the stress invariants approach by Sines (1959), is to reduce the complex multiaxial stress states to an equivalent uniaxial stress state. Thus, they are essentially the extensions of static yield theories to fatigue conditions. The most significant advantages of these approaches are their simplicity and their correlation to uniaxial fatigue cases, for which a large amount of existing uniaxial fatigue data is available. Accordingly, the equivalent stress approaches often have a high level of acceptance in design practice. Of course, they lack insights into fatigue crack path and crack propagation rate as they just "average" the stresses with no regard to crack growth direction. Pook (2007) states that these methods have good agreement with some experimental data on metallic materials in crack initiation-dominated fatigue situations. But some researchers have claimed that these criteria might cause non-conservative and unsatisfactory predictions (Miller, 1982; Brown, 1983), and they are often not applicable for non-proportional fatigue loadings (Suresh, 1998; Zenner, 2004).

The critical plane approaches were first postulated by Findley (1959) and then Brown and Miller (1973, 1985), and further developed with various variants for different materials and loading modes (see for example, Kussmaul et al., 1991; McDiarmid, 1994; Macha et al., 1999). These are the fatigue criteria based on cracking observations and the recognition that multiaxial fatigue damage is essentially a directional process: cracking usually takes place initially on a particular plane, i.e. "critical plane", with certain critical combination of shear stress and normal stress acting on it. Obviously, the major advantage of the critical plane approaches is their ability of physical interpretation of the fatigue cracking behavior under multiaxial loadings. In light of this, active studies are still focusing on this direction (Liu and Mahadevan, 2005). The main drawback of these approaches is that the proposed models show a lack of a wide applicability as they are restricted to specific materials or loading conditions, and thus different models define different critical planes (Pook, 2007).

Dang Van's multiscale approach has gained popularity recent years for the HCF regime, and has been used successfully in predicting some fretting fatigue failures that occurred in aerospace and automotive industries (Petiot et al., 1995; Arrieta et al., 2003). Dang Van initially formulated this approach in his PhD thesis in 1973 with later refinements with his co-workers to make it easier to use and provide better correlation (Dang Van et al., 1989~2003). These fatigue limit criteria are classified as multiscale methods because the material description at the mesoscopic scale (i.e. the scale of the metal grains of a metallic aggregate) is introduced in addition to the usual macroscopic scale of continuum mechanics. The methodology is based on the assumption that a structure will not have fatigue fracture if a stabilized "elastic shakedown" state is reached at both scales under HCF loading. Its detailed mechanical and mathematical formulations can be found in Dang Van (2003). In practice, in order to implement these criteria on a structure, different steps and algorithms have to be performed with an iterative computational process, and thus require a reliable numerical fatigue analysis computing code (Ballard et al., 1995; Maitournam, 2003).

In conclusion, to the author's knowledge, in spite of the extensive research carried out in recent decades, it is so far not yet possible to make definitive statements on which multiaxial fatigue criteria are the most appropriate in particular circumstances, let alone their general application. Thus, this subject is still a widely open and rapidly developing research area, with theories continuing to be developed, tested and modified.

5.6.2 Fretting Fatigue Lifing Approach for Conductors

Fretting fatigue of overhead line conductors in their service environment is among the most difficult fatigue phenomena to describe as it involves a large number of interactive factors with variable amplitudes and complex stress-strain states. In particular, the mechanics behavior at the edge of the clamp mouth contact region is highly multiaxial with steep stress gradients, as presented in Section 5.5. Our goal herein is to develop a lifing methodology that is able to capture the key features of conductor fretting fatigue, but yet is simple enough to be incorporated in a practical design.

Before presenting the detailed approach, it should be noted that an important simplified treatment for lifing is made in the present study**:** Like other types of metal fatigue, fretting fatigue damage may also accumulate under variable amplitude fatigue loads, leading to the so-called *cumulative fatigue damage* (Frost et al., 2011), and many efforts have been made to tackle this problem, such as the simplest and most widely used linear damage Miner's rule (1945), nonlinear damage theories (Collins, 1981), and the associated loading cycle identification (cycle counting) techniques based on highly-controlled tests, statistics and random process theory (Stephens et al., 2001; Schijve, 2009). As a preliminary study under the scope of this thesis, a fretting fatigue life model for the Drake conductor is proposed based on constant-amplitude fatigue loads.

As stated above, there is presently no existing lifing criterion that is universally accepted. Each technique has its own strengths and limitations and thus a selection needs to be tailored to particular applications. Actually, the uses of all three types of multiaxial lifing methods in different fretting fatigue cases were reported in the literature (Farris et al., 2003; Nicholas, 2006). In this section, a practical scheme is proposed in an attempt to bridge the technology gap between academia and industry practice to reasonably estimate fretting fatigue life of overhead line conductors, and to be cost-effective to implement within a conductor design cycle. Of course, for a FEA-based conductor fretting fatigue lifing, a reliable computational modeling for accurate evaluation of the local stress-strain states is the key requirement and may be a major technical challenge, which has been overcome in the preceding sections. The following discussions present the author's approach in the selection of an appropriate fatigue lifing criterion.

In view of the nature of fretting fatigue mainly associated with HCF, and the fact that the fretting fatigue mechanism of conductors is not fully understood yet, and the effects and contributions of fretting crack behavior (crack nucleation and crack growth) on total fatigue life still generate considerable controversy (Nicholas, 2006), a **stress-based method** is thus preferred. Another practical consideration for this selection is also due to many years of experience in the industry with stress-life methods, thus leading to much higher degree of confidence, while those sophisticated approaches may very possibly decrease the level of acceptance to keep them from design practice.

Encouraged by the success in predicting fretting crack nucleation for titanium alloys using an **"equivalent stress" method** developed for General Electric Aircraft Engines (Anton, 1999), the same type of multiaxial lifing approach is employed here for the Drake conductor, but the fatigue criterion equations are taken from Stephens et al. (2001). A significant advantage of this approach is that the conductor fretting fatigue life can be predicted only with knowledge of the contact stress states, and the calculations are independent of the coordinate system and with straightforward formulations. No further information is required, which vastly simplifies the procedures and thus benefit the design community to apply it as an efficient tool for a fatigue life prediction.

After the determination of a selective criterion, the most expeditious means of accomplishing this goal of lifing relies on how to employ the stress results from FE analysis to implement the fatigue model effectively to calculate the most damaging stress state at the contact regions and relate it to available uniaxial testing data. An analysis strategy is proposed by the author and the detailed scheme is outlined below.

Firstly, we need to determine which stress variables are supposed to be included in the fatigue calculations. Although the precise nature of the *most damaging stress* is still under debate in fretting community, “alternating stress” (also called “stress amplitude”, $\mathbf{S_a} = (S_{max} - S_{min})/2$) remains the decisive quantity for fatigue failure in a general fatigue case, and the fatigue crack typically propagates normal to the maximum principal stress (Schütz, 1996). Consequently, principal stresses have been used widely in many multiaxial fatigue cases, for example, the aircraft fatigue lifing practiced in Boeing (Farahmand, 2001). Moreover, some empirical efforts at United Technologies have shown that the principal stresses can be reasonably assumed as the most damaging stresses to drive fretting damage (Anton, 1999). Accordingly, **principal stresses** are also chosen in the present work for conductor lifing calculations.

Secondly, the detailed formulations employed in the Drake conductor lifing are summarized herein. An *equivalent von Mises alternating stress,* $\mathbf{S_{qa}}$, can be defined as:

$$\mathbf{S_{qa}} = \frac{1}{\sqrt{2}}\sqrt{(S_{1a} - S_{2a})^2 + (S_{2a} - S_{3a})^2 + (S_{3a} - S_{1a})^2} \tag{5.1}$$

where S_{1a}, S_{2a}, and S_{3a} are alternating principal stresses, i.e.

$$S_{1a} = (S_{1,max} - S_{1,min})/2;\ \ S_{2a} = (S_{2,max} - S_{2,min})/2;\ \ S_{3a} = (S_{3,max} - S_{3,min})/2 \tag{5.2}$$

An *equivalent mean stress,* $\mathbf{S_{qm}}$, can be given by the sum of the mean principal stresses:

$$\mathbf{S_{qm}} = S_{1m} + S_{2m} + S_{3m} \tag{5.3}$$

where S_{1m}, S_{2m}, and S_{3m}, are mean principal stresses, i.e.

$$S_{1m} = (S_{1,max} + S_{1,min})/2;\ \ S_{2m} = (S_{2,max} + S_{2,min})/2;\ \ S_{3m} = (S_{3,max} + S_{3,min})/2 \tag{5.4}$$

Once the equivalent alternating stress ($\mathbf{S_{qa}}$) and mean stress ($\mathbf{S_{qm}}$) are obtained, the multiaxial stress state is “reduced” to an equivalent uniaxial stress state, and thus uniaxial *S-N* equations can be used for the fatigue calculations. The popular finite life “modified Goodman” equation (Stephens et al., 2001) was chosen to estimate the fatigue strength:

$$\frac{S_{qa}}{S_{Nf}} + \frac{S_{qm}}{S_u} = 1 \tag{5.5}$$

where $\mathbf{S_u}$ is ultimate tensile strength (UTS) of the material; $\mathbf{S_{Nf}}$ is the endurance limit.

In addition, after obtaining the alternating stress (S_{qa}), the so-called *Cigré Safe Border Line* (SBL) method (Cigré, 1979~1995) for multilayer ACSR conductors can be used to estimate the fatigue life (N_f) by the approximate equations:

$$S_{qa} = 450 * N_f^{-0.20} \quad \text{for } N \leq 1.56 * 10^7 \text{ cycles} \tag{5.6}$$

$$S_{qa} = 263 * N_f^{-0.17} \quad \text{for } N > 1.56 * 10^7 \text{ cycles} \tag{5.7}$$

The empirical Cigré SBL equations are derived from *S-N* curves obtained by a number of experimental data sets with multilayer ACSR conductors mounted on various types of clamps, and thus they are usually regarded as the conservative lower limit for a conductor fatigue life (Azevedo et al., 2009).

Last, but not the least, it is necessary to interpret the approach used to extract stress results from the FE analyses. Generally, in academic/research laboratory environment, material fatigue data are obtained using standard specimens under either uniaxial or multiaxial load conditions. In industry practice, fatigue analyses are applied to various real structures, but engineers mostly tend to use uniaxial testing data and criteria to determine individual component fatigue life due to the simplicity in calculations. That is, local stresses or strains in the critical locations of the component are used in its life estimate by correlating with uniaxial specimen life. As known already, multiaxial lifing is conducted in the present work. Furthermore, in light of the fact that an electrical conductor is essentially a multi-component assembly with all aluminum wires having the same material properties (in conductor fretting fatigue analyses, we only focus on aluminum wires and thus there is no necessity to consider the steel core.), the proposed lifing methodology is thus developed at an **integrated assembly level** to estimate the fatigue life of the conductor aluminum wires as an overall structure, instead of individual wires or layers. Without an attempt for great rigor, Table 5.8 presents the distinctions of the methodologies employed in academia, industry and current work. In addition, since the aluminum wires exhibit their highest peak stresses and steepest stress gradient at KE, only the results on this cross section are used in fatigue analysis. That is, the peak values (maximum and minimum) of the three principal stresses calculated during one entire fretting cycle on both the outer and inner layers at KE are extracted, as summarized in Table 5.9 (for Y_b =1.3mm).

Table 5.8 Stress-based lifing methodologies in HCF regime

	Object		Fatigue model
Traditional		specimen	uniaxial fatigue criteria
Academic (modern)		specimen	multiaxial fatigue criteria
Industry practice		component	uniaxial fatigue criteria
Current work		assembly	multiaxial fatigue criteria

Table 5.9 Peak values of principal stresses at KE during entire fretting cycle (Y_b =1.3mm)

Principal stresses		Peak values (MPa)	Location	Time
Maximum Principal **(S_1)**	Max.	113.67	Outer layer	t = 3s
	Min.	-120.57	Outer layer	t = 1s
Intermediate Principal **(S_2)**	Max.	38.82	Outer layer	t = 3s
	Min.	-173.16	Outer layer	t = 1s
Minimum Principal **(S_3)**	Max.	1.63	Inner layer	t = 1s
	Min.	-252.07	Outer layer	t = 1s

Using formulas (5.1) ~ (5.5), the calculated alternating stress, $\mathbf{S_{qa}}$ = 18.08 MPa, and the fatigue strength, $\mathbf{S_{Nf}}$ = 8.81 MPa are obtained. These values are in agreement with the minimum value from Drake ACSR fretting fatigue test at the first wire break, $\mathbf{S}_a \approx 19$ MPa (EPRI, 2006) and the suggested value of endurance limit, 8.5 MPa, for multilayer ACSR conductors (EPRI, 2006). Additionally, it has been identified by FE analysis that the prime critical zone, where dominant fretting cracks are most likely to initiate, is located at KE, and the wire breakage locations are mainly at the "Upper Half-Section" of the conductor, between the outer and inner layers. The next critical zone is in the wires of the outer layer in the vicinity of the LPC. These numerical findings are also consistent with the ones observed from the tests (Zhou et al., 1994). Certainly, it needs to be mentioned that, in reality, the particular location of a conductor wire failure associated with fretting fatigue depends also on many other factors, such as fretting amplitude.

In conclusion, fretting fatigue of overhead line conductors is primarily a HCF problem with complex multiaxial stress state in the suspension clamp mouth contact region. A FEA-based and design-oriented multiaxial fretting fatigue lifing scheme is developed successfully in this section. Not only is it efficient (easy to implement) to be suited to the conductor design environment, but also it predicts conductor fretting fatigue life at an integrated assembly level, which is of higher practical value for conductor fatigue design.

5.7 Parametric Study on Fretting Amplitude

As indicated in Chapter 2, various parameters may play important roles in the fretting fatigue performance of a transmission line conductor. In this thesis, only the effects of fretting amplitude, one of the primary factors, will be examined numerically. By means of experimental “fretting charts” and the “fretting map” theory, the effects of bending fretting amplitude on conductor fretting were investigated in-depth (Zhou et al., 1994, 1996). Using the simulation approach to address this topic will be obviously an essential supplement.

A parametric study is conducted by selecting several imposed bending fretting amplitudes, ranging from **0.43 to 1.3 mm** based on available testing data in the open literature, while all other aspects in the Drake fatigue FE model are kept the same. Some computational results and conclusions are summarized as below. (The detailed results from Y_b=1.3mm have been discussed in the previous two sections.)

Drake conductor fretting contact behavior and its fretting fatigue strength are very sensitive to the imposed fretting amplitudes:

(1) It has been found that contact kinematics states in the clamp mouth fretting region vary with the increase of fretting amplitudes, and agree well with experimental observations.

(i) The size of the critical fretting fatigue zone is affected strongly by fretting amplitudes. As stated before, a fretting zone may be revealed via the longitudinal stress field (S_{zz}) on contacting surfaces. Figures 5.30~5.32 exhibit distinctly the impact of Y_b on the size of the conductor fretting zone. When Y_b increases, the conductor fretting fatigue zone enlarges significantly.

(ii) Fretting contact states on the inner layer of aluminum wires can be changed drastically by a slight variation in fretting amplitude. At low amplitude, the inner aluminum layer and steel core behave much like one composite solid with unperceivable relative slips. With the increase of Y_b, the partial slip contact regime expands gradually on the inner layer with increasing relative slips, and the stick regime reduces correspondingly, as shown in Figures 5.33~5.35.

(iii) An increase in fretting amplitude may also affect the fretting marks among wire contact surfaces. The size and number of fretting marks on the inner layer are larger at higher bending amplitude (Figures 5.36~5.38), while the differences on the outer layer are negligible.

(iv) For the contact states between the outer layer of wires and the suspension clamp body, the effects of fretting amplitude are not significant. This can be attributed mainly to the large clamping force acting directly on the mating surfaces.

(2) The conductor fretting fatigue strength decreases with the increase of fretting amplitudes. The lifing results under different Y_b using the approach in the preceding section are presented in Table 5.10 and Figure 5.39.

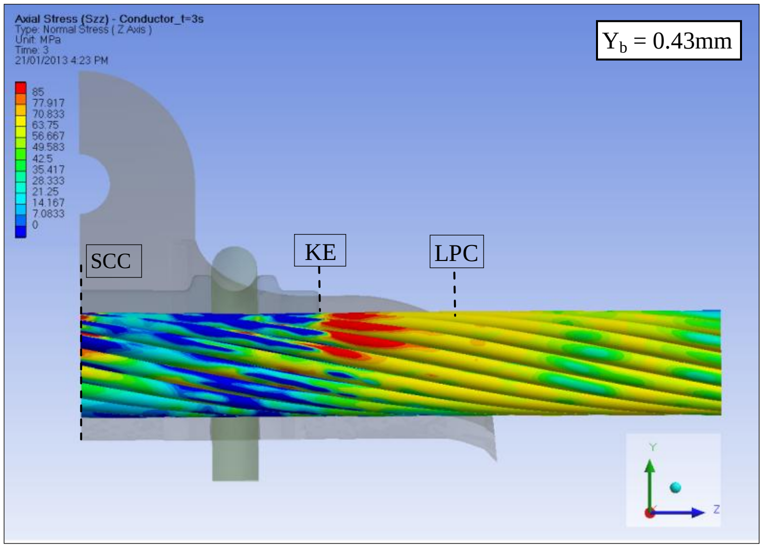

Figure 5.30 S_{zz} of Drake conductor (Y_b = 0.43mm)

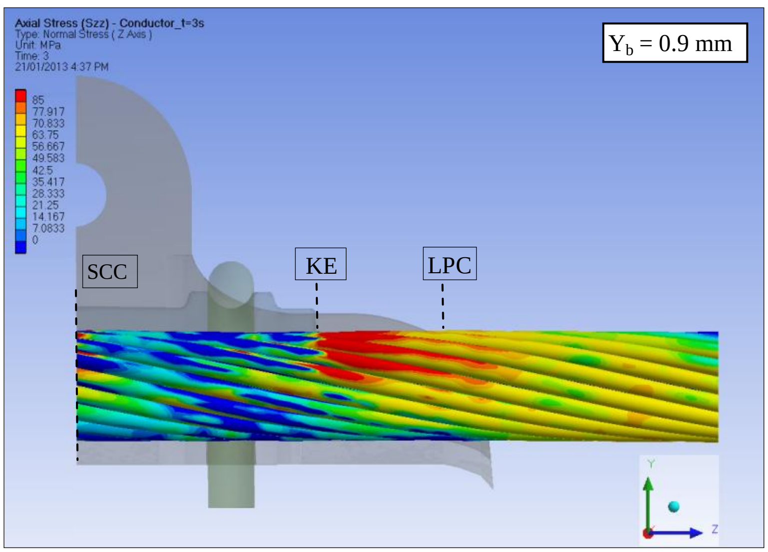

Figure 5.31 S_{zz} of Drake conductor (Y_b = 0.9mm)

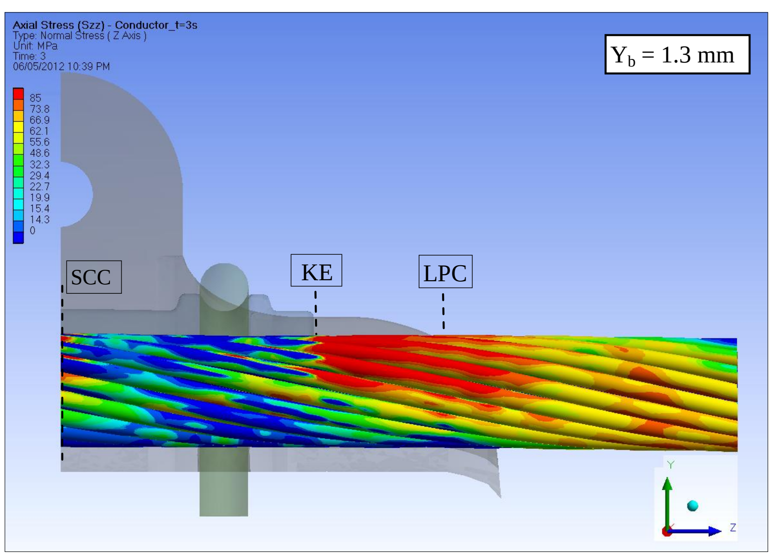

Figure 5.32 S_{zz} of Drake conductor (Y_b = 1.3mm)

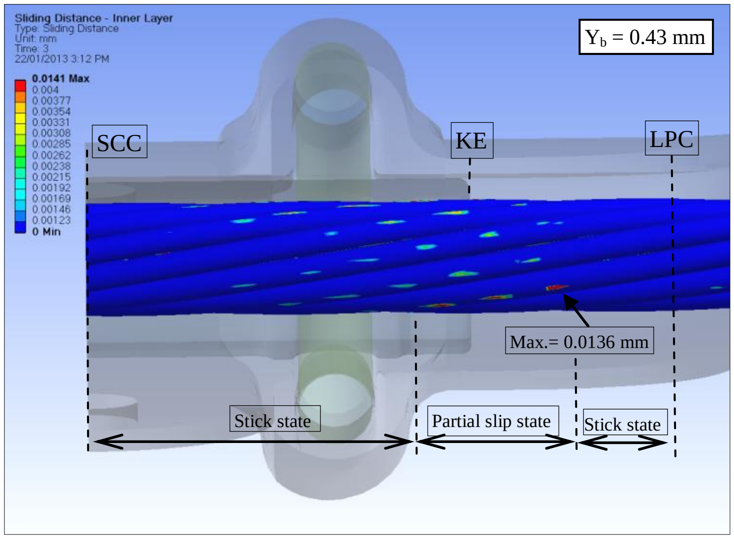

Figure 5.33 Fretting contact state on inner layer (Y_b=0.43 mm)

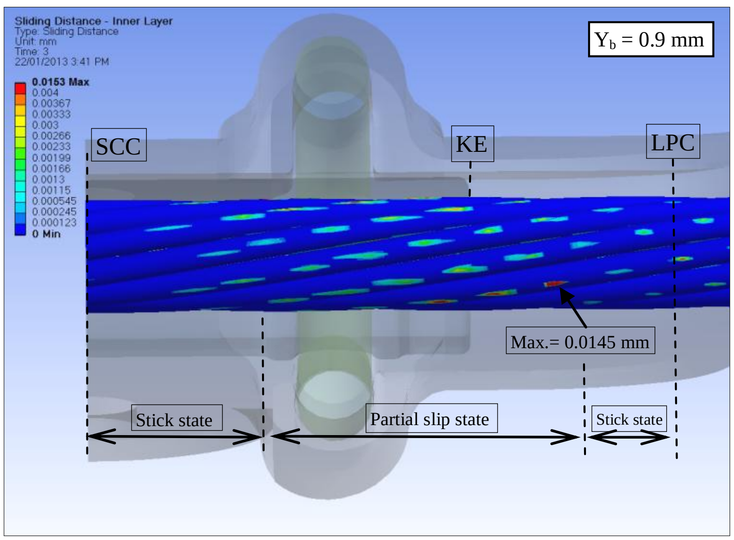

Figure 5.34 Fretting contact state on inner layer (Y_b=0.9 mm)

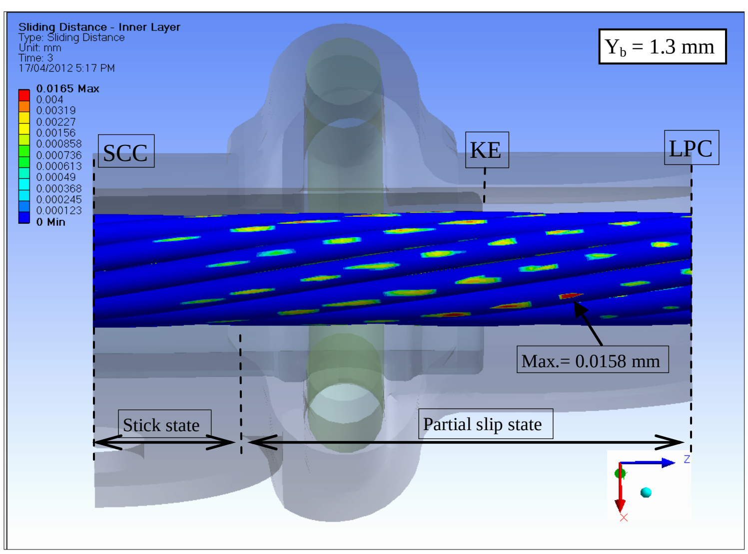

Figure 5.35 Fretting contact state on inner layer (Y_b=1.3 mm)

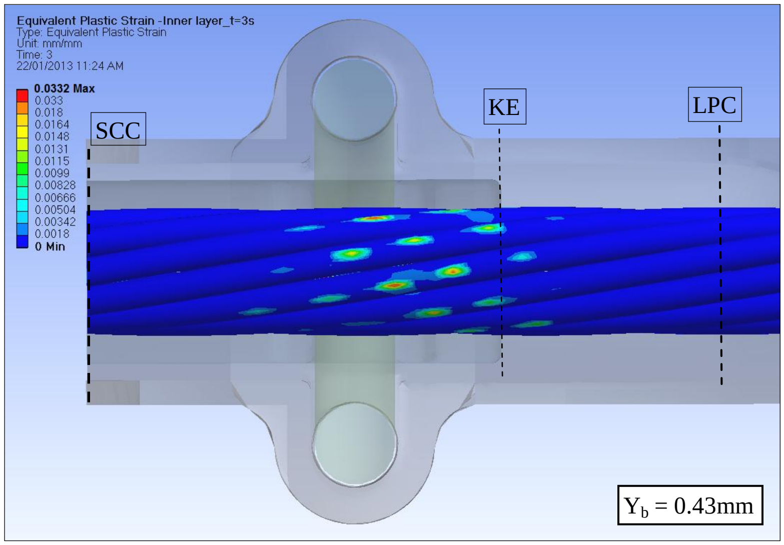

Figure 5.36 Fretting marks on inner layer (Y_b = 0.43 mm)

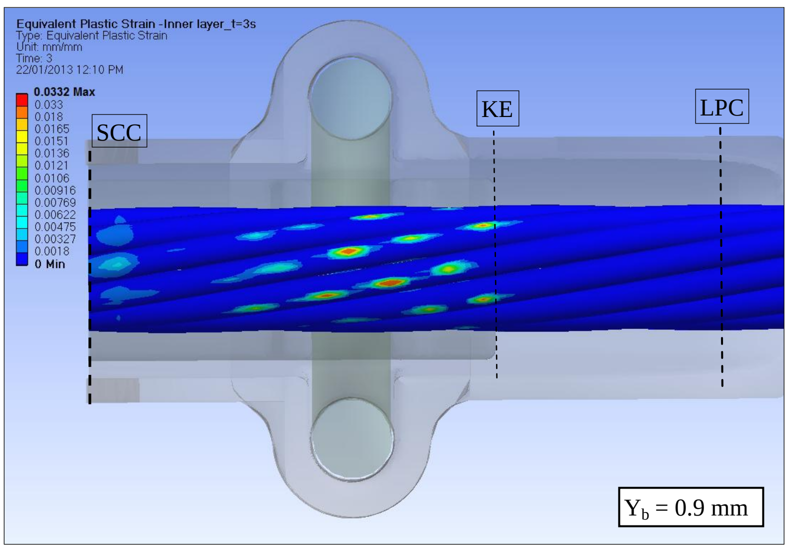

Figure 5.37 Fretting marks on inner layer (Y_b = 0.9 mm)

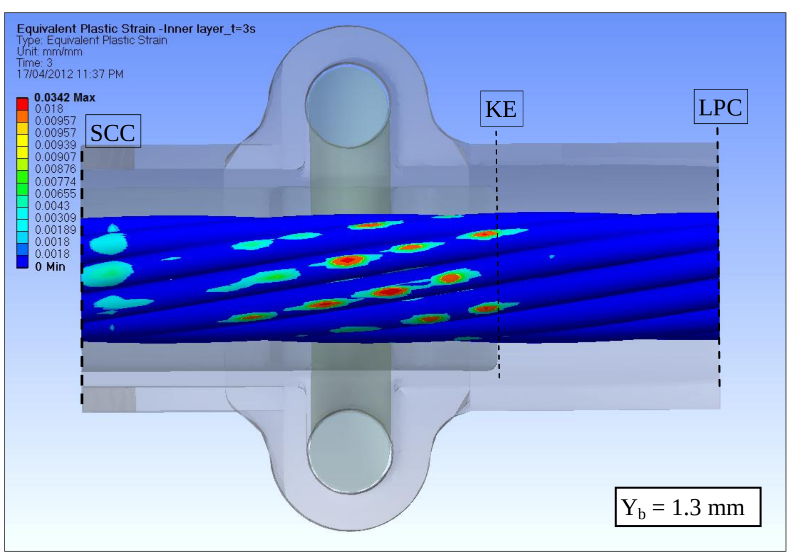

Figure 5.38 Fretting marks on inner layer (Y_b= 1.3 mm)

Table 5.10 Drake conductor fretting fatigue strength under different Y_b

Fretting amplitude (**Y_b**, mm)	Alternating stress (**S_{qa}**, MPa)	Endurance limit (**S_{Nf}**, MPa)
0.43	32.25	16.58
0.6	28.22	14.13
0.8	23.73	11.69
0.9	20.38	9.92
1.3	18.08	8.81

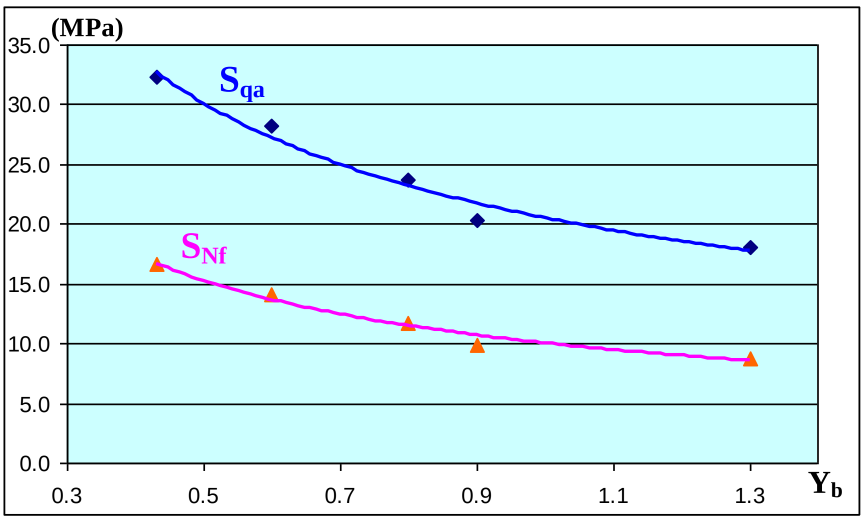

Figure 5.39 Drake conductor fretting fatigue strength under different Y_b

5.8 Summary Remarks

Continuing the journey of detailed conductor stress analysis, this long chapter has focused on the computational modeling of contact damage of electrical conductors under fretting fatigue conditions. The "Drake" ACSR fatigue FE model has much larger computational size (274,478 contact elements and multi-stepped loadings), higher nonlinearities and uncertainties than its strength model, bringing about many realistic challenges to overcome. This study provides an accurate and clearer insight of the contact states and the associated stress states among the conductor wires in the conductor-clamp system under the bending fretting fatigue conditions. Based on high accuracy of the stress analysis, a practical multi-axial fretting fatigue lifing scheme is suggested. The numerical fatigue results, including the calculated endurance limit and the findings about the critical locations for conductor wire failure, are in excellent agreement with experimental measurements and field observations in the open literature. These validations demonstrate again that the transmission line conductor FE modeling and lifing methodologies developed in this thesis are accurate, successful and dependable.

Chapter 6

Conclusions

6.1 Summary of Research Findings

The main goal of this thesis was to study the complex stress states and relevant influencing factors of stranded electrical conductors, using finite element analysis approaches, in order to accurately capture the detailed mechanical response of conductors under design and fretting fatigue conditions. All these objectives have been achieved. The main research activities and their conclusions are summarized as below:

- The first effort in this research was to largely improve a coarse stress analysis model for optical ground wires (OPGW) that are typically used in overhead high-voltage transmission lines. With the aim to predict the cable mechanical response with satisfactory accuracy, least computational cost, and a reliable solution process, a detailed and refined 3-D FE stress analysis model was constructed, which included all the essential nonlinear characteristics of the problem. The stress analysis procedures were presented in detail, and the quality of the mathematical model and the involved numerical solution techniques were studied thoroughly. Specifically, element performance, mesh design, contact condition establishment, boundary conditions and load treatments were examined carefully. The key numerical solution techniques, including computational contact algorithms, solution schemes for nonlinear algebraic equations and for large linear algebraic systems, were assessed empirically (with numerical experiments) to develop a robust solution methodology. The numerical results of the OPGW case study show agreement with the analytical solutions and significantly improve on a previous coarse model, demonstrating the high quality of the refined FE model. By means of this study, a new-generation, high-fidelity FE modeling methodology was developed for reliable and accurate computational stress analysis of stranded transmission line conductors. This analysis methodology can also be generalized to other complex stranded cable structures and wire ropes used widely in civil works and mechanical applications.

- A 795 kcmil Drake (28.13-mm outer diameter) ACSR overhead conductor was selected as a benchmark conductor to investigate the tensile strength and stress states of a complete conductor under extreme design conditions. A large-size 3-D elastic-plastic, large kinematics, multi-body frictional contact FE model of this conductor was constructed. Good solution accuracy was obtained with stable convergence. This study demonstrated again the capability and significance of using refined FE modeling to achieve a clear understanding of the highly nonlinear mechanics behavior of transmission line conductor cables, as well as the validity of the modeling approach developed in this thesis.

- It was found that, under design conditions, the longitudinal stresses in the Drake conductor wires are contributed from the combined tensile stresses and tangential contact stresses, while the effects of tangential contact stresses induced by friction may be significant. A sensitivity study was thus conducted to examine the effects of the magnitude of the frictional coefficient among conductor wires on the mechanical response of helically stranded electrical conductors under axial loading. It was shown that the effects of the frictional coefficient (μ_s) on the conductor axial stresses are evident under low friction. But, the stress variations with different frictional coefficients are negligible when μ_s increases to above 0.57. This conclusion implies that the frictional coefficients will become insensitive to the stress states as long as the conductor wire surfaces are kept in dry and clean operational conditions. However, after years of service, the aging conductors may not be so clean in polluted areas, and the effects of the magnitude of the frictional coefficient may be perceptible.

- The author is using a computational applied mechanics perspective to investigate fretting fatigue of transmission line stranded conductors. A large 3-D FE stress analysis model with comprehensive nonlinearities was developed and implemented to simulate the actual fretting fatigue test of an ACSR conductor-clamp system. The model comprised all structural components of the conductor-clamp system - adding up to 323,731 nodes, 309,805 solid finite elements and 274,478 contact elements. A hierarchical modeling approach was applied during modeling and analysis to overcome the many challenges encountered to effectively solve such a highly nonlinear and computationally demanding problem. This study provides accurate and clear insight into the contact states and the associated stress states among the helically stranded conductor wires in the conductor-clamp system under bending fretting fatigue amplitudes (such fretting is typically resulting from aeolian vibrations). The numerical results clearly demonstrate that the critical zone for conductor fretting fatigue failure is located in the suspension clamp mouth region between the keeper edge (KE) and the last point of contact (LPC), and the fretting micro cracks mostly initiate from contacting surfaces under partial slip contact state (i.e. mixed regimes), during which the axial stress plays an essential role. The agreement between the predictions of the numerical models and the experimental data is considered to be highly satisfactory.

- A practical (design-oriented) multi-axial fatigue lifing methodology was developed to estimate the local fretting fatigue strength of overhead stranded electrical conductors. The proposed lifing scheme recognized the complexity of conductor fretting fatigue but used realistic simplifications to incorporate its essence without overburdening designers to have to perform complex fatigue analysis. Thus, it may have the practical value to guide a more reliable and cost-effective OHL conductor design.

- A parametric study was performed to examine the influence of fretting amplitudes on the mechanical response of conductor-clamp system. As expected, it has been found that contact kinematics states in the clamp mouth fretting region vary with the increase of fretting amplitudes, and the conductor fretting fatigue strength reduces with the increase of fretting amplitudes.

- Based on the refined stress and fatigue analyses, a practical simplified procedure was proposed for design practice: A fretting fatigue knock-down factor (KDF) is necessary to be taken into account when a transmission line conductor is designed. Waterhouse

(1972) once pointed out that the "Strength Reduction Factor" due to fretting for aluminum alloys may be between 1.59~2.79. Later, Cowles (1996) and Hoeppner et al. (2000) claimed that the HCF strength reduction for fretting fatigue should be around 30%~50%. This computational research verifies that the stresses may be reduced by about half in the ACSR conductor critical regions susceptible to fretting fatigue. That is, KDF=0.5 is thus suggested for a transmission line aluminum conductor design in order to ensure that the component will not fail prematurely due to fretting fatigue. In other words, the strength allowable of the aluminum wires used for electrical conductor design should be set as 50% of the aluminum alloy material strength limit.

- Finally, it should be noted that, although experiments were not conducted as part of this this research, the validations of all the computational models and related numerical observations in this thesis had been achieved by comparing with experimental data provided by several manufacturers and some from the open literature.

6.2 Recommendations for Future Research

Although the mechanical behavior of stranded conductors is very complex and fretting fatigue is not a problem that can be eliminated completely from any mechanical and structural systems, numerical modeling approaches targeted to better understand the progressive damage mechanisms associated with partial slip contact states, as the work done in this thesis, are much beneficial to gain insights into managing and minimizing the effects of fretting fatigue on the degradation of product durability. Of course, such a research effort may have significant implications for conductor design improvements and manufacturing processes. Therefore, the author is strongly convinced that this is a very promising direction that is worthy of continued exploration. Some recommendations for future research from the computational modeling perspective are listed as below:

(1) The assumptions and simplifications in Chapter 5 for the fretting fatigue modeling already imply some improvement for the future work. In particular, the variation of frictional coefficients is significant with fretting cycles and is affected by many factors, and thus it needs to be included in future models provided that reliable experimental data are available. Fretting debris is also to be taken into account in the future macroscopic level modeling as the effects of the debris on contact stresses and fretting cracking behavior are actually not negligible.

(2) It is well known that the suspension clamping force is one of the two leading factors that have great influences on the conductor fretting contact states and fretting cracking behaviors. Thus, a parametric study to quantify its effects will be very meaningful.

(3) The impact and variations of various fretting damage parameters in the conductor fretting fatigue mechanisms are to be studied extensively. That is, developing quantifiable relationships between the fretting contact parameters and fretting fatigue crack behavior is expected. To this end, accurate highly-localized numerical models of the fretting contact surfaces are to be established and validated by a series of well-characterized experiments. Accounting for variability in the physics-based FE models faces tremendous challenges that have not been fully dealt with to date. This is a very open area of substantial scientific endeavor for future research.

(4) In-depth numerical study of the propagation of fretting cracks is to be carried out. For example, the development of a reliable 3-D fretting crack growth law to predict the cracking behavior has great significance. Many fretting fatigue crack analyses have been conducted on aerospace materials, such as Ti-6Al-4V, based on fracture mechanics methodology. For OHL conductors, Ouaki et al. (2003) initiated such an effort with simplified 2-D crack hypothesis. The relevant research is far from mature, and further study is certainly to be encouraged.

(5) Applying continuum damage mechanics with finite element methods to fretting damage may break new ground in terms of research methodology in this subject. Fracture mechanics is based on the analysis of existing cracks. But for fretting,

studying the evolution of internal damage/subsurface damage (before macro-cracks become evident) might be more important. Because once macro-cracks occur, it might be too late to stop a final rupture. Damage mechanics has the focus on such a “precursory state” of cracks, and it has matured to such a status for real applications.

(6) Further development of improved fretting fatigue lifing methods for various conductor types is of course another long term goal that needs to be pursued.

(7) Room temperature fretting fatigue of conductors is investigated in this thesis, while the author has realized that the fretting fatigue strength and fatigue life at high temperature may reduce significantly comparing with the ones under ambient temperature conditions. Actually, this issue, as well as the related topic of a composite conductor response to high temperature loads, is an increasingly arisen concern in the transmission line industry and research community. The strong thermal-mechanical coupling and highly nonlinear material creep behavior will increase drastically the difficulties for faithful numerical simulations, and thus must bring about greater challenges for any such a future research.

References

Abé, H., Kusumi, Y. and Saka, M. 1989. Deformation of slot rods in a slot-type optical fiber cable. Nippon Kikai Gakkai Ronbunshu, 55 (514): 1462-1468. (Paper in Japanese with abstract in English).

Abel, J. F. and Shephar, M. S. 1979. An algorithm for multipoint constraints in finite element analysis. International Journal for Numerical Methods in Engineering, 14 (3): 464-467.

ADINA R&D, Inc. 2008. ADINA theory and modeling guide, Volume I: ADINA solids & structures, Watertown, MA, U.S.A.

Aggarwal, R. K., Johns, A. T., Jayasinghe, J. A. S. B. and Su, W. 2000. An overview of the condition monitoring of overhead lines. Electric Power Systems Research, 53 (1): 15-22.

Ainsworth, M. and Oden, J. T. 1993. A unified approach to a posteriori error estimation based on element residual methods. Numerical Mathematics, 65: 23-50.

Akin, J. E. 2005. Finite element analysis with error estimators, Butterworth-Heinemann.

Aliabadi, M. H. and Brebbia, C. A. 1993. Computational methods in contact mechanics, Computational Mechanics Publications.

Alic, J. A. and Kantimathi, A. 1979. Fretting fatigue with reference to aircraft structures. SAE Report Number: SAE-790612.

Anderson, B. and Li, H. 2006. Simulation of the cross arm failure due to unequal ice loading of two 500 kV transmission towers through numerical modeling, in Electrical Transmission Line and Substation Structures: Structural Reliability in a Changing World. Nickerson, R. E. (ed.), ASCE.

Anderson, T. L. 2005. Fracture mechanics: fundamentals and applications, 3rd edition, CRC Press.

ANSYS Inc. 2007. Introduction to ANSYS DesignModeler training manual, Canonsburg, PA, USA.

ANSYS Inc. 2007. Theory reference for ANSYS and ANSYS Workbench, Canonsburg, PA, USA.

Anton, D. L. 1999. Simultaneous fretting and fatigue of Ti-6Al-4V. United Technologies Research Center, A report in “Improved high-cycle fatigue (HCF) life prediction, Part 3, Appendix 6D, University of Dayton Research Institute (2001).

Arrieta, H., Wackers, V. P., Dang Van, K., Constantinescu, A. and Maitournam, H. 2003. Modelling attempts to predict fretting-fatigue life on turbine components. The RTO AVT Specialists’ Meeting on “The Control and Reduction of Wear in Military Platforms”, Williamsburg, USA, and also published as a report ADM201869, RTO-MP-AVT-109.

ASME. 1979. Cases of ASME boiler and pressure vessel code, code case N-47-12, American Society of Mechanical Engineers.

ASTM International. 1996. Fatigue and fracture (ASM Handbook Vol.19), American Society for Metals.

ASTM International. 2002. Failure analysis and prevention (ASM Handbook Vol.11), American Society for Metals.

ASTM International. 2004. Standard specification for aluminum 1350-H19 wire for electrical purposes. Annual Book of ASTM Standards, 02.03: 92-95, ASTM B 230/B 230M-99.

ASTM International. 2004. Standard specification for concentric-lay-stranded aluminum conductors, coated-steel reinforced (ACSR). Annual Book of ASTM Standards, 02.03: 107-122, ASTM B 232/B 232M-01.

ASTM International. 2004. Standard specification for zinc-coated (galvanized) steel core wire for aluminum conductors, steel reinforced (ACSR). Annual Book of ASTM Standards, 02.03: 216-219, ASTM B 498/B 498M-98.

Atluri, S. N. 2004. The Meshless Method for Domain and BIE Discretizations. Tech Science Press.

Attia, M. Helmi and Waterhouse, R. B. 1992. Standardization of Fretting Fatigue Test Methods and Equipment, ASTM International.

Avallone, E.A. and Baumeister, T. (eds.). 1997. Marks' Standard Handbook for Mechanical Engineers, 11th ed., McGraw-Hill, Inc.

Azevedo, C.R.F., and Cescon, T. 2002. Failure analysis of aluminum cable steel reinforced (ACSR) conductor of the transmission line crossing the Parana River. Engineering Failure Analysis, 9(6): 645–664.

Azevedo, C.R.F., Henriques, A.M.D., Pulino Filho, A. R., Ferreira, J. L. A. and Araujo, J. A. 2009. Fretting fatigue in overhead conductors: Rig design and failure analysis of a Grosbeak aluminium cable steel reinforced conductor. Engineering Failure Analysis, 16: 136–151

Babuška, I. 1988. The p- and hp-versions of the finite element method: the state of the art. in Finite elemnts: theory and applications, edited by D. L. Dwoyer, M. Y. Hussaini and R. G. Voigt, Springer-Verlag, pp.199-239.

Babuška, I. and Rheinboldt, W. 1978. Error estimates for adaptive element computation. SIAM Journal of Numerical Analysis, 15: 736-754.

Babuška, I. and Strouboulis, T. 2001. The finite element method and its reliability, Oxford University Press.

Babuška, I. and Suri, M. 1990. The p- and hp-versions of the finite element method: a overview. Computers Methods in Applied Mechanics and Engineering, 80:5-26.

Babuška, I., Whiteman, J. R. and Strouboulis, T. 2011. Finite elements: An introduction to the method and error estimation, Oxford University Press.

Bahke, E. 1985. 150 years of research on wire rope. Wire, 35(4): 148-152.

Bahke, E. 1985. 150 years of research on wire rope II. Wire, 35(5): 203- 207.

Ballard, P. Dang Van, K. Deperrois, A. and Papadopulos, I. V. 1995. High cycle fatigue and finite element analysis. Fatigue and Fracture of Engineering Materials and Structures, 18 (3): 397-411.

Bannantine, J. A., Comer, J. J. and Handrock, J. L. 1990. Fundamentals of metal fatigue analysis, Prentice Hall.

Basquin, O. H. 1910. The exponential law of endurance tests. Procedings ASTM, 10: Part II, 625.

Bathe, K. J. 1996. Finite element procedures, Prentice Hall, Englewood Cliffs, NJ, USA.

Bathe, K. J. and Cimento, A. P. 1980. Some practical procedures for the solution of nonlinear finite element equations. Computer Methods in Applied Mechanics and Engineering, 22: 59-85.

Bathe, K. J., Lee, N. S. and Bucalem, M. L. 1990. On the use of hierarchical models in engineering analysis. Computer Methods in Applied Mechanics and Engineering, 82: 5-26.

Beaver, P. W. Multiaxial fatigue and fracture: a literuature review. 1984. Structures Report 410 (AR-003-931). Aeronautical Research Laboratories, Defence Sinence & Technology Organisation, Department of Defence, Australia.

Becker, R. and Rannacher, R. 1996. A feed-back approach to error control in finite element methods: Basic analysis and examples. EAST-WEST Journal of Numerical Mathematics, 4: 237-264.

Belytschko, T., Kronggauz, Y., Organ, D. et al. 1996. Meshless methods: An overview and recent developments. Computer Methods in Applied Mechanics and Engineering, 139 (1-4): 3-47.

Belytschko, T., Liu, W. K. and Kennedy, J. M. 1984. Hourglass control in linear and nonlinear Problems. Computer Methods in Applied Mechanics and Engineering, 43: 251–276.

Belytschko, T., Liu, W. K. and Moran, B. 2000. Nonlinear finite elements for continua and structures, John Wiley & Sons.

Belytschko, T., Lu, Y. Y. and Gu, L. 1994. Element-free Galerkin methods International Journal for Numercial Method in Engineering, 37 (2): 229-256.

Berthier, Y., Vincent, L. and Godet, M. 1988. Velocity accommodation in fretting. Wear, 125: 25-38.

Berthier, Y., Vincent, L. and Godet, M. 1989. Fretting fatigue and fretting wear. Tribology International, 22(4): 235-242.

Bjorkman, G., Klarbring, A., Sjodin, A. et al. 1995. Quadratic programming for non-linear elastic contact problems. International Journal for Numerical Methods in Engineering, 38: 137-165.

Boniardi, M., Cincera, S., D'Errico, F. and Tagliabue, C. 2007. Fretting fatigue phenomena on an all aluminium alloy conductor. Key Engineering Materials, 348-349: 5-8

Bonet, J. and Wood, R. D. 2008. Nonlinear continuum mechanics for finite element analysis, 2nd edition, Cambridge University Press.

Boyer, H. E. 1986. Atlas of fatigue curves, ASTM International.

Braess, D. 2007. Finite elements: theory, fast solvers, and applications in elasticity theory, 3rd edition, Cambridege University Press.

Broek, D. 1982. Elementary engineering fracture mechanics, Springer.

Broek, D. 1988. The practical use of fracture mechanics, Springer.

Brown, M. W. and Miller, K. J. 1973. A theory for fatigue failure under multiaxial stress-strain conditions. Proceedings of the Institution of Mechanical Engineers, 187: 65-73.

Brown, M. W. 1983. Multiaxial fatigue tesing and analysis. in Fatigue at High Temperatures. Applied Science Publishers, 97-133.

Bucalem, M. L. and Bathe, K. J. 2011. The mechanics of solids and structures: hierarchical modeling and the finite element solution, Springer.

Calhoun, D. A., Helzel, C. and LeVeque, R. J. 2008. Logically rectangular grids and finite volume methods for PDEs in circular and spherical domains. SIAM Review, 50 (4): 723-752.

Campbell, W. E. 1969. “Fretting” in boundary lubrication: A review of world literature. ASME.

Cardou, A., Dalpé, C. and Hardy, C. 1997. Fretting fatigue of the Drake ACSR electrical conductor under cyclic bending at suspension clamp. ISF'97, Chengdu, China, pp. 200-214.

Cardou, A., Cloutier, L., Lanteigne, J. and M'Boup, P. 1990. Fatigue strength characterization of ACSR conductors at suspension clamps. Electric Power Systems Research, 19(1): 61-71.

Cardou, A., Cloutier, L., St-Louis, M. and Leblond, A. 1992. ACSR electrical conductors fretting fatigue at spacer clamps. in “Standardization of Fretting Fatigue Test Methods and Equipment”, Attia, M. H. and Waterhouse, R. B. (eds.), pp. 231-242.

Cardou, A., Leblond, A. and Cloutier, L. 1993. Suspension clamp and ACSR electrical conductor contact conditions. Journal of Energy Engineering, 119 (1): 19-31.

Cardou, A., Leblond, A., Goudreau, S. and Cloutier, L. 1994. Electrical conductor bending fatigue at suspension clamp: a fretting fatigue problem. in: Fretting Fatigue, Waterhouse, R. B., and Lindley, T.C., (Eds.), Mechanical Engineering Publications, pp. 257-266.

Carpinteri, A., Freitas, M. D. and Spagnoli, A. 2003. Biaxial multiaxial fatigue and fracture, Elsevier Science.

Cescotto, S. and Charilier, R. 1992. Frictional contact finite elements based on mixed variational principles. International Journal for Numercial Method in Engineering, 36: 1681-1701.

Cescotto, S. and Zhu, Y. Y. 1994. Large strain dynamic analysis using solid and contact finite elements based on a mixed Formulation - application to metalforming. Journal of Metals Processing Technology, 45: 657-663Chan, K. S., Davidson, D.L., Lee, Y-D., and Hudak, S.J., Jr. 2001. A fracture mechanics approach to high cycle fretting fatigue based on the worst case fret concept: Part I - Model development. International Journal of Fracture, 112: 299-330.

Chen, Y., Lee, J. and Eskandarian, A. 2006. Meshless methods in solid mechanics. Springer.

Chiang, Y. J. 1996. Characterizing simple-stranded wire cables under axial loading. Finite Element in Analysis and Design, 24 (2): 49-66.

Cigré Study Committee 22 (working group 04). 1979. Recommendations for the evaluation of the lifetime of transmission line conductors. Electra, 63: 103-145.

Cigré Study Committee 22 (working group 04). 1985. Guide for endurance tests of conductors inside Cclamps. Electra, 100: 77-86.

Cigré Study Committee 22 (working group 04). 1988. Endurance capability of conductors, Final Report.

Cigré Study Committee 22 (working group 02). 1995. Guide to vibration measurements on overhead lines. Electra, 162: 125-137.

Cloutier, L., Dalpé, C., Cardou, A., Hardy, C. and Goudreau, S. 1999. Studies of conductor vibration fatigue tests, flexural stiffness and fretting behavior. Third International Symposium on Cable Dynamics, pp. 197-202.

Coffin, L. F. 1954. A study of the effects of cyclic thermal stresses on a ductile metal. Transactions of the American Society of Mechanical Engineers, 76: 931-950.

Collins, J. A. 1981. Failure of meterials in mechanical design, Wiley-Inerscience.

Colombie, C., Berthier, Y., Floquet, A., Vincent, L. and Godet, M. 1984. Fretting: load carrying capacity of wear debris. Journal of Tribology, 106(2): 194-201.

Comyn, R. H. and Furlani, C. W. 1963. Fretting corrosion: A literature survey. Report No. TR-1169, U.S. Army Material Command, Harry Diamond Laboratories, pp.100.

Conry, T. F. and Seireg, A. 1971. A mathematical programming method for design of elastic bodies in contact. Journal of Applied Mechanics, 38 (2): 387-392.

Cook, R. D., Malkus, D. S., Plesha, M. E. and Witt, R. J. 2001. Concepts and applications of finite element analysis, 4th edition, John Wiley & Sons.

Cowles, B. A. 1996. High cycle fatigue in aircraft gas turbines - an industry perspective. International Journal of Fracture, 80: 147-163.

Costello, G. A. 1997. Theory of wire rope, 2nd ed., Springer.

Crisfield, M. A. 1991. Non-linear finite element analysis of solids and structures, V. 1: Essentials, Wiley.

Crisfield, M. A. 1997. Non-linear finite element analysis of solids and structures, V. 2: Advanced Topics, Wiley.

Dalpé, C., Cardou, A., and Cloutier, L. 2001. Fatigue strength characterization of the Drake ACSR electrical conductor performed on two test systems. CANCAM 01, Canadian Congress of Applied Mechanics, St John's, NF. pp. 79-80.

Dalpé, C., Cardou, A., and Vincent, L. 1999. Fretting behavior of two aluminum wires in contact under a cyclic imposed displacement. CANCAM 99, Canadian Congress of Applied Mechanics, Hamilton, Ont. pp. 391-392.

Dang Van, K., Griveau, B. and Message, O. 1989. On a new multiaxial fatigue limit criterion: theory and application. Biaxial and Multiaxial Fatigue, EGF Publications 3 (Edited by M. W. Brown and K. J. Miller), 479-496.

Dang Van, K. 1993. Macro-Micro approach in high-cycle multiaxial fatigue. Advances in multiaxial fatigue, (D.L. McDowell and R. Ellis, Eds.), ASTM, 120-130.

Dang Van, K. and Maitournam, M. H. 2002. On some recent trends in modelling of contact fatigue and wear in rail,. Wear, 253(1-2): 219-227.

Dang Van, K. 2003. Introduction to fatigue analysis in mechanical design by the multiscale approach. High-cycle Metal Fatigue: From theory to Applications (K. Dang Van and I. Papadoupoulos, Eds), CISM International Centre for Mechanical Sciences, Springer, 57-88.

Dassault Systèmes, 2010. Abaqus 6.10 theory manual. Dassault Systèmes Simulia Corp., Providence, RI, USA.

Dastous, J. B. 2005. Nonlinear finite-element analysis of stranded conductors with variable bending stiffness using the tangent stiffness method. , IEEE Ttransactions on Power Delivery, 20(1): 328-338.

Davis, J. R. 1994. Aluminum and aluminum alloys. ASM Specialty Handbook, Davis & Associates.

De Borst, R., Crisfield, M., Remmers, J. and Verhoosel, C. 2012. Non-linear finite element analysis of solids and structures, Wiley.

Demmel, J. W. 1997. Applied numerical linear algebra, Society for Industrial and Applied Mathematics (SIAM).

Dhondt, G. 2004. The finite element method for three-dimensional thermomechanical applications, John Wiley & Sons.

Dowling, N. E. 2006. Mechanical behavior of materials: engineering methods for deformation, fracture, and fatigue, Prentice Hall.

Eck, C., Janusek, J. and Krbec, M. 2005. Unilateral contact problems: Variational methods and existence theorems, CRC Press.

Eck, C., Steinbach, O. and Wendland, W. L. 1999. A symmetric boundary element method for contact problem with friction. Mathematics and Computers in Simulation, 50 (1-4): 43-62.

Eck, C. and Wendland, W. L. 1998. An adaptive boundary element method for contact problems. Mathematical Aspects of Boundary Element Method / Eds. M. Bonnet et al., 116-127.

Eden, E.M., Rose, W.N. and Cunningham F. L. 1911. The endurance of metals - experiments on rotating beams at University of College. Proc. Inst. Mech. Engrs., 4: 839–974.

El-Fashny, K., Chouinard, L., and McClure, G. 1999. Reliability analysis of telecommunication towers. Canadian Journal of Civil Engineering, 26(1): 1-12.

Ellyin, F. 1996. Fatigue damage, crack growth, and life prediction, Chapman & Hall.

EMI Transmission Limited. 2007. Suspension clamp (Envelop type) suitable for “Zebra” ACSR Conductor (Drawing).

Endo, K. and Goto, H. 1976. Initiation and propagation of fretting fatigue cracks. Wear, 38: 311-324.

Engine Structural Integrity Program (ENSIP). 1984. MIL-HDBK-1783B (USAF).

Engine Structural Integrity Program (ENSIP). 2002. MIL-HDBK-1783B (USAF).

Engineering ToolBox. Friction theory and coefficients of friction for some common materials and materials combinations, www.engineeringtoolbox.com.

EPRI. 1979. Transmission Line Reference Book: Wind-induced Conductor Motion, Electric Power Research Institute. Palo Alto, CA. U.S.A.

EPRI. 2006. Transmission Line Reference Book: Wind-induced Conductor Motion, Electric Power Research Institute. Palo Alto, CA. U.S.A.

Eterovic, A. L. and Bathe, K. J. 1991. On the treatment of inequality constraints arising from contact conditions in finite element analysis. Computers and Structures, 40 (2): 203-209.

Faanes. S., and Fernando, U. S. 1994. Life prediction in fretting fatigue using fracture mechanics, in Fretting Fatigue, ESIS 18, Waterhouse, R. B., and Lindley, T. C., (eds.), 149-159.

Farahmand, B. 2001. Fracture mechanics of metals, composites, welds, and bolted joints - application of LEFM, EPFM, and FMDM theory, Springer.

Faridafshin, F. and McClure, G. 2008. Seismic response of tall guyed masts to asynchronous multiple-support and vertical ground motions. ASCE Journal of Structural Engineering, 134(8): 1374-1382.

Farris, T. N., Murthy, H., and Matlik, J. F. 2003. “Fretting fatigue”, Comprehensive Structural Integrity. Ritchie, R. O. and Murakami, Y. eds, Elsevier. Vol. 4: 281-326.

Farzaneh, M. and Savadjiev, K. 2007. Evaluation of tensile strength of ACSR conductors based on test data for individual strands. IEEE Transactions on power delivery, 22 (1): 627-633.

Feyrer, K. 2010. Wire Ropes: tension, endurance, reliability. Springer.

Findley, W. N. 1959. A theory for the effect for mean stress on fatigue of metals under combined tortion and axial load or bending. Journal of Engineering for Industry, 81(4): 301-306

Flanagan, D. P., and Belytschko, T. 1981. A uniform strain hexahedron and quadrilateral with hourglass control. International Journal for Numerical Methods in Engineering, 17: 679-706.

Foulquier, J. 1988. Comportement en fretting fatigue des alliages T7175 et 2124 T351, Rapport Aerospatiale, Suresnes-France.

Francavilla, A. and Zienkiewicz, O. C. 1975. A note on numerical computation of elastic contact problems. International Journal for Numerical Methods in Engineering, 9: 913-924.

Freitag, L. A. and Knupp, P. M. 2002. Tetrahedral mesh improvement via optimization of the element condition number. International Journal for Numerical Methods in Engineering, 53: 1377–1391.

Frey, P. and Georg, P. L. 2008. Mesh generation, 2nd edition, Wiley-ISTE.

Fricke, W. G. Jr., and Rawlins, C. B. 1968. Importance of fretting in vibration fatigue of stranded conductors. IEEE Transactions Paper. PAS-87. 6: 1381-1384.

Frost, N. E., Marsh, K. J, and Pook, L. P. 2011. Metal fatigue, Dover Publications.

Galin, L. A. 2008. Contact problems: the legacy of L.A. Galin, Springer.

Gallagher, J. P., et al., 2001. Improved high-cycle fatigue (HCF) life prediction. Research Report (Report No. AFRL-ML-WP-TR-2001-4159), University of Dayton Research Institute.

Garud, Y. S. 1981. Multiaixal fatigue: a survey of the state of the art. Journal of Testing and Evaluation, 9(3): 165-178.

Gdoutos, E. E. 2005. Fracture mechanics: An introduction, 2nd ed., Springer.

General Cable. 2007. Modulus and expansion calculations using Teynolds (General Cable) coefficient values. (Internal test report)

General Cable. 2010. ACSR/GA Drake certified test report.

General Cable. 2010. Cable design for concentric round conductor.

Georg, P. L. 1991. Automatic mesh generation: application to finite element methods, John Wiley & Sons Inc.

Gerber, W. 1874. Bestimmung der zulassigen Spannungen in Eisen-konstructionen. Zeitschrift des Bayerischen Architeckten und Ingenieur-Vereins, 6: 101-110.

Giglio, M., and Manes, A. 2005. Life prediction of a wire rope subjected to axial and bending loads, Engineering Failure Analysis, 12(4): 549-568.

Gladwell G. M. L., 1980. Contact problems in the classical theory of elasticity, Springer.

Godet, M. 1990. Third-bodies in tribology. Wear, 136(1): 29-45.

Golub, G. H. and Van Loan, C. F. 1996. Matrix computations, 3rd edition, The Johns Hopkins University Press.

Goodman, J. 1899. Mechanics Applied to Engineering, Longmans-Green, London.

Goryacheva, I. G. 1998. Contact mechanics in tribology, Kluwer.

Griffiths, B. J. 1985. White layer formation at machined surfaces and their relationship to white layer formations at worn surfaces. Journal of Tribology, 107: 165-170.

Gunther, F. C. and Liu, W. K. 1998. Implementation of boundary conditions for meshless methods. Computer Methods in Applied Mechanics and Engineering, 163 (1-4): 265-230.

Hackbusch, W. 1994. Iterative solution of large sparse systems, Springer.

Hall, H. M. 1951. Stresses in small wire ropes. Wire and Wire Products, 26: 228, 257-259.

Hamilton, G. M. and Goodman, L. E. 1966. The stress field created by a circular sliding contact. Journal of Applied Mechanics, 371-376.

Harris, W. J. 1967. The influence of fretting on fatigue, North Atlantic Treaty Organization Advisory Group for Aerospace Research and Development, Report Number: AGARD-AR-8.

Harris, W. J. 1972. The influence of fretting on fatigue, Part III, North Atlantic Treaty Organization Advisory Group for Aerospace Research and Development, Report Number: AGARD-AR-45.

Heoppner, D. W., Adibnazari, S. and Moesser, M. W. 1994. Literature review and preliminary studies of fretting and fretting fatigue including special applications to aircraft joints. Final report, Report Number: DOT-FAA-CT-93-2, Utah University.

Heoppner, D. W., Elliot, C. B., and Moesser, M. W. 1996. The role of fretting fatigue on aircraft rivet hole cracking. Final report, Report Number: DOR-FAA-AR-96-10, Utah University.

Hertz, H. 1882. Uber die Beruhrung fester elastischer Korper. J. Reine Angew. Math., 92: 156-171.

Hertzberg, R. W. 1996. Deformation and fracture mechanics of engineering materials. 4th ed., Wiley.

Heywood, R. B. 1962. Designing against Fatigue, Chapman and Hall, London.

Hills, D. A., Kelly, P. A., Dai, D. N. and Korsunsky, A. M. 1996. Solution of Crack Problems: The Distributed Dislocation Technique, Springer.

Hills, D. A. and Nowell, D. 1994. Mechanics of fretting fatigue, Kluwer Academic Publishers.

Hills, D. A., Nowell, D., and O'Connor, J. J. 1998. On the mechanics of fretting fatigue. Wear, 125: 129-146.

Hlavacek, I., Haslinger, J., Necas, J., Lovisek, J. 1988. Solution of variational inequalities in mechanics, Springer.

Hoeppner, D. W. 2002. Fretting/fretting fatigue and aircraft joints, presentation at Pratt & Whitney Canada.

Hoeppner, D. W., Chandrasekaran, V. and Elliott Charles B. 2000. Fretting fatigue: current technology and practices, ASTM International.

Hruska, F. H. 1951. Calculation on stresses in wire ropes. Wire and Wire Products, 26: 766–767, 799–801.

Hruska, F. H. 1952. Radial forces in wire ropes, Wire and Wire Products, 27: 459–463.

Hruska, F. H. 1953. Tangential forces in wire ropes. Wire and Wire Products, 28: 455–460.

Huang, X. and Vinogradov, O. 1992. Interwire slip and its influence on the dynamic properties of tension cables. Proceedings of the Second International Offshore and Polar Engineering Conference, San Francisco, USA, 392-396.

Huang, X. and Vinogradov, O. 1994. Analysis of dry friction hysteresis in a cable under uniform bending. Structural Engineering and Mechanics, 2(1): 63-80.

Huang, X. and Vinogradov, O. 1996. Dry friction losses in axially loaded cables. Structural Engineering and Mechanics, 4(3): 330-344.

Huang, X. and Vinogradov, O. 1996. Extension of a cable in the presence of dry friction. Structural Engineering and Mechanics, 4(3): 313-329.

Hughes, T. J. R. 2000. The finite element method, Dover Publications, Inc..

Hurricks, P. L. 1970. The mechanism of fretting: A review. Wear, 15: 389-409.

Hutson, A., Nicholas, T., and John, R. 2005. Fretting fatigue crack analysis in Ti-6Al-V4. International Journal of Fracture, 27: 1582-1589

Ibrahimbegovic, A. 2009. Nonlinear solid mechanics: theoretical formulations and finite element solution methods, Springer.

IEEE. 1966. Standardization of conductor vibration measurement. Committee Report, IEEE Trans. Power, Apparatus Systems, PAS-85, IEEE (1): 10-20.

Inagaki, K., Ekh, J. and Zahrai, S. 2007. Mechanical analysis of second order helical structure in electrical cable. International Journal of Solids and Structures , 44 (5): 1657-1679.

IREQ, Laboratoire Grande Puissance. 1994. 96 Hours traction test on 19 mm OPGW. Institut de recherche d'Hydro-Québec, Test report #84274B. Montréal, Canada.

Irwin, G. R. 1957. Analysis of stresses ans strains near the end of the crack transversing a plate. Journal of Applied Mechanics, 24: 361-364.

Jamaleddine, A., McClure, G., Rousselet, J., and Beauchemin, R. 1993. Simulation of ice shedding on electrical transmission lines using ADINA. Computers & Structures, 47(4/5): 523-536.

Jiang, W. G. and Henshall, J. L. 1999. The analysis of termination effects in wire strand using the finite element method. Journal of Strain analysis, 34(1): 31-38.

Jiang, W. G and Henshall, J. L. 2000. A novel finite element model for helical springs. Finite Elements in Analysis and Design, 35(4): 363-377.

Jiang, W. G, Henshall J. L. and Walton, J. M. 2000. A concise finite element model for 3-layer straight wire rope strand. International Journal of Mechanical Sciences, 42(1): 63-86.

Jiang, W. G, Warby, M. K. and Henshall, J. L. 2008. Statically indeterminate contacts in axially loaded wire strand. European Journal of Mechanics A/Solids, 27(1): 69-78.

Jiang, W. G., Yao, M. S., and Walton, J. M. 1999. A consise finite element model for simple straight wire rope strand. International Journal of Mechanical sciences, 41(2): 143-161.

Johnson, K. L. 1985. Contact mechanics, Cambridge University Press.

Jolicoeur, C. and Cardeau, A. 1996. Semicontinuous mathematical model for bending of multilayered wire strands. ASCE Journal of Engineering Mechanics, 122: 643-650.

Kálmán, T., Farzaneh, M. and McClure, G. 2007. Numerical analysis of the dynamic effects of shock-load-induced ice shedding on overhead ground wires. Computers & Structures, 85: 375-384.

Kardestuncer, H. and Norrie, D. H. 1987. Finite element handbook, McGraw Hill.

Kelley, C. T. 1995. Iterative methods for linear and nonlinear equations, Society for Industrial and Applied Mathematics (SIAM).

Kelley, C. T. 2003. Solving nonlinear equations with Newton's method, Society for Industrial and Applied Mathematics (SIAM).

Keyhan, H., McClure, G. and Habashi, W. G. 2011. Computational study of surface roughness and ice accumulation effects on wind loading of overhead line conductors. International Review of Civil Engineering (IRECE), 2(4): 208-214.

Keyhan, H., McClure, G. and Habashi, W. G. 2013. Dynamic analysis of an overhead transmission line subject to gusty wind loading predicted by wind-conductor interaction. Computers & Structures. DOI:10.1016/j.compstruc.2012.12.022.

Khedr, M., and McClure, G. 1999. Earthquake amplification factors for self-supporting telecommunication towers. Canadian Journal of Civil Engineering, 26(2): 208-215.

Khedr, M., and McClure, G. 2000. A simplified method for seismic analysis of lattice telecommunication towers. Canadian Journal of Civil Engineering, 27(3): 533-542.

Kiessling, F., Nefzger, P., Nolasco, J. F. and Kaintzyk, U. 2010. Overhead power lines: planning, design, construction. 1st edition, Springer.

Kikuchi, N. and Oden, J. T. 1988. Contact problems in elasticity: A study of variational inequalities and finite element methods, Society of Industrial and Applied Mathematics.

Kinyon, S. E., Hoppner, D. W. and Mutoh, Y. 2003. Fretting Fatigue: Advances in Basic Understanding and Applications, ASTM International.

Klarbring, A. 1986. A mathematical programming approach to three-dimensional contact problems with friction. Computer Methods in Applied Mechanics and Engineering, 58: 175-200.

Klarbring, A. and Bjorkman, G. 1988. A mathematical programming approach to contact problems with friction and varying contact surface. Computer and Structures, 30 (5): 1185-1198.

Kurtus, R. 2005. Coefficient of friction values for clean surfaces, www.school-for-champions.com/science/friction_coefficient.htm.

Kussmaul, K. F., McDiarmid, D. L. and Socie, D. F. 1991. Fatigue under biaxial and multiaxial Loading, ESIS Publication 10, Elsevier Science.

Kutz, M. (ed.) 1986. Mechanical Engineers' Handbook, John Wiley and Sons.

Lanteigne, J., Cardou, A., and Cloutier, L. 1985. Fatigue tests on a typical ACSR conductor. Transactions of Canadian Electrical Association, Engineering and Operating Division, Conductor Vibration Workshop, Montréal, Vol. 5.

Lao, H. J., Zhao, X. Z. and Cao, Z. 2009. Stress finite element analysis of clamping region of overhead transmission line. Journal of China Three Gorges University, 31(1): 45-47. (in Chinese)

Laursen, T. A. 1995. Review of computational methods in contact mechanics. American Scientist, 83: 196-198.

Laursen, T. A. 2002. Computational contact and impact mechanics: fundamentals of modeling interfacial phenonemna in nonlinear finit element analsyis, Springer.

Laursen, T. A. and Simo, J. C. 1993. A continuum-based finite element formulation for the implicit solution of multibody, large-deformation, frictional, contact problems. International Journal for Numerical Methods in Engineering, 36: 3451-3486.

Laursen, T. A. and Simo, J. C. 1993. Algorithmic symmetrization of Coulomb frictional problems using augmented lagrangians. Computers Methods in Applied Mechanics and Engineering, 108 (1&2): 133-146.

Laursen, T. A. and Oancea, V. G. 1994. Automation and assessment of Augmented Lagrangian algorithms for frictional contact problems. Journal of Applied Mechanics, 61 (4): 956-963.

LeClaire, R. A. 1989. Upper bound to mechanical power transmission losses in wire rope. Journal of Engineering Mechanics-ASCE, 115(9): 2011-2019.

LeClaire, R. A. 1991. Axial response of multilayered strands with compliant layers. Journal of Engineering Mechanics-ASCE, 117(12): 2884-2903.

Leine, R. I. and Wouw, N. 2008. Stability and convergence of mechanical systems with unilateral constraints, Springer.

Leissa, A. W. 1959. Contact stresses in wire ropes. Wire and Wire Products, 34: 307–314, 372–373.

Liling Orient Power Co., Ltd. 2009. Power Fittings: Suspension Clamps. (Product specifications)

Liseikin, V. D. 2009. Grid generation methods (scientific computation), Springer-Verlag.

Liu, Y. and Mahadevan, S. 2005. Multiaxial hing-cycle fatigue criterion and life prediction for metals. International Journal of Fatigue, 27:790-800.

Love, A. E. H. 1944. A treatise on the mathematical theory of elasticity. Dover Publications Inc., New York.

Luo, G., Xu, L. and Zhang, J. 2000. Analysis of parallel groove clamp with finite element method, IEEE, 230-237.

Macha, E., Bedkowski, W. and Lagoda, T. 1999. Multiaxial fatigue and fracture, Elsevier Science.

Machida, S. and Durelli, A. J. 1973. Response of a strand to axial and torsional displacements. Journal of Mechanical Engineering Science, 15(4): 241-251.

Mahinthakumar, G. and Hoole, S. R. H. 1990. A parallelized element by element Jacobi conjugate gradients algorithm for field problems and a comparison with other schemes. Applied Electromagnetics in Materials, 1: 15-28.

Maitournam, H. 2003. Finite element applications; numerical tools and specific faigue problems. High-cycle Metal Fatigue: From theory to Applications (K. Dang Van and I. Papadoupoulos, Eds), CISM International Centre for Mechanical Sciences, Springer, 169-187.

Manson, S. S. 1953. Bahavior of materials under conditions of thermal stress. Heat Transfer Symposium, University of Michigan Engineering Research Institute, 9-75.

Maouche, N., Maitournam, M. H. and Dang Van, K. 1997. On a new method of evaluation of the inelastic state due to moving contacts. Wear, 203-204: 139-147.

Mattingly, J. D., Heiser, W. H., and Pratt, D. T. 2002. Aircraft engine design. 2nd ed., AIAA Publications.

McClure, G., and Guevara, E. 1994. Seismic behavior of tall guyed telecommunications towers. Bulletin of the International Association for Shell and Spatial Structures, 35(115): 93-99.

McClure, G. and Lapointe, M. 2003. Modeling the structural dynamic response of overhead transmission lines. Computers & Structures, 81: 825-834.

McClure, G., and Tinawi, R. 1987. Mathematical modeling of the transient response of electric transmission lines due to conductor breakage. Computers & Structures, 26(1/2): 41-56.

McDevitt T. W. and Laursen, T. A. 2000. A mortar finite element formulation for frictional contact problems. International Journal for Numerical Methods in Engineering, 48: 1525-1547.

McDiarmid, D. L. 1994. A shear stress based cricital-plane criterion of multiaxial fatigue failure for design and life prediction. Fatigue & Fracture of Engineering Materials and Structures, 17(12): 1475-1484.

McDowell, D. L. and Ellis, R. 1993. Advances in multiaxial fatigue, ASTM STP 1191.

McVeigh, P. A. 1999. Analysis of fretting fatigue in aircraft structures: stresses and stress intensity factors and life predictions. Ph.D. thesis, School of Aeronautics and Astronautics, Purdue University.

McVeigh, P. A. and Farris, T.N. Analysis of surface stresses and stress intensity factors present during fretting fatigue. 1999. Proceedings of the 40th AIAA/ASME/ASCE/ ASC Structures, Structural Dynamics, and Materials Conference, 2: 1188-1196

Miller, K. J. and Brown, M. W. 1985. Multiaxial fatigue: a symposium sponsored by ASTM Committees E-9 on Fatigue and E-24 on Fracture Testing, ASTM.

Miller, K. J. 1982. Fatigue under multiaxial stress strain conditions. Mechanical and Thermal Behavior of Metallic Materials, North Holland Publishing Co., 145-164.

Milne, I., Ritchie, R. O. and Karihaloo, B. 2003. Comprehensive structural integrity, Elsevier Science.

Mindlin, R. D. 1949. Compliance of elastic bodies in contact, ASME Journal of Applied Mechanics, 16: 259-268.

Miner, M. A. 1945. Cumulative damage in fatigue. Journal of Applied Mechanics, 12: 159-164.

Mirshafiei, F., McClure, G., and Farzaneh, M. 2013. Modelling the dynamic response of iced transmission lines subjected to cable rupture and ice shedding. IEEE Transactions on Power Delivery. DOI:10.1109/TPWRD.2012.2233221.

Mocks, L. 1970. Damage caused by oscillations to conductor cables. Bulletin of the Swiss Electrotechnical Association. 69(5): 223-227.

MSC.Software Corporation. 2010. Marc 2010 Volume A: Theory and user information, Santa Ana, CA, U.S.A.

Nawrocki A. and Labrosse M. 2000. A fnite element model for simple straight wire rope strands. Computers and Structures, 77(4): 345-359.

Nguyen, D. T. 2006. Finite element methods: parallel-sparse statics and eigen-solutions, Springer.

Nicholas, T. 2006. High cycle fatigue: A mechanics of materials perspective, Elsevier Science.

Nicholas, T., Hutson, A., John. R., and Olson, S. 2003. A fracture mechanics methodology assessment for fretting fatigue. International Journal of Fracture, 25: 1069-1077.

Nickerson, R. E. 2006. Electrical Transmission Line and Substation Structures: Structural Reliability in a Changing World, ASCE.

Nishioka, K. and Hirakawa, K. 1969. Fundamental investigation of fretting fatigue. Bull. JSME, 12: 180-187, 397-414, 692-697.

Nix, K. and Lindley, T. C. 1988. The influence of relative slip range and contact material on the fretting fatigue proprieties of 35NiCrMoV rotor steel. Wear, 125: 147-162.

Nowell, D. and Hills, D. A. 1990. Crack initiation criteria in fretting fatigue. Wear, 136: 329-343.

Oberg, E., Jones, F. D., Horton, H. L. and Ryffel, H. H. 1996. Machinery's Handbook, 25th ed., Industrial Press.

Odfalk, M., and Vingsbo, O. 1992. An elastic-plastic model for fretting contact. Wear, 157: 435-444.

Oden, J. T. and Prudhomme, S. 2002. Estimation of modeling error in computational mechanics. Journal of Computational Physics, 182: 496-515.

Ouaki, B., Goudreau, S., and Cardou, A. 1997. Experimental study of wire strains in a conductor suspension clamp under cyclic bending loading. CANCAM 97, 16ème Congrès canadien de mécanique appliquée, Québec, pp. 149-150.

Ouaki, B., Goudreau, S., Cardou, A. and Fiset, M. 2003. Fretting fatigue analysis of aluminum conductor wires near the suspension clamp: Metallurgical and fracture mechanics analysis. Journal of Strain Analysis for Engineering Design, 38(2): 133-147.

Páczelt, I. and Beleznai, R. 2011. Nonlinear contact-theory for analysis of wire rope strand using high-order approximation in the FEM. Computers & Structures, 89(11-12): 1004-1025.

Panagiotopoulos, P. D. 1985. Inequality problems in mechanics and applications. Birkhauser.

Papailiou, K. O. 1995. Improved calculations of dynamic conductor bending stresses using a variable bending stiffness. Cigre sc 22-wg1 1, paper 138.

Papailiou, K. O. 1997. On the bending stiffness of transmission line conductors. IEEE Trans Power Delivery, 12 (4) : 1576-1588.

Papanikolas, P. 1995. Axial fatigue of multi-layered wire strands, PhD thesis, University of Alberta.

Paris, P. C. 1998. Fracture mechanics and fatigue: a historical perspective. Fatigue and Fracture of Engineering Materials and Structures, 21(5): 535-540.

Paris, P. C. and Erdogan, F. 1963. A critical analysis of crack propagation laws. Journal of Basic Engineering, Transactions of the American Society of Mechanical Engineers, 85: 528-534.

Paris, P. C., Gomez, M. P. and Anderson, W. E. 1961. A rational analytic theory of fatigue. The Trend in Engineering, 13: 9-14.

Peabody, AB, and McClure, G. 2010. Modeling the EPRI-Wisconsin Power and Light Broken Wire Tests, IEEE Transactions on Power Delivery, 25(3): 1826-1833.

Petiot, C., Vincent, L., Dang Van, K., Maouche, N., Foulquier, J., and Journet, B. 1995. An analysis of fretting-fatigue failure combined with numerical calculations to predict crack nucleation. Wear, 181-183: 101-111.

Phillips, J. W. and Costello, G. A. 1973. Contact stresses in twisted wire cables. Journal of the Engineering Mechanics Division, Proceedings of the American Society of Civil Engineers. 99: 331-341.

Pian, T. H. H. and Wu, C. 2005. Hybrid and incompatible finite element methods, Chapman and Hall/CRC.

Pook, L. 2007. Metal fatigue: what it is, why it matters, Springer.

Preformed Line Products (Canada) Ltd. 2009. Ductile Iron Suspension Clamp. (Product specifications)

Puso, M. A. 2000. A highly efficient enhanced assumed strain physically stabilized hexahedral element. 2000. International Journal for Numerical Methods in Engineering, 49: 1029–1064.

Puso, M. A. and Laursen, T. A. 2004. A mortar segment-to-segment contact method for large deformation solid mechanics. Computer Methods in Applied Mechanics and Engineering, 193: 601-629.

Puso, M. A. and Laursen, T. A. 2004. A mortar segment-to-segment frictional contact method for large displacements. Computer Methods in Applied Mechanics and Engineering, 193: 4891-4913.

Qi, G., Wu, C. and Zhang, N. 2000. Precise analysis of 3-D elastic contact of tenon and mortise joint in turbine. Shipbuilding of China, 41 (3): 69-73. (in Chinese)

Qi, G., Wu, C. and Zhang, N. 2001. A study on modeling and algorithm of precise FE analysis of engine connecting-rods. China Mechanical Engineering, 12 (3): 282-284.

Quarteroni, A., Sacco, R. and Saleri, F. 2007. Numerical mathematics, 2nd ed., Springer.

Quarteroni, A. and Valli, A. 1997. Numerical approximation of partial differential equations, Springer.

Ramey, G. E. and Townsend, J. S. 1981. Effects of clamps on fatigue of ACSR conductors. ASCE, 107:103-109.

Ramsdale, R. 2006. Coefficient of Friction, www.EngineersHandbook.com

Raoof, M. and Hobbes, R., E. 1988. Analysis of Multilayered Structural Strands. Journal of Engineering Mechanics, 114(7): 1166-1182.

Rawlins, Charles B. 2005. Analytical elements of overhead conductor fabrication. Fultus Corporation.

Reybet-Degat, P., Zhou, Z. R., and Vincent, L. 1997. Fretting cracking behavior on pre-stressed aluminum alloy specimens. Tribology International, 30 (3): 215-223.

Rice, C. R. 1997. SAE fatigue design handbook, SAE International.

Roshan Fekr, M. 1998. A survey of publications on stress analysis of helical wires, optical fibers and optical ground wires. Department of Civil Engineering and Applied Mechanics, McGill University, Structural Engineering report, No. 97-12, 32p.

Roshan Fekr, M. 1999. Stress analysis of an optical ground wire. Department of Civil Engineering and Applied Mechanics, McGill University, Ph.D. Thesis, 201p.

Roshan Fekr, M. and McClure, G. 1998. Numerical modelling of the dynamic response of ice shedding on electrical transmission lines. Atmospheric Research, 46: 1-11.

Roshan-Fekr, M., McClure, G., and Farzaneh, M. 1999. Application of ADINA to stress analysis of an optical ground wire. Computers & Structures, 72: 301-316.

Ruiz, C., Boddington, P. H. B., and Chen, K. C. 1984. A investigation of fatigue and fretting in a dovetail joint. Experimental Mechanics. 24(3): 208-217.

Saad, Y. 2003. Iterative methods for sparse linear systems, 2nd ed., Society for Industrial and Applied Mathematics (SIAM).

Sato, K., Fuji, H. and Kodama, S. 1986. Crack propagation behavior in fretting fatigue. Wear, 107: 245-262.

Sauger, E., Fouvry, S., Ponsonnet, L., Kapsa, Ph., Martin, J. M. and Vincent, L. 2000. Tribologically transformed structure in fretting. Wear, 245: 39-45.

Sauger, E., Ponsonnet, L., Martin, J. M. and Vincent, L. 2000. Study of the tribologically transformed structure created during fretting tests. Tribology International, 33: 743-750.

Schijve, J. 2009. Fatigue of structures and materials, Springer.

Schütz, W. 1996. A history of fatigue. Engineering Fracture Mechanics, 54(2): 263-300.

Serway, R. A. 1995. Physics for scientists and engineers, 4th edition, Harcourt Brace College Publishers.

Shehata, A. Y. and El-Damatty, A. A. 2005. Finite element modeling of transmission line under downburst wind loading. Finite Element in analysis and Design, 42: 71-89.

Shigley, J. E. 1972. Mechanical Engineering Design, 2nd ed., McGraw-Hill, Inc.

Shrivastava, S. 2005. CIVE 601: Course notes of “Finite Element Analysis”, Departmant of Civil Engineering and Applied Mechanics, McGill University.

Simo, J. C. and Laursen, T. A. 1992. An Augmented Lagrangian treatment of contact problems involving friction. Computers and Structures, 42 (1): 97-116.

Simo, J. C. and Rifai, M. S. 1990. A class of assumed strain methods and the method of incompatible modes. International Journal for Numerical Methods in Engineering, 29: 1595-1638.

Sines, G. 1959. Behaviour of metals under complex stresses. In: Metal fatigue, Sines, G. and Waisman, J. L. (ed.), McGraw-Hill, 145-169.

Smailys A., and Brownridge, C. 1987. Design for fretting fatigue free joints in turboprop engine gearboxes, P&WC, UTC, AIAA Report Number: AIAA-87-2046.

Smith, E. H. (ed.). 1998. Mechanical Engineer's Reference Book, Elsevier.

Sofonea, M. and Matei, A. 2012. Mathematical models in contact mechanics (London Mathematical Society Lecture Note Series), Cambridge University Press.

Sonsino, C. M., Zenner, H. and Portella, P. D. 2004. 7th ICBMFF: Proceedings of 7th International Conference on Biaxial, Multiaxial Fatigue and Fracture, Berlin, Germany, 17-25.

Specialists meeting on fretting in aircraft systems. 1974. NATO-AGARD Conference Proceedings, No.161, AGARD.

Stampacchia, G. and Lions, J. L. 1967. Variational inequalities. Commun. Pure Appl. Math., 20: 493-519.

Stanova, E., Fedorko, G. Fabian, M. and Kmet, S. 2011. Computer modeling of wire strands and ropes Part I: theory and computer implementation. Advances in Engineering Software, 42(6): 305-315.

Stanova, E., Fedorko, G. Fabian, M. and Kmet, S. 2011. Computer modeling of wire strands and ropes Part II: finite element-based applications. Advances in Engineering Software, 42(6): 323-331.

Starkey W. L. and Cress, H. A. 1959. An analysis of critical stresses and mode of failure of a wire rope. J. Eng. Ind, Trans ASME 81: 807–816.

Stein, E. 2003. Error-controlled adaptive finite elements in solid mechanics, John Wiley & Sons, Inc.

Stein, E. 2005. Adaptive finite elements in linear and nonlinear solid and structural mechanics, SpringerWienNewYork.

Stephens, R. I., Fatemi, A., Stephens, R. R. and Fuchs, H. O. 2001. Metal fatigue in engineering, Wiley-Interscience.

Strang G. 1986. Introduction to applied mathematics, Wellesley-Cambridge Press.

Strang G. 2005. Linear algebra and its applications, 4th ed. Brooks Cole.

Strang G. 2007. Computational science and engineering, Wellesley-Cambridge Press.

Studer, C. 2009. Numerics of unilateral contacts and friction: Modeling and numerical time integration in non-smooth dynamics, Springer.

Suresh, S. 1998. Fatigue of materials. 2nd ed., Cambridge University Press.

Szabo, B. and Babuška, I. 1991. Finite element analysis, John Wiley & Sons, Inc.

Szabo, B. and Babuška, I. 2011. Introduction to finite element analysis: formulation, verification and validation, John Wiley & Sons, Inc.

Szolwinski, M. and Farris, T. 1996. Mecahnics of fretting fatigue crack formation. Wear, 198: 93-107.

Takahashi, S. 1991. Elastic contact analysis by boundary elements, Springer.

Timothy, A. D. 2006. Direct methods for sparse linear systems, Society for Industrial and Applied Mathematic (SIAM).

Tomlinson, G. A. 1927. The rusting of steel surfaces in contact. Proc. Roy. Society (London), A115: 472–483.

Tomlinson, G. A., Thorpe, P. L. and Gough, H. J. 1939. Investigation of the fretting corrosion of closely fitting surfaces. Proc. Inst. Mech. Engrs., 141: 223.

Topping, B. H. V. J., Muylle, P. I. and Putanowicz, R. 2002. Finite element mesh generation, Saxe-Coburg Publications.

Trefethen, L. N. and Bau, D. 1997. Numerical linear algebra, Society for Industrial and Applied Mathematics (SIAM).

UGS Corp. 2006. I-DEAS 12m2 NX Help Library, Plano, Texas. USA.

United States Patent No. 3602956. 1971. Cable Clamp, invented by Eddens, F. C. and Reed, K. F., patented on Sept. 7, 1971.

Utting, W. S. 1994a. Survey of the literature on the behaviour of steel wire rope - Part I. Journal of Wire Industry, 633-635.

Utting, W. S. 1994b. Survey of the literature on the behaviour of steel wire rope-Part II. Journal of Wire Industry, 746-748.

Utting, W. S. 1995c. Survey of the literature on the behaviour of steel wire rope-Part III. Journal of Wire Industry, 269-270.

Utting, W. S., and Jones, N. 1984. Survey of the literature on the behaviour of steel wire rope. Journal of Wire Industry, 623-629.

Uttings, W. S. and Jones, N. 1987. The response of wire rope strands to axial tensile loads-Part II. Comparison of experimental results and theoretical predictions. International Journal of Mechanical Science, 29(9)9: 621-636.

Uttings, W. S. and Jones, N. 1987. The response of wire rope strands to axial tensile loads-Part I. Experimental results and theoretical predictions. International Journal of Mechanical Science, 29(9): 605-619.

Vingsbo, O. and Odfalk, M. 1990. Conditions for elastic contact in fretting. Proceedings of Japan International Tribology Conference, 833-838. Tokyo.

Vingsbo, O., Odfalk, M., and Shen, Ning-E. 1990. Fretting maps and fretting behavior of some FCC metal alloys. Wear, 138(1-2): 153-167.

Vingsbo, O. and Schon, J. 1993. Gross slip criteria in fretting. Wear, 162-64(A): 347-356.

Vingsbo, O. and Soderberg, S. 1988. On fretting maps. Wear, 126(2): 131-147.

Wang, J. J., Lara-Curzio, E., and Tom, J. King Jr. 2008. The integrity of ACSR full tension single-stage splice connector at higher operation temperature. Report No. ORNL/TM-2008/156, Oak Ridge National Laboratory, U.S.A.

Wang, Y. Y. and Yao, W. X. 2004. Evaluation and comparison of several multiaxial fatigue criteria. International Journal of Fatigue, 26 (1):17-25.

Waterhouse, R. B. 1955. Fretting corrosion. Proc. Inst. Mech. Engrs. (London), 169: 1157.

Waterhouse, R. B. 1969. “Fretting” in Treatise on Materials Science and Technology. Vol. 13, Wear, Scott, D. (ed.), Academic Press, London.

Waterhouse, R. B. 1972. Fretting corrosion, Pergamon Press, Oxford.

Waterhouse, R. B. 1977. The role of adhesion and delamination in the fretting Wear of metallic materials, Wear, 45: 355-364.

Waterhouse, R. B. 1981. Fretting Fatigue, Elsevier Applied Science, London.

Waterhouse, R. B. 1984. Fretting wear. Wear, 100: 107-118.

Waterhouse, R. B. 1992. Fretting fatigue. International Material Review, 37: 77-97.

Waterhouse, R. B. 1992. Fretting wear. ASM Handbook, Vol. 18, Friction, Lubrication, and Wear Technology, ASM International.

Waterhouse, R. B. 2003. Fretting in steel ropes and cables: a review. ASTM STP1425.

Waterhouse, R. B. and Lindley, T. C. 1994. Fretting fatigue, ESIS Publication 18, London.

Watkins, D. S. 2010. Fundamentals of matrix computations, 3rd edition, John Wiley & Sons, Inc.

Wilson, E. L. and Ibrahimbegovic, A. 1990. Use of incompatible displacement modes for the calculation of element stiffness and stresses. Finite Elements in Analysis and Design, 7: 229-241.

Wöhler, A. 1867. Wöhler’s experiments on the strength of metals. Engineering, 2:160-161.

Wong, J. C. and Miller, M. D. 2009. Guidelines for Electrical Transmission Line Structural Loading. Third edition, Asce Manuals and Reports on Engineering Practice, No. 74.

Wriggers, P. 2006. Computational contact mechanics, 2nd edition, Springer.

Wriggers, P. 2008. Nonlinear finite element method, Springer.

Wriggers P. and Laursen T. A. 2008. Computational contact mechanics. CISM Courses and Lectures, Vol. 498, Springer.

Wriggers, P. and Nackenhorst, U. 2006. Analysis and simulation of contact problems, Springer.

Wriggers, P. and Nackenhorst, U. 2006. IUTAM Symposium on computational methods in contact mechanics, Springer.

Wriggers, P. and Panagiotopoulos, P. 1999. New developments in contact problems. CISM courses and lectures, No. 384, Springer.

Xu, L. Q., Clough, S., Howard, P. et al. 1995. Laboratory assessment of the effect of white layers on wear resistance for digger teeth. Wear, 181-183: 112-117.

Yang, B. 2009. Mortar finite element methods for large deformation contact mechanics, VDM Verlag Dr. Müller.

Yastrebov, V. A. 2013. Numerical methods in contact mechanics, Wiley-ISTE.

You, B. R. and Lee, S. B. 1996. A critical review on multiaxial fatigue assessments of metals. International Journal of Fatigue, 18 (4):235-244.

Zenner, H. 2004. Multiaxial fatigue - methods, hypotheses and applications, an overview. In: 7th ICBMFF. Proceedings of 7th International Conference on Biaxial, Multiaxial Fatigue and Fracture, Berlin, Germany, 3-16.

Zhang, H. W., Liao, A. H., Xie, Z. Q., Chen B. S. and Wang, H. 2006. Some advances in mathematical programming method for numerical simulation of contact problems. IUTAM Symposium on computational methods in contact mechanics, Springer.

Zhang, Z. and Costello, G. A. 1996. Fatigue design of wire rope. Wire Journal International, 29 (2): 106-112.

Zhong, Z. H. 1993. Finite element procedures for contact-impact problems. Oxford University Press.

Zhong, Z. H. and Mackerle, J. 1994. Contact-impact problems: A review with bibliography. Applied Mechanics Review, 47 (2): 55-76.

Zhong, Z. H. and Nilsson, L. 1994. Automatic contact searching algorihm for dynamic finite element analysis. Computers and Structures, 52 (2): 187-197.

Zhong, Z. H. and Nilsson, L. 1994. Lagrange multiplier approach for evaluation of friction in explicit finite-element analysis. Computer Methods in Applied Mechanics and Engineering, 10 (3): 249-255.

Zhou, Z. R., Cardou, A., Fiset, M., and Goudreau, S. 1994. Fretting fatigue in electrical transmission lines. Wear, 173: 179-188.

Zhou, Z. R., Cardou, A., Goudreau, S., and Fiset, M. 1994. Fretting patterns in a conductor-clamp contact zone. Fatigue and Fracture of Engineering Materials & Structures, 17(6): 661–669.

Zhou, Z. R., Cardou, A., Goudreau, S., and Fiset, M. 1996. Fundamental investigations of electrical conductor fretting fatigue. Tribology International, 29(3): 221-232.

Zhou, Z. R., Fayeulle, S., and Vincent, L. 1992. Cracking behaviour of various aluminum alloys during fretting wear. Wear, 155(2): 317-330.

Zhou, Z. R., Fiset, M., Cardou, A., Cloutier, L., and Goudreau, S. 1995. Effect of lubricant in electrical conductor fretting fatigue. Wear, 189: 51-57.

Zhou, Z. R., Fiset, M., Cardou, A., and Goudreau, S. 1993. Fretting behavior of overhead electrical conductors under cyclic bending at suspension clamps. International Symposium on Tribology, 475-484.

Zhou, Z. R., Goudreau, S., Fiset, M., and Cardou, A. 1995. Single wire fretting fatigue tests for electrical conductor bending fatigue evaluation. Wear, 181: 537-543.

Zhou, Z. R., Gu, S. R., and Vincent, L. 1997. An investigation of the fretting Wear of two aluminum alloys. Tribology International, 30: 1-7.

Zhou, Z. R., Kapsa, P. H., and Vincent, L. 1998. Grease lubrication in fretting. Journal of Tribology, Transactions of the ASME, 120(4): 737.

Zhou, Z. R., Sauger, E., Liu, J. J. and Vincent, L. 1997. Nucleation and early growth of tribologically transformation structure (TSS) induced by fretting. Wear, 212: 50-58

Zhou, Z. R. and Vincent, L. 1993. Effect of external loading on wear maps of aluminum alloys. Wear, 162-64(A): 619-623.

Zhou, Z. R and Vincent, L. 1995. Mixed fretting regime. Wear, 181-183(2): 531-536.

Zhou, Z. R. and Vincent, L. 1997. Cracking induced by fretting of aluminum alloys. Journal of Tribology, Transactions of the ASME, 119 (1): 36.

Zhou, Z. R. and Vincent, L. 1999. Lubrication in fretting - A review. Wear, 225-229: 962-927.

Zhou, Z. R. and Vincent, L. 2002. Fretting wear, Science Press (in Chinese).

Zhu, J. Z. and Zienkiewicz, O. C. 1990. Superconvergence recovery techniques and a posteriori error estimators. International Journal for Numerical Methods in Engineering, 30: 1321-1339.

Zienkiewicz, O. C. and Taylor, R. L. 2005. The finite element method for solid and structural mechanics, 6th edition, Butterworth-Heinemann.

Zienkiewicz, O. C., Taylor, R. L., and Zhu, J. Z. 2005. The finite element method: Its basis and fundamentals, 6th edition, Butterworth-Heinemann.

Zienkiewicz, O. C., and Zhu, J. Z. 1987. A simple error estimator and adaptive procedure for practical engineering analysis. International Journal for Numerical Methods in Engineering, 24: 337-357.

Zienkiewicz, O. C., and Zhu, J. Z. 1992. The superconvergent patch recovery and a posteriori error estimates. Part 1: The recovery technique. International Journal for Numerical Methods in Engineering, 33: 1331-1364.

Zienkiewicz, O. C. and Zhu, J. Z. 1992. The superconvergent patch recovery and a posteriori error estimates. Part 2: Error estimates and adaptivity. International Journal for Numerical Methods in Engineering, 33: 1365-1382.

“雄关漫道真如铁，而今迈步从头越 ”